Experimental and theoretical mechanistic studies of transition-metal free and copper-catalyzed reactions

Indira Fabre

THÈSE DE DOCTORAT

de l'Université de recherche Paris Sciences et Lettres
PSL Research University

Préparée à l'Ecole Normale Supérieure

Experimental and theoretical mechanistic studies of transition-metal free and copper-catalyzed reactions

Études expérimentales et théoriques de mécanismes de réactions non catalysées par des métaux de transition et catalysées au cuivre

Ecole doctorale n°388

CHIMIE PHYSIQUE ET CHIMIE ANALYTIQUE DE PARIS CENTRE

Spécialité CHIMIE THEORIQUE, PHYSIQUE, ANALYTIQUE

COMPOSITION DU JURY :

Pr. Hélène GERARD
Université Pierre et Marie Curie, Présidente du jury

Dr. Marine DESAGE-EL MURR
Université Pierre et Marie Curie, Rapporteur

Pr. Emilia SICILIA
Università della Calabria, Rapporteur

Pr. Olivier RIANT
Université Catholique de Louvain, Membre du jury

Dr. Ilaria CIOFINI
Chimie ParisTech, Directrice de thèse

Dr. Laurence GRIMAUD
Ecole Normale Supérieure, Directrice de thèse

Soutenue par Indira FABRE
le 10 juillet 2017

Dirigée par **Dr. Ilaria CIOFINI**
et **Dr. Laurence GRIMAUD**

ENS ÉCOLE NORMALE SUPÉRIEURE

Chimie Paris ParisTech

PSL RESEARCH UNIVERSITY PARIS

Experimental and theoretical mechanistic studies of transition-metal free and copper-catalyzed reactions

Indira Fabre

Thèse de doctorat

Table of content

Acknowledgements 7

Introduction 9

List of abbreviations 13

Chapter 1 - Methods for mechanistic studies 15

Experimental techniques 17

Nuclear magnetic resonance spectroscopy 17

Cyclic voltammetry 18

Radical trapping and radical-clock experiments 20

Theoretical methods 24

The theoretical toolbox 24

Selected tools and methods used in this thesis 43

Chapter 2 - *t*BuOK/DMF mediated alpha-arylation of enolizable aryl ketones – mechanistic evidence for a radical process and synergistic role of the base and solvent 49

State of the art 51

Transition metal free methods of alpha-arylation of ketones by $S_{RN}1$ mechanism 51

*t*BuOK/DMF-promoted alpha-arylation of aryl ketones 55

Mechanisms of initiation of radical chain processes by organic additives 58

Mechanistic study of the *t*BuOK/DMF promoted alpha-arylation of aryl ketones 70

$S_{RN}1$ Mechanism 70

DFT computational details 72

Initiation by outer-sphere electron transfer to PhI 73

Initiation by inner-sphere electron transfer to PhI 74

Initiation by outer-sphere electron transfer to the solvent 76

Initiation by deprotonation of the solvent 77

Developments and precisions following our work 88

Conclusion 92

Chapter 3 – Mechanistic study of the copper-catalyzed *N*-arylation of pyrazoles with arenediazonium salts generated *in situ* from anilines under ligand-free conditions 93

State of the art 95

Table of content

Methodology and scope for the copper-catalyzed arylation of nitrogen heterocycles from anilines 95

Arenediazonium salts as an alternative to aryl halides 97

Existing DFT methods for the study of transition metal catalytic cycles 108

Mechanistic study of the copper-catalyzed *N*-arylation of pyrazoles from anilines 110

First step: the triazene-diazonium equilibrium modulated by acetic acid 111

The oxidation state of the active copper species - at the frontier between radical and non-radical reactions 117

DFT for the study of the $Cu^{(I)}/Cu^{(III)}$ catalytic cycle 121

Evaluation of alternative mechanisms 130

The nature of the active copper species 131

Complementary results - the case of imidazole 137

Conclusion 141

Chapter 4 – Stereoselective access to trisubstituted fluorinated alkenyl thioethers 143

State of the art 145

Interest of fluorine and sulfur in drug development 145

Methods of functionalization of alkenyl thioethers 147

Difluoroacetylation methods by C-H functionalization 150

Methodology for the copper–catalyzed difluoroacetylation of alkenyl thioethers 161

Optimization of the conditions 161

Scope of the reaction 165

Selectivity of the reaction 167

Reactivity with other substrates and post-functionalization 169

Mechanistic study of the copper-catalyzed difluoroacetylation of alkenyl thioethers 172

Experimental evidence for a radical process 172

Study of the initiation of the reaction 173

Addition on the alkenyl thioether 181

Generalization of the mechanism to other substrates 183

Perspectives 186

Reactivity of fluorinated alkenyl thioethers 186

Isotetronic acids 188

Table of content

Conclusion 190
General conclusion 191
Appendix 193
General considerations 193
Appendix to chapter 2 194
Appendix to chapter 3 195
Appendix to chapter 4 205
References 233

Acknowledgements

Je tiens tout d'abord à remercier Laurence Grimaud et Ilaria Ciofini, mes deux directrices de thèse. Au-delà de leurs compétences scientifiques et de leur implication dans tous les sujets qui ont été abordés au cours de cette thèse, elles ont su faire preuve de grandes qualités humaines et ce fut un réel plaisir de travailler avec elles. Je les remercie de m'avoir fait confiance dès le début et de m'avoir permis, au cours de ces trois années, de m'épanouir dans un travail réellement collaboratif.

Merci à Marine Desage-El Murr et à Emilia Sicilia pour leur lecture minutieuse de ce manuscrit et leurs rapports détaillés. Merci aussi à Hélène Gérard et Olivier Riant qui m'ont fait l'honneur d'être membres du jury.

Je souhaite remercier le département chimie de l'ENS, ainsi que Chimie ParisTech, PSL, l'Université Pierre et Marie Curie et le CNRS, qui ont permis à cette thèse pluridisciplinaire d'exister. Je souhaite également remercier l'Ecole Normale Supérieure Paris-Saclay qui m'a attribué une bourse de thèse pour ces trois années.

Je tiens à remercier Anny Jutand, pour nos discussions fructueuses et toujours éclairantes. Je souhaite remercier tout particulièrement Luca, pour sa grande disponibilité et ses immenses qualités de chercheur, mais aussi Baptiste, Alexandra, Na, Aude et Pierre-Adrien qui m'ont accompagnée à la paillasse et ont été d'une aide précieuse, et de très bons amis.

Je souhaite également remercier Carlo Adamo et toute l'équipe des chimistes théoriciens, trop nombreux au cours de ces trois années pour tous les nommer. J'aimerais adresser un merci tout particulier à Liam, qui a avancé dans sa thèse au même rythme que moi et a été d'un réel soutien. Merci aussi à Stefania, Alexandra, Frederica, Ashwani, et Alistar.

Merci à nos collaborateurs Thierry Ollevier et Marc Taillefer. Merci à l'Ecole Nationale Supérieure de Chimie de Montpellier, qui m'a permis de travailler dans ses laboratoires, et merci aux membres de l'Institut Charles Gerhardt pour leur accueil.

Merci à Isabelle Gillaizeau, Xavier Pannecoucke et Thomas Poisson pour leur implication dans une collaboration fructueuse. Merci également à Maria Ivanova pour son aide précieuse et sa gentillesse. Merci aussi à Laurence Miesch pour son énergie et sa confiance.

Merci également à Vincent Jactel, de l'Ecole Polytechnique, et à Céline Fosse et Claudine Fleurant de Chimie ParisTech pour leur disponibilité et leur efficacité dans le traitement des diverses analyses.

Merci à mes parents, à mes sœurs, et à mes amis, qui m'ont accompagnée pendant ces trois années. Je tiens à féliciter ceux parmi eux qui m'ont précédée sur cette voie et je souhaite le meilleur à ceux qui sont en train de la suivre, ou viennent juste de s'y engager.

Enfin, merci à Thibault pour sa patience, son soutien à toute épreuve et pour tout le reste.

Introduction

Nowadays, there is a constant need for the development of new chemical reactions, for industrial or pharmaceutical applications. The purpose can be to access new kinds of active molecules, or to develop new synthetic routes, for cheaper, less toxic processes, that produce less waste.

Nevertheless, such innovations require a fine understanding of the phenomena involved. This understanding is not always trivial, and many discoveries are made by chance, or in an incremental fashion starting from an already known method, which limits the possibilities of breakthrough discoveries. This thesis has the ambition to help change the way new reactions are developed. In this thesis, we focus on a parallel work between methodology development and mechanistic study. We are half-way between classical conditions for screening and optimization and usual mechanistic studies, that are often done years after the reaction is first published, sometimes by a different research group.

The mechanism of a reaction is the step by step description of the transformations that occur during a chemical reaction. It includes the description of all the intermediates, but also the description of the transition states. A complete reaction mechanism must account for all the reactants and products, but also for the catalysts, and describe the stereochemistry of the products formed. Ideally, the reaction conditions (solvent, temperature…) are also taken into account.

Investigation of mechanisms allows a deeper understanding of the fundamental reactivity of species, especially in catalysis, allowing one to reduce the tedious work of conditions screening. In the ideal case, both conditions optimization and mechanistic studies are made in parallel, avoiding a blind choice of conditions. Mechanistic investigations can be generalized and provide keys for the understanding of several related reactions, and improve the development of new reactions.

Mechanistic studies are already used for industrial processes where they can help anticipate the rate of reactions and the amount of by-products to optimize the processes. This approach may allow to save time and money.

In this thesis, all the mechanistic studies presented use a complementary approach, with both experiments and calculations. Experiments allow one to obtain kinetic data and information on the structure of some intermediates. They are performed in the "true" reaction conditions. For the theoretical part, Density Functional Theory methods are used to answer questions that cannot be addressed experimentally. Theoretical insights for instance allow one to postulate the nature of short-lived species that cannot be isolated or charaterized. On the other hand, one limit of this approach is that it does not account for the actual complexity of the reaction medium. Several mechanistic hypotheses can be tested and compared, in accordance with the experimental results. Complementary experiments can then be performed, with a coming and going between theory and experiments.

For the reactions studied, we focused on solving key points that can be generalized. We are interested in reactions that happen in mild conditions, either in the absence of transition metal catalyst or with copper, which is a cheap metal of low toxicity and which displays interesting reactivity. This thesis is composed of four independent chapters. The first chapter presents the methods that are used in the following ones.

The second chapter presents the mechanistic study of the alpha-arylation of aryl ketones mediated by *t*BuOK and DMF. This reaction proceeds in the absence of a transition-metal catalyst. The state of the art and the development of the method by Martin Pichette Drapeau under the supervision of Marc Taillefer and Thierry Ollevier is presented. A $S_{RN}1$ mechanism was suspected but the initiation of the radical process required a fully detailed study. The experimental and theoretical results obtained are presented. The main goal of this chapter is the understanding of the peculiar and unique role of the *t*BuOK/DMF couple in the initiation of this radical reaction.

The third chapter concerns the mechanistic study of the copper-catalyzed arylation of pyrazoles. The first part presents the optimized conditions for the reaction studied which were developed by Fouad Ouazzani and Marc Taillefer. The advantages of the use of diazonium salts are then presented, along with an overview of their reactivity, with and without transition metal catalysts. The second part of this chapter consists of the mechanistic study of the reaction, done during this thesis. It is composed of both experimental and theoretical results. It involves in particular a screening of the DFT approaches for this reaction, which was one of the goals of

this study. This work also allows the understanding of the mechanism of the double catalytic cycle involved in this reaction.

The fourth chapter presents the copper-catalyzed difluoroacetylation of alkenyl thioethers. We first explain the interest of the combined presence of fluorine and sulfur in small molecules and expose the state of the art for the functionalization of alkenyl thioethers and for difluoroacetylation reactions. The second part focuses on the results obtained during this thesis: the synthetic methodology for the difluoroacetylation of alkenyl thioethers, and the experimental and theoretical results for the mechanistic study of this reaction. Understanding the mechanism of this reaction allows one to generalize it to analogous transformations on enamides and benzofuranes. The chapter ends on synthetic perspectives for the access to new isotetronic acids structures.

List of abbreviations

AIBN: azobisisobutyronitrile

BHAS: base-promoted homolytic aromatic substitution

BHT: 3,5-di-*tert*-4-butylhydroxytoluene

BSSE: basis set superposition error

CV: cyclic voltammetry

DBU: 1,8-diazabicyclo[5.4.0]undec-7-ene

DFT: density functional theory

DMEDA: *N*,*N*'-dimethylethylenediamine

DMF: *N*,*N*-dimethylformamide

DMSO: dimethylsulfoxide

EDG: electron donating group

EPR: electron paramagnetic resonance

Equiv: equivalent

ESI-MS: electrospray ionization-mass spectrometry

EWG: electron withdrawing group

FDA: food and drug administration

FG: functional group

GC: gas chromatography

GC-MS: gas chromatography-mass spectroscopy

GGA: generalized gradient approximation

GTO: Gaussian type orbital

HF: Hartree-Fock

HOESY: two-dimensional heteronuclear overhauser effect spectroscopy

HIV: human immunodeficiency virus

HMPA: hexamethylphosphoramide

HOMO: highest occupied molecular orbital

ID: intramolecular deprotonation

IRC: intrinsic reaction coordinate

LCAO: linear combination of atomic orbitals

LDA: lithium diisopropylamide

List of abbreviations

LDA: local density approximation

LE: ligand exchange

LED: light-emitting diode

LUMO: lowest unoccupied molecular orbital

MP: Møller Plesset

MS: mass spectrometry

NE: nitrogen extrusion

NMP: *N*-methylpyrrolidine

NMR: nuclear magnetic resonance

NOESY: two-dimensional nuclear overhauser effect spectroscopy

OA: oxidative addition

PCM: polarizable continuum model

Phen: 1,10-phenanthroline

Ppm: parts per million

RE: reductive elimination

RMSD: root mean square deviation

ROHF: restricted open shell Hartree-Fock

SCE: saturated calomel electrode

SCF: self-consistent field

SET: single electron transfer

SHE: standard hydrogen electrode

S_NAr: aromatic nucleophilic substitution

$S_{RN}1$: radical nucleophilic aromatic substitution

STO: Slater type orbital

TFA: trifluoroacetic acid

TEMPO: (2,2,6,6-tetramethylpiperidin-1-yl)oxyl

THF: tetrahydrofuran

TMEDA: tetramethylethylenediamine

TMHD: 2,2,6,6-tetramethyl-3,5-heptanedione

TMS: trimethylsilyl

UHF: unrestricted Hartree-Fock

UV: ultraviolet

Chapter 1 - Methods for mechanistic studies

In this chapter, an overview of some selected experimental techniques used in this thesis is given. The theoretical methods that have been used are also briefly detailed.

Experimental techniques

In this thesis, we use a combination of various experimental techniques to investigate reaction mechanisms.

Nuclear magnetic resonance spectroscopy

Nuclear magnetic resonance (NMR) spectroscopy is a routine powerful non-selective and non-destructive analytical tool that allows the determination of molecular structures, concentrations, and interactions. ^{1}H and ^{13}C are classically used for the complete characterization of isolated compounds.

^{1}H represents 99.98 % of naturally abundant hydrogen and has a spin ½. It is highly responsive to NMR spectroscopy. One of the drawbacks of this spectroscopy, in the context of mechanistic study, is that protons are present in all organic chemical species, in particular in solvents (which leads to the use of deuterated solvents). This can make the study of a complex reaction medium difficult because of the high number of signals and because of their possible superposition. Nevertheless, no-deuterium proton NMR is becoming popular for analyzing reactions.[1]

^{13}C has also a spin of ½, but this isotope is naturally present at only 1.1 %, whereas the major isotope of carbon, ^{12}C (98.93 %), has a spin of zero and is not detectable by NMR. This low sensitivity implies long acquisition times for ^{13}C NMR spectra. These timescales are not compatible with the study of the mechanisms of reactions that happen within minutes. In addition, the same drawbacks as ^{1}H NMR relative to the high number of signals exists.

In this context, ^{19}F is highly responsive to nuclear magnetic resonance spectroscopy. It has a nuclear spin of ½ and this isotope of fluorine represents 100 % of naturally abundant fluorine. For these reasons, ^{19}F NMR measurements are very fast. ^{19}F NMR chemical shift range is wide, between -50 and -200 ppm for the most commonly encountered signals.

Fluorine is not present in many organic molecules and solvents. This heteroatom can be selectively introduced on some molecules to study the evolution of a limited number of species, directly in a complex reaction mixture. We typically use a DMSO-d_6 insert for the reference for

the NMR acquisition, to avoid the use of deuterated solvent inside the reaction medium. Moreover, the presence of fluorine induces coupling with ^{13}C and ^{1}H. The signals can be decoupled, but the coupling can give useful information on the structure of the products. To have quantitative signals for ^{19}F NMR, the relaxation delay *d1* must be long enough, to allow the spins to return at the equilibrium. We typically use *d1* of 10 s in all our experiments.

Cyclic voltammetry

Molecular electrochemistry is a powerful tool to study the mechanisms of reactions that imply changes in the oxidation state of species.[2]

In this thesis, cyclic voltammetry (CV) was used as an electrochemical analytical method. It consists of the observation of the current of a system at an imposed potential that varies linearly with time. The conditions are non-stationary: the experiments are performed without stirring the solution, which suppresses convection, and the observed properties are governed by the diffusion. The migration of the charged species in the electric field due to the potential between the electrodes is suppressed by the addition of a support electrolyte. This electrolyte is present in the solution at a high concentration (typically 0.3 $mol.L^{-1}$, in 100-fold excess with respect to the observed species) to ensure a good conductivity. It also limits the non-faradaic contributions of the measured intensity. The electrolyte must be soluble, non-electroactive and chemically inert. It must allow the elimination of the migration mode of mass transport, and a high conductivity (with a low ohmic drop) and allow a high and constant ionic strength. In organic solvents, the commonly used electrolytes are ammoniums: $R_4N^+BF_4^-$ or $R_4N^+PF_6^-$. We generally choose nBu$_4$NBF$_4$ which is non-hygroscopic and easy to handle. The solvent used must be able to conduct with a high dielectric constant, and must be non-electroactive (or exhibit a large domain of electroactivity). Polar organic solvents are good candidates (DMF, CH_3CN, THF, MeOH, CH_2Cl_2, $CHCl_3$, DMSO), and are compatible with many current reactions.

A three-electrode set up is used (Figure 1.1). The potential is imposed between the working electrode (a gold or glassy carbon disk in our case) and the counter-electrode (a platinum wire). The potential is measured between the working electrode and the reference electrode. We used a saturated calomel electrode (SCE, E_{ref} = 0.244 V/SHE at 25 °C, $Hg_{(l)}$ /

$Hg_2Cl_{2(s)}$ / $KCl_{saturated}$). The current is measured between the working electrode and the counter-electrode.

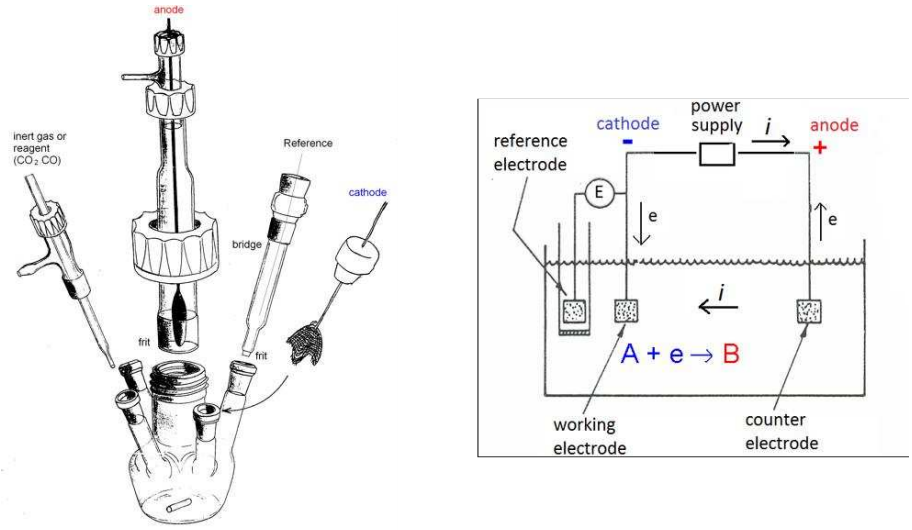

Figure 1.1 - Three-electrode set up for cyclic voltammetry (left) and its equivalent electrical scheme (right)

The reference electrode is separated from the solution by a bridge containing the solvent and the supporting electrolyte. In practice, the imposed potential is an affine function of time, with a chosen scan rate. Starting from an initial potential E_i, at which no reaction occurs, the potential reaches E_f. The obtained voltammogram is called cyclic if the potential reaches E_i again at the end of the measurement (Figure 1.2, left). To avoid any problem of natural convection, the scan rate is chosen greater that 50 $mV.s^{-1}$. The change of potential induces the reduction of a species A to form B by electron transfer, and an electrical current is detected ($A + e^- \rightarrow B$). This current decreases again when all the species A in the diffusion layer is consumed. By symmetry a peak is also obtained for the oxidation of B in A in the case of a reversible system ($B \rightarrow A + e^-$) (Figure 1.2, right). During the reduction of A, the working electrode is the cathode and the counter electrode is the anode. During the oxidation of B, it is the opposite.

With this technique, electroactive organometallic species can be characterized by their oxidation or reduction potentials. Cyclic voltammetry can generate short-lived species by electrochemical oxidation or reduction. This allows the investigation of reactive species that cannot be observed with spectroscopic techniques (NMR, UV-vis). Reduction or oxidation

currents are proportional to the concentration of the electroactive species in the bulk, and their reactivity can be followed.

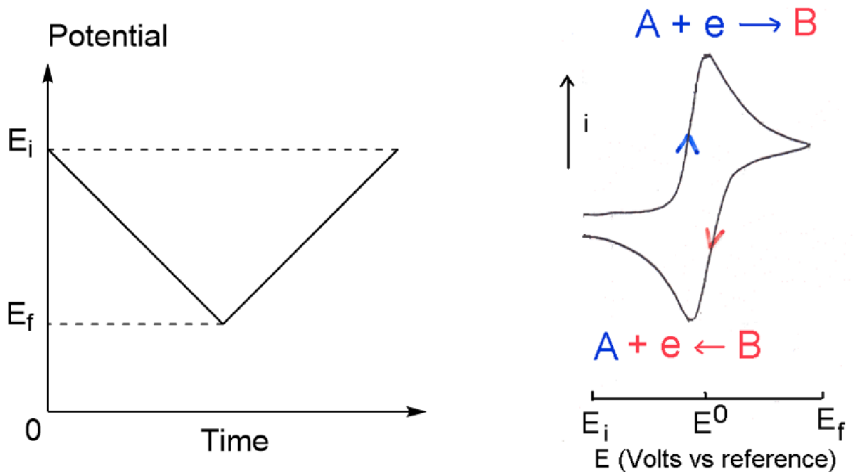

Figure 1.2 – Evolution of the potential during a cycle (left) and intensity/potential answer of the system (right)

Radical trapping and radical-clock experiments

Radicals are very reactive and usually short-lived species. When electrochemically generated, radicals tend to adsorb at the surface of the electrode. The grafting of an organic layer on the electrode blocks the access of electroactive species to the electrode for further analysis. Indeed, for example, the grafting of aryl radical starting from diazonium salts is a known and well-developed technique for the functionalization of electrodes and other surfaces.[3,4] This phenomenon makes the study of radical reactions by CV challenging.

Other techniques can be used to evidence the formation of radicals, and to identify their nature. In this thesis we used two strategies: the introduction of radical scavengers, and radical clock experiments.

Radical scavengers

Radical scavengers can be of various nature. Galvinoxyl and (2,2,6,6-tetramethylpiperidin-1-yl)oxyl (TEMPO) (Figure 1.3) are both stable radicals that can be easily

introduced in the reaction medium. If radicals are formed during the reaction, a radical-radical coupling is likely to occur and stop the propagation of the reaction. TEMPO is the most commonly used nitroxide. It is commercially available and it is an efficient trap for carbon-centered radicals.

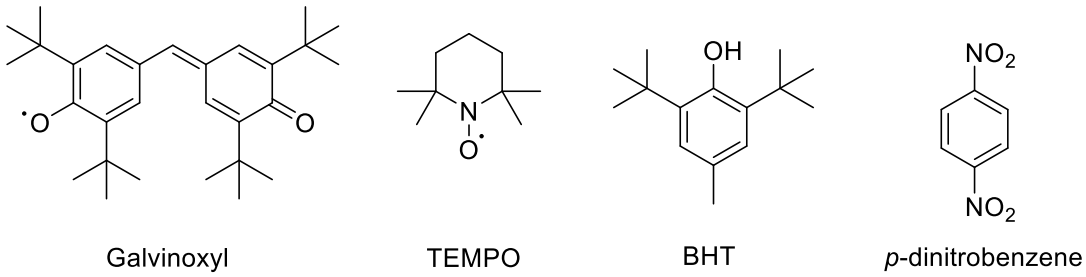

Figure 1.3 – Commonly used radical scavengers

3,5-Di-*tert*-4-butylhydroxytoluene (BHT) and *p*-dinitrobenzene are non-radical aromatic molecules (Figure 1.3). BHT in easily oxidized, especially with reactive oxygen species, and can form a phenoxy radical. It is a commonly used antioxidant in food, cosmetics, pharmaceuticals and chemicals. *p*-Dinitrobenzene, when reduced, forms a very stable radical.

Those radical scavengers are typically introduced in stoichiometric amount in the reaction medium of the system studied, with no modification of the reaction conditions. If their introduction greatly affects the yield of the reaction, it is generally considered as a proof that the main mechanistic pathway for the reaction involves free radicals. In some cases, adducts between the radical scavenger and a reactant can be isolated and this gives further information on the nature of the radical species involved. Nevertheless, if the presence of radical scavengers does not affect the yield of the reaction, it does not necessarily imply that the reaction does not involve radicals. Indeed, there is the possibility to produce very short-lived radicals during the reaction, for example in the coordination sphere of transition metal complexes. These radicals might not have time to be trapped by the radical scavenger before they react.

More generally, in the case of radical trapping studies, it is important to keep in mind that the introduction of these radical scavengers can affect the reaction due to their oxidizing or reducing properties, and not only because radicals are formed.

Radical-clock experiments

To address the issue of very short-lived radicals, another possible method is the use of radical-clocks. The term "radical-clock" is used to describe a unimolecular reaction with known kinetics. This reaction can be applied to "time" a given radical reaction. Some typical radical-clock reactions are reported in Figure 1.4.

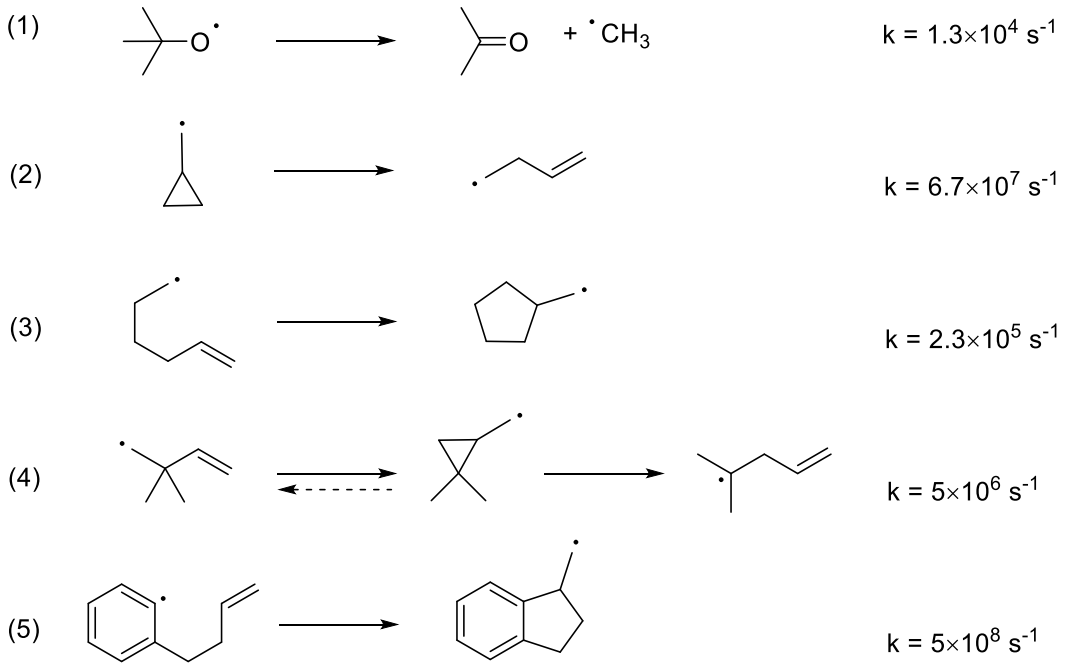

Figure 1.4 – Typical radical-clock reactions, and their rate constants[5]

In opposition to the introduction of radical scavengers, which is straightforward, this method requires the synthesis of new substrates for the reaction studied. For example, if the formation of an alkyl radical is suspected, the substituents from Figure 1.4, equations (2), (3) or (4) can be introduced. If an aryl radical is suspected, the substituent from Figure 1.4, equation (5) can be introduced. An example is depicted in Figure 1.5.

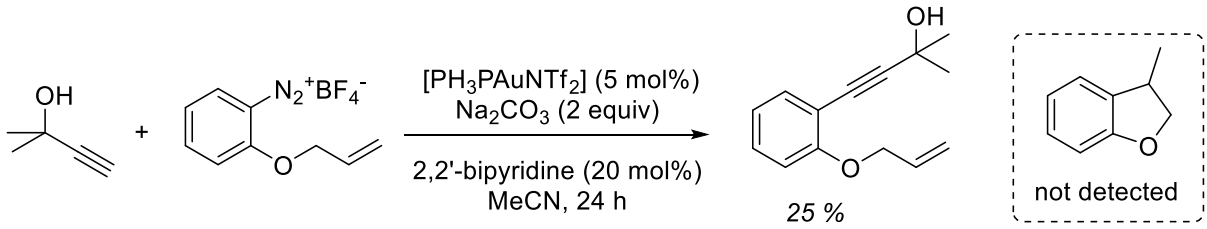

Figure 1.5 – Radical-clock experiment in the case of gold-catalyzed cross-coupling[6]

Radical-clock experiments can also give access to useful kinetic data, since the rate constants for the radical-clock reactions are known and tabulated (Figure 1.4). In our case, we used these reactions for qualitative results only, that is to evidence - or not - the formation of a radical. No kinetic data were therefore derived from these experiments.

Theoretical methods

Theoretical methods are used in combination with experimental techniques for the elucidation of reaction mechanisms.

The theoretical toolbox[7–9]

Fundamental aspects of the electronic structure

The fundamental equation of quantum mechanics is the Schrödinger equation[10] which, in its time-independent version, can be written:

$$\hat{H}|\Psi\rangle = E|\Psi\rangle \qquad (1.1)$$

In this equation, $\hat{H}$ represents the Hamiltonian of the system, Ψ the total wave-function of the system and E the total energy of the system. This equation allows to describe the physical properties of macroscopic systems. It can be exactly solved only for simple systems with one electron. Different approaches exist for the mathematical approximated resolution of this equation for polyelectronic systems.

Usually, methods that do not rely on the use of parameters in the resolution of this equation are called "*ab initio*". They aim at finding the polyelectronic wave-function of the system. They usually start with the Hartree-Fock (HF) approximation, eventually followed by different corrections aiming at introducing the missing correlation energy in the original HF method (see below for further explanation).

Nonetheless, it has been shown that the ground state of an n electrons system can be fully defined by its density (which is actually an observable). The energy E can be thus expressed as a functional of the electronic density. Approaches of this type are rooted on Density Functional Theory (DFT).

All HF and post-HF as well as DFT methods that were used in this thesis will be briefly detailed in this section.

The Schrödinger equation

The Hamiltonian of a generic system constituted by n electrons and N nuclei can be written as the sum of the kinetic ($\hat{T}$) and potential ($\hat{V}$) energy.

$$\hat{H} = \hat{T} + \hat{V} \tag{1.2}$$

These two terms can both be decomposed into their electronic and nuclear contributions.

$$\hat{T} = \hat{T_e} + \hat{T_N} = -\sum_{i,e^-}^{n} \frac{\hbar^2}{2m_e}\nabla_i^2 + \sum_{I,noyaux}^{N} -\frac{\hbar^2}{2M_I}\nabla_i^2 \tag{1.3}$$

$$\begin{aligned}\hat{V} &= \hat{V_{Ne}} + \hat{V_{ee}} + \hat{V_{NN}} \\ &= -\sum_{I,noyaux}^{N}\sum_{i,e^-}^{n}\frac{e^2 Z_I}{4\pi\mathcal{E}_0 r_{iI}} + \sum_{i,e^-}^{n}\sum_{j>i}\frac{e^2}{4\pi\mathcal{E}_0 r_{ij}} + \sum_{I,noyaux}^{N}\sum_{J>I}\frac{e^2 Z_I Z_J}{4\pi\mathcal{E}_0 r_{IJ}}\end{aligned} \tag{1.4}$$

$\hat{T_e}$ represents the electronic kinetic energy and $\hat{T_N}$ the nuclear kinetic energy. $\hat{V_{Ne}}$, $\hat{V_{ee}}$ and $\hat{V_{NN}}$ represent the nuclei-electron, electron-electron and nuclei-nuclei coulombic electrostatic interaction respectively.

I and J run over the N nuclei, i and j run over the n electrons of the system. m_e is the mass of the electron, M_I is the mass of the nucleus I, $\hbar$ is the Planck constant divided by 2π, e is the charge of the electron, $\mathcal{E}_0$ is the electric constant, Z_I the charge of the nucleus I and r_{ab} is the distance between particles a and b. ∇_i^2 is the Laplacian operator, defined as a sum of differential operators (in cartesian coordinates).

$$\nabla_i^2 = \frac{\partial^2}{\partial x_i^2} + \frac{\partial^2}{\partial y_i^2} + \frac{\partial^2}{\partial z_i^2} \tag{1.5}$$

In atomic units, $m_e = 1$, $\hbar = 1$, $e = 1$, $\frac{1}{4\pi\varepsilon_0} = 1$, and the Hamiltonian of the system can be written:

$$\hat{H} = -\frac{1}{2}\sum_{i,e^-}^{n}\nabla_i^2 - \frac{1}{2}\sum_{I,noyaux}^{N}\frac{1}{M_I}\nabla_I^2 - \sum_{I,noyaux}^{N}\sum_{i,e^-}^{n}\frac{Z_I}{r_{iI}} + \sum_{i,e^-}^{n}\sum_{i<j}\frac{1}{r_{ij}} + \sum_{I,noyaux}^{N}\sum_{I<J}\frac{Z_I Z_J}{r_{IJ}} \quad (1.6)$$

The Born-Oppenheimer approximation

In order to simplify the Hamiltonian, the coupling between the movement of the electrons and the nuclei can be neglected. The electrons can be considered as instantaneously moving in the field generated by fixed nuclei. This approximation is known as the Born-Oppenheimer approximation.

Indeed, under typical physical conditions, the nuclei of a molecular system are moving much slower than the electrons, since protons and neutrons are about 1800 times heavier than electrons. The nuclear kinetic energy $\widehat{T_N}$ can be neglected and $\widehat{V_{NN}}$, the nuclei-nuclei coulombic electrostatic interaction can be considered constant, which leads to a simplification of the total Hamiltonian:

$$\hat{H} = \widehat{H_{el}} + \widehat{V_{NN}} \quad (1.7)$$

with:

$$\widehat{H_{el}} = \widehat{T_e} + \widehat{V_{Ne}} + \widehat{V_{ee}} \quad (1.8)$$

The electronic wave-function of the system can thus be derived as:

$$\widehat{H_{el}}|\Psi_{el}\rangle = E_{el}\,|\Psi_{el}\rangle \quad (1.9)$$

While the total energy of the system reads:

$$E = E_{el} + \sum_{I,noyaux}^{A}\sum_{I<J}\frac{Z_I Z_J}{r_{IJ}} \quad (1.10)$$

By analyzing more carefully the electronic Hamiltonian, it can be decomposed into mono and bielectronic terms, that is:

$$\widehat{H_{el}} = \sum_{i,e^-}^{n} \widehat{h_1}(i) + \sum_{i,e^-}^{n} \sum_{i<j} \widehat{h_2}(i,j) \tag{1.11}$$

The monoelectronic operators ($\widehat{h_1}$) collect the kinetic energy and the interactions of each electron with the nuclei.

$$\widehat{h_1} = -\frac{1}{2}\nabla_i^2 - \sum_{I,noyaux}^{A} \frac{Z_I}{r_{iI}} \tag{1.12}$$

While the bielectronic term ($\widehat{h_2}$) represents the electron-electron coulombic repulsion.

$$\widehat{h_2} = \frac{1}{r_{ij}} \tag{1.13}$$

For polyelectronic systems, because of the two-electron interactions, the Schrödinger equation cannot be solved exactly. Approximations have been developed to solve this problem.

Variational principle

The variational principle allows to systematically approach the wave-function of the ground state Ψ_0, which is the state that delivers the lowest energy E_0. It states that, for a normalized wave-function, the computed energy will be an upper bond to the true energy.

$$\langle \Psi_{trial} | \widehat{H} | \Psi_{trial} \rangle = E_{trial} \geq E_0 = \langle \Psi_0 | \widehat{H} | \Psi_0 \rangle \tag{1.14}$$

The equality holds if and only if $\Psi_{trial} = \Psi_0$. In order to find the ground state energy and the ground state wave-function, the functional $E[\Psi]$ has to be minimized by searching through all n-electron suitable wave-functions:

$$E_0 = \min_{\Psi \to n} E[\Psi] = \min_{\Psi \to n} \langle \Psi | \widehat{H} | \Psi \rangle \tag{1.15}$$

$\Psi \to n$ means that Ψ is an allowed n-electrons wave-function. This principle can be applied to a set of chosen possible functions, and the result obtained will be the best approximation to the exact wave-function that can be obtained from this particular set.

The basis set

The ensemble of functions that will be combined to represent the n electron wave-function is called a basis set. The many electrons wave-function can be approximated using mono-electronic wave-functions. The mono-electronic functions $\chi_i(x)$ are called molecular spin orbitals and are composed of a spatial orbital $\phi_i(r)$ and of a spin function $\sigma(s)$ with the following relationship:

$$\chi_i(x) = \phi_i(r)\sigma(s), \quad \sigma = \alpha, \beta \tag{1.16}$$

It means that for each spatial orbital, two spin orbitals can be obtained, $\phi_i(r)\alpha(s)$ and $\phi_i(r)\beta(s)$. x represents all the coordinates of the electron: the spatial coordinates r and the spin coordinate s. The spin functions have the property of being orthonormal.

$$\begin{aligned} \int \alpha^*(s)\alpha(s)ds &= \int \beta^*(s)\beta(s)ds = 1 \\ \int \alpha^*(s)\beta(s)ds &= \int \beta^*(s)\alpha(s)ds = 0 \end{aligned} \tag{1.17}$$

The spin orbitals themselves are usually chosen to be orthonormal as well.

$$\int \chi_i^*(x)\chi_j(x)dx = \delta_{ij} \tag{1.18}$$

where δ_{ij} is the Kronecker symbol which equals 1 if $i = j$ and 0 otherwise.

In the LCAO (Linear Combination of Atomic Orbitals) approach, the spatial component $\phi(r)$ of these molecular spin orbitals is expressed as a linear combination of basis functions $\varphi_v(r)$, called atomic orbitals.

$$\phi_i(r) = \sum_{v=1}^{K} c_{vi}\varphi_v(r) \tag{1.19}$$

The c_{vi} coefficients are the coefficients for the development of the molecular orbital $\phi_i(r)$ on the basis functions $\varphi_v(r)$.

The molecular orbital is represented by a finite number K of basis functions. This is an approximation since an accurate representation of this molecular orbital would require a complete basis, with an infinite number of basis functions. The mathematical expression of the basis functions has to account for the physics of the system, but also to be practical when it comes to the calculations of the required integrals.

Exponential functions, with a radial decay in e^{-r} are good candidates: they converge to zero as the distance between the electron and the nucleus increases, and they are known to be exact solutions for the hydrogenoic atoms. These are the Slater functions or Slater Type Orbitals (STO), where ζ, n, l and m are parameters:

$$\varphi_v(r,\theta,\varphi) = NY_{l,m}(\theta,\varphi)r^{n-1}e^{-\zeta r} \tag{1.20}$$

Unfortunately, they turn out to be computationally challenging for practical application. Gaussian functions, with a radial decay in e^{-r^2}, describe less accurately the electronic structure. Indeed, they have no cusp at the nucleus and their reduction in amplitude with distance is too rapid. Nevertheless, they are much easier to handle computationally. These are the Gaussian Type Orbitals (GTO):

$$\varphi_v(r,\theta,\varphi) = NY_{l,m}(\theta,\varphi)r^{2n-2-l}e^{-\zeta r^2} \tag{1.21}$$

To have a better description of the electronic behavior near the nucleus using GTOs, the behavior of the Slater functions can be reproduced using a linear combination of GTOs.

A basis function composed of a linear combination of GTOs is called a “contracted” basis function. The individual GTOs are called “primitives”.

To sum up, the wave-function is represented using mono-electronic molecular spin orbitals. Their spatial components are expressed as linear combinations of basis functions centered on atoms called atomic orbitals. These latter are a linear combination of GTOs. The mathematical expression of the wave-function itself, as a function of the molecular spin orbitals, still remains to be defined.

The Hartree-Fock approach

In the case of the Hartree-Fock approximation, the complicated many-electron wave-function is approached by an antisymmetrized product of n one-electron wave-functions $\chi_i(x_i)$, referred to as the Slater determinant Φ_{SD}.

$$\Psi_0 \approx \Phi_{SD} = \frac{1}{\sqrt{n!}} \det \begin{pmatrix} \chi_1(x_1) & \chi_2(x_1) & \dots & \chi_n(x_1) \\ \chi_1(x_2) & \chi_2(x_2) & \dots & \chi_n(x_2) \\ \vdots & \vdots & & \vdots \\ \chi_1(x_n) & \chi_2(x_n) & \dots & \chi_n(x_n) \end{pmatrix} \quad (1.22)$$

The prefactor $\frac{1}{\sqrt{n!}}$ is a normalization factor. This determinant is antisymmetric since it changes sign when exchanging two rows or two columns. This is in agreement with the fermion nature of the electrons. The Pauli principle is also respected: two electron cannot occupy the same spin orbital. It would mean having two columns identical, and the determinant would equal zero.

With this expression in hand for the wave-function, solving the electronic Schrödinger equation reduces to find the Slater determinant yielding the lowest energy by varying the spin orbitals χ_i under the constraint that they remain orthonormal.

$$E_{HF} = \min_{\Psi_{SD} \to n} E[\phi_{SD}] \quad (1.23)$$

The wave-function is optimized variationally by using the molecular orbital coefficients as variational parameters. The variational freedom arises from the choice of the orbitals.

The Hartree-Fock method was the first *ab initio* method to be developed. The restricted Hartree-Fock (RHF) method is used for systems in which a pair of electrons with opposed spins occupies the same spatial orbital. Using the electronic Hamiltonian defined in equation (1.11) on the Slater determinant of equation (1.22), the HF energy is given by:

$$E_{el\,HF}[\phi_{SD}] = \int \phi_{SD}^* \widehat{H_{el}} \phi_{SD}\, dx \quad (1.24)$$

$$= \sum_{i=1}^{n} \int \chi_i^*(x) \left[-\frac{1}{2} \nabla_i^2 - \sum_{I,noyaux}^{N} \frac{Z_I}{r_{iI}} \right] \chi_i(x)\, dx$$
$$+ \frac{1}{2} \sum_{i=1}^{n} \sum_{j=1}^{n} [\int \int \chi_i^*(x_1) \chi_j^*(x_2) \frac{1}{r_{12}} \chi_i(x_1) \chi_j(x_2) dx_1 dx_2$$
$$- \int \int \chi_i^*(x_1) \chi_j^*(x_2) \frac{1}{r_{12}} \chi_i(x_2) \chi_j(x_1) dx_1 dx_2]$$

The first term is the one-electron energy. The second term is the Coulomb integral, the classical repulsion between the charge of electron i and electron j. The third term is the exchange integral, resulting from the antisymmetric nature of the Slater determinant. The two latter represent the two-electron energy.

In a shorter notation:

$$E_{el\,HF} = \sum_{i=1}^{n} h_{ii} + \frac{1}{2} \sum_{i=1}^{n} \sum_{j=1}^{n} [J_{ij} - K_{ij}] \tag{1.25}$$

One can notice that $J_{ii} = K_{ii}$, which compensates the Coulombic interaction of an electron with itself. From this expression, the one-electron Fock operator can be introduced:

$$\hat{f}_i = -\frac{1}{2} \nabla_i^2 - \sum_{I}^{N} \frac{Z_I}{r_{iI}} + V_{HF}(i) \tag{1.26}$$

The condition of minimal energy for the spin orbitals results in the Hartree-Fock equations:

$$\hat{f}_i \chi_i = \varepsilon_i \chi_i \tag{1.27}$$

The ε_i have the physical interpretation of the orbital energies. $V_{HF}(i)$ is the Hartree-Fock potential. It is the average repulsive potential experienced by the electron i due to the other $n-1$ electrons. The electron-electron repulsion is taken into account in an average way (mean field approximation) and instantaneous electron-electron interactions are thus neglected if one excepts the exchange interaction term. It has the following expression:

$$V_{HF}(x_1) = \sum_{j=1}^{n} (J_j(x_1) - K_j(x_1)) \tag{1.28}$$

The Coulomb operator J is defined as:

$$J_j(x_1) = \int \chi_j^*(x_2)\frac{1}{r_{12}}\chi_j(x_2)dx_2 \tag{1.29}$$

It represents the potential that an electron at position x_1 experiences due to the average charge distribution of another electron in the spin orbital χ_j.

The exchange operator K has no classical interpretation and can only be defined through its effect on a spin orbital:

$$K_j(x_1)\chi_i(x_1) = \int \chi_j^*(x_2)\frac{1}{r_{12}}\chi_i(x_2)dx_2\chi_j(x_1) \tag{1.30}$$

It leads to an exchange of the variables in the two spin orbitals. As a consequence, this exchange contribution exists only for electrons of the same spin because the $\frac{1}{r_{12}}$ operator is spin independent and the spin functions are orthonormal.

Using the LCAO approximation, the n Hartree-Fock equations (1.27) can be written as:

$$\hat{f}_i\sum_{v=1}^{K} c_{vi}\chi_v = \varepsilon_i\sum_{v=1}^{K} c_{vi}\chi_v \tag{1.31}$$

By multiplying from the left by a specific basis function and integrating, one can write under matrix notation the Roothaan-Hall equations:

$$\begin{gathered} FC = SC\varepsilon \\ F_{\mu v} = \langle\chi_\mu|\hat{F}|\chi_v\rangle \\ S_{\mu v} = \langle\chi_\mu|\chi_v\rangle \end{gathered} \tag{1.32}$$

The F matrix contains the Fock matrix elements, the S matrix contains the overlap elements between basis functions. The C matrix is the matrix of the $c_{\mu v}$ coefficients.

The Fock operator depends on the spin orbitals through the HF potential. For this reason, this set of equations has to be solved iteratively. This technique is called the self-consistent field (SCF) procedure.

Starting from an initial geometry, a guess set of orbitals is chosen. With this set, the HF equations are solved, providing a new set of orbitals and an estimate of the HF energy of the system. This new set of orbitals is used in the next iteration, and a new value for the energy is obtained. These two parameters are controlled and iterations are performed until the convergence criteria are reached.

The restricted Hartree-Fock method described up to now works for closed-shell systems, that is the ones possessing an even number of all paired electrons. In this case, the spatial orbitals are all doubly occupied: two spin orbitals share the same spatial orbital, and have opposite spin functions. They have thus the same orbital energy.

For open-shell systems, in which not all the electrons are paired in one spatial orbital, two methods can be used: the restricted open shell Hartree-Fock (ROHF) method or the unrestricted Hartree-Fock (UHF) method.

The UHF approach allows for a more flexible description of open shell systems. Each spin orbital is allowed to have its own spatial part. The α and β orbitals experience different potentials and can have different orbital energies. The major disadvantage of this method is that the wave-function is no longer an eigenfunction of the total spin operator. This can result in a contamination of the determinant by functions corresponding to states of higher multiplicity, and give less physically meaningful results.

The limits of Hartree-Fock

The HF wave-function is not an exact wave-function, since it consists of a single Slater determinant, describing n electrons in a mean field. Each electron experiences an average field due to the presence of the n-1 other electrons. Therefore, the electron correlation is an electron-electron energy contribution missing in a HF calculation.

$$E_{corr} = E_0 - E_{HF} \tag{1.33}$$

The correlation energy is traditionally decomposed in two parts: the so-called *dynamical correlation*, due to the instantaneous interactions between electrons of opposite spins, and the *non-dynamical* or *static correlation*, due to the possible existence of different configurations close in energy, that a single determinant is not able to represent.

To deal with the electron correlation problem, a large variety of methods has been developed during the years. The most computationally affordable approach is the Møller Plesset perturbation theory. This approach has been used in our work and it will be described in the next section.

The Møller Plesset perturbation theory

The Møller Plesset (MP) method is based on the perturbation theory. The main idea of the perturbation theory is that if the Hamiltonian describing our system is very close to one that can be solved (ie for which solutions are known), then the energy associated to the true Hamiltonian can be computed from the wave-function of the known unperturbed system.

In a more formal way, a given Hamiltonian for which the solution is unknown is separated into two parts: a reference Hamiltonian for which solutions are known (H^0), while the remaining interactions, which can be considered as a perturbation, are collected together (H'). λ is a dimensionless parameter, ranging between 0 and 1, allowing to transform the reference Hamiltonian into the real one.

$$H = H^0 + \lambda H' \tag{1.34}$$

Defining E_k as the eigenvalue associated to Ψ_k, which is the k-state eigenfunction for H:

$$H\Psi_k = E_k\Psi_k \tag{1.35}$$

And knowing that the solutions for the reference Hamiltonian are $E_k^{(0)}$ and $\Psi_k^{(0)}$:

$$H^0\Psi_k^{(0)} = E_k^{(0)}\Psi_k^{(0)} \tag{1.36}$$

It can be demonstrated by making use of a Taylor expansion in power of the perturbation parameter that:

$$\lambda^n\colon H^0\Psi_k^{(n)} + H'\Psi_k^{(n-1)} = \sum_{i=0}^{n} E_k^{(i)}\,\Psi_k^{(i-1)} \tag{1.37}$$

In MP perturbation theory, the unperturbed Hamiltonian is chosen as a sum of Fock operators defined as before ($\widehat{f_i} = -\frac{1}{2}\nabla_i^2 - \sum_I^A \frac{Z_I}{r_{iI}} + V_{HF}(i)$).

$$H^0 = \sum_{i=1}^{K} f_i \tag{1.38}$$

Where K is the number of basis functions. Ψ_0 is the ground state eigenfunction for H, E_0 is the ground state eigenvalue for H. $\Psi_0^{(0)}$ is the ground state eigenfunction for H^0, $E_0^{(0)}$ is the ground state eigenvalue for H^0.

$\Psi_0^{(0)}$ is taken as the HF wave-function, which is a Slater determinant formed of the occupied orbitals. The eigenvalue of H^0 when applied to the HF wave-function is the sum of the occupied orbital energies (eigenvalues of f_i):

$$H^0\Psi_0^{(0)} = \sum_{i=1}^{occ} \varepsilon_i \Psi_0^{(0)} \tag{1.39}$$

The MP zeroth order wave-function $\Psi_0^{(0)}$ is the HF determinant and the zeroth order energy $E_0^{(0)}$ is just a sum of molecular orbitals energies. The orbital energy is the energy of an electron in the field of all the nuclei and mean field all the other electrons. For this reason, the sum of the orbital energies counts the electron-electron repulsion twice.

This will be corrected with the perturbation Hamiltonian, H', which allows to correctly introduce the electron-electron repulsion.

$$H' = \sum_{i}^{occ} \sum_{j>i}^{occ} \frac{1}{r_{ij}} - \sum_{i}^{occ}\sum_{j}^{occ}\left[J_{ij} - \frac{1}{2}\,K_{ij}\right] \tag{1.40}$$

The first term is the proper way to compute electron repulsion, and the second one arises from computing it by summing over the Fock operators. J and K are the Coulomb and exchange operators.

This way, the energy corrected at the first order by operating on the HF wave-function is

$$\begin{aligned} E_0^{(0)} + E_0^{(1)} &= \left\langle \Psi_0^{(0)} \middle| H_0 \middle| \Psi_0^{(0)} \right\rangle + \left\langle \Psi_0^{(0)} \middle| H' \middle| \Psi_0^{(0)} \right\rangle \\ E_0^{(0)} + E_0^{(1)} &= \left\langle \Psi_0^{(0)} \middle| H_0 + H' \middle| \Psi_0^{(0)} \right\rangle \\ E_0^{(0)} + E_0^{(1)} &= \left\langle \Psi_0^{(0)} \middle| H \middle| \Psi_0^{(0)} \right\rangle \\ E_0^{(0)} + E_0^{(1)} &= E_{HF} \end{aligned} \tag{1.41}$$

The MP first order corrected energy $E_0^{(0)} + E_0^{(1)}$is the Hartree-Fock energy. To obtain an estimation of the correlation energy, one thus has to go at least up to the second order correction. To achieve that, the first order wave-function is needed. This function can be expressed as a linear combination of the complete set of eigenfunctions of H^0, using the excited Slater determinants, which means for the ground state:

$$\Psi_0^{(1)} = \sum_{i>0} c_i \Psi_i^{(0)} \tag{1.42}$$

Using this formula and the previous equations, the expression of the second order energy correction can be obtained:

$$E_0^{(2)} = \sum_{j>0} \frac{\left| \left\langle \Psi_j^{(0)} \middle| H \middle| \Psi_0^{(0)} \right\rangle \right|^2}{E_0^{(0)} - E_j^{(0)}} \tag{1.43}$$

According to the Slater-Condon rules, only singly and doubly excited determinants have to be considered. Moreover, according to the Brillouin's theorem, the integrals involving the singly excited determinants will all be zero, which leaves only doubly excited determinants. The second order MP energy is then:

$$E_0^{(2)} = \sum_{i}^{occ} \sum_{j>i}^{occ} \sum_{a}^{virt} \sum_{b>a}^{virt} \frac{[(ij|ab) - (ia|jb)]^2}{\varepsilon_i + \varepsilon_j - \varepsilon_a - \varepsilon_b} \qquad (1.44)$$

The sum of $E_0^{(0)}$, $E_0^{(1)}$ and $E_0^{(2)}$ defines the MP2 energy. The MP2 theory is a method that allows to take into account a part of the electron correlation in a computationally-affordable way.

The Density Functional Theory

DFT is today probably the most used quantum approach. DFT relies on the use of the electronic density as basic variable to express the total energy and properties of a given system.

The electronic density can be expressed as a function of the wave-function as:

$$\rho(r) = N \int \dots \int |\Psi(x_1, x_2 \dots x_n)|^2 \, dx_1 dx_2 \dots dx_n \qquad (1.45)$$

Where each electron is described by $x_i = (r_i, s_i)$, spatial and spin coordinates. The n electron density of a system is an observable and represents the probability to find an electron in a volume dr with any spin, the $n - 1$ other electrons being at any position in space with any spin.

The basic idea of DFT is that the exact energy of the system is a functional of the electronic density only:

$$E_0 = E[\rho] \qquad (1.46)$$

Historically, the first model of DFT dates back to 1927, even before a formal proof of the energy functional dependence was given.[11,12] It is the Thomas-Fermi model, proposed for a uniform gas of electrons. Indeed, it was only in 1964[13] that the formal proof of DFT was derived by Hohenberg and Kohn.

The *first Hohenberg and Kohn theorem* states that all properties of the many-body system are determined by the ground state density ρ_0. ρ_0 defines the external potential V_{Ne} (except for a constant) and thus all properties. Knowing V_{Ne} allows to express the Hamiltonian

and to solve the system. Each property is a functional of the ground state density ρ_0 which is written as $f[\rho_0]$.

The *second Hohenberg and Kohn theorem* states that the ground state density is a variational quantity. The electronic energy is minimal if and only if the electronic density is the one of the ground state. Like for wave-function methods, linear variation techniques can be employed to optimize the density.

The total energy can be expressed as sum of three density functionals: a kinetic term (T_e), a term of nucleus-electron coulombic interaction (V_{Ne}), and a term of electron-electron coulombic interaction (V_{ee}).

$$E[\rho] = T_e[\rho] + V_{Ne}[\rho] + V_{ee}[\rho] \tag{1.47}$$

According to the variational principle:

$$E_0 = \min_{\rho \to n} \min_{\Psi \to \rho} \langle \Psi | \widehat{T_e} + \widehat{V_{Ne}} + \widehat{V_{ee}} | \Psi \rangle \tag{1.48}$$

In DFT calculations, variational optimization proceeds with a double minimization of the energy, on all the electronic densities with n electrons, and on all the wave-functions for a given density. There is a unique match between the electronic density and the wave-function of the system.

Unfortunately, the first Hohenberg and Kohn theorem provides a proof of existence but does not give any hint concerning the form of the exact energy functional.

The exact expression of the first term $T_e[\rho]$ is difficult to determine and is the main problem behind initial DFT formalisms. On the other hand, the second term $V_{Ne}[\rho]$ can be easily and exactly calculated. A part of the electron-electron interaction $V_{ee}[\rho]$ can be represented by the energy of repulsion between two charges $J[\rho]$.

$$J[\rho] = \iint \frac{\rho(r_1)\rho(r_2)dV_1dV_2}{|r_1 - r_2|} \tag{1.49}$$

This interaction does not take into account the correlation (the fact that the movement of two electrons is not independent). The electron has a presence density defined in any point

of the space including r_1 and r_2 meaning that it can interact with itself (self-interaction). It does not take into account the electronic exchange interaction, related to the spin of the electron, which specifies that two electrons with an identical spin cannot be located in the same position. This can be represented by a second non classical term $V_{nc}[\rho]$.

$$V_{ee}[\rho] = J[\rho] + V_{nc}[\rho] \tag{1.50}$$

Therefore, the formulation proposed by Hohenberg and Kohn is exact but does not provide any real solution.

Kohn and Sham proposed in 1965 to solve this problem by replacing the real system of interacting electrons by a virtual system of non-interacting electrons having an overall ground-state density equal to the density of the real system. This allows to separate the kinetic energy of the electrons T_e in a term that can be calculated exactly, T_{KS}, that considers the electrons as non interacting particles, and a correction calculated with an approximate functional, accounting for the electron-electron interaction.

Equations (1.47) and (1.50) become:

$$E[\rho] = T_{KS}[\rho] + (T_e[\rho] - T_{KS}[\rho]) + V_{Ne}[\rho] + J[\rho] + V_{nc}[\rho] \tag{1.51}$$

Which can be simplified under the form:

$$E[\rho] = T_{KS}[\rho] + V_{Ne}[\rho] + J[\rho] + E_{XC}[\rho] \tag{1.52}$$

Where $E_{XC}[\rho]$ is called the exchange-correlation functional. It is the only unknown entity and will have to be approximated as well as possible. It expresses the correction to the kinetic energy for the existing interaction between the electrons, and all the non-classical corrections to the electron-electron repulsion term.

With an orbital formulation, the ground state energy of a system with n electrons and N nuclei can be written:

$$E[\rho] = -\frac{1}{2}\sum_{i=1}^{n}\int \Psi_i^*(r_1)\nabla_i^2\Psi_i(r_1)dr_1 - \sum_{I=1}^{N}\int \frac{Z_I}{r_{Ii}}\rho(r_1)dr_1 + \frac{1}{2}\int\int \frac{\rho(r_1)\rho(r_2)}{r_{12}}dr_1dr_2 + E_{XC}[\rho] \quad (1.53)$$

The Ψ_i are the Kohn-Sham orbitals. The first term is the kinetic energy of the non-interacting electrons. The second term represents the nuclear-electron interactions. The third term is the Coulombic repulsions between the total charge distribution at r_1 and r_2. The last term is the exchange correlation term. The description of this last term is the current challenge in DFT developments.

The ground-state electron density $\rho(r)$ can be written making use of Kohn-Sham orbitals:

$$\rho(r) = \sum_{i=1}^{n}|\Psi_i(r)|^2 \quad (1.54)$$

The Kohn-Sham orbitals are determined by solving the Kohn-Sham equations:

$$\hat{h}_{i\,KS}\Psi_i(r) = \varepsilon_i\Psi_i(r) \quad (1.55)$$

$\hat{h}_{i\,KS}$ is the Kohn-Sham monoelectronic operator and ε_i is the Kohn-Sham orbital energy associated. The Kohn-Sham Hamiltonian can be written as:

$$\hat{h}_{i\,KS} = -\frac{1}{2}\nabla_i^2 - \sum_{I=1}^{N}\frac{Z_I}{r_{Ii}} + \int \frac{\rho(r_2)}{r_{12}}dr_2 + V_{XC}(r_1) \quad (1.56)$$

V_{XC} is the functional derivative of the exchange-correlation energy:

$$V_{XC} = \frac{\partial E_{XC}[\rho]}{\partial \rho} \quad (1.57)$$

The Kohn-Sham equations are solved in a self-consistent fashion. The starting point is a guess charge density ρ, along with a chosen approximate form of the functional to describe the dependence of E_{XC} on the electron density that allows to calculate V_{XC} with equation (1.57).

The Kohn-Sham equations (1.55) can then be solved, giving an initial set of Kohn-Sham orbitals. This set is used to calculate an improved density from equation (1.54). This entire procedure is then repeated until the density and the exchange-correlation energy satisfy a given convergence criterion. At this point, the electronic energy is calculated from equation (1.53).

There is a strong analogy between the Kohn-Sham method and the Hartree-Fock method presented earlier in terms of resolution of the equations and description of the orbitals. Both methods involve a self-consistent procedure. Like for the Hartree-Fock method, the Kohn-Sham orbitals are expressed in terms of a set of basis functions, and solving the Kohn-Sham equations is determining the coefficients of the linear combination of basis functions.

The exchange-correlation energy

There is no universal analytical form for the exchange-correlation functional $E_{XC}[\rho]$. The expression will depend on the system studied.

The dependence of $E_{XC}[\rho]$ on the electronic density can be expressed as an interaction between an energy density depending on ρ, which is the exchange-correlation energy per particle of a uniform electron gas, and the electronic density itself, the probability that an electron is at this position:

$$E_{XC}[\rho] = \int \rho \, \varepsilon_{XC}[\rho] \, dr \qquad (1.58)$$

It is generally divided into two separate terms, an exchange term E_X and a correlation term E_C:

$$E_{XC}[\rho] = E_X[\rho] + E_C[\rho] \qquad (1.59)$$

The main source of inaccuracy in DFT is a result of the approximate nature of the exchange-correlation functional. The development of new functionals aims at getting as close as possible to the chemical accuracy.

The simplest way to evaluate the exchange-correlation energy is the *Local Density Approximation* (LDA) which locally considers the electronic density as a uniform gas of

electrons. The advantage is that this is the only system for which there are excellent interpolations of the exchange and correlation energies.

The exchange and correlation energy can be calculated using:

$$E_{XC}^{LDA}[\rho] = \int \rho\, \varepsilon_{XC}[\rho]\, dr \qquad (1.60)$$

In an unrestricted approach, if the system has a different number of electrons α and electrons β, the density is separated in two distinct parts. This is the Local Spin-Density Approximation:

$$\rho(r) = \rho_\alpha(r) + \rho_\beta(r) \qquad (1.61)$$

In most systems, the electronic repartition is far from being locally uniform, and the LDA leads to a very bad description of the bonding energies, among others. A more accurate approach it the *Generalized Gradient Approximation* (GGA) which takes into accounts the spatial variations of the electronic density with the introduction of the first spatial derivative of the density ($\nabla\rho$) as variable in the exchange correlation functional:

$$E_{XC}^{GGA}[\rho] = \int \rho\, \varepsilon_{XC}[\rho, \nabla\rho]\, dr \qquad (1.62)$$

Both LDA and GGA do not properly consider the self-interaction phenomenon, and the long range correlation effects.

The next improvement for the accuracy of the functionals is the introduction on non-local terms: in meta-GGA functionals, the energy density also depends on the Laplacian of the electronic density.

$$E_{XC}^{meta-GGA}[\rho] = \int \rho\, \varepsilon_{XC}[\rho, \nabla\rho, \nabla^2\rho]\, dr \qquad (1.63)$$

Hybrid functionals, on the other hand, describe part of the exchange term with the exchange energy computed in a HF fashion. Indeed, HF theory treats the exchange interaction exactly though it does not take into account the electronic correlation. In such a way a global hybrid general form reads:

$$E_{XC}^{hybrid}[\rho] = E_{XC}^{KS}[\rho] + aE_X^{HF}[\rho] + (1-a)E_X^{DFT}[\rho] \qquad (1.64)$$

Contrary to global hybrids, in range-separated functionals, the percentage of HF exchange introduced depends explicitly on the interelectronic distance, giving rise to functional forms slightly more complex than that reported in equation (1.64). The choice of functional strongly depends on the system and property considered and will be detailed for each study of this thesis. The functionals used and their characteristics are given in Table 1.1.

Table 1.1 – Functionals used and their characteristics

Functional	Family	Characteristics
BLYP[14,15]	GGA	
PBE0[16]	Hybrid GGA	25 % HF exchange
B3LYP[14,15,17]	Hybrid GGA	20 % HF exchange
CAM-B3LYP[18]	Hybrid GGA	Range separated, 19 % HF exchange at short range, 65 % HF exchange at long-range
MPW91[19]	Hybrid GGA	Improved long-range behavior
M06[20]	Meta hybrid GGA	27 % HF exchange
M062X[20]	Meta hybrid GGA	54 % HF exchange

Selected tools and methods used in this thesis

All the calculations were performed using the Gaussian09 software (Revision A.02).[21]

Choice of the basis set

First rows atoms

In this thesis, for all first rows atoms, we use a Pople triple zeta basis set 6-311+G(d,p).[22,23] Core orbitals are described as a contraction of six primitives GTO while valence orbitals are described using three (which explains the name *triple zeta*) contracted orbitals, composed of three, one and one primitives respectively. For a better description of the system, polarization and diffuse functions are added.

Polarization functions allow a better description of inter and intra molecular interactions, such as hydrogen bonding. These are orbitals with a secondary quantum number

superior to the valence number (atomic orbital p for the hydrogen, atomic orbital d for the second row elements). The level of polarization used in this thesis adds these polarization orbitals on all atoms including hydrogen. This is indicated by the "(d,p)" notation.

A basis set that describes well a neutral molecule will describe equally well its cation, but not necessarily its anion (because an electron is added and not removed). Diffuse orbitals have a broader spatial extension and are able to improve the description of the anions. The basis set chosen in this thesis adds these orbitals on all atoms but hydrogen. This is indicated by the "*" notation.

Copper

For the copper we use the Los-Alamos double zeta basis set Lanld2z and its associated pseudo potential.[24–26] The pseudo potential approximation separates the description of the core electrons from the description of the valence electrons. Indeed, for heavy elements, which have a large number of core electrons, the valence electrons can be considered as the only responsible for the reactivity of the molecules and complexes that are studied. The core electrons are not described as particles, but the valence electrons evolve in an average electrostatic potential created by the core electrons.

Basis set superposition error

The basis set superposition error (BSSE) problem arises when the interaction of two distinct chemical species A and A' is computed, where A and A' are not described by the same basis set. We consider A, described by the basis set B and A', described by the basis set B'.

When A and A' are separated, their energy is:

$$E\{A + A'\} = E_B\{A\} + E_{B'}\{A'\} \tag{1.65}$$

When A and A' are interacting, for example in a transition state, both species are computed in the same calculation. A can borrow basis functions from A', and A' can borrow basis functions from A. The energy is in fact calculated in a larger base: A' is computed in a base B_+, and A' is computed in a base B'_+.

$$E\{[AA']\} = E_{B_+}\{A\ in\ [AA']\} + E_{B'_+}\{A' in [AA']\} \qquad (1.66)$$

The bigger the basis, the lower the energy (and the closest to the energy of the real system). There is for this reason an underestimation of the energy of the system $[AA']$. The energy obtained is in fact:

$$E\{[AA']\} = E_B\{A\ in\ [AA']\} + E_{B'}\{A' in [AA']\} - E_{BSSE} \qquad (1.67)$$

In this thesis, to evaluate the BSSE energy we use the Counterpoise algorithm in Gaussian09.[27–29] The energy of each part of the interacting system is calculated in the "non-polluted" base, and a value for E_{BSSE} is obtained.

Solvent description

The solvent can be described using different methods. In this work, we used an implicit description of the solvent: the Polarized Continuum Model (PCM).[30] The solvent is described as a continuous medium acting on the solute. Punctual charges surround the Van der Waals cavity of the molecules considered.

The PCM model allows to take into account both electrostatic effects (Keesom forces) and dispersion-repulsion effects (Debye and London forces). The free energy of solvation is calculated as follows:

$$G_{solvation} = G_{electrostatic} + G_{dispersion-repulsion} + G_{cavitation} \qquad (1.68)$$

Solvation effects are particularly important when a reaction involves charge separation, which is very disfavored in vacuum, whereas ions are stabilized in polar solvents. In some cases that are specified in this work, solvent molecules were also added explicitly in order to take into account direct solute-solvent interaction that cannot be described using a continuum model.

Reaction pathway

The elucidation of a reaction path is the computation of keypoints on a potential energy surface. Two families of points are considered:

- the local minima which are stable states and can be reactive species, intermediates or products

- the local maxima, linking these minima, which are transition states

For the research of both local extrema, the structure found must be related to a first order derivative of the energy equal to zero relative to all geometry coordinates. The difference between a stable intermediate and a transition state relies in the second order derivatives. If these are all positive, the point is a local minimum (potential well), if one of them is negative (saddle point), it is a first order local maximum. Frequency calculations on optimized structures allow to calculate the second order derivatives of the energy. For the transition states, in order to check that the structure found really links the two considered intermediates, an Intrinsic Reaction Coordinate (IRC) calculation is performed.[31,32] With such a procedure, following the direction of the negative derivative, forward and backward, step by step, the convergence to the intermediates is validated.

Calculated energies and entropy considerations

The Gaussian09 software gives access to the usual thermodynamic functions. In this thesis, depending on the system, we report values for the total energy (E), which includes both electronic energy and the contributions from the repulsions of the nuclei, and values for the enthalpy (H) and the Gibbs free energy (G = H-TS). These are by default calculated considering the system as an ideal gas.

Unser this assumption, the free energy is evaluated as the one of an ideal gas, which introduces major errors in the evaluation of the entropic contribution in condensed phases such as solution.

Indeed, it does not take into account the reorganization of the solvation layer, or the electronic interaction between two reactants getting closer. The accurate estimation of the entropy is particularly problematic when considering association and dissociation reactions. The PCM model also does not take into account this type of entropic effects. Because all the reactions studied are in solution, this is particularly problematic. For these reasons, in this thesis, we chose to discuss mainly enthalpies.

Several options exist to answer the problem of the accurate evaluation of the entropy. Maseras and coworkers[33] suggest to perform PCM single-point calculations on gas-phase optimized geometries. To this energy obtained in solution, the entropic correction from the gas phase was added. This method overestimates the entropy, which is greater in gas phase than in solution.

$$\Delta G_{solv} = \Delta E_{solv} + (\Delta G_{gas} - \Delta E_{SCF,gas}) \quad (1.69)$$

Other propositions were done, for example by Sakaki and coworkers who considered that the translational and rotational contributions of entropy were greatly diminished in solution. They used only the vibrational term of entropy as calculated in gas phase.[34,35] This method underestimates the entropy, since translation and rotation movements are not completely suppressed in solution. The true value would be somewhere between the two methods, closer to the latter method.

In this work we optimized the geometries with the PCM. The effect of the solvent is taken into account for the geometry and for the energy. But the frequencies, and for this reason the entropy, are still calculated by considering the molecules as an ideal gas, and the entropic factor is greatly overestimated by our method.

Chapter 2 - *t*BuOK/DMF mediated alpha-arylation of enolizable aryl ketones – mechanistic evidence for a radical process and synergistic role of the base and solvent

This work was done in collaboration with the teams of Dr. Marc Taillefer (Ecole Nationale Supérieure de Chimie de Montpellier, ENSCM) and Pr. Thierry Ollevier (Université Laval). In a first part, this chapter presents an overview of the literature regarding the alpha-arylation of ketones in transition metal-free conditions, followed by the methodology developed by Martin Pichette Drapeau, at Université Laval and ENSCM. The literature related to the initiation of radical-chain processes is then exposed.

In a second part, the results for the mechanistic study of the *t*BuOK/DMF promoted alpha-arylation of aryl ketones are presented.

This work was published: Transition-metal-free α-arylation of enolizable aryl ketones and mechanistic evidence for a radical process, M. Pichette Drapeau, I. Fabre, L. Grimaud, I. Ciofini, T. Ollevier, M. Taillefer, *Angew. Chem. Int. Ed*, 2015, **54**, 10587-10591.

State of the art

Alpha-arylation of carbonyl compounds is a transformation of high importance for synthetic organic chemistry, and the alpha-arylation of carbonyl derivatives with aryl halides under metal catalysis has been known for decades. Alpha-arylated carbonyl moieties are present in many organic compounds that exhibit interesting pharmacological and biological properties.[36,37]

In the late nineties, the groups of Buchwald,[38] Hartwig,[39] and Miura,[40] inspired by the development of palladium-catalyzed arylation of heteroatom nucleophiles, independently reported methods based on palladium catalysis for the intermolecular alpha-arylation of ketones with aryl halides. Improved palladium[41,42] and nickel-catalyzed[43,44] protocols have since been disclosed. Aryl halides could be replaced by phenol derivatives with nickel catalysts.[45] Moreover, historically difficult mono-alpha-arylation of acetone is now achieved by palladium catalysis, with aryl halides[46,47] but also tosylates,[48] imidazoylsulfonates[49] and mesylates.[50] As a complementary approach, Taillefer and coworkers reported the copper-catalyzed alpha-arylation of benzyl phenyl ketones (Figure 2.1).[51,52]

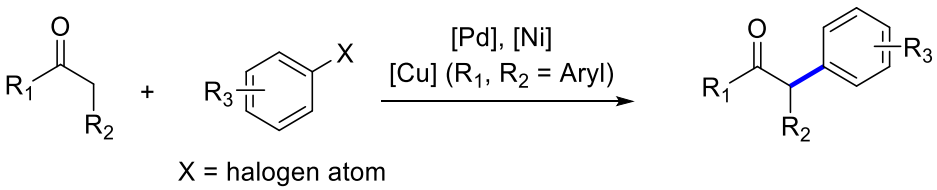

Figure 2.1 - Transition metal-catalyzed alpha-arylation of carbonyl compounds starting from aryl halides

Transition metal free methods of alpha-arylation of ketones by $S_{RN}1$ mechanism

Radical methods to synthesize alpha-aryl ketones were known before the use of metal catalysts.[53] Selected examples of these methods are given below.

Metallic Na/K in ammonia

In 1972, Bunnett described the first protocol of radical nucleophilic aromatic substitution ($S_{RN}1$) using potassium enolate of acetone **2-1** and iodobenzene **2-2** to form

phenylacetone **2-3** (Figure 2.2).[54] The reaction was performed in liquid ammonia in the presence of metallic potassium or sodium.

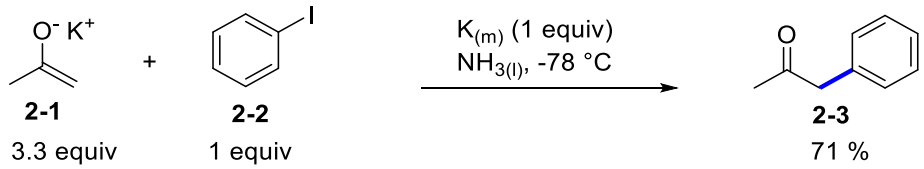

Figure 2.2 - Phenylacetone synthesis by arylation of potassium enolate of acetone with iodobenzene *via* $S_{RN}1$

The $S_{RN}1$[55] mechanism is detailed in Figure 2.3. In the initiation step, a radical is generated by the reduction of the aryl halide in the reaction medium. This reduction can be effected electrochemically,[56–60] chemically or photochemically. The two latter mechanisms will be presented in this chapter. The aryl radical generated reacts with the nucleophile, to form a radical anion. In the propagation step, this radical anion can reduce another molecule of aryl halide, form the product and regenerate an aryl radical.

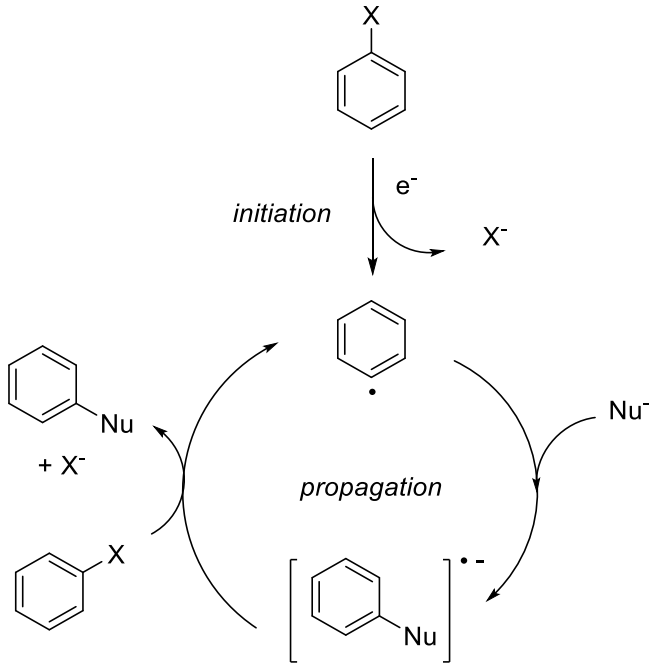

Figure 2.3 - The $S_{RN}1$ mechanism (X = halogen)

In the case of the reaction of alpha-arylation reported by Bunnett, the metallic potassium (or sodium) reduces the arylhalide in the initiation step, and the enolate of the ketone plays the role of the nucleophile.

This methodology of arylation with metallic sodium or potassium in liquid ammonia was developed during the 70's and 80's. The same conditions were applied to other aliphatic ketones.[61] Enolates of aromatic ketones are more stabilized and less reactive. For this reason, their arylation is harder to perform. The arylation of the enolate of acetophenone **2-4** was nevertheless achieved in 57 % yield with chloronaphthalene **2-5** (Figure 2.4).[62]

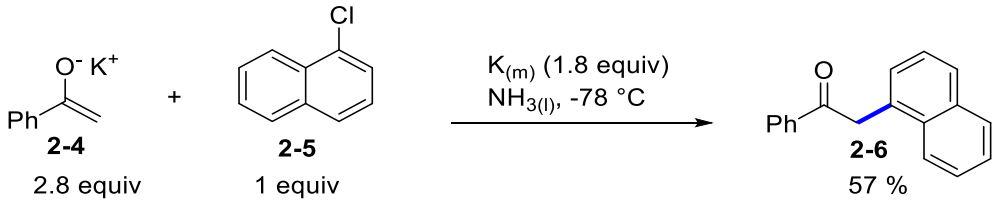

Figure 2.4 – Arylation of accetophenone with chloronaphthalene

Using a Na(Hg) amalgam in liquid ammonia, Austin et al. reported the coupling of enolates of acetone **2-1** and acetophenone **2-4** with chloronaphtalene **2-5**, chloropyridine and chloroquinoline.[63]

One of the drawbacks of these methods is the need to prepare the potassium enolate of the ketone by acid-base reaction with *t*BuOK before the reaction. Moreover, these reactions use metallic potassium in liquid ammonia which are harsh conditions.

Photochemical stimulation in ammonia or DMSO

Another development of this methodology was done with the generation of the radicals by photochemical stimulation.[62,64] The first case was reported in 1973 by Bunnett where this stimulation was used as an alternative for the generation of radicals using metallic sodium or potassium.[61] Photochemical stimulation is able to assist the intermolecular electron transfer to initiate the reaction.

Rossi, Pierini, and coworkers later reported a method for the arylation of aromatic ketones under photochemical stimulation.[65,66] More recently, the synthesis of benzo-fused heterocycles by intramolecular alpha-arylation of ketone enolates was reported (Figure 2.5).[67] The enolate of pinacolone acts as an electron-donor to generate the radical of the aryl halide under irradiation.

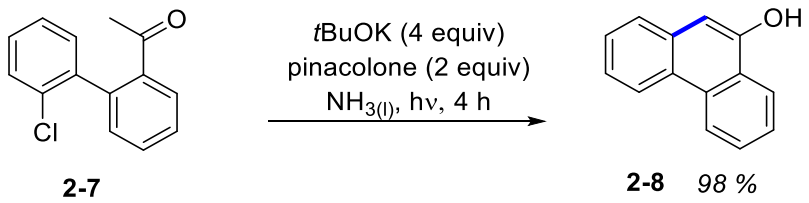

Figure 2.5 – Synthesis of benzo-fused heterocycles by intramolecular alpha-arylation of ketone enolates

The same method of arylation of aliphatic ketones by photo stimulation in ammonia works with halogenated pyrimidines, pyridazines, and pyrazines.[68]

_t_BuOK/DMSO under microwave irradiation

Recently, the alpha-arylation of acetophenone derivatives with iodoarenes using *t*BuOK and DMSO under microwave conditions was described (Figure 2.6).[69]

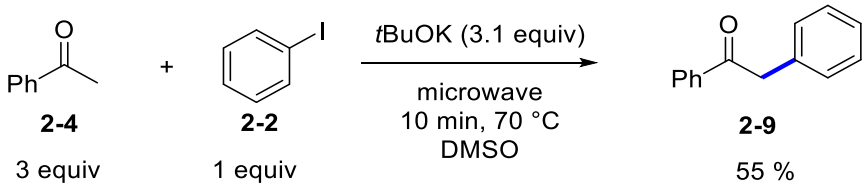

Figure 2.6 – Microwave-induced alpha-arylation of acetophenone

The yields obtained by this method are modest and seldom above 50 %. According to the authors, this would be due to the competitive reduction of the aryl radical to benzene mediated by the solvent.

They performed a mechanistic study to understand the role of the microwave irradiation in this $S_{RN}1$ reaction.[70] In the absence of base and ketone, iodobenzene was stable under microwave irradiation. This led them to conclude that the microwave-induced homolytic rupture of the C-I bond was not involved in the radical initiation process. They also showed that the presence of ionic and dipolar species allowed a faster heating rate, but that these species did not participate in the initiation of the reaction. They finally concluded that an electron transfer from the nucleophile or from tBuO$^-$ was produced by a thermal effect.

As a general trend, DMSO and liquid ammonia were found to be the best solvents for $S_{RN}1$ reactions.[71,72] Liquid ammonia has a boiling point of -33 °C, is very basic and corrosive

and its inhalation may cause asphyxia. Moreover, it requires distillation prior to use, which implies careful manipulation.

Overall, the arylation of aliphatic ketones is easier than the arylation of aryl ketones. Very harsh conditions are used, generally involving photochemical stimulation. Simpler and safer conditions to achieve good yields still need to be developed.

*t*BuOK/DMF-promoted alpha-arylation of aryl ketones

Recently, Martin Pichette-Drapeau, under the supervision of Pr. Thierry Ollevier and Dr. Marc Taillefer, developed a methodology for the potassium *tert*-butoxide promoted alpha-arylation of various enolizable aryl ketones with aryl halides. This reaction proceeds in the absence of metal catalyst and ligand. As listed below, it thus presents several advantages over the methods presented above.

Optimization of the conditions

Optimization studies were performed for the reaction between propiophenone **2-10** and iodobenzene **2-2**, as depicted in Figure 2.7. The results are detailed in Table 2.1.

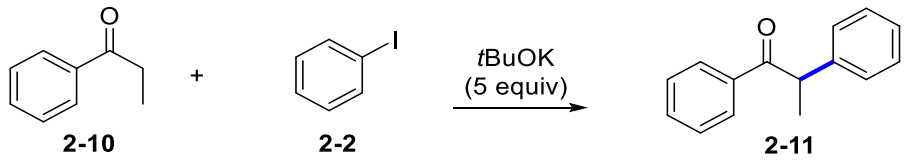

Figure 2.7 – Alpha-arylation of propiophenone with iodobenzene

Without the addition of a metal catalyst, a low yield (24 %) of **2-11** was obtained using a 1.2:1 ratio of propiophenone to iodobenzene, with 3 equiv of *t*BuOK in DMF at 40 °C (Table 2.1, entry 1). The use of 4 and 5 equiv of *t*BuOK slightly increased the yield (Table 2.1, entries 2 and 3) while increasing the temperature to 60 °C was also moderately beneficial (Table 2.1, entry 4). A quantitative yield of **2-11** was finally obtained using a 2:1 ratio of propiophenone to iodobenzene, with 5 equiv of *t*BuOK (Table 2.1, entry 5). The amount of base (5 equiv) could not be lowered. Both propiophenone and the product of the reaction are enolizable ketones deprotonated by the base in the reaction medium.

The reaction also proceeded smoothly using undistilled DMF under an air atmosphere, and an 85 % yield was obtained (Table 2.1, entry 6). The alpha-phenylation could also proceed at room temperature to give 85 % yield of **2-11** after 48 h, the reaction being complete after 72 h (Table 2.1, entry 7).

Among the other bases tested in the conditions of entry 5, *t*BuOLi and *t*BuONa gave very poor conversions (Table 2.1, entries 8 and 9). Moderate yields were nevertheless obtained at higher temperatures (Table 2.1, entries 10 and 11). Cs_2CO_3, CsOH and NaH were completely ineffective (Table 2.1, entries 12–14). A solvent screening revealed that THF, toluene, acetonitrile and DMSO were unsuitable for this reaction (Table 2.1, entries 15–18). *t*BuOK and DMF was the combination of choice.

Table 2.1- Optimization of the conditions of arylation of propiophenone

Entry	Base (x equiv)	Solvent	2-10/2-2	Temperature (°C)	Yield of 2-11 (%)[a]
1	*t*BuOK (3)	DMF	1.2:1	40	24
2	*t*BuOK (4)	DMF	1.2:1	40	31
3	*t*BuOK (5)	DMF	1.2:1	40	37
4	*t*BuOK (5)	DMF	1.2:1	60	56
5	*t*BuOK (5)	DMF	2:1	60	99 (97)
6	*t*BuOK (5)	DMF	2:1	60	85[b]
7	*t*BuOK (5)	DMF	2:1	23	85[c]
8	*t*BuOLi (5)	DMF	2:1	60	<5
9	*t*BuONa (5)	DMF	2:1	60	<5
10	*t*BuOLi (5)	DMF	2:1	120	36
11	*t*BuONa (5)	DMF	2:1	120	52
12	Cs_2CO_3 (5)	DMF	2:1	60	0
13	CsOH (5)	DMF	2:1	60	0
14	NaH (5)	DMF	2:1	60	0
15	*t*BuOK (5)	THF	2:1	60	0
16	*t*BuOK (5)	PhMe	2:1	60	0
17	*t*BuOK (5)	MeCN	2:1	60	0
18	*t*BuOK (5)	DMSO	2:1	60	<1

Reactions performed on 1 mmol scale, in 3 mL solvent during 13 h. a. Yield determined by ^{1}H NMR spectroscopy using 1,3,5-trimethoxybenzene as internal standard. The isolated yield for the best entry is given in parentheses. b. The yield was 85% by using undistilled DMF (3 mL) under an air atmosphere. c. The reaction was performed for 48 h. The yield was 99% after 72 h.

Since undesired metal contaminants in commercial *t*BuOK could catalyze the reaction,[73] the base was resublimed. The use of this purer base led to the same quantitative yield (Table 2.1, entry 5), ensuring that the reaction was not metal-catalyzed.

Scope of the reaction

This reaction has a wide scope and substituted aryl halides and propiophenones could be used. No regiomers were observed when substituted aryl halides were used. Aryl bromides could be used as well as aryl chlorides in a few cases. The latter required higher temperature and gave lower yields than aryl iodides (Table 2.2).

Table 2.2 – Selected scope for the arylation of propiophenone **2-10**

Entry	Temperature	ArX	Yield of 2-11
1	60 °C	PhI	97 %
2	120 °C	PhBr	75 %
3	120 °C	PhCl	29 %

Reactions performed on 1 mmol scale, yields of isolated products. Standard conditions of Table 2.1, entry 5. For X = I, T = 60 °C; for X = Br or Cl, T = 120 °C.

A radical chain mechanism, the SRN1 pathway

As the reaction was suspected to proceed through radical intermediates, common radical scavengers were added to the reaction mixture. 2,6-Di-tert-butyl-α-(3,5-di-tert-butyl-4-oxo-2,5-cyclohexadien-1-ylidene)-p-tolyloxy (Galvinoxyl) and (2,2,6,6-tetramethylpiperidin-1-yl)oxyl (TEMPO) completely inhibited the coupling of propiophenone with iodobenzene (see structures on Figure 2.8).

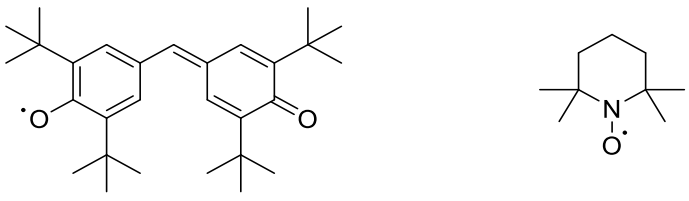

Galvinoxyl TEMPO

Figure 2.8 – Structures of the radical scavengers used

Complementary experiments showed that the reaction was not inhibited in the dark (78 % yield of **2-11** after 48 h at room temperature), and good conversions were achieved under UV irradiation (46 % yield after 2 h at room temperature, $\lambda = 365$ nm).

This led to the hypothesis of a $S_{RN}1$ mechanism, like for the other transition metal free methods presented for this reaction. This mechanism is detailed in Figure 2.9. In the initiation step, a benzene radical is generated from the reduction of iodobenzene in the reaction medium. This aryl radical reacts with the enolate of the ketone to form the radical anion of the product. Then this radical anion can reduce another molecule of iodobenzene to form the product and regenerate an aryl radical. In this case, the enolate of the ketone plays the role of the nucleophile.

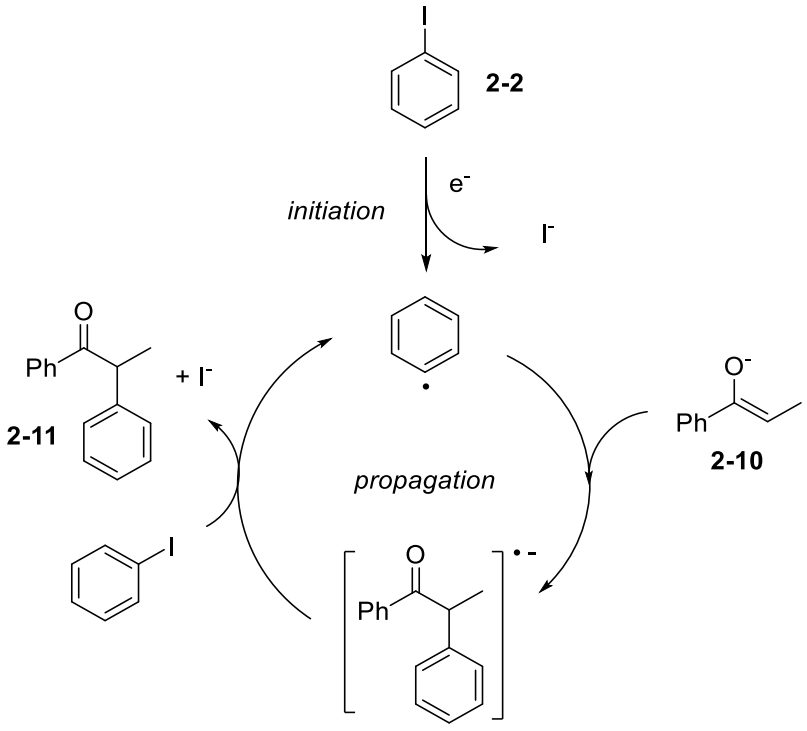

Figure 2.9 - $S_{RN}1$ mechanism for the alpha-arylation of arylketones

Mechanisms of initiation of radical chain processes by organic additives

Radical initiation and electron catalysis

Free radical reactions, and among them the reactions of C-C bond formation by radical chain processes are important in the synthetic toolbox of the organic chemist. The initiation process of this kind of reactions is a key step. The most often used method for the initiation of radical chain reactions is the thermic decomposition of radical initiators having thermolabile

chemical bonds such as peroxides (for example benzoyl peroxide) and azo compounds (for example AIBN, see Figure 2.10).

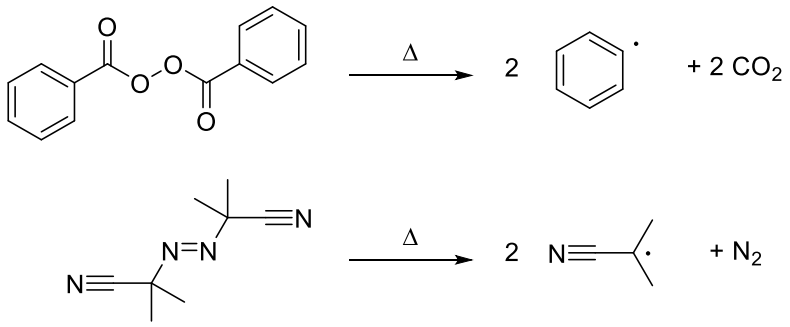

Figure 2.10 – Formation of radicals the radical initiators benzoyl peroxide and AIBN

Since 2008,[74] new ways of initiation of radical chain processes have been developed for the metal-free C-C bond formation. They involve small organic molecule additives in the presence of a base. These additives can be ligand-type molecules such as 1,10-phenanthroline,[75–77] 1,2-diamines,[78] alcohols,[79,80] 1,2-diols,[81] amino acids,[82,83] hydrazine derivatives,[84,85] *N*-heterocyclic carbenes[86] or solvents such as pyridine[87] or DMF[88–90] (Figure 2.11).

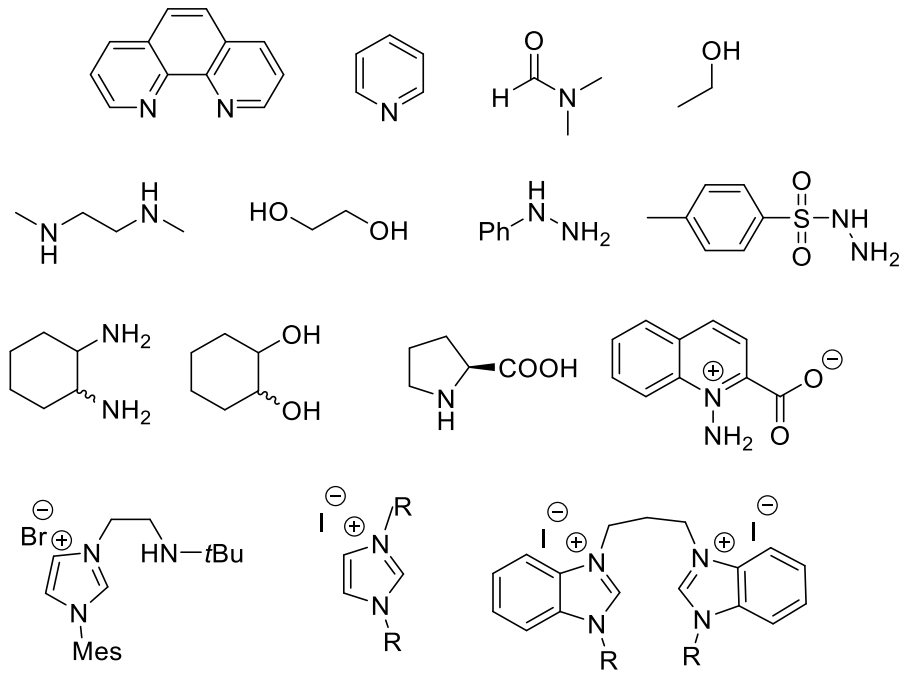

Figure 2.11 – Selected examples of additives known to initiate radical processes

The role of these various additives can be mistaken for a ligand or a solvent role. For this reason, whereas the chain propagation mechanism for radical reactions has been understood

for a long time, the radical initiation mechanism is still a problem of interest in radical chemistry. A general mechanistic hypothesis is that the organic additive works as an electron donor or generates an electron donor in the reaction medium. This electron donor can reduce the aryl halide and can generate the aryl radical to initiate the reaction. This is the case for the $S_{RN}1$ reactions.

This $S_{RN}1$ mechanism can be part of a much more general family of reactions called "electron-catalyzed reactions". A formal mechanism is depicted in Figure 2.12, where the electron is regenerated at the end of each cycle.[91] The initiator can also be called precatalyst because it generates the actual catalyst, the electron.

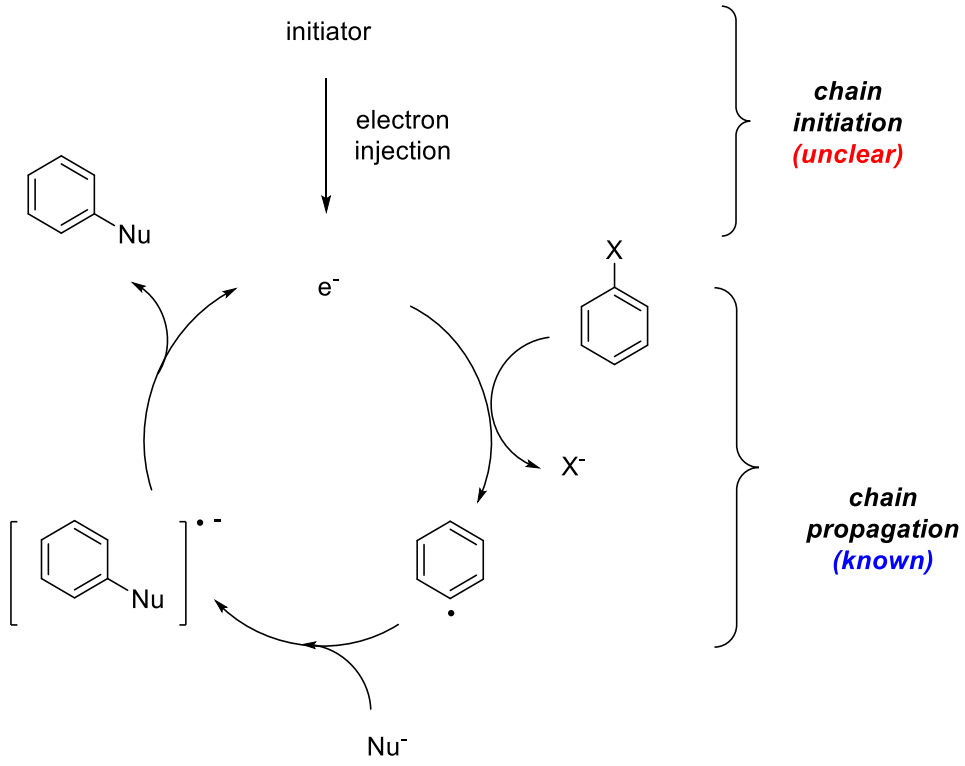

Figure 2.12 - $S_{RN}1$ process considering the electron as a catalyst

Selected examples from the literature

A selection of these electron-catalyzed reactions, initiated by small organic molecule additives is presented below.

DMEDA/*t*BuOK systems

Base-promoted homolytic aromatic substitutions (BHAS) are reactions that occur through electron catalysis. In 2010, Liu and coworkers reported the *N*,*N*'-dimethylethylenediamine (DMEDA) catalyzed direct C-H arylation of unactivated benzene[78] (Figure 2.13).

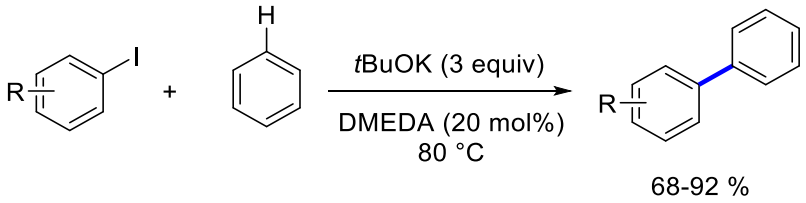

Figure 2.13 - DMEDA catalyzed direct C-H arylation of unactivated benzene

Murphy's team investigated the radical initiation mechanism of these cross-coupling reactions initiated with diamine.[92] They suggested, starting from the diamine **2-12** in the presence of the base, the formation of an imine **2-13** through expulsion of hydride followed by deprotonation. This imine would then undergo further deprotonation to afford the formation of an enamine salt **2-14** that would be the electron donor (Figure 2.14).

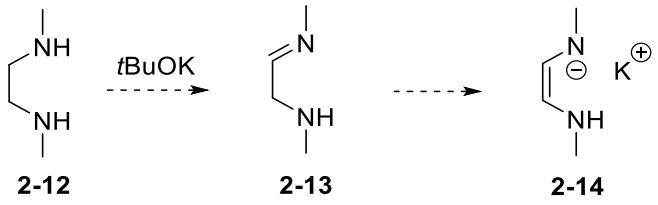

Figure 2.14 – Formation of the radical initiator from DMEDA

They prepared the deuterated derivatives of **2-12** DMEDA-d_4, DMEDA-d_6 and DMEDA-d_{10} (Figure 2.15). DMEDA-d_4 and DMEDA-d_{10} exhibited no radical initiation activity, whereas only a small drop of the reaction yield was observed with DMEDA-d_6. They analyzed these results as a primary isotope effect for the cleavage of an ethylene C-H/(D) bond. They concluded that this step plays a significant role in the radical initiation process. For the ethylene-deuterated derivatives, the formation of the initiator **2-14** is slowed down, and the yield of the reaction drops down. Their results are thus consistent with the initiation of the reaction by an organic electron donor that is formed by the oxidation of the amines under basic conditions. Nevertheless, the nature of the oxidant that forms the imine **2-13** is not clear in this study.

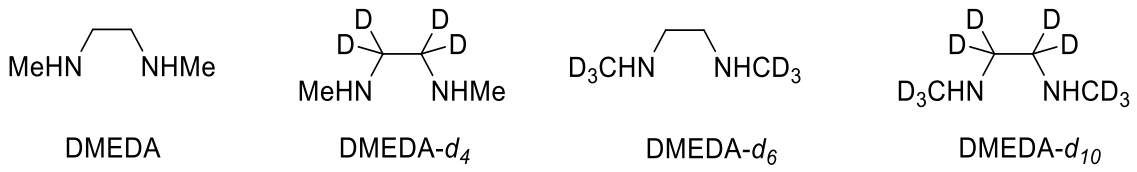

Figure 2.15 – Deuterated derivatives of DMEDA

Two years later, Jiao and coworkers investigated the same mechanism and found different conclusions which led them to rule out this simple redox-type initiation pathway.[93] Indeed they reported an activity for the deuterated diamines. They observed an induction period for the global reaction that they linked to the formation of the monoimine **2-13**. The mechanism proposed for its formation is described in Figure 2.16.

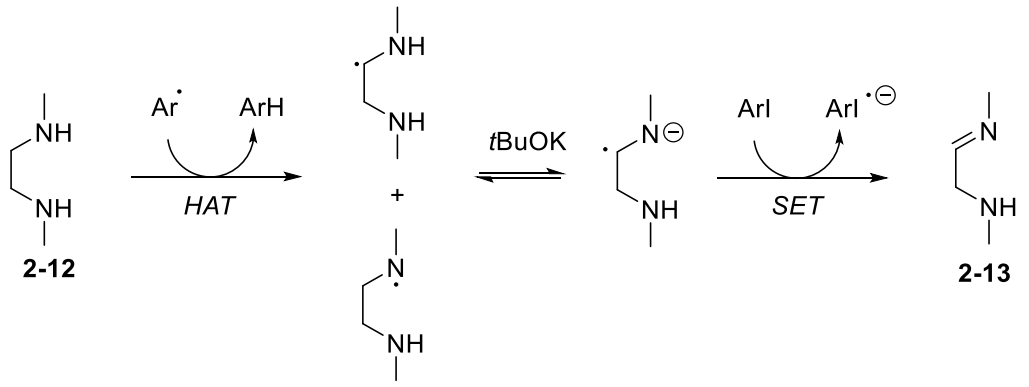

Figure 2.16 – Formation of the monoimine **2-13** from the diamine **2-12**

They proposed a double role for this monoimine **2-13**, as a radical amplifier (radical proliferation), and as a radical regulator (radical homeostasis), as described in Figure 2.17.

In their experiments, the activity of the deuterated analogs followed the order DMEDA-d_4 < DMEDA-d_{10} < DMEDA < DMEDA-d_6. Deuteration on the ethylene bridge made the initiation less effective to form the monoimine **2-13**, and also the formation of **2-14**, slowing down the radical proliferation. On the opposite, deuteration on the *N*-Me groups slowed down the consumption of the monoimine **2-13** to form **2-16** which favored the radical proliferation pathway instead of the radical homeostasis and increased the activity. Their study was supported by DFT calculations.

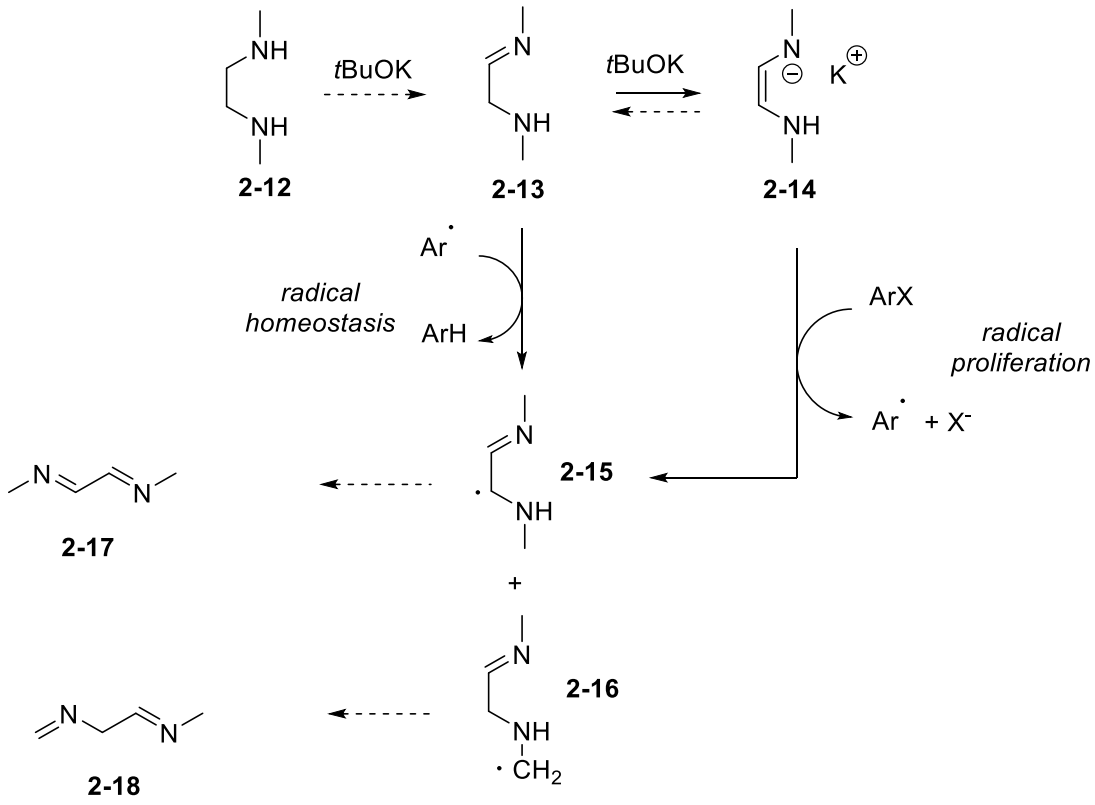

Figure 2.17 – Mechanism of radical proliferation and radical homeostasis starting from DMEDA

This example shows the complexity of the initiation mechanisms, compared to the main chain reaction. Jiao and coworkers suggested that a hydrogen atom donor moiety next to a heteroatom-H bond might be the key structural feature for many successful initiators of radical reactions, including diols, amino alcohols, hydrazines and amino acids.

1,10-Phenanthroline/*t*BuOK systems

In 2010, Shi and coworkers reported the C-H functionalization of arenes with aryl iodides or bromides. This reaction is mediated by *t*BuOK as a base and 1,10-phenanthroline as organic additive.[75] The reaction works both in inter and intra molecular version (Figure 2.18).

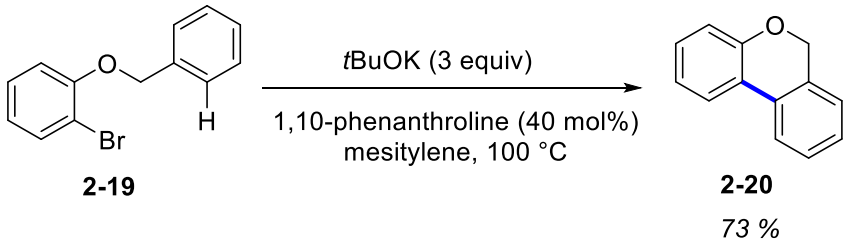

Figure 2.18 – *t*BuOK/1,10-phenanthroline promoted intra molecular cross-coupling to prepare 6*H*-benzo[*c*]chromene

Under similar reaction conditions, with 1,10-phenanthroline[76] or bathophenanthroline[77] Heck-type reactions can be achieved (Figure 2.19).

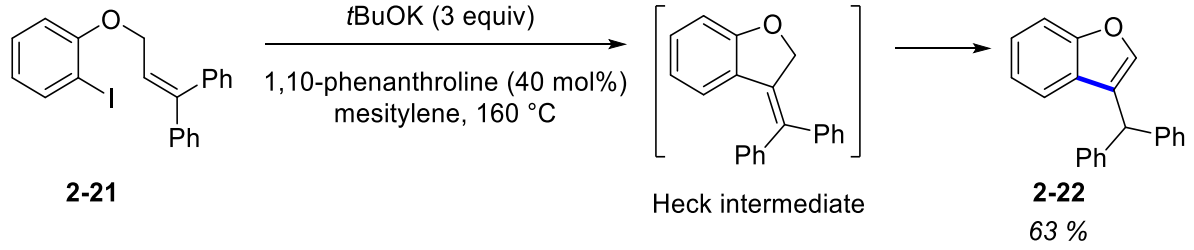

Figure 2.19 - Potassium *tert*-butoxide mediated Heck-type cyclization/isomerization to form benzofurans

Wilden and coworkers studied the interaction between *t*BuOK and 1,10-phenanthroline and showed that *tert*-butoxide rapidly reduced 1,10-phenanthroline to its radical anion, which could then reduce an aryl halide.[94] They suggested that phenanthroline derivatives allow storing electrons temporarily. These conclusions are in agreement with the work of Lei and Jutand who investigated the initiation of the *t*BuOK/1,10-phenanthroline promoted BHAS reaction using EPR and electrochemistry.[95] They evidenced an inner-sphere electron transfer from the *tert*-butoxide anion to 1,10-phenanthroline to form the phenanthroline radical anion and the *t*BuO$^{\bullet}$ radical. The phenanthroline radical anion intermediate reduces aryl bromides by outer-sphere electron transfer to form aryl radicals. They also suggested that the potassium cation is complexed by 1,10-phenanthroline, which brings the *tert*-butoxide anion closer to favor an inner sphere electron transfer within the intermediate complex (Figure 2.20).

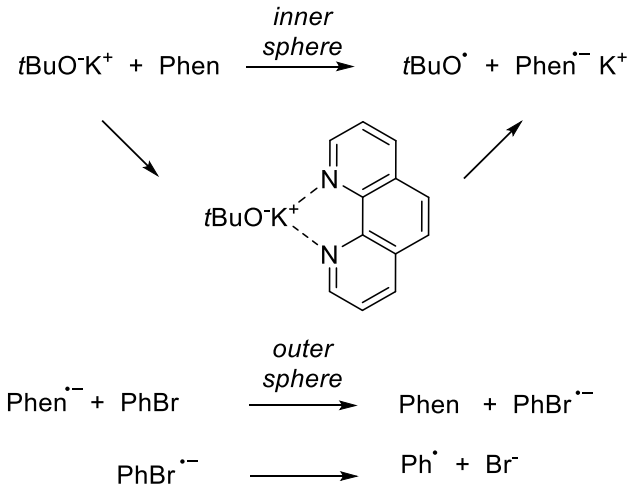

Figure 2.20 – Formation of aryl radical with *t*BuOK and 1,10-phenanthroline

In their study,[96] Murphy and coworkers computed the free energy change for this reaction between potassium *tert*-butoxide, 1,10-phenanthroline and iodobenzene (Figure 2.21).

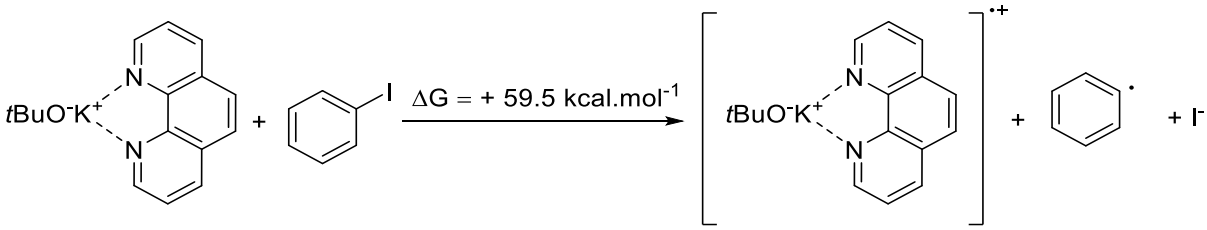

Figure 2.21 – Computed free energy for the reduction of iodobenzene by a *t*BuOK/1,10-phenanthroline complex

Due to the high energy value obtained ($\Delta G = 59.5$ kcal.mol^{-1}), they rather suggested the formation of a super electron donor **2-26** by deprotonation of 1,10-phenanthroline to form **2-24** and addition of this nucleophile on another 1,10-phenanthroline molecule. They isolated the oxidized product of the phenanthroline dimer **2-26** (Figure 2.22).

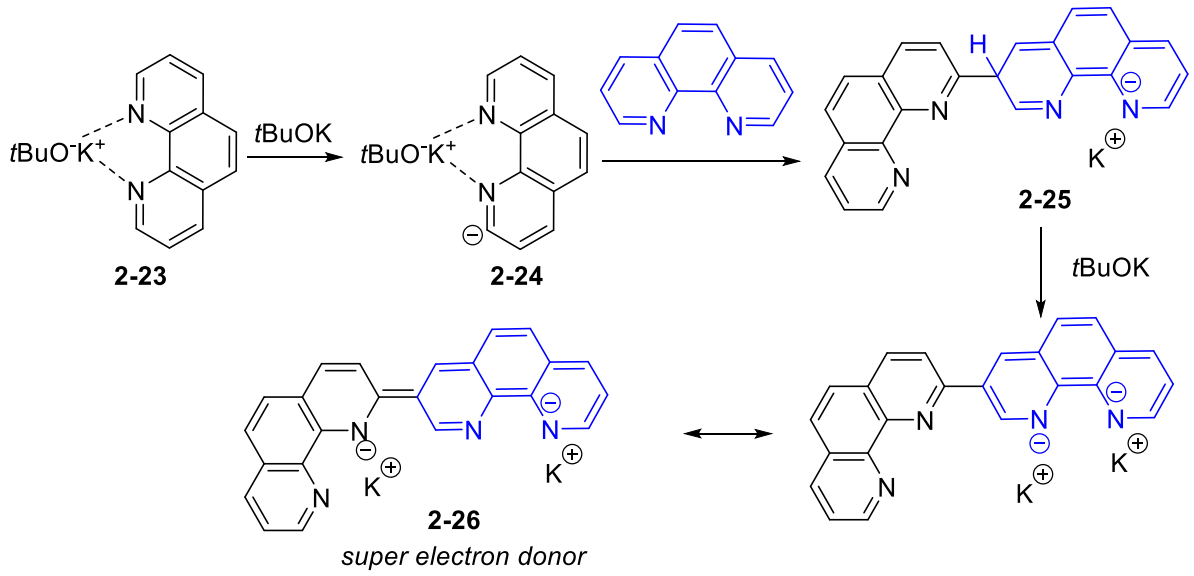

Figure 2.22 – Formation of a super-electron-donor in the presence of 1,10-phenanthroline and *t*BuOK

_t_BuOK/DMF systems

DMF is known to have a role apart from being a solvent.[97,98] It can be an active participant in chemical reactions, and it can in particular be a source of radicals or a source of reducing agents. Yan and coworkers developed a series of reactions using *t*BuOK in DMF (selected example in Figure 2.23).[88–90]

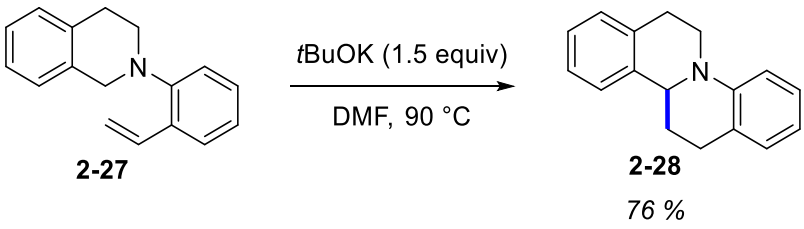

Figure 2.23 – Cyclisation of *N*-2-ethenyl-phenyl tetrahydroisoquinoline in DMF in the presence of *t*BuOK

In their work, Yan and coworkers suggested a mechanism involving deprotonation of the DMF by the *tert*-butoxide to generate an electron-rich carbamoyl anion **2-29**, able to reduce DMF to generate a DMF radical species **2-30**. Hydrogen abstraction from the substrate **2-27** would then generate the active radical **2-31** (Figure 2.24).

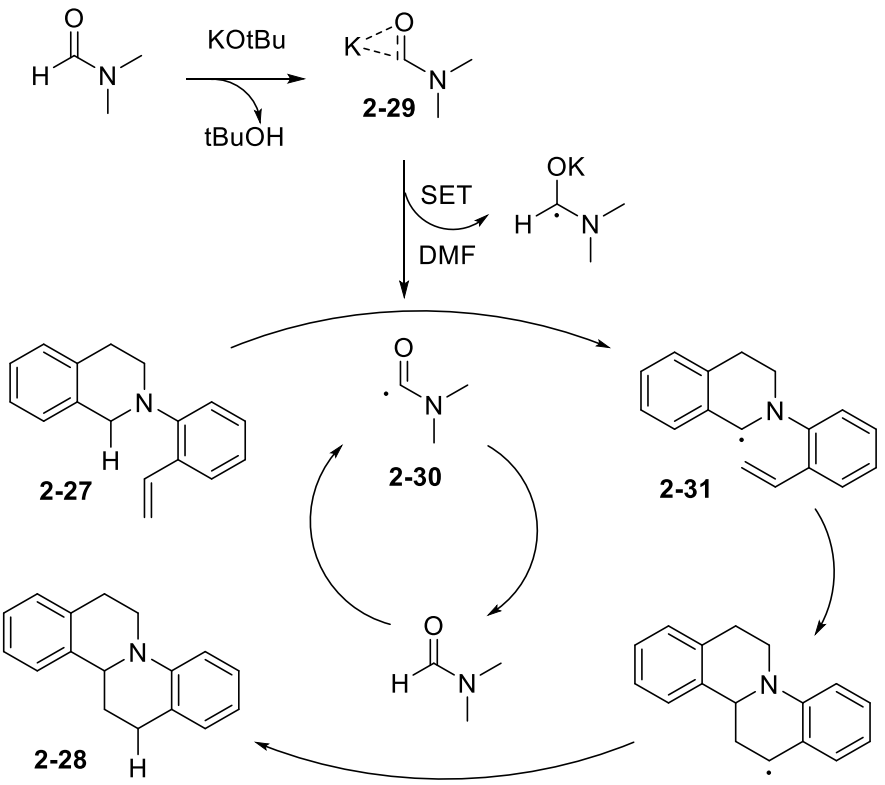

Figure 2.24- Proposed mechanism for the cyclisation of *N*-2-ethenyl-phenyl tetrahydroisoquinoline in DMF in the presence of *t*BuOK

In 2011, Hayashi and coworkers developed a Mizoroki-Heck type reaction mediated by potassium *tert*-butoxide in DMF (Figure 2.25).[79] In their suggested mechanism, the *tert*-butoxide transfers an electron to iodobenzene to form a benzene radical. The role of ethanol as an additive was not clear.

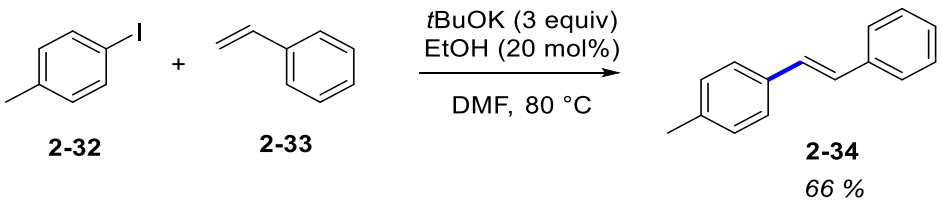

Figure 2.25 - Mizoroki–Heck-type reaction mediated by potassium *tert*-butoxide in the presence of ethanol

_t_BuOK alone

*t*BuOK alone can also promote reactions, without phenanthroline or diamine additives, as described by Wilden and coworkers (see Figure 2.26).[94] In this case the reaction requires higher temperatures.

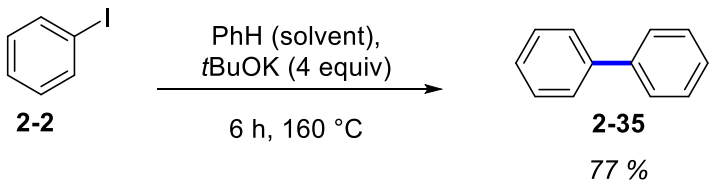

Figure 2.26 – Transition metal free biaryl coupling promoted by *t*BuOK in the absence of additives

In this case, the commonly proposed initiation mechanism is a direct electron transfer from the *tert*-butoxide anion to the aryl halide to generate the aryl radical. Wilden and coworkers suggested that the most important factor is the dissociation degree between the cation (K^+, Na^+, Li^+) and the *tert*-butoxide. The reducing ability of the latter increases with the dissociation. 1,10-phenanthroline is required to help the dissociation of the ion pair with *t*BuONa, but not with *t*BuOK.

Nevertheless, given the computed thermodynamics for the electron transfer to aryl iodide with the base complexed by 1,10-phenanthroline (Figure 2.21), Murphy and coworkers suggested a different initiation mechanism,[96] involving the conversion of iodobenzene **2-2** to benzyne **2-36** by deprotonation, which has already been reported in the literature.[99] This pathway would be only the initiation step for the cases where the regioselectivity of the reaction cannot be explained by a benzyne intermediate. Indeed, only small amounts of benzyne are predicted to be formed by this reaction which is endergonic, with a barrierless reverse reaction (Figure 2.27).

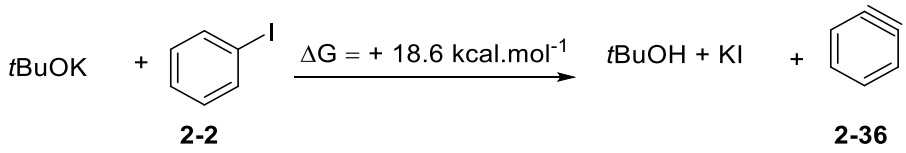

Figure 2.27 – Computed free energies for the formation of benzyne by deprotonation of iodobenzene

This benzyne **2-36** could then attack benzene in a radical fashion to form **2-37**. Hydrogen abstraction from benzene, which generates a first aryl radical, and deprotonation would form **2-39** which is a potential electron donor to reduce iodobenzene (Figure 2.28). The calculated energies predict an overall exergonic reaction (ΔG = -29.1 kcal.mol^{-1}) with a maximum barrier of 12.2 kcal.mol^{-1}.

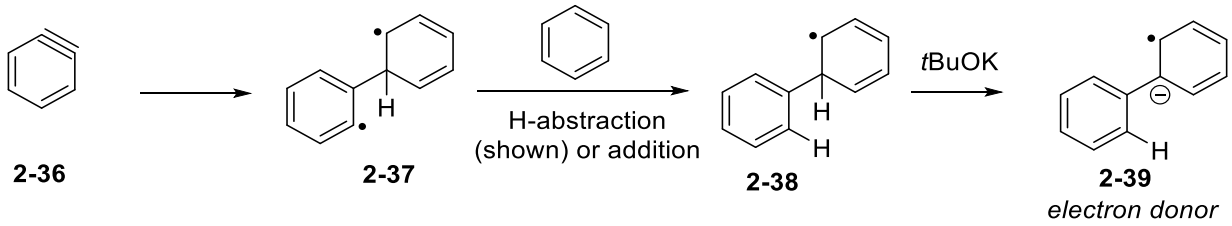

Figure 2.28 – Proposed mechanism for the generation of radicals from benzyne

These selected examples of initiation mechanisms for radical coupling in analogous conditions show that the mechanism of action of the additives is neither trivial nor systematically the same. Nevertheless, the effect of the initiation step is always to generate an organic electron donor in the reaction medium.

Mechanistic study of the *t*BuOK/DMF promoted alpha-arylation of aryl ketones

The main challenge in the mechanistic study of the *t*BuOK/DMF promoted alpha-arylation of aryl ketones (Figure 2.29) is the identification of the radical initiator. This must be achieved by taking into account the specificity of the base and of its counterion and the specificity of the solvent used, DMF. Indeed, whereas according to the literature DMSO is one of the best solvents for the alpha-arylation of ketones, less than 1 % of product is formed with this solvent in our conditions.

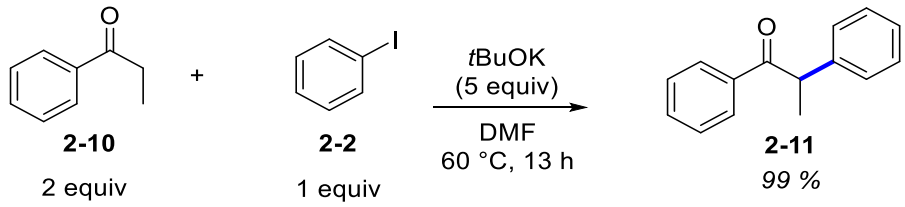

Figure 2.29 - Optimized conditions for the alpha-arylation of propiophenone by iodobenzene

$S_{RN}1$ Mechanism

The reaction is completely inhibited by radical scavengers which suggests a radical mechanism. A benzyne intermediate, as proposed by Murphy[96] was in our case not considered as the main mechanistic pathway since a very good regioselectivity was observed on substituted halide derivatives (Table 2.2 and Figure 2.30). Benzyne as an initiator in our case will be discussed at the end of the study.

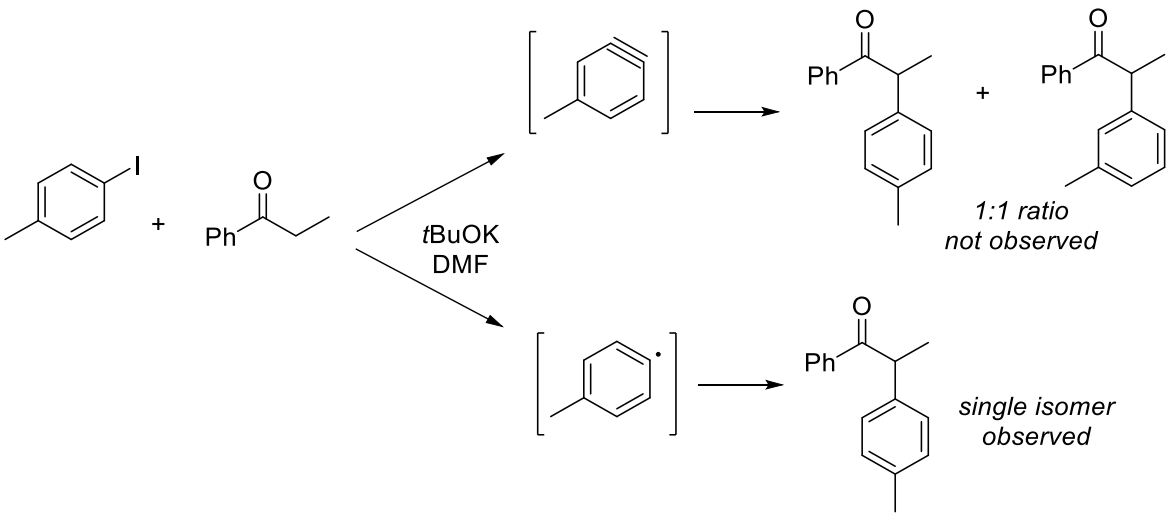

Figure 2.30 – Expected products in the case of a benzyne or benzene radical intermediate

We considered a $S_{RN}1$ mechanism with the formation of a benzene radical from iodobenzene (Figure 2.31). An electron donor can reduce iodobenzene **2-2** according to a single electron transfer (SET) to form its radical anion **2-40** that would dissociate into a benzene radical **2-41** and an iodide anion.

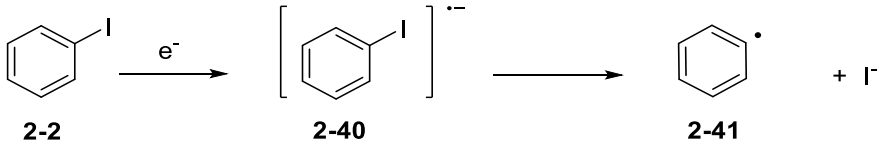

Figure 2.31 - Benzene radical formation from iodobenzene

The radical **2-41** can then react with the enolate of the ketone **2-10** to form the radical anion of the product **2-42**. This radical anion can reduce a new molecule of iodobenzene by a SET to form the product **2-11** and to regenerate a benzene radical **2-41** to ensure the propagation of the radical chain (Figure 2.32).

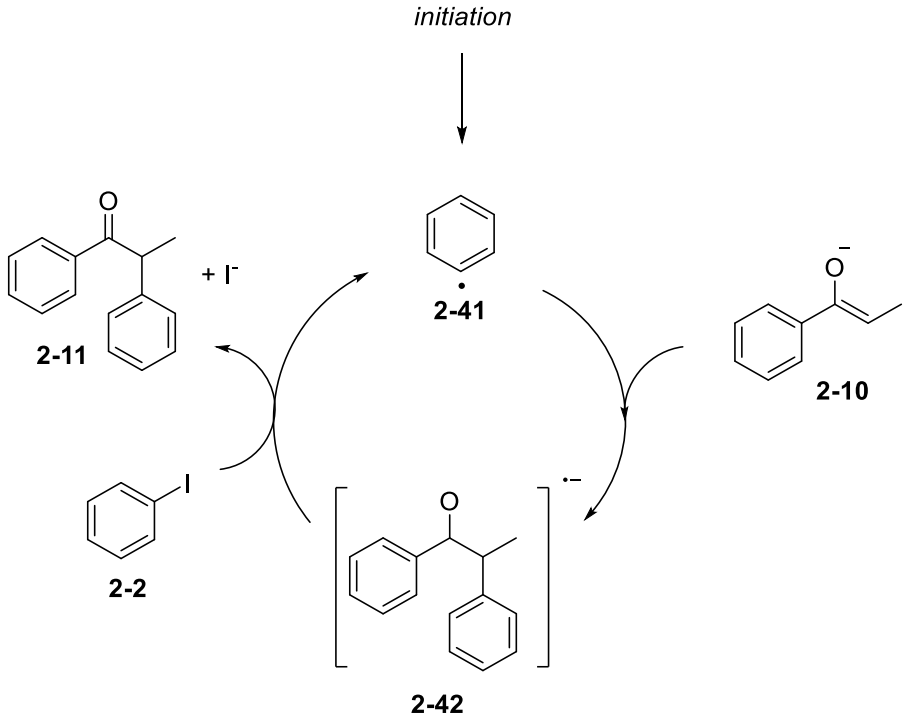

Figure 2.32 - $S_{RN}1$ mechanism for the alpha-arylation of aryl ketones

In a preliminary study, different possible initiation mechanisms to form the benzene radical were investigated at the DFT level. Two types of SET can be defined: the outer-sphere electron transfer, where an electron is exchanged between two separate reagents, and the inner-sphere electron transfer, where the electron is exchanged between two reagents linked together in a molecular complex (Figure 2.33).

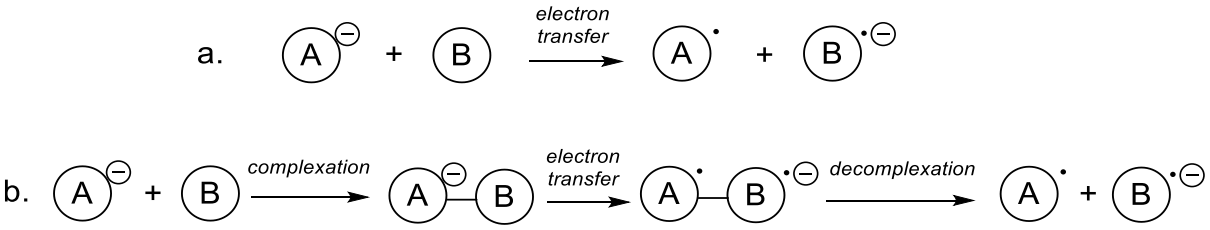

Figure 2.33 – SET a. outer-sphere electron transfer b. inner-sphere electron transfer

DFT computational details

The energy profiles were computed for the $S_{RN}1$ pathway in DMF using the 6-311+ G(d,p) basis sets for all atoms but I, described using 6-311G(d,p). Bulk solvent effects for DMF were included by means of a PCM. Some explicit molecules of solvent (DMF) were added when the solvent was involved in the reaction steps. Counterpoise correction was included when

indicated. Different functionals were used at the beginning of the study: PBE0[16], M06[20], M062X[20], B3LYP.[14,15,17] Total energies, free energies and enthalpies are given for the reactions. Enthalpies and free energies were calculated for standard conditions at 298.15 K.

Initiation by outer-sphere electron transfer to PhI

We first considered the reduction of iodobenzene by an electron rich species *via* outer-sphere electron transfer. The *tert*-butoxide anion itself is commonly proposed as an electron donor for the initiation of the reaction.[94] Murphy and coworkers suggested that enolates formed from alcohols could be efficient electron donors in the coupling reactions of haloarenes to arenes involving alcohols and 1,2-diols as additives.[92] In our reaction conditions, after deprotonation of the ketone, the base, *tert*-butoxide, is in three-fold excess and the enolate of the ketone is in two-fold excess. Both can be partially consumed in the initiation step.

Table 2.3 – Reaction energies computed for the outer-sphere electron transfer to iodobenzene (in kcal.mol^{-1})

(2-1) Electron transfer from *t*BuO$^-$

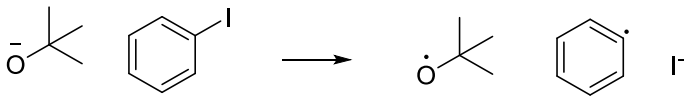

(2-2) Electron transfer from the enolate

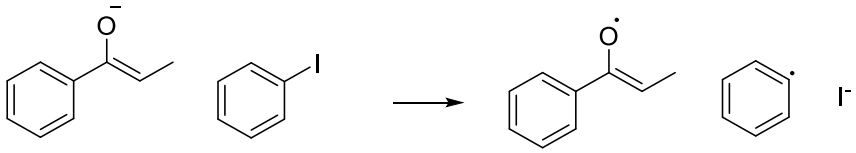

	Energy ΔE				**Free energy ΔG**				**Enthalpy ΔH**			
	PBE0	B3LYP	M06	M062X	PBE0	B3LYP	M06	M062X	PBE0	B3LYP	M06	M062X
(2-1)	32.86	31.11	42.45	35.27	22.85	20.97	32.07	25.65	32.38	30.52	41.68	34.98
(2-2)	23.71	20.74	30.50	26.29	14.13	10.88	20.38	16.76	23.07	20.07	29.76	25.65

The same trends are found independently on the functional used. The electron transfer from the enolate (equation (2-2)) is easier as it requires around 10 kcal.mol^{-1} less energy than the electron transfer from the *tert*-butoxide (equation (2-1)). Nevertheless, the computed reaction energies and enthalpies are all above 20 kcal.mol^{-1}, which is too high for this reaction which can proceed at room temperature.

Initiation by inner-sphere electron transfer to PhI

Because the energies required for the outer-sphere electron transfer are too high, an inner-sphere electron transfer was considered. Indeed, a complexation bringing closer the reagents could favor the electron transfer.

For a given complex between an electron rich species and iodobenzene, we computed the transposition of one electron from an occupied orbital localized on the electron donor to an unoccupied orbital localized on the aryl iodide, that we will call *alter* operation. After relaxation performed in an unrestricted formalism, if the electron transfer is evidenced, the spin density of the molecular complex is different from zero and the negative charge is localized on the iodobenzene (Figure 2.34).

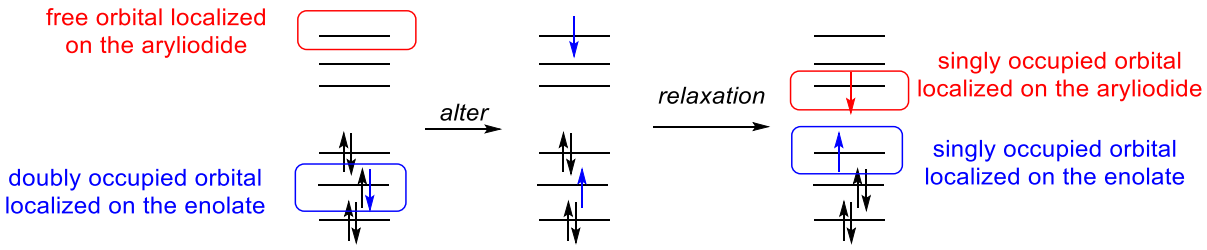

Figure 2.34 – Schematic representation of the *alter* operation

We first explored this possibility for the enolate as electron-donor, since the energies for this transfer were lower than the ones for the *tert*-butoxide. It could form a molecular complex with iodobenzene *via* halogen bonding.[100] We computed the reaction energies for the formation of the halogen bond, then we performed the *alter* operation (Table 2.4).

Table 2.4 – Computed inner-sphere electron transfer *via* halogen bond between iodobenzene and the enolate. Reaction energies for the complexation (in kcal.mol^{-1})

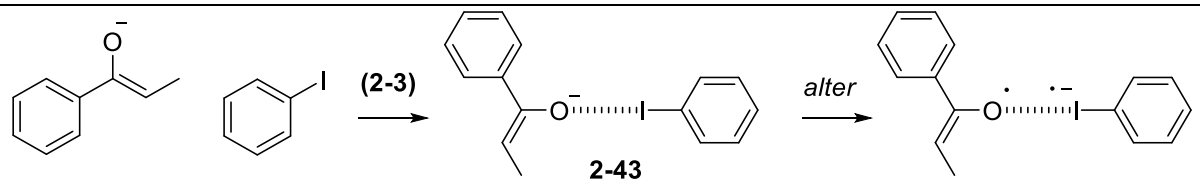

	Energy ΔE				Free energy ΔG				Enthalpy ΔH			
	PBE0	B3LYP	M06	M062X	PBE0	B3LYP	M06	M062X	PBE0	B3LYP	M06	M062X
(2-3)	-3.51	-1.90	-6.64	-5.38	7.34	9.01	4.83	6.27	-2.23	-0.59	-5.32	-4.03

The halogen bond between the enolate and iodobenzene induces a small stabilization of the complex (ΔH from -1.59 to -5.32 kcal.mol^{-1} depending on the functional used).

For the *alter* operation, different combinations of occupied and unoccupied orbitals were considered. For complex **2-43**, the highest occupied molecular orbital (HOMO), localized on the enolate, and the lowest unoccupied molecular orbital (LUMO), localized on iodobenzene are represented as an example in Figure 2.35. Relaxation after *alter* operation always led back to the initial complex **2-43**, and no inner-sphere electron transfer could be found.

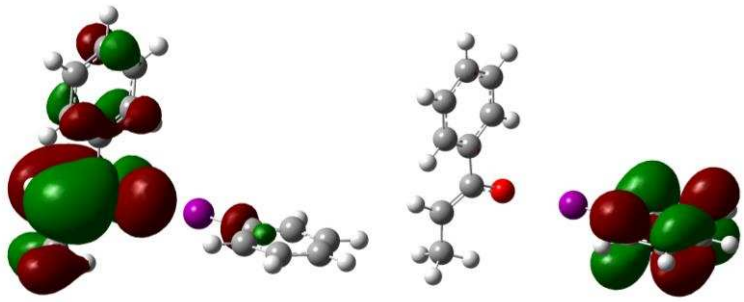

Figure 2.35- HOMO of the complex **2-43**, localized on the enolate (left), LUMO of the complex **2-43**, localized on the aryl iodide (right)

The same methodology was then applied to a similar complex with a potassium cation, since its presence was found necessary for the success of the reaction (Table 2.5). This cation can stabilize the complex before the electron transfer, but also the negative charge after the electron transfer to iodobenzene. In a last step it can also help with the dissociation of the radical anion of iodobenzene into the aryl radical and iodide.

Table 2.5 – Computed inner-sphere electron transfer *via* halogen bond between iodobenzene and the enolate with complexation by K^+. Reaction energies for the complexation (in kcal.mol^{-1})

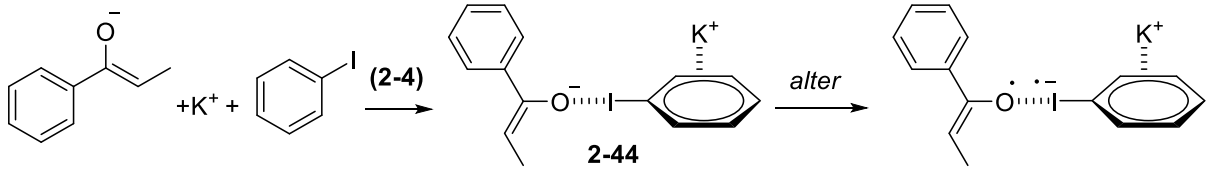

	Energy ΔE				Free energy ΔG				Enthalpy ΔH			
	PBE0	B3LYP	M06	M062X	PBE0	B3LYP	M06	M062X	PBE0	B3LYP	M06	M062X
(2-4)	-5.32	-3.24	-8.62	-7.90	13.02	15.06	10.70	12.00	-3.67	-2.24	-6.85	-6.13

The presence of the potassium ion induces a more favorable formation of the complex **2-44**, (ΔH between -2.24 and -6.85 kcal.mol^{-1} depending on the functional used). Nevertheless, relaxation after *alter* operation always led back to the initial complex **2-44**, and no inner-sphere electron transfer could be found.

Next, the methodology was applied to a similar complex with a halogen bond between iodobenzene and *tert*-butoxide stabilized by a potassium cation (Table 2.6).

Table 2.6 – Computed inner-sphere electron transfer *via* halogen bond between iodobenzene and *tert*-butoxide with complexation by K^+. Reaction energies for the complexation (in kcal.mol^{-1})

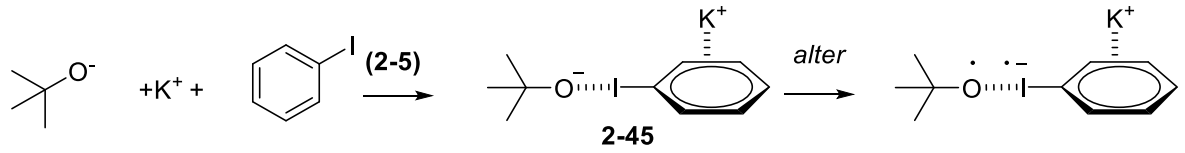

	Energy ΔE				Free energy ΔG				Enthalpy ΔH			
	PBE0	B3LYP	M06	M062X	PBE0	B3LYP	M06	M062X	PBE0	B3LYP	M06	M062X
(2-5)	-8.59	-5.17	-11.57	-10.17	10.16	12.67	7.07	8.11	-6.69	-3.34	-9.71	-8.44

With *tert*-butoxide, the halogen bonding is more favorable than with the enolate (ΔH from -3.34 to -9.71 kcal.mol^{-1} depending on the functional used). Nevertheless, in this case as well, relaxation always led back to the initial complex **2-45**, without electron transfer.

In the results above, Counterpoise correction was estimated for complexes **2-43**, **2-44** and **2-45** but found to be very small (below 1.06 kcal.mol^{-1}) for all functionals considered.

To conclude from these results, an electron transfer from the enolate of from the *tert*-butoxide to the aryl iodide seems not energetically favoured.

Initiation by outer-sphere electron transfer to the solvent

In an attempt to justify the specificity of the solvent in our reaction, we then considered that the DMF could be a relay for the electron transfer as an electron acceptor. The *tert*-butoxide or the enolate could in a first step transfer an electron to the DMF.

Table 2.7 – Computed reaction energies for the outer-sphere electron transfer to DMF (in kcal.mol^{-1})

(2-6) Electron transfer from *t*BuO$^-$

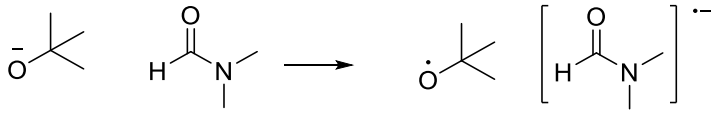

(2-7) Electron transfer from the enolate

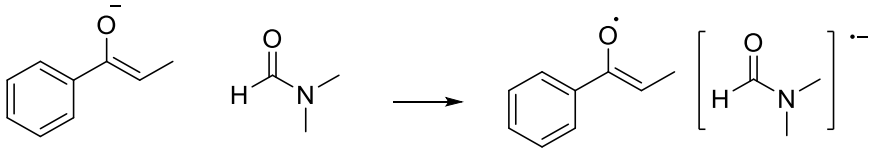

	Energy ΔE				Free energy ΔG				Enthalpy ΔH			
	PBE0	B3LYP	M06	M062X	PBE0	B3LYP	M06	M062X	PBE0	B3LYP	M06	M062X
(2-6)	78.17	79.40	82.86	81.09	74.85	75.90	79.40	78.76	75.93	77.03	80.39	79.16
(2-7)	69.03	69.03	70.91	72.11	66.14	65.82	67.72	69.86	66.61	66.58	68.47	69.83

The computed energies are much higher than the ones obtained for the reduction of the aryl iodide (ΔH above 60 kcal.mol^{-1} in all cases). Therefore, this hypothesis of mechanism cannot be retained.

To sum up, electron transfer from *tert*-butoxide or from the enolate to iodobenzene or to DMF, by inner- or outer-sphere requires energies that are not compatible with the experimental conditions, especially because our reaction can proceed at room temperature.

Initiation by deprotonation of the solvent

At this point, we turned our attention to a mechanism suggested by Yan et al,[88] in which the base car deprotonate DMF to form a carbamoyl anion.

The first report for the generation of carbamoyl anion was in 1967, when Gerhart and coworkers prepared diethylcarbamoyllithium from bis(diethylcarbamoyl)mercury and trapped it with carbonyl electrophiles.[101] In 1973, Banhidai and coworkers reported the formation of carbamoyl anion by treating formamides with LDA. This anion can be trapped with carbonyl electrophiles.[102,103] The formation of such an intermediate was reported by Reeves and coworkers, in the presence of LDA or *t*BuLi and the carbamoyl intermediate was characterized by ^{13}C NMR at low temperature.[104]

We considered a deprotonation of the solvent, DMF, by the base, with the hypothesis that the carbamoyl anion could then be the electron-donor.

Table 2.8 – Computed reaction energies for the deprotonation of DMF (in kcal.mol^{-1})

(2-8)

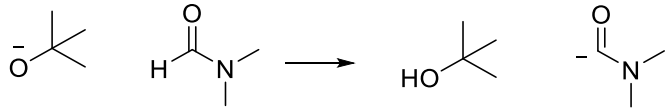

	Energy ΔE				Free energy ΔG				Enthalpy ΔH			
	PBE0	B3LYP	M06	M062X	PBE0	B3LYP	M06	M062X	PBE0	B3LYP	M06	M062X
(2-8)	19.66	20.06	19.11	16.92	18.98	19.15	18.54	16.04	19.44	19.72	18.97	16.59

These reaction energies (ΔH from 16.59 to 19.44 kcal.mol^{-1} depending on the functional used), are lower than those for all previous hypotheses and are compatible with our reaction conditions.

At this point we chose M062X as the functional for all the study, which gives the lowest energies for the deprotonation. The M06 functional gives the highest energies in all studied cases, and it is known to be adapted to the study of organometallic and inorganometallic thermochemistry. The M062X functional is well performing for the study of noncovalent interactions that will occur between the ions present and with the solvent.[20] PBE0 and B3LYP are known to provide a more balanced description of spectroscopic properties and reactivity.

Experimental observation of the deprotonation of DMF

These promising results led us to the experimental investigation of the deprotonation of the solvent. A solution of *t*BuOK (100 mg, 0.9 mmol) in 0.5 mL DMF-d_7 was monitored by ^{1}H NMR and ^{13}C NMR during several hours at room temperature.

We observed an increase of the integration of the formamide proton, which is consistent with a D exchange between the deuterated solvent DMF-d_7 and water in the presence of the base (Figure 2.36).

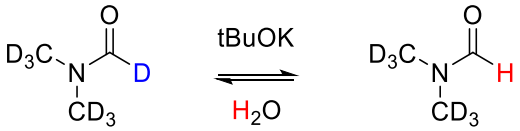

Figure 2.36 - Observed deuterium/proton exchange in the presence of base and water

With a fixed integration of 3 for the CH_3 signals of DMF, the formamide proton signal integration increased from 2.39 after 4 minutes to 10.56 after 9 hours (Figure 2.37 and Figure 2.38).

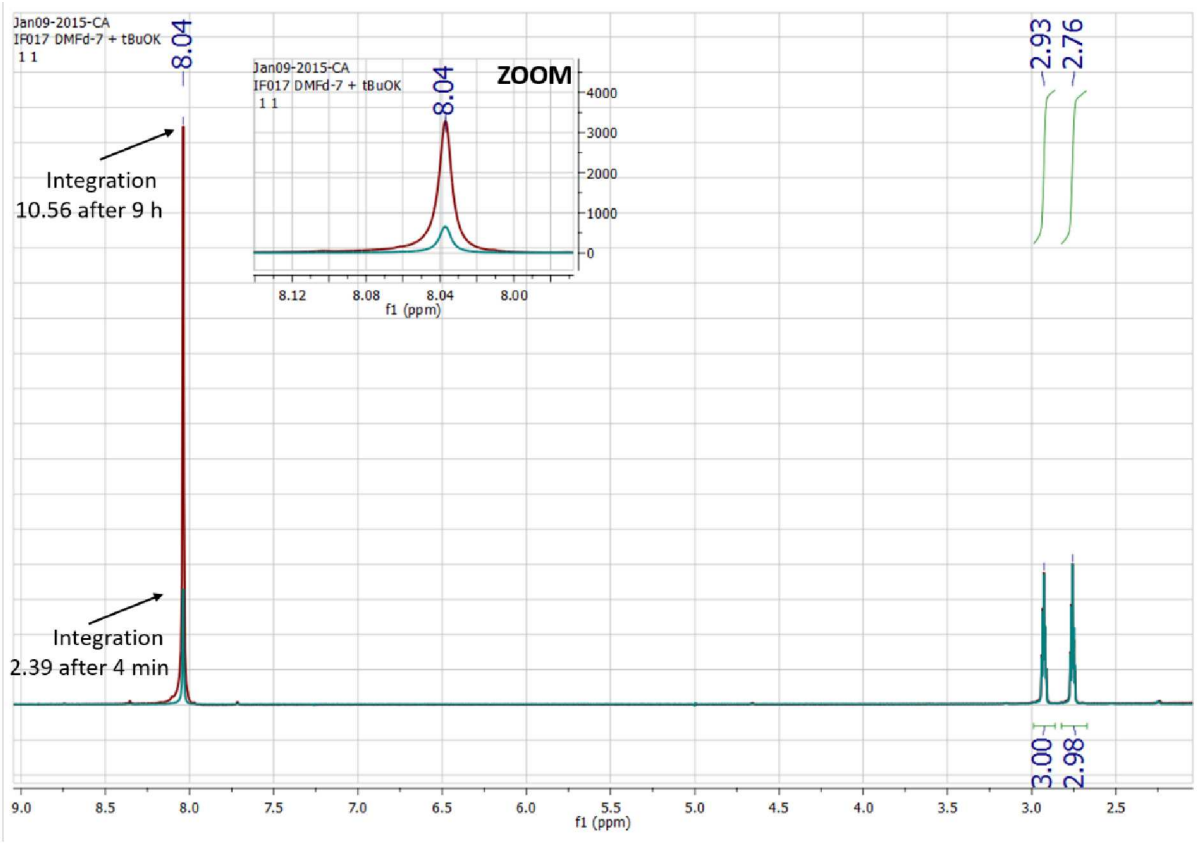

Figure 2.37- ^{1}H NMR after 4 min (in red) and after 9 h (in blue) of a solution of *t*BuOK in DMF-d_7. The CH_3 proton signal integration was calibrated to 3.0.

On the ^{13}C NMR spectrum, the triplet for the carbon bearing the formamide deuterium turned into a singlet illustrating the exchange of the deuterium with a proton from water promoted by the presence of the base (Figure 2.39).

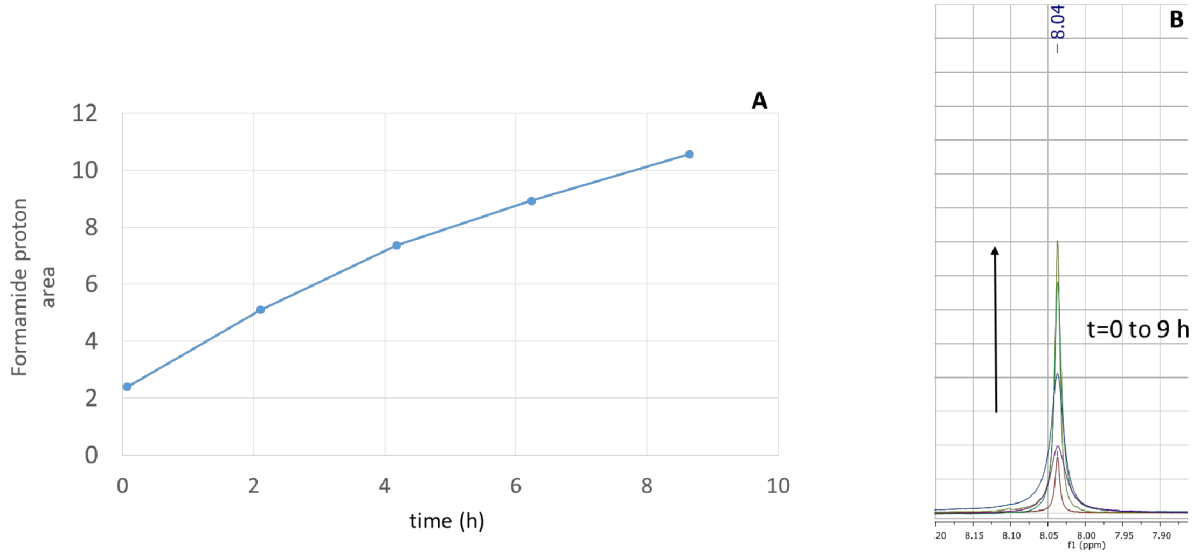

Figure 2.38 - Evolution of the formamide proton integration with time. A: Representation of the ^{1}H NMR integration as a function of time. B: superimposed ^{1}H NMR spectra of the formamide proton signal.

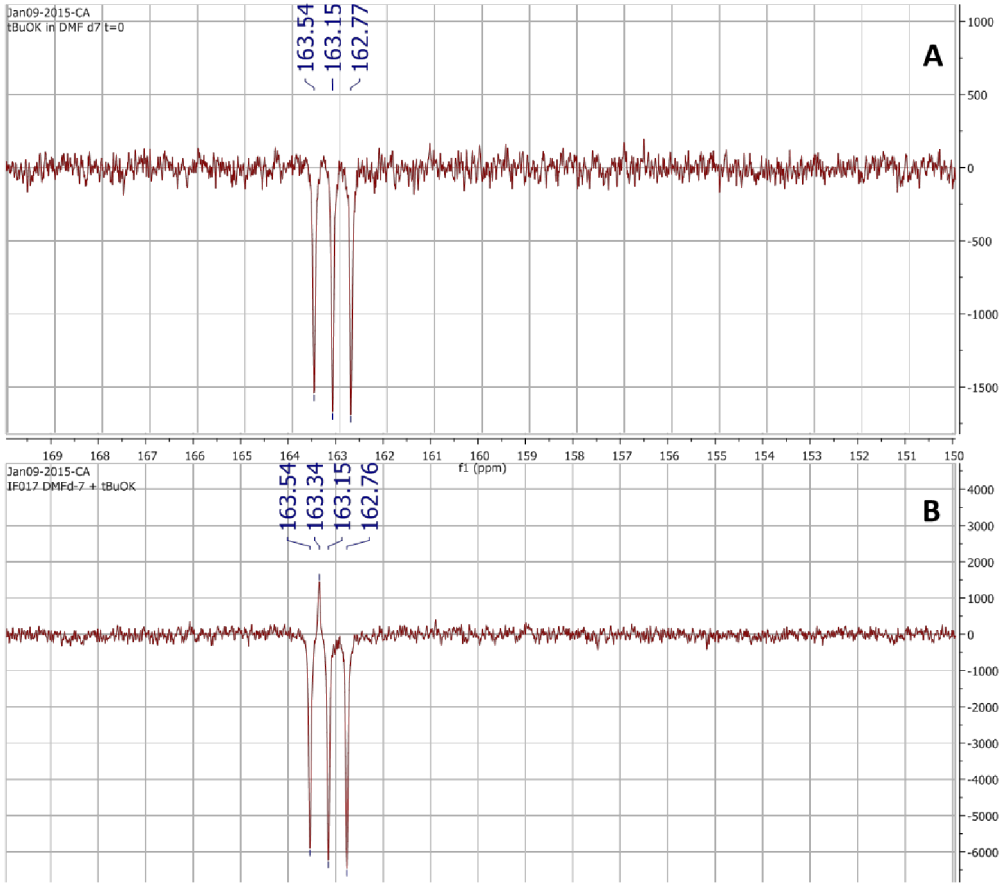

Figure 2.39- ^{13}C NMR after 20 min (**A**) and after 9 h (**B**) of a solution of *t*BuOK in DMF-d_7.

Importantly, in the absence of base, no modification of the initial signal was observed by ^{1}H or ^{13}C NMR. In the presence of *t*BuOK, even after prolonged reaction times, no dimerization product of DMF was detected by NMR. It is noteworthy that no proton exchange was observed after 12 hours under the same conditions when *t*BuONa was used, which might be due to the lower solubility of this base.

These experimental observations confirmed the computational results, and the whole mechanism was more finely described using DFT calculations, with the M062X functional.

Computational results for the deprotonation of DMF

The reaction paths were computed in the absence and in the presence of the cation (K^+ or Li^+) to understand its role (Figure 2.40). Though the following results reported are neglecting Basis Set Superposition Error (BSSE), the latter was evaluated using Counterpoise method and the values found were always below 1.1 kcal.mol^{-1}, as presented in the preliminary results.

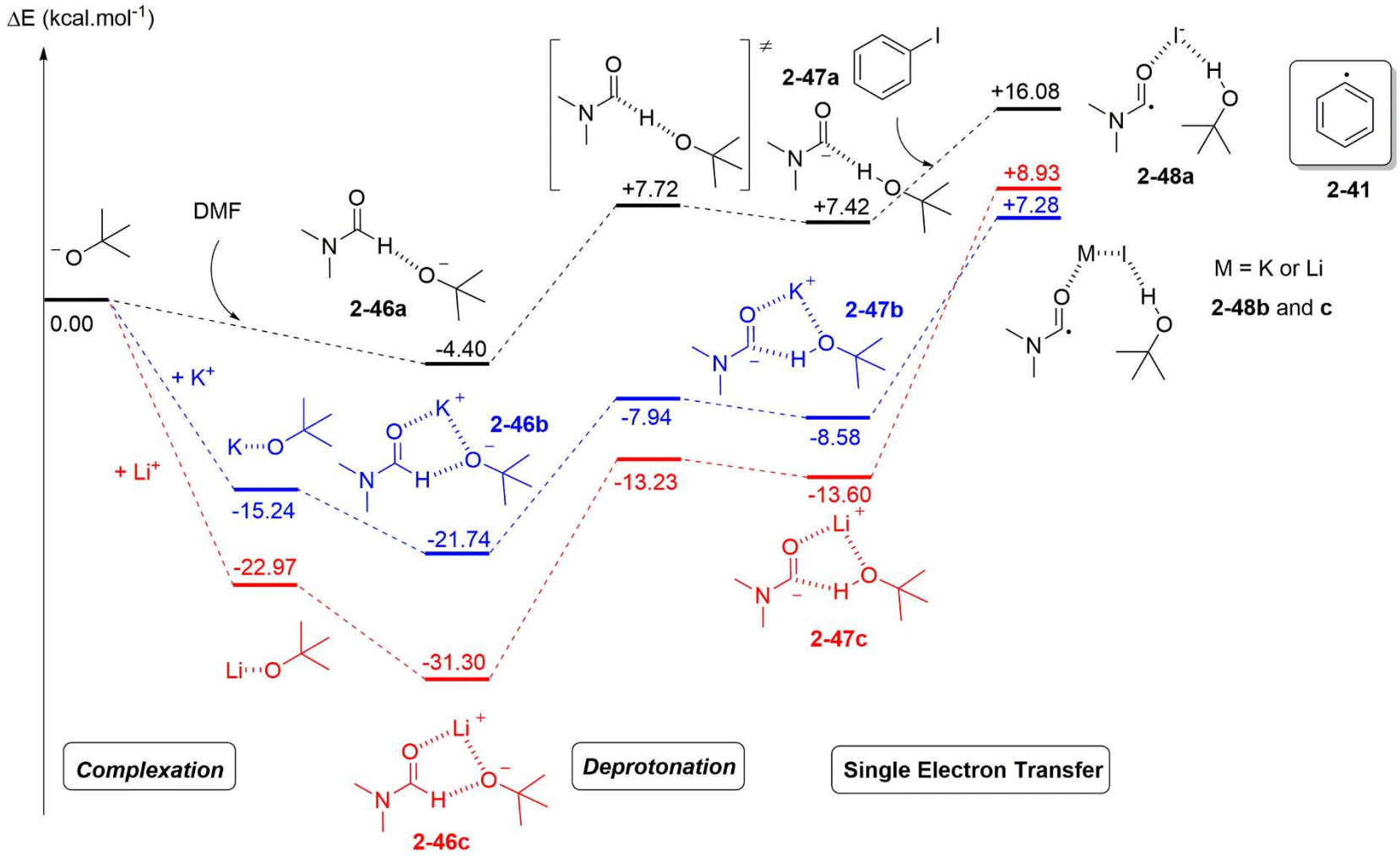

Figure 2.40 - Mechanism of the initiation by deprotonation of the solvent. Electronic energies in kcal.mol^{-1}

DMF and tBuO$^-$ are able to form a stable intermediate **2-46a** owing to hydrogen bonding. (ΔE = -4.40 kcal.mol^{-1}). However, the presence of a cation leads to much more stable complexes: ΔE = -21.74 kcal.mol^{-1} for **2-46b** with K^+ and ΔE = -31.30 kcal.mol^{-1} for **2-46c** with Li^+. Successive deprotonation is then achievable with a reasonably low activation barrier: E_a = 12.12 kcal.mol^{-1} (no cation), E_a = 13.80 kcal.mol^{-1} (K^+), E_a = 18.07 kcal.mol^{-1} (Li^+). In all cases, the computed transition state is very close in energy to the product of the reaction, a carbamoyl anion stabilized by *tert*-butanol through hydrogen bonding (**2-47a**, **b** and **c**).

Overall, the computed reaction barriers are consistent with the experimental conditions and clearly show the synergistic role played by the base and the solvent in the initiation process.

Apart from these three distinct pathways, an equilibrium can be envisaged between the intermediates with and without the stabilization by a cation, the deprotonation being easier for the latter. This exchange is more favorable for K^+ than for Li^+ because of the higher dissociation energy required for Li^+.

After the deprotonation, the electron-rich carbamoyl anions **2-47a**, **b** and **c** can react with iodobenzene through a SET mechanism to form the corresponding benzene radical **2-41**. Calculations demonstrated that the radical anion of iodobenzene dissociated spontaneously to the corresponding iodide anion and benzene radical.

The variation of the total energy associated with this SET process is computed to be higher in the presence of K^+ (ΔE = 15.86 kcal.mol^{-1}) and Li^+ (ΔE = 22.53 kcal.mol^{-1}) than in the absence of a cation (ΔE = 8.66 kcal.mol^{-1}). This step represents the rate-determining step of the reaction. This allows to explain why the reaction is more favorable using tBuOK instead of tBuOLi.

These values (ΔE = 8.66 kcal.mol^{-1} in the absence of cation, and ΔE = 15.86 kcal.mol^{-1} in the presence of K^+), are much smaller than the one computed with other reducing species in the previous section.

Table 2.9 reports the reaction energies for the complexation and the deprotonation described in Figure 2.40.

Table 2.9 – Computed reaction energies for the deprotonation of the solvent (in kcal.mol^{-1})

	Energy ΔE			**Free energy ΔG**			**Enthalpy ΔH**		
	No cation	K+	Li+	No cation	K+	Li+	No cation	K+	Li+
Complexation	- 4.40	- 21.74	- 31.30	+ 7.86	- 3.64	- 11.10	- 2.92	- 19.64	- 28.54
Ea deprotonation	+ 12.12	+ 13.80	+ 18.07	+ 8.34	+ 10.21	+ 15.76	+ 8.30	+ 9.88	+ 14.54
ΔE deprotonation	+ 11.82	+ 13.16	+ 17.70	+ 8.67	+ 12.44	+ 17.59	+ 10.21	+ 11.83	+ 16.56

The SET step was computed in two different ways: with the stabilizing interaction between the cation M (M = K^+ or Li^+), iodide and the radical from DMF (**2-48)** as depicted in Figure 2.40, and without this interaction and the formation of **2-49** and the MI salt instead. Both results are detailed in Table 2.10.

Table 2.10 – Computed reaction energies for the electron transfer from **2-47** to iodobenzene (in kcal.mol^{-1})

	Energy ΔE			**Free energy ΔG**			**Enthalpy ΔH**		
	No cation	K+	Li+	No cation	K+	Li+	No cation	K+	Li+
Stabilization by MI	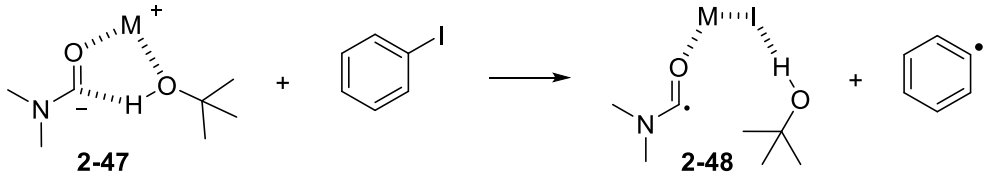 **2-47** **2-48**								
	+ 8.66	+ 15.86	+ 22.53	+ 7.76	+ 13.22	+ 20.30	+ 10.46	+ 17.10	+ 23.56
No stabilization	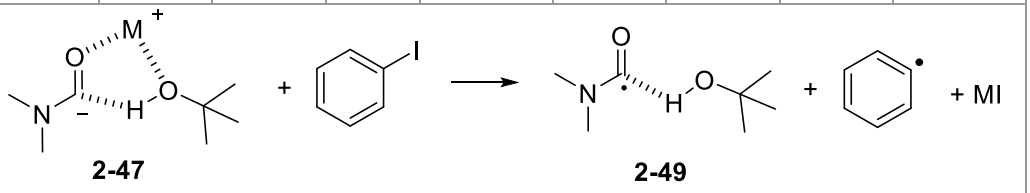 **2-47** **2-49**								
	+ 12.10	+ 22.91	+ 28.75	+ 3.51	+ 10.01	+ 13.62	+ 13.82	+ 23.45	+ 28.55

Reaction energies are lower when the radical formed is stabilized by the MI ion pair: **2-48**. Nevertheless, it is important to stress that all issues related to solubility, which can play an important role in this process, cannot be addressed by our computational approach. Owing to the difficulty associated with estimating the energy of formation of LiI and KI in solution using the current theoretical approach, the computed energy values associated with the SET

elementary step should be considered as an upper boundary to the reaction energies. However, even if the SET energies are overestimated, the overall conclusions of this mechanistic study will not be affected.

From a thermodynamic point of view, the overall reaction is driven by the last steps, which are extremely favorable. Indeed, a ΔE value of – 56.57 kcal.mol^{-1} was computed for the reaction of the enolate **2-10** with the benzene radical **2-41** to form the radical anion **2-42**, which can then react (by SET) with iodobenzene (ΔE = -9.07 kcal.mol^{-1}) to yield the final product **2-11**, along with the regeneration of the benzene radical **2-41** (Figure 2.41 and Table 2.11).

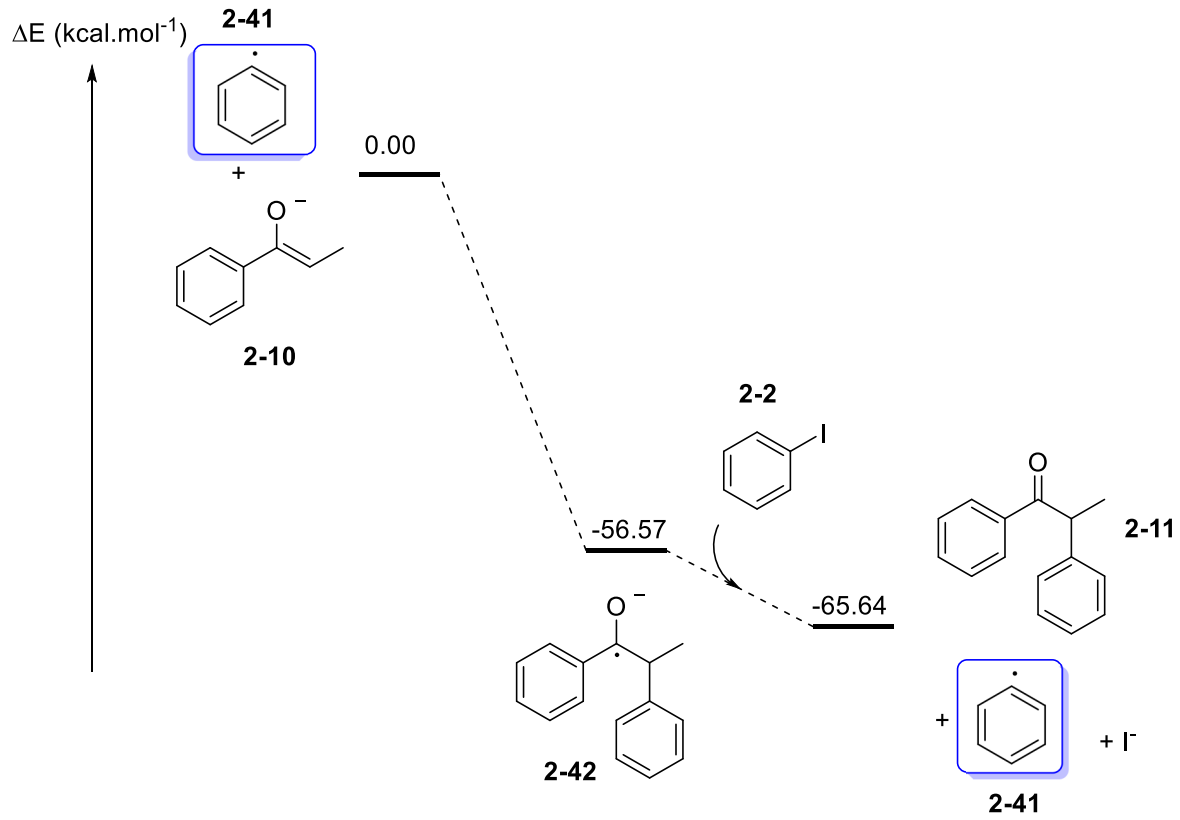

Figure 2.41 - Radical chain steps of the reaction

Table 2.11 – Computed reaction energies for the radical chain steps of the reaction (in kcal.mol^{-1})

	Electronic energy ΔE	**Free energy ΔG**	**Enthalpy ΔH**
ΔE addition	-56.57	-41.01	-54.05
ΔE SET	-9.07	-16.34	-8.27

Whereas the roles of the DMF and tBuO$^-$ are relatively clear from the computed reaction paths, it is more delicate to define the role of the cation, and to justify the peculiar efficiency observed with K^+. It is clear that the cation can help the stabilization of reaction intermediates. Indeed, the lower barrier found in the presence of potassium with respect to lithium can give some, albeit non exhaustive, information on the role of the cation. Too much stabilization, such as in the case of Li^+, can be deleterious, as it translates into too high reaction barriers (for deprotonation) or energies (SET). It is worth noting that deprotonation of DMF was only observed experimentally with *t*BuOK and not with *t*BuONa.

Cyclic voltammetry experiments support the fact that the cation promotes the SET process, as the reduction potential of iodobenzene is lowered when alkali salts are added to the reaction mixture (Figure 2.42). The cation can favor the formation of the arene radical **2-41** from iodobenzene by capturing the iodide anion.

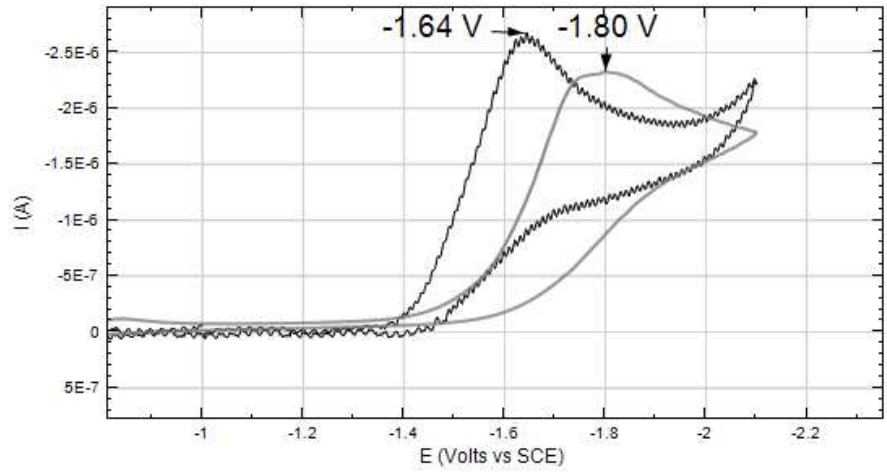

Figure 2.42- Cyclic voltammetry: reduction of PhI (2 mM) in DMF containing nBu$_4$NBF$_n$ (0.3 M) at a steady gold-disk electrode (d = 0.5 mm) at a scan rate of 0.1 V.s^{-1} at 20°C (in grey) and after addition of *t*BuOK (6 mM) (in black)

Different reactivity with ArI, ArBr and ArCl

Aryl bromides and aryl chlorides have a lower reactivity than aryl iodides in this reaction. They require higher temperatures and give lower yields (see Table 2.2). This can be explained with the SET step of the reaction. The energies associated to the SET reactions for PhI, PhBr and PhCl have been computed in absence of counterion and reported in Table 2.12.

Table 2.12 – Computed reaction energies (ΔE in kcal.mol^{-1}) calculated for X = I, Br, Cl, for the reduction of the arylhalide by SET

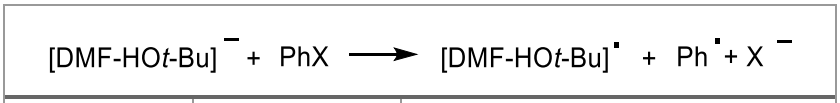

Entry	X	ΔE
1	I	+ 12,10
2	Br	+ 15,18
3	Cl	+ 20,73

These computed energies are in agreement with the standard reduction potentials of PhI, PhBr and PhCl, which are experimentally known (Table 2.13).

Table 2.13- Reduction potential of PhX measured vs SCE in DMF (0.1 M nBu_4NBF_4)[105]

Entry	ArX	E^0 (V)
1	PhI	-1,91
2	PhBr	-2,43
3	PhCl	-2,76

These values are in agreement with the experimental results (Table 2.2), showing that the reaction is more difficult with PhCl than with PhBr and more difficult with PhBr than with PhI.

We evaluated different possibilities for the initiation mechanism of the *t*BuOK/DMF promoted alpha arylation of aryl ketones. Different reducing agents (enolate, base, solvent) were envisaged both by inner- and outer-sphere electron transfer. Experiments and calculations give evidence for the deprotonation of the DMF by the base in the reaction medium, and for the ability of the generated carbamoyl anion to transfer an electron to the aryl iodide. The complete mechanism of the reaction is depicted in Figure 2.43.

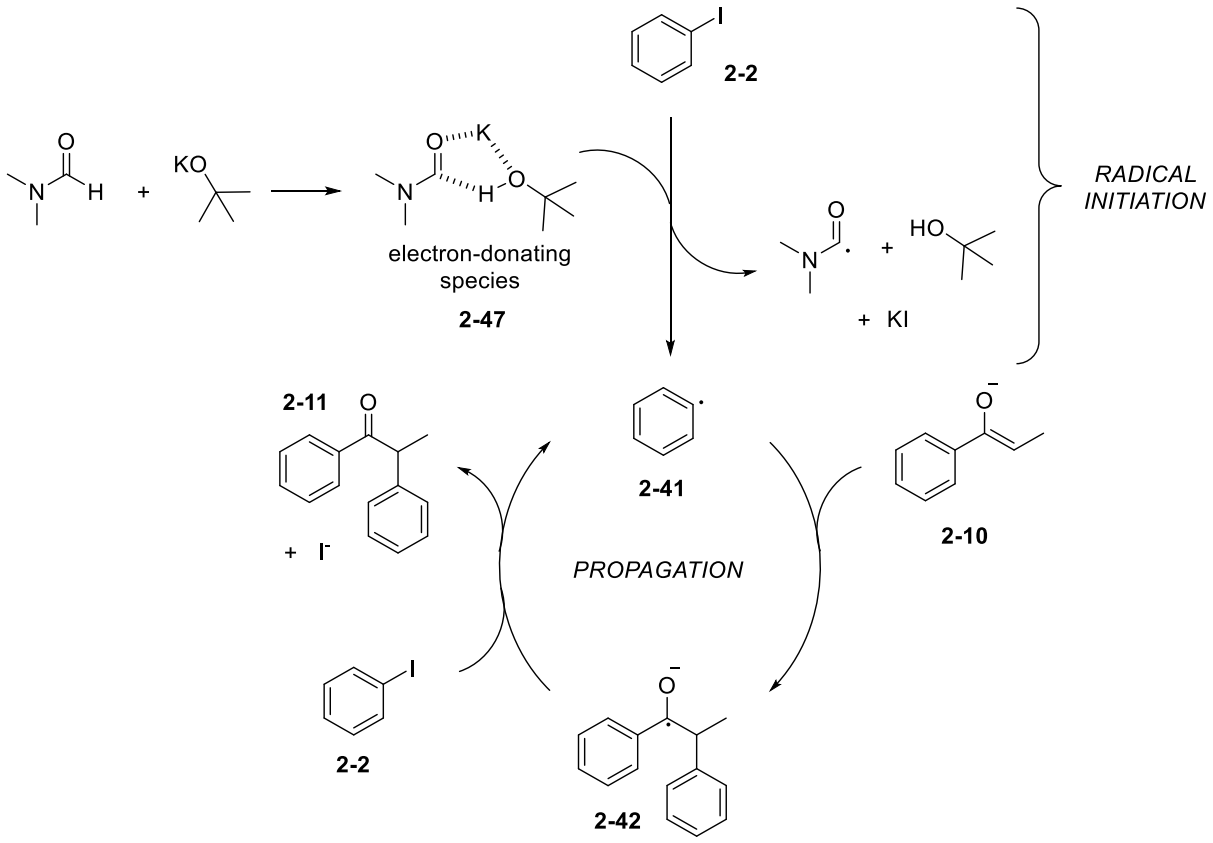

Figure 2.43 – Mechanism for the *t*BuOK/DMF promoted alpha-arylation of aryl ketones

Our results can be compared with the initiation by the formation of benzyne, as proposed by Murphy and coworkers.[96] They computed a reaction free energy for the formation of benzyne by deprotonation of iodobenzene of 18.6 kcal.mol^{-1} which is higher than the values obtained for our proposed mechanism. If this reaction can occur, calculations confirm that it is not the main reaction pathway.

Developments and precisions following our work

One year after the publication of our work[106], Murphy and coworkers investigated the same initiation mechanism[107] for a biaryl coupling reaction (Figure 2.44).

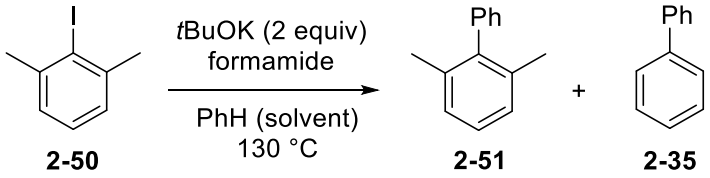

Figure 2.44 – Reactivity of formamides in a biaryl coupling reaction that uses *t*BuOK as base

Carbamoyl anions are known to act as nucleophiles,[104] and reactions of carbamoyl anions with formamides have already been reported in the literature.[108] For this reason, Murphy and coworkers suggested the attack of the carbamoyl **2-29** on a second DMF molecule, to form the enolate **2-53** that could act as an electron donor. Further deprotonation could form the dianion **2-54**, even more electron-rich (Figure 2.45). In our study, no NMR signal for the formation of such a dimeric species could be identified when *t*BuOK was dissolved in deuterated DMF-d_7.

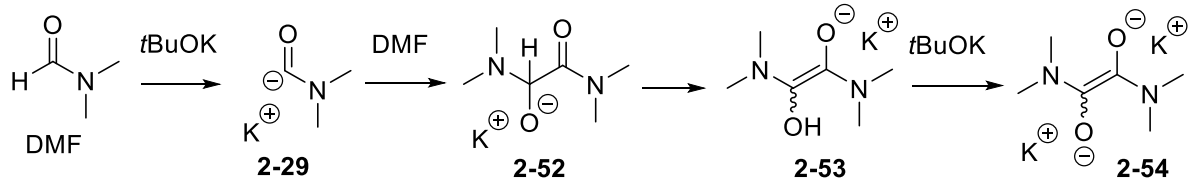

Figure 2.45 – Formation of electron donors from DMF

They compared the reactivity of DMF, and of the diformamides **2-55** and **2-58** with the following hypothesis in mind: if the carbamoyl anion **2-29** is the electron donor, **2-55** and **2-58** should exhibit twice the activity of DMF. If the electron-transfer agent is **2-53** or **2-54** when DMF is used, **2-55** should exhibit more than twice the activity of DMF, because of the easier intramolecular reaction to form the electron donor. **2-58** should work even better because of its restricted conformation (Figure 2.46). This is what they observed, as reported in Table 2.14.

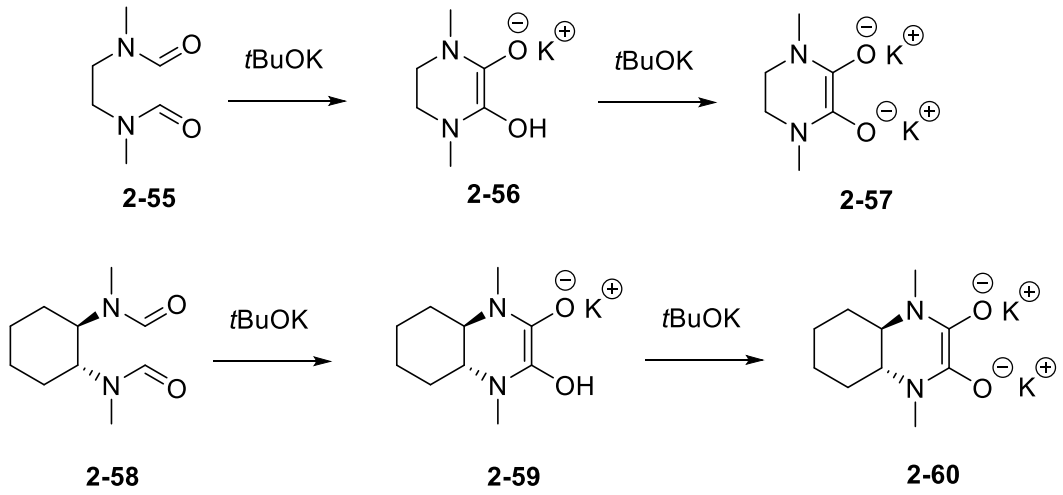

Figure 2.46- Formation of electron donors from various formamides

Table 2.14 – Comparison of the reactivity of DMF and formamides in biaryl coupling reaction

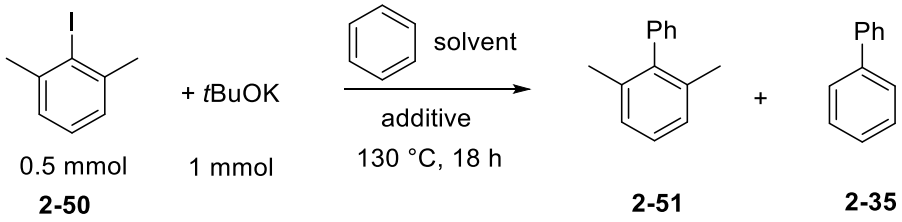

Entry	Additive	2-51 + 2-35 (%)
1	None	0.5
2	DMF (0.1 mmol)	0.6
3	**2-55** (0.05 mmol)	8.0
4	**2-58** (0.05 mmol)	16.1

They also computed the reaction energies for different electron donors in benzene: the carbamoyl anion we proposed, the dianion **2-54** (for the *Z* and *E* isomers) and **2-60**. The results are reported in Table 2.15. There is a huge difference with the results they found in DMF (entry 1), highlighting the importance of the solvent. Their results do not explain the very good activity of **2-60** (entry 5).

Table 2.15- Computed free energies for the SET between an electron donor and **2-50** (in kcal.mol^{-1})

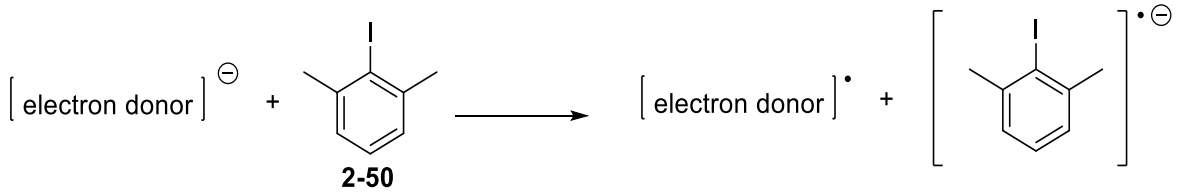

2-50

Entry	Solvent	Electron donor	Ga	ΔG
1	DMF	**2-29**	23.9	10.2
2	Benzene	**2-29**	51.9	49.0
3	Benzene	**2-54** (*Z*)	30.2	18.5
4	Benzene	**2-54** (*E*)	23.6	8.7
5	Benzene	**2-60**	28.1	16.0

In the study by Murphy and coworkers, the reactions are performed in benzene, and not in DMF, which is only present in small amounts, as an additive. This is major difference with our arylation of enolates. The computed reaction energies are in the same range as ours (ΔG around 10 kcal.mol^{-1}), and do not really show an easier electron transfer with the dianion of DMF. Moreover, no experimental evidence is given to support the formation of the dimeric species **2-54** and the reaction studied by Murphy is an aryl-aryl coupling, proceeding at higher temperatures than our arylation of enolates. Overall, this study provides interesting results that are complementary to ours, and does not contradict our conclusions about an initiation relying on the deprotonation of DMF.

Conclusion

In this chapter, we reported experimental and computational studies providing unambiguous evidence that DMF is an active species in the initiation step of the alpha-arylation of aryl ketones. The deprotonation of the solvent is possible under the experimental conditions, and the carbamoyl anion generated is able to promote the $S_{RN}1$ process, leading to the product.

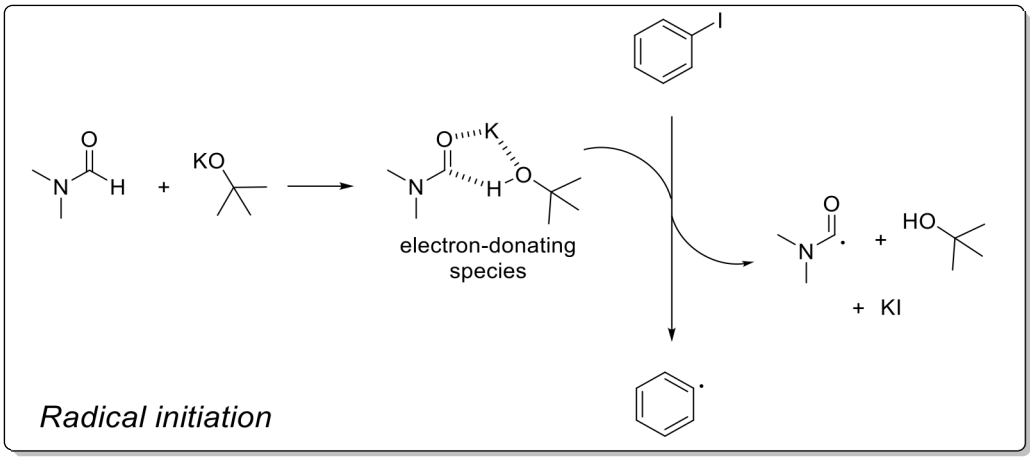

Chapter 3 – Mechanistic study of the copper-catalyzed *N*-arylation of pyrazoles with arenediazonium salts generated *in situ* from anilines under ligand-free conditions

This chapter presents the mechanistic study of a copper-catalyzed C-N bond formation between an aryl group and a nitrogen heterocycle. This reaction involves arenediazonium salts generated *in situ* from anilines. After a brief presentation of the reaction, an overview of the literature is given, regarding the use of arenediazonium salts and their reactivity in the absence and in the presence of transition metal catalysts.

The mechanism of the reaction was investigated using mainly ^{19}F NMR and DFT calculations. A benchmark of functionals was performed to choose the most suitable methodology for our system. The results obtained prove the formation of a triazene in the reaction medium as a safe diazonium reservoir, show the antagonistic role of the acetic acid present in the reaction medium and allow to explain the difference in reactivity observed between pyrazole and imidazole.

This work was done in collaboration with the team of Dr. Marc Taillefer (ENSCM) and was published: Antagonistic effect of acetates in C-N bond formation with in situ generated diazonium salts: a combined theoretical and experimental study, I. Fabre, L. A. Perego, J. Bergès, I. Ciofini, L. Grimaud, M. Taillefer, *Eur. J. Org. Chem*, 2016, 5887-5896.

State of the art

Methodology and scope for the copper-catalyzed arylation of nitrogen heterocycles from anilines

The methodology for the copper-catalyzed *N*-arylation of pyrazoles with arenediazonium salts was developed by Dounia Toummini, Dr. Anis Tlili and Julien Bergès under the supervision of Pr. Fouad Ouazzani and Dr. Marc Taillefer and was published in 2014.[109] This is the first copper-catalyzed reaction involving nitrogen-containing nucleophiles and diazonium salts reported in the literature.

In this reaction, the arylation of pyrazole is achieved by coupling arenediazonium salts generated *in situ* from aniline using a catalytic system with copper salts. The aniline **3-1** is treated with an excess of *tert*-butylnitrite and a catalytic amount of acetic acid in methanol at 0 °C for 30 min. The diazonium salt of the aniline is expected to be formed. This solution is then added to a mixture of copper salts and pyrazole **3-2**, in methanol (Figure 3.1).

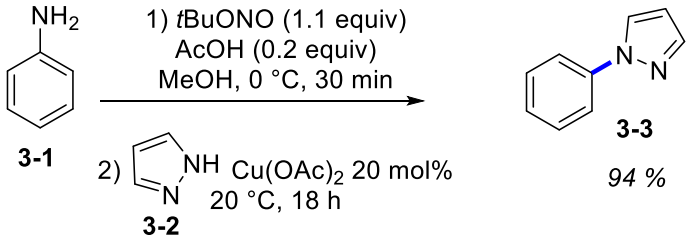

Figure 3.1 - Copper-catalyzed arylation of pyrazole with aniline

This reaction gives a quantitative yield of *N*-arylpyrazole **3-3** (94 %) after 18 h. It works with a variety of substituents. A small selection of the scope of this reaction is available in Table 3.1. Ortho substituted anilines give lower yields as illustrated by the comparison of entries 2 and 3 of Table 3.1.

Table 3.1 – Selected scope of the arylation of pyrazole with various anilines

Entry	Aniline	Yield (%)
1	**3-1** 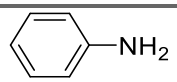	94
2	**3-4** 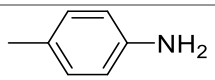	98
3	**3-5** 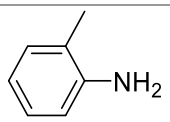	64
4	**3-6** 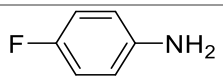	90

Various copper sources can be used, at different oxidation states: $Cu^{(0)}$, $Cu^{(I)}$, $Cu^{(II)}$ (Table 3.2). The most efficient one is $Cu(OAc)_2$ (Table 3.2, entry 4).

Table 3.2 – Performance of various copper catalysts for the arylation of pyrazole **3-2** with **3-1**

Entry	[Cu] (20 mol%)	Yield of 3-3 (%)
1	Cu	78
2	CuI	50
3	CuOAc	22
4	$Cu(OAc)_2$	94

The arylation of other nitrogen heterocycles, in particular imidazole derivatives, is less efficient in these conditions (42 % of **3-8** obtained with the imidazole **3-7**). Achieving good yields of **3-8** requires a two steps procedure with the presence of an additive (NBu_4I), high temperatures (120 °C instead of rt), and the addition of two equivalents of base (Figure 3.2).

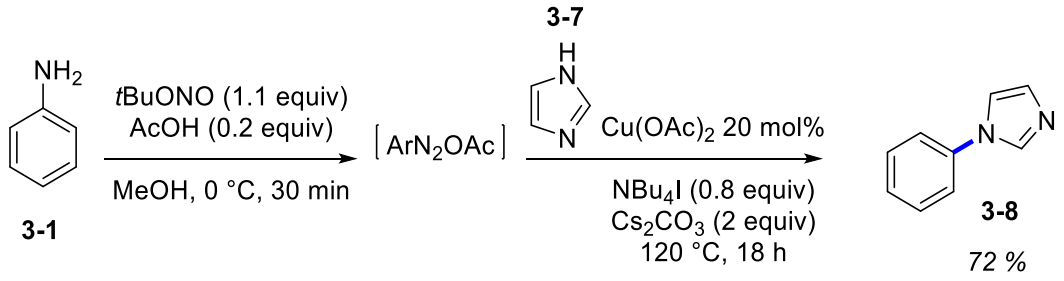

Figure 3.2 – Optimized conditions for the copper-catalyzed arylation of imidazole with aniline

The reaction in these different conditions may involve the conversion of the arenediazonium in aryl iodide, followed by the reaction with the imidazole catalyzed by copper. This different mechanism will not be studied in this chapter, but the difference in reactivity observed between both heterocycles will be discussed during the mechanistic study.

Preliminary mechanistic experiments showed that in the absence of copper, the *N*-arylheterocycles are not formed, ruling out uncatalyzed pathways such as aromatic nucleophilic substitution (S_NAr)[110] or $S_{RN}1$.[55] The reaction is regioselective with substituted anilines which also rules out elimination-addition mechanisms via arynes intermediates.[111] In the presence of radical scavengers such as TEMPO or Galvinoxyl, the formation of aryl pyrazoles is not inhibited. A copper-catalyzed pathway involving the formation of radicals seems unlikely, and this will be discussed more in details during the mechanistic study.

Arenediazonium salts as an alternative to aryl halides

In the reaction presented above, an arenediazonium salt is generated in situ from the aniline.

Preparation of arenediazonium salts

Arenediazonium salts constitute a potential alternative to aryl halides as starting materials and have been used for many years.[112] They are very reactive electrophiles displaying various reactivities, from free radical to organometallic synthesis. These compounds exhibit several interesting features; they are prepared from widely available and inexpensive aniline derivatives, they often react under very mild reaction conditions without any additional bases or additives, and the leaving group (N_2) is intert towards the reaction mixtures. They can be

prepared in water using sodium nitrite and a strong acid, or in organic solvents using organic nitrite. The mechanism of their formation is depicted in Figure 3.3. The acid chosen determines the counterion of the diazonium and its reactivity.

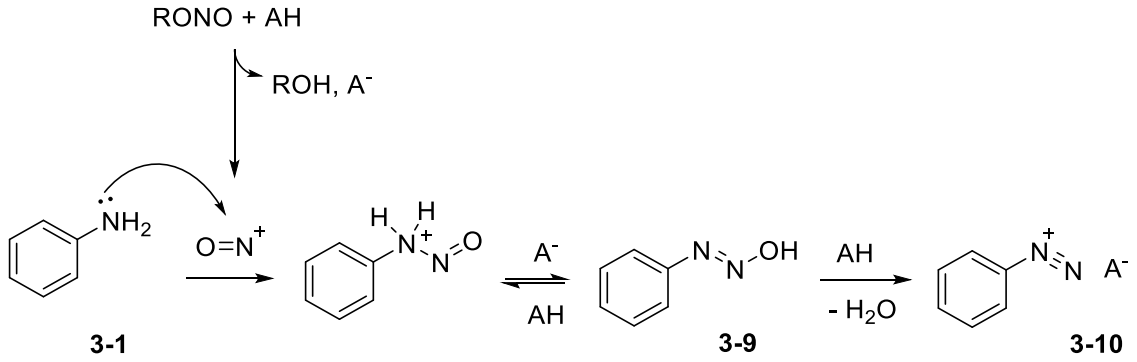

Figure 3.3 – General mechanism of formation of arenediazonium salts

Reactivivty of arenediazonium salts without catalysts

Different types of reactivity of arenediazonium salts in the absence of catalyst are depicted in Figure 3.4. The N_2 group is labile and can be removed during the reaction. Thermal elimination of nitrogen is possible with BF_4^- as counterion and allows the formation of arylfluoride, known as the Balz-Schiemann reaction.[113] The Gomberg-Bachmann reaction occurs in the presence of a benzene derivative in basic medium, and the aryl moiety replaces nitrogen.[114]

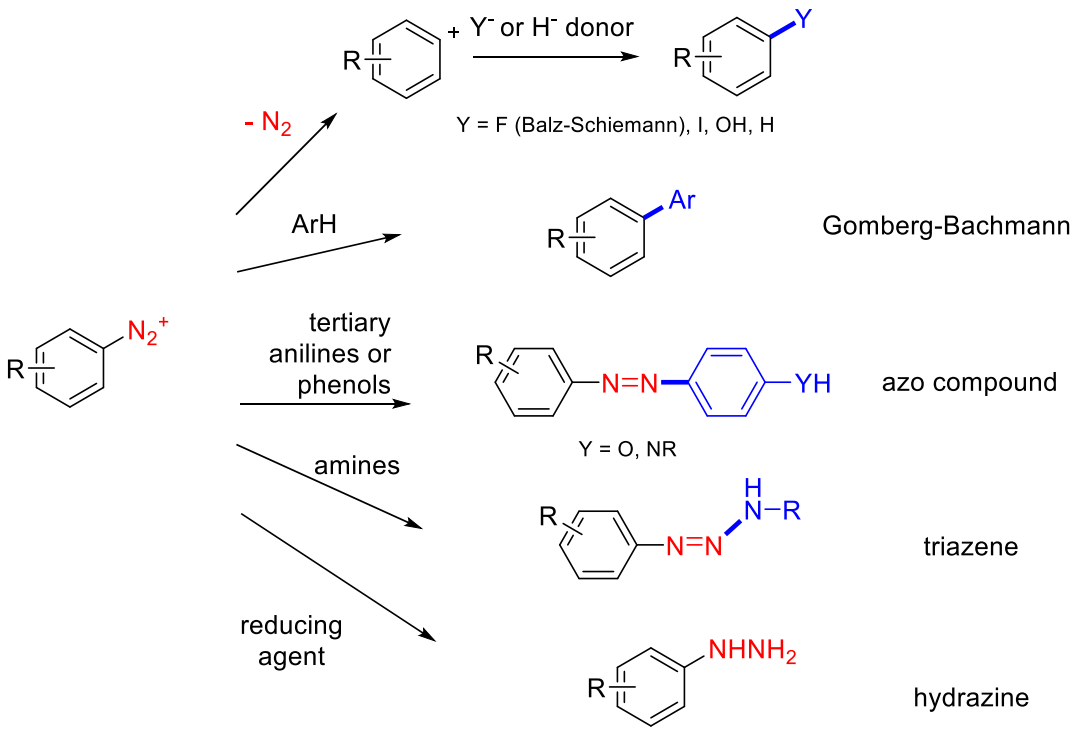

Figure 3.4 – Reactivity of arenediazonium salts in the absence of catalyst

In some cases, the N_2 group is maintained during the reaction. The coupling of arenediazonium with highly nucleophilic tertiary anilines[115] or phenolate[116] can form azo compounds that are used for commercial dyes.[117] The addition of free amines on diazoniums forms triazenes.[118] Some reducing agents, for example Na_2SO_3, retain the N-N bond to afford aryl hydrazines.[119]

Arenediazonium salts can be reduced by alcoholic solvents. Dediazoniation via a homolytic pathway can happen in neutral,[120–124] basic[125–128] or acidic[129–135] media, in the presence or not of water. Previous work by DeTar et al.[125,126,129] showed that it is favored by the presence of acetate in methanol, resulting in the formation of arene and formaldehyde. Some studies[125] also suggest a reaction of the acetate on the diazonium to form a covalent bond before radicals formation with release of nitrogen.

A proposed radical mechanism for the homolytic reaction of arenediazonium ions with methanol, with the formation of arene and formaldehyde[135] is detailed in equations (3.1) to (3.4):

$$ArN_2^+ + MeOH \longleftrightarrow Ar - N = NOMe + H^+ \qquad (3.1)$$

$$Ar - N = NOMe \longrightarrow Ar^{\cdot} + MeO^{\cdot} + N_2 \quad (3.2)$$

$$Ar^{\cdot} + MeOH \longrightarrow ArH + {}^{\cdot}CH_2OH \quad (3.3)$$

$$2\ {}^{\cdot}CH_2OH \longrightarrow CH_3OH + CH_2O \quad (3.4)$$

Reactivity of arenediazonium salts with transition metal catalysts

Arenediazonium salts can also react via non-radical pathways, with transition metal catalysis. They are highly attractive coupling partners that have been used extensively in palladium-catalyzed Heck, Suzuki–Miyaura, Stille and carbonylative cross-coupling reactions (Figure 3.5).[136–138] Some reactions involving arenediazonium salts and palladium catalysts are used in industrial processes,[139] showing their attractiveness.

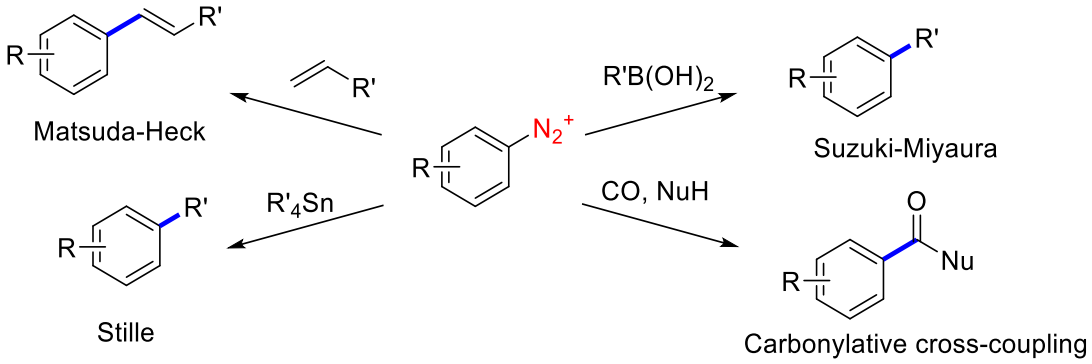

Figure 3.5 – Reactivity of arenediazonium salts with palladium catalysts

Some recent mechanistic studies evidenced the non-radical nature of reactions with diazonium salts involving transition metals: Shi and coworkers studied the gold-catalyzed C(sp)–C(sp^2) and C(sp^2)–C(sp^2) cross-coupling reactions using preformed diazonium salts.[6] They ruled out a radical mechanism based on radical-clock experiments. NMR and ESI-MS experiments allowed them to evidence the complexation of the diazonium on $Au^{(I)}$ and to propose a $Au^{(I)}/Au^{(III)}$ catalytic cycle (Figure 3.6).

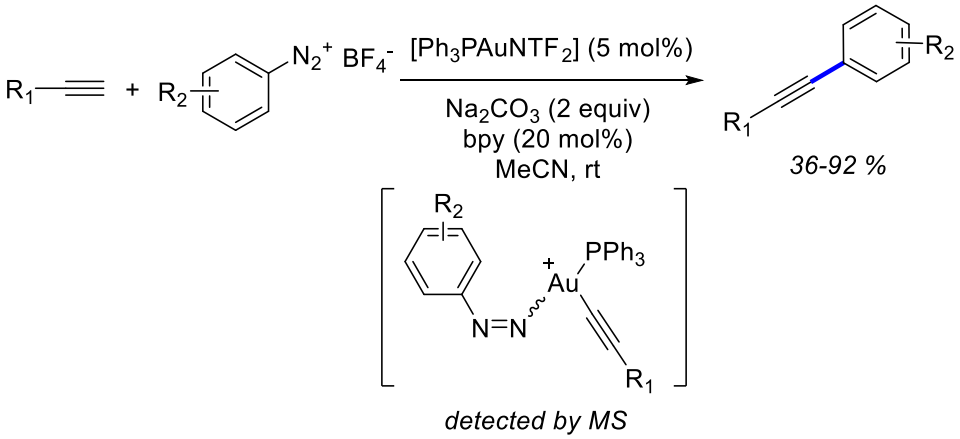

Figure 3.6 – Ligand-assisted gold-catalyzed cross-coupling with arenediazonium salts

Shin and coworkers reported the C-H arylation of arenes and alkenes using preformed diazonium salts.[140] Relying on DFT calculations, they proposed an $Ir^{(III)}/Ir^{(V)}$ catalytic cycle (Figure 3.7).

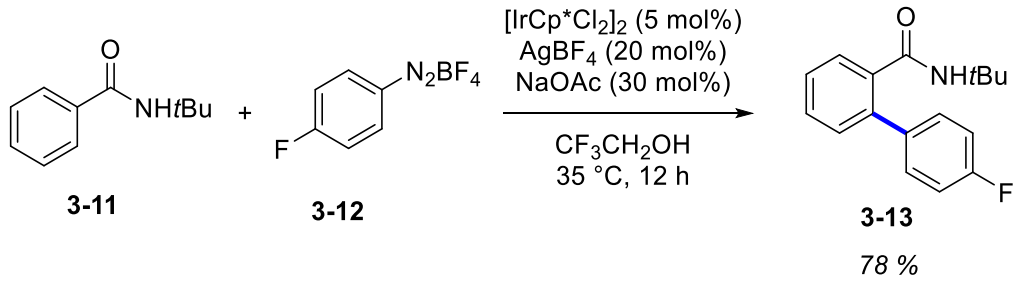

Figure 3.7 – Iridium-catalyzed C-H arylation of arenes with arenediazonium salts

Working under safer conditions with diazonium salts

Unfortunately, the leaving group ability of the diazonium function, giving N_2 release, is a major safety issue. Indeed, arenediazonium salts are able to undergo spontaneous and violent decomposition, potentially leading to explosions. The need to isolate and to dry them before using them limits their utility and the scalability of the reactions. Different methods allow to work under safer conditions, with no need of isolation of diazonium species. These methods involve the *in situ* generation of diazonium salts (with catalytic or stoichiometric amounts of acid) from anilines or from acetanilides (Figure 3.8),[141] the use of triazenes as latent diazonium salts (Figure 3.9),[142] and reactions in continuous flow.[143] These alternatives were mainly explored for palladium catalyzed reactions.[144]

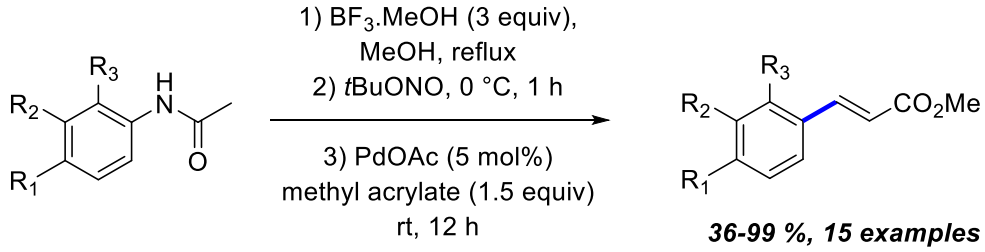

Figure 3.8 – Palladium-catalyzed C-C bond formation with acetanilides

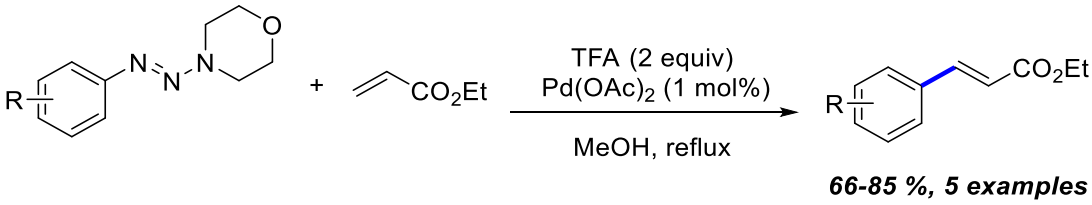

Figure 3.9 – Heck reaction on aryltriazenes

If a catalytic amount of acid is used for the *in situ* generation of diazonium salts, there is no need for their isolation, and, more importantly, they are only present in substoichiometric amount in the reaction medium. This allows to avoid hazard issues and to have a better control over the selectivity of the reaction by limiting possible parallel reactions. This is the strategy successfully developed by Felpin and coworkers for the Heck-Matsuda reaction with palladium (Figure 3.10).[145–147]

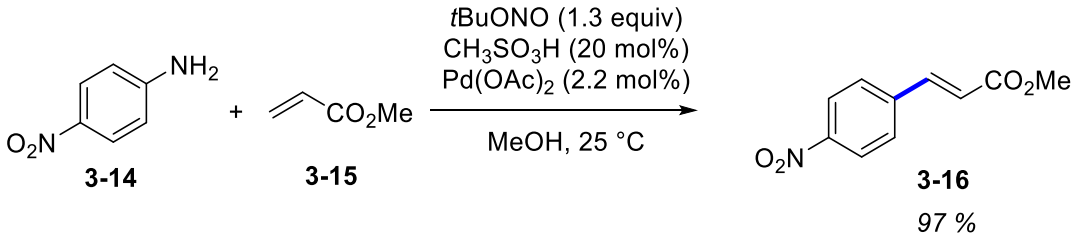

Figure 3.10 - Heck-Matsuda reaction with substoichiometric use of arenediazonium salts

Based on DFT calculations, Sotiropoulos and Felpin[146] proposed a $Pd^{(0)}/Pd^{(II)}$ catalytic cycle for this reaction. The mechanism is depicted in Figure 3.11.

Methanesulfonic acid, present in catalytic amount, allows to form a small amount of diazonium salt **3-17**. Oxidative addition of the diazonium on $Pd^{(0)}$ forms a $Pd^{(II)}$ complex **3-18** bearing the aryl group. Then the olefin inserts in the metal-carbon bond to form **3-19** and β-elimination forms the product **3-16**, regenerating both the $Pd^{(0)}$ catalyst and methanesulfonic acid. The reaction thus proceeds via a double catalytic cycle.

It is noteworthy that in the optimization studies for this reaction, using 4-bromoaniline, led to the formation of triazene due to the coexistence of the diazonium salt in catalytic amount with the unreacted free aniline. The formation of the triazene was not reversible in the experimental conditions, thus inhibiting the reaction. To overcome this issue, a slow addition of the aniline over 24 h was performed.

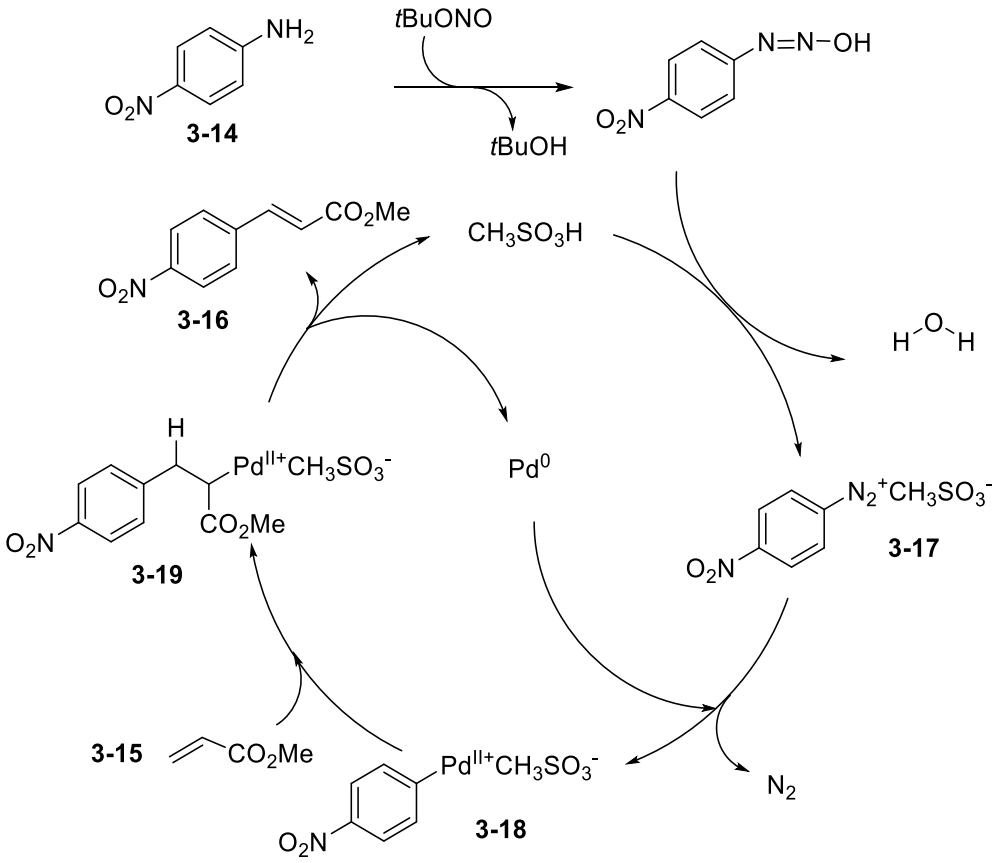

Figure 3.11 – Mechanism for the Heck-Matsuda reaction with substoichiometric use of arenediazonium salts *via* a double catalytic cycle

Reactivity of arenediazonium salts with copper catalysts

In the presence of $Cu^{(I)}$, the reactivity of arenediazonium salts is different from their reactivity with other transition metals. Elimination of one nitrogen molecule is frequently observed by SET to the arenediazonium.

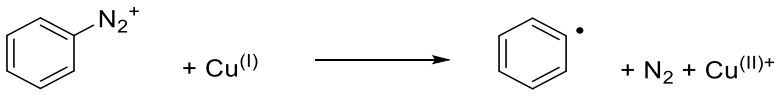

Figure 3.12 – Formation of aryl radical from arenediazonium in the presence of $Cu^{(I)}$

The aryl radical formed can then react with various nucleophiles (Sandmeyer reaction[148]) or with olefins (Meerwein reaction[149]) (Figure 3.13).

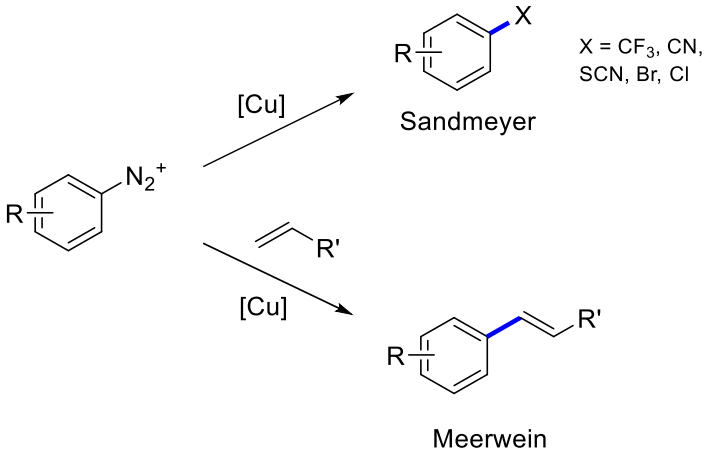

Figure 3.13 – Reactivity of arenediazonium salts in the Sandmeyer and Meerwein reactions

The Sandmeyer copper-mediated reaction

The first reaction of arenediazonium salts with stoichiometric amounts of copper for the synthesis of aryl halides was disclosed more than a century ago by Sandmeyer.[148] The first example reported was the synthesis of arylchloride from copper chloride (Figure 3.14).

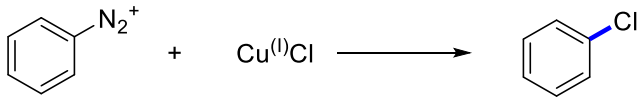

Figure 3.14 – First example of the Sandmeyer reaction

Changing the nature of the copper salt, allows various functionalization of the aromatic ring. Aryl bromide and aryl cyanides could be synthesized in the same manner.[150]

A radical mechanism is generally proposed for the Sandmeyer reaction[151–153] (Figure 3.15). $Cu^{(I)}$ reduces the diazonium to form nitrogen, an aryl radical and $Cu^{(II)}$. Then the nucleophile reacts with the aryl radical to form the product and $Cu^{(I)}$ is regenerated. The catalyst

should be able to enter a new cycle, but the first versions of the Sandmeyer reactions used stoichiometric amounts of copper.

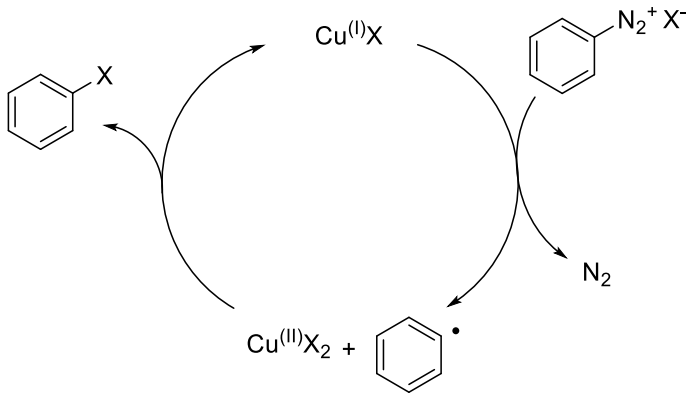

Figure 3.15 - Mechanism of the Sandmeyer reaction

The Sandmeyer copper-catalyzed reactions

The first catalytic version of the Sandmeyer reaction was described by Beletskaya et al. who reported the copper/phenanthroline catalyzed formation of aryl halides,[154] aryl nitriles[155] and aryl thiocyanates[156] under very mild conditions (Figure 3.16). All these systems use a mixture of $Cu^{(I)}$ and $Cu^{(II)}$ catalyst with 1,10-phenanthroline as ligand and the crown ether dibenzo-18-crown-6 as phase transfer co-catalyst.

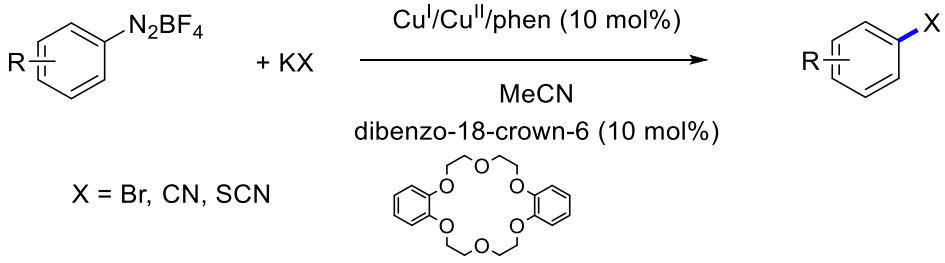

Figure 3.16 - Copper/phenanthroline catalyzed formation of aryl halides, aryl nitriles and aryl thiocyanates

The copper mediated (0.6 equivalent) trifluoromethylation and trifluoromethylthiolation of arenediazonium tetrafluoroborates have also been reported recently by Danoun and coworkers[157,158] (Figure 3.17).

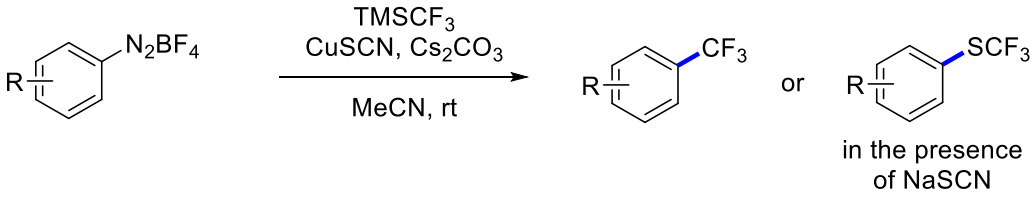

Figure 3.17 - Copper mediated trifluoromethylation and trifluoromethylthiolation of arenediazonium tetrafluoroborates

These copper-catalyzed reactions use preformed arenediazonium tetrafluoroborate salts. In all cases, a $Cu^{(I)}/Cu^{(II)}$ catalytic cycle, involving aryl radical intermediates was proposed, in accordance with the mechanism of the Sandmeyer reaction.

Copper-catalyzed arylation with *in situ* generated diazonium salts

After the successful development of safe conditions for palladium-catalyzed reactions involving diazonium salts, Felpin and coworkers reported the copper-catalyzed C-H arylation of benzoquinones[159] and pyrroles[160] (Figure 3.18) with arenediazonium salts generated *in situ* from anilines.

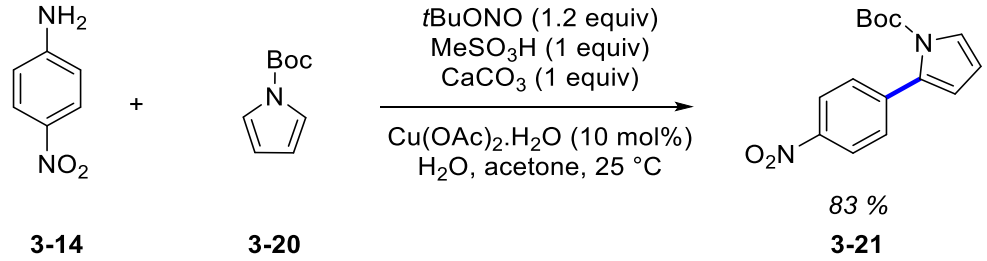

3-14 **3-20** **3-21**

Figure 3.18 – Copper-catalyzed C-H arylation of pyrroles with *in situ* generated diazonium

A free-radical pathway is proposed for the arylation of pyrroles. The $Cu^{(I)}$-catalyzed homolytic dediazoniation of the in situ generated diazonium salt **3-17** gives the corresponding aryl radical **3-22**, quickly intercepted by the pyrrole **3-20**. The radical intermediate **3-23** is oxidized by $Cu^{(II)}$ into the corresponding cation **3-24**, regenerating $Cu^{(I)}$. After deprotonation, **3-24** provides the coupling product **3-21**.

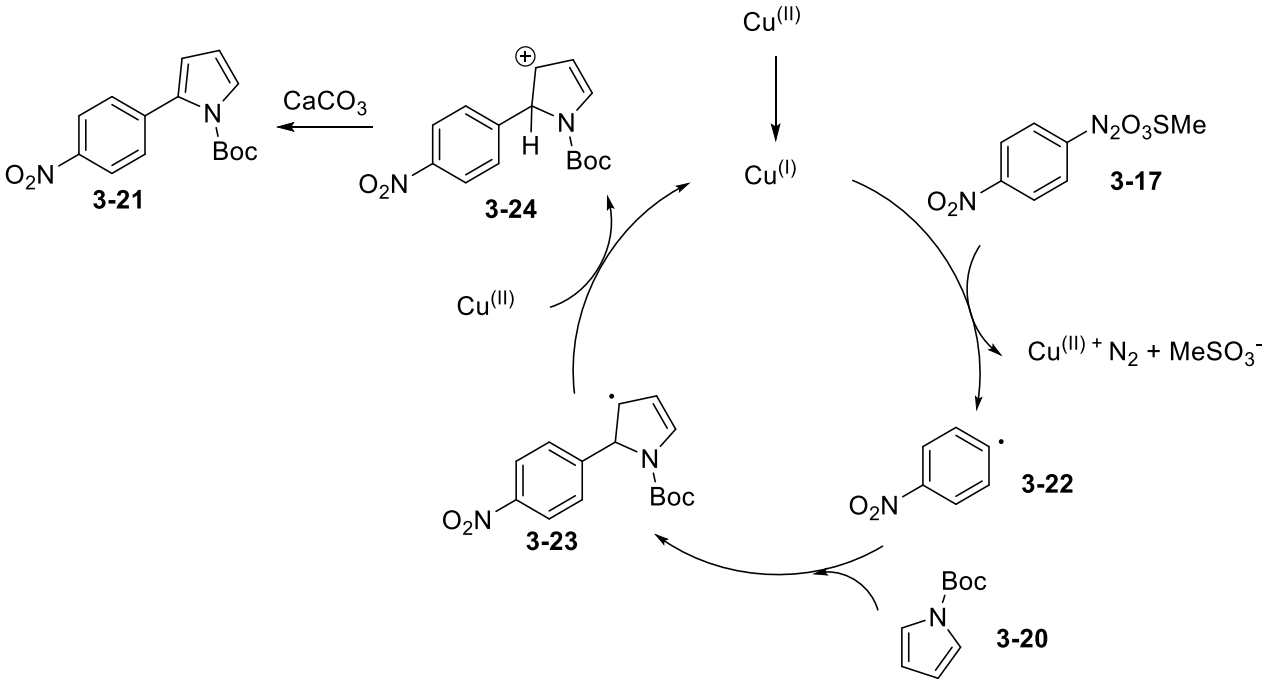

Figure 3.19 – Mechanism for the copper-catalyzed C-H arylation of pyrroles with in situ generated diazonium salts

Copper catalyzed C-N bond formation with aryl halides

The reaction studied in this chapter is the copper-catalyzed C-N bond formation using arenediazonium salts, aryl halides surrogates. The copper-mediated formation of carbon-nitrogen bond from aryl halides is known since the work of Ullman and Goldberg at the beginning of the XXth century.[161–164] Ullman reported the formation of a C-N bond between an aryl group and an aniline, starting from an aryl chloride as depicted in Figure 3.20. Goldberg reported the formation of a C-N bond with an amide using an arylbromide (Figure 3.21).

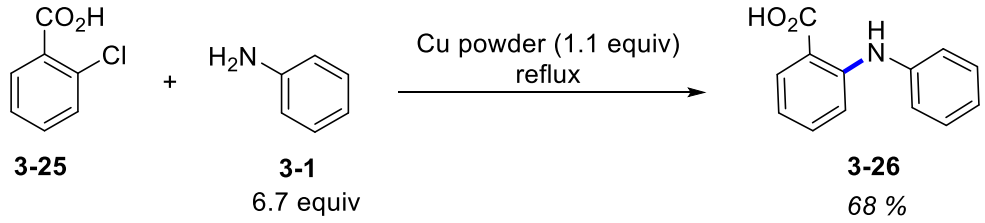

Figure 3.20 – Amination of arylchloride as reported by Ullmann in 1903[161]

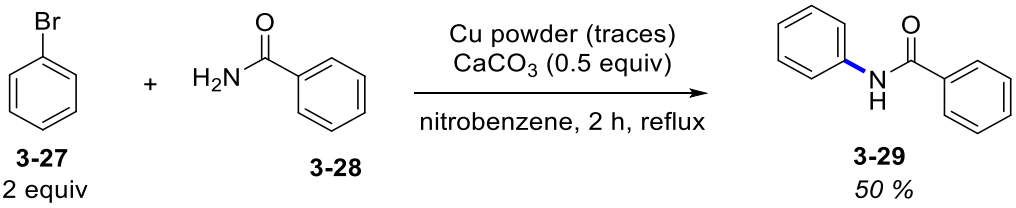

Figure 3.21 – Amidification of arylbromide as reported by Goldberg in 1906[162]

However, the need of stoichiometric amounts of copper, high temperatures (often above 200 °C) and polar solvents severely limited the synthetic potential of these reactions. Nevertheless, in comparison to other transition metals (Pd, Rd, Ru, Ni), copper has an undeniable advantage of cost and toxicity. For this reason, during the last twenty years, extensive work was done to increase the efficiency of these reactions in terms of copper loading, and to widen their scope. The use of copper-based catalytic systems allowed to overcome these drawbacks.[165–169] The main modifications relied on the use of oxygen or nitrogen coordinating ligands.

Existing DFT methods for the study of transition metal catalytic cycles

In this chapter, we use DFT calculations to study the mechanism of the copper-catalyzed *N*-arylation of pyrazoles. DFT methods, especially when used in conjugation with hybrid exchange-correlation functionals, have become powerful tools to study a large number of catalytic reactions. They provide reliable energetic, structural and electronic values of the intermediates involved at low computational cost.[170–172] In particular, DFT approaches have proven their accuracy in the mechanistic investigations of copper catalyzed C-N bond forming reactions, enabling to compare multiple reaction pathways, determine their rate limiting steps and the nature of the active catalyst.[168,173,174] Several studies were focused on Ulmann-type reactions (coupling an aryl halide and an amine or alcohol derivative). Ligand directed selectivities in *N*- versus *O*-arylation reactions could be explained with DFT methods by comparing the nucleophile formation and aryl halide activation steps.[175,176] In spite of the many successes of the method, the accuracy obtained strongly depends on the exchange-correlation functional used. This latter has to be carefully chosen, especially when transition metal are involved.

If several benchmark sets were developed in recent years to test exchange correlation functionals performances (such as atomization energies, noncovalent interactions, and

thermochemistry and kinetics[177] or excited states[178]), less extensive benchmark exists in the field of transition metal chemistry, especially in bond activation by transition metal catalysts. This field was first explored by Siegbahn and Blomberg during the eighties and nineties using as reference ab initio values.[179–181] Later, benchmark studies for DFT methodologies on catalytic reactions were made mainly for palladium-based catalysts,[182–187] while less extensive work was performed for nickel,[186] iridium,[185] platinium,[185] rhodium,[185,187] ruthenium[187] or iron[188]-based catalysts. To the best of our knowledge, an extensive analysis of the exchange-correlation functional effect on copper-catalyzed reactions is still not fully developed. In this respect, we decided to analyze the performance of a selection of representative new generation exchange and correlation functionals for the description of the C-N copper catalyzed reaction reported in this chapter. It will be detailed in the next section.

Mechanistic study of the copper-catalyzed *N*-arylation of pyrazoles from anilines

The mechanism of the copper-catalyzed *N*-arylation of pyrazoles is studied in detail in this section. We focused on understanding the double catalytic cycle, by identifying the role of the acid, the oxidation state of copper, and the nature of the complexes involved. We also explain the difference in reactivity observed between the pyrazole and the imidazole. This study leads us to a DFT benchmark of various functionals to choose the most suitable method for our system.

In the reaction (Figure 3.22), the first step is most likely the diazotization of the aniline **3-1** in the presence of *t*BuONO and acetic acid to form the corresponding diazonium acetate salt **3-30**.[189–191] The diazonium generated *in situ* could then be involved in the copper-catalyzed cross-coupling with one equivalent of pyrazole **3-2** to form the desired aryl pyrazole **3-3**.

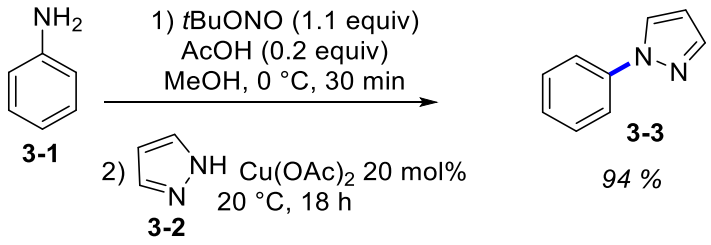

Figure 3.22 - Copper-catalyzed arylation of pyrazole with aniline

However, using a catalytic amount of acetic acid (20 mol%), the diazonium **3-30** should be present at low concentration. Therefore, the overall reaction should most probably rely on two concerted catalytic processes (Figure 3.23). The primary goal of this study will thus be to elucidate which are the active reagents and to identify the active copper catalyst.

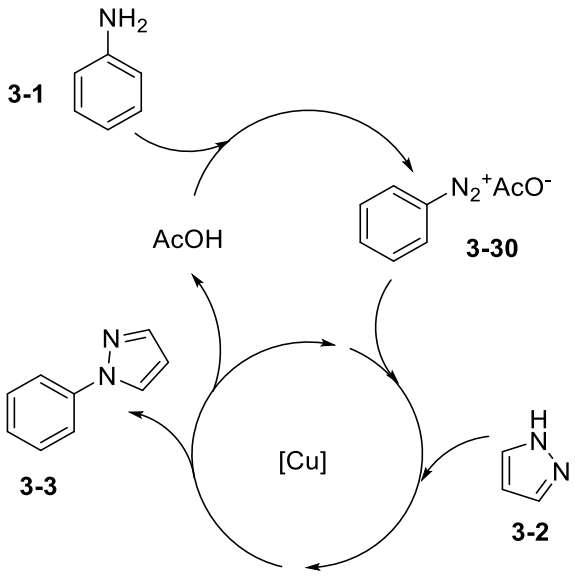

Figure 3.23 – Schematic representation of the double catalytic cycle

First step: the triazene-diazonium equilibrium modulated by acetic acid

Formation of triazene in the absence copper

Felpin and coworkers[147] showed that when using electron-rich anilines in the palladium-catalyzed arylation of olefins, triazene species were immediately formed in the reaction medium due to the coexistence of the diazonium salt and excess of aniline. The sensitivity of the triazene species toward acidic conditions (methanesulfonic acid in this case) was suspected to stop the catalytic cycle. Nevertheless, triazenes are not necessarily unreactive species and can be used as concealed diazoniums or protected amines[192–194] regenerated by acidic treatment (usually 5 % trifluoroacetic acid, weaker than $MeSO_3H$). As we suspected a similar behavior, the formation of the diazonium acetate salt was monitored by ^{19}F NMR, choosing the 4-fluoroaniline **3-6** as model substrate, both with a catalytic (standard conditions) and a stoichiometric amount of acetic acid, and with an excess of aniline (Figure 3.24).

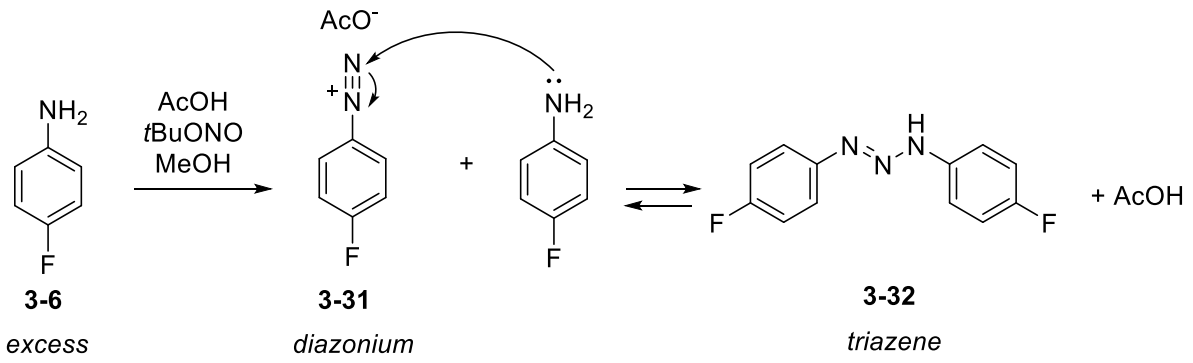

Figure 3.24 – Formation of diazonium acetate and triazene from 4-fluoroaniline as monitored by ^{19}F NMR

In all cases, the aniline was fully converted within a few hours into a single species identified as the triazene **3-32** by comparison with the NMR spectra of an authentic sample prepared independently (Figure 3.25).

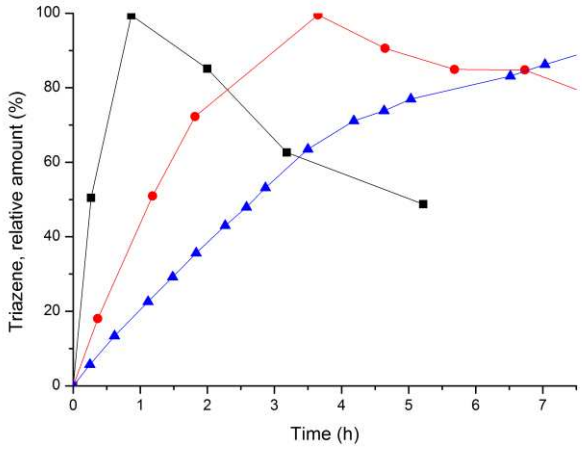

Figure 3.25 - ^{19}F NMR monitoring of the formation and decomposition of the triazene starting from 4-fluoroaniline in different conditions: 1 equiv of aniline, 0.2 equiv of AcOH, 1.1 equiv of *t*BuONO (black, ■, standard conditions); 1 equiv of aniline, 1 equiv of AcOH, 1.1 equiv of *t*BuONO (red, ●); 2.5 equiv of aniline, 1 equiv of AcOH, 1.1 equiv of *t*BuONO (blue, ▲). α,α,α-trifluorotoluene was used as internal standard. The relative amount is calculated against the limiting reactant: aniline for ■ and ●, and *t*BuONO for ▲.

This species decomposed after a few hours yielding fluorobenzene **3-33** as the main product, regenerating 4-fluoroaniline, (Figure 3.25 and Table 3.3).

Table 3.3 - ^{19}F NMR fluorobenzene yields after 5 h for the experiment in Figure 3.25

Entry	Conditions	Fluorobenzene yield (%)
1	1 equiv of aniline, 0.2 equiv of AcOH, 1.1 equiv of *t*BuONO (black, ■)	10
2	1 equiv of aniline, 1 equiv of AcOH, 1.1 equiv of *t*BuONO (red, ●)	2
3	2.5 equiv of aniline, 1 equiv of AcOH, 1.1 equiv of *t*BuONO (blue, ▲)	0

In our standard conditions (fig 1, ■**)** the triazene species can be quantitatively formed because the substoichiometric amount of acetic acid is consumed by the formation of diazonium but regenerated by the formation of triazene. The rates of both formation and decomposition of the triazene were found faster when low amounts of acetic acid were used (fig 1, ■). The weak acidity of acetic acid (pKa = 4.75 in water), allows a reasonable stability of the triazene and its formation does not stop the reaction with copper.

Reactivity of the triazene with copper under different conditions: a safe diazonium reservoir

We then explored the ability of the triazene **3-32** to react with the nucleophile **3-2** to give the corresponding coupling product. Gas chromatography (GC) analysis of the reaction between the triazene, $Cu(OAc)_2$ and pyrazole (slight excess, 1.3 equiv) in presence of a catalytic amount of acetic acid (0.5 equiv) proved the slow formation of the desired 4-fluorophenylpyrazole **3-34** along with para-fluoroaniline **3-6**, confirming the reactivity of the triazene species. 80 % of product (GC yield) were formed after 48 h at room temperature (Figure 3.26).

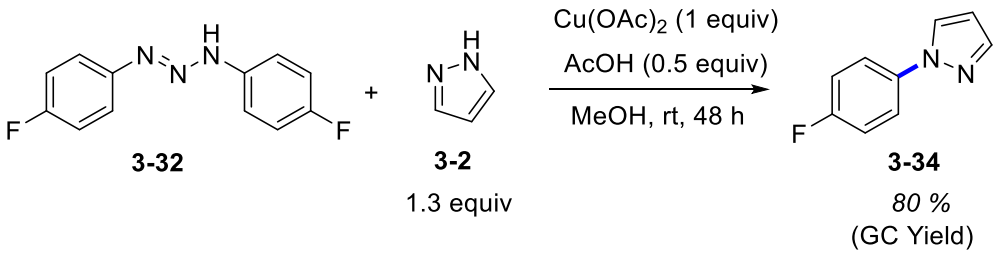

Figure 3.26 – Copper-mediated reaction between the triazene and pyrazole

This result confirms that the triazene is an efficient resting state for the diazonium species. Triazene species can form complexes with copper[193,195] and are stable towards neutral or basic conditions. To verify that the diazonium was the active species and not the triazene, we performed ^{19}F NMR kinetics of the arylation of pyrazole, starting from the triazene, in different conditions, assuming that the presence of acid favored the equilibrium shift towards the formation of the diazonium intermediate. The results are presented in Figure 3.27 and Table 3.4.

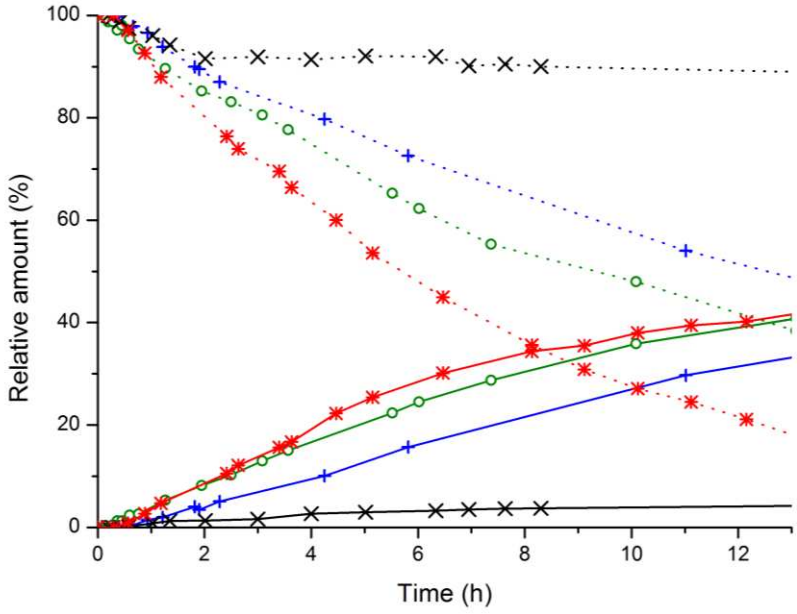

Figure 3.27 - Kinetics of the reactivity of the triazene **3-32** (1 equiv) in MeOH in presence of pyrazole (1.3 equiv) and $Cu(OAc)_2$ (1 equiv) and different additives, as monitored by ^{19}F NMR spectroscopy: 1 equiv K_2CO_3 (black, ×), no additive (blue, +), 0.5 equiv AcOH (green, ○), 1 equiv AcOH (red, *). α,α,α-trifluorotoluene was used as internal standard. Dotted decreasing curves show the consumption of the triazene **3-32**, solid increasing curves show the formation of **3-34**.

The reaction without AcOH proceeded, albeit slowly. The yield of **3-34** was 53 % after 24 hours and 70 % after 48 hours. The addition of an inorganic base (1 equiv K_2CO_3) instead of acetic acid, decreased the rate and almost shut down the reaction. Indeed, the yield was only 5 % after 48 hours of reaction.

Table 3.4 - *Para*-fluorophenyl pyrazole yields after prolonged reaction times for the experiment in Figure 3.27

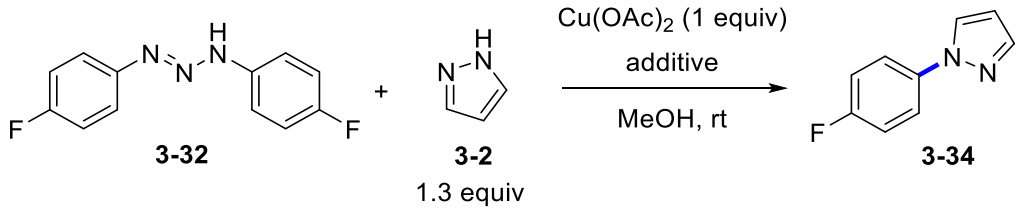

Entry	Additive	3-34 yield (%) after 24 h	3-34 yield (%) after 48 h
1	1 equiv K_2CO_3	5	5
2	No additive	53	70
3	0.5 equiv AcOH	61	80
4	1 equiv AcOH	48 (94 % conversion of pyrazole)	-

In the presence of acid (0.5 equiv or 1 equiv, to be compared with no additive), the decomposition of the triazene, and the formation of the expected **3-34** were faster. With 0.5 equivalents of AcOH, the yield was 61 % after 24 h and 80 % after 48 hours. But when 1 equivalent of AcOH is used, the yield is 48 % after 24 hours with 94 % of conversion of the triazene. This can be explained by the formation of fluorobenzene **3-33**, represented in Figure 3.28. After 12 h, almost 30 % of fluorobenzene is formed in this case. When the acidity of the reaction medium decreases, the amounts of fluorobenzene drop down, with less than 10 % after 10 h with 0.5 equivalents of AcOH or no additive, and under 5 % with K_2CO_3. These results are consistent with the hypothesis that the triazene **3-32** is in equilibrium with the diazonium **3-31** which is the active species: basic conditions prevent the regeneration of the diazonium salt and stop the reaction.

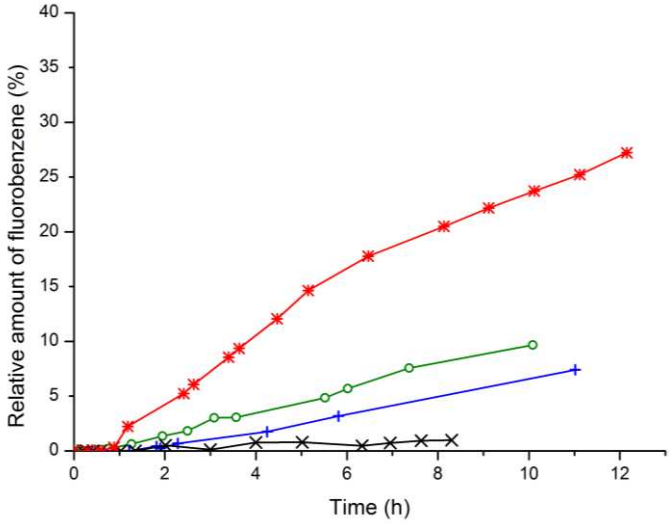

Figure 3.28 - Kinetics of the formation of fluorobenzene **3-33** under the following conditions: 0.4 M triazene in MeOH in presence of pyrazole (0.52 M) and $Cu(OAc)_2$ (0.4 M) and different additives as monitored by ^{19}F spectroscopy: 1 equiv K_2CO_3 (blue, ▲), no additive (red, ●), 0.5 equiv AcOH (black, ■), 1 equiv AcOH (green, ▼). α,α,α-trifluorotoluene was used as internal standard.

Solvent and AcOH/AcO^- influence on the decomposition of the arenediazonium

Acetic acid plays an ambivalent role as it is required to generate the active diazonium from the unreactive triazene but has a deleterious effect at high concentrations (1 equiv) by accelerating its decomposition, increasing the quantity of arene formed, and limiting the final yield (Figure 3.27 and Figure 3.28). Indeed, the amount of arene obtained allows us to explain the moderate yields of phenyl pyrazole observed.

As exposed in the previous section, diazonium salts can be reduced by alcoholic solvents, especially in the presence of acetate. As a supplementary evidence, benzyl alcohol was used as a model alcoholic solvent. The addition of *para*-fluorophenyldiazonium tetrafluoroborate and tetrabutylammonium benzoate in stoichiometric amounts showed immediate gas evolution (N_2) and formation of benzaldehyde was confirmed by both ^1H NMR and GC. ^{19}F NMR showed total conversion of the diazonium after a few minutes, with fluorobenzene as the main product (see the Appendix page 199-200). This confirms an *in situ* reduction of the diazonium salt by the alcohol, generating small amounts of radicals. Nevertheless, MeOH turned out to be the best solvent, mainly for solubility issues.

The oxidation state of the active copper species - at the frontier between radical and non-radical reactions

Kinetics under catalytic conditions starting from the aniline

In order to gain further insight into the mechanism, the kinetics of the global reaction under catalytic conditions was followed by ^{19}F NMR (see Figure 3.29).

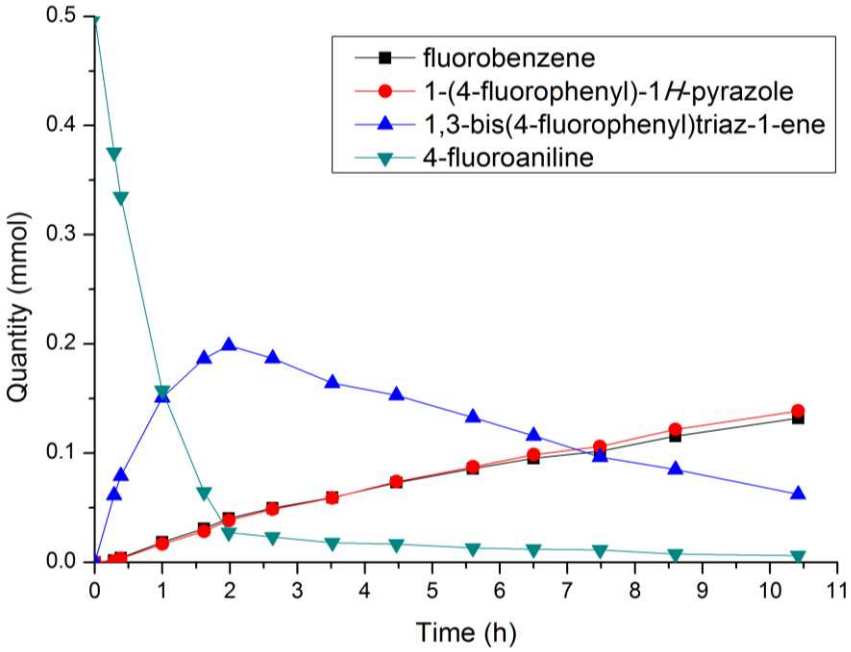

Figure 3.29 - Kinetics of the conversion of 4-fluoroaniline (0.5 mmol) in the presence of $Cu(OAc)_2$ (0.066 mmol), pyrazole (0.33 mmol), *t*BuONO (0.55 mmol), and AcOH (0.1 mmol) in MeOH (0.5 mL), as monitored by ^{19}F NMR spectroscopy. α,α,α-Trifluorotoluene was used as internal standard.

Consumption of 4-fluoroaniline **3-6** was fast from the beginning and both triazene **3-32** and 1-(4-fluorophenyl)-1*H*-pyrazole **3-34** formed immediately. After two hours, the amount of triazene started decreasing, and the product was formed slowly along with fluorobenzene **3-33**.[1] The formation of the product is rate-limiting compared to the triazene formation. In the previous section, when evaluating the reactivity of the triazene species, its decomposition in the absence

[1] The important amount of fluorobenzene formed in these conditions as compared to the reaction performed in optimized Schlenk conditions can be due to the difference in the procedure (addition of the aniline), temperature and concentration. These parameters were adjusted to allow NMR monitoring.

of copper afforded the aniline and the arene. The latter is formed by reduction of the diazonium, and should involve an aryl radical intermediate.

Radical trapping experiments

When optimized conditions are applied, high yields are achieved, meaning that the rate of decomposition of the triazene is slower than the reaction rate, and that only a small amount of radical species is produced by reaction with the solvent. When radical scavengers (Galvinoxyl and TEMPO) were used in the optimized conditions, the formation of the product was not inhibited. This suggests that free radicals are not involved in the cross-coupling process, but rather in a by-path process, explaining the need for an excess of aniline to overcome its loss. Nevertheless, a negative result in radical trapping experiments by using classical radical scavengers does not necessarily exclude the involvement of very short-lived radicals in the coordination sphere of the metal. Therefore, we performed a radical-clock experiment (Figure 3.30).

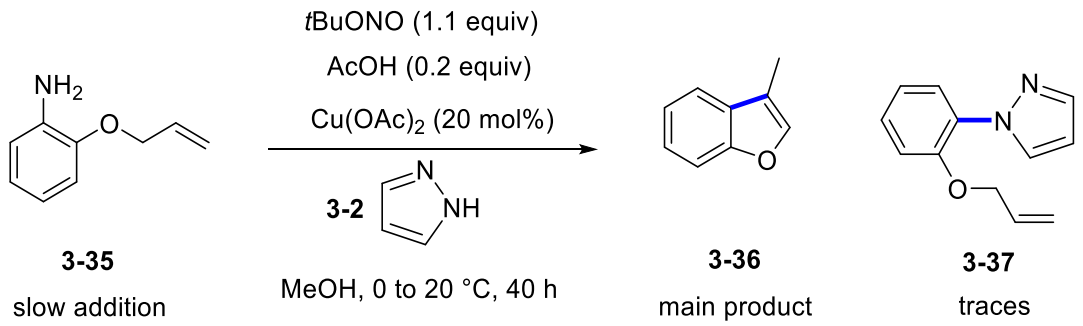

Figure 3.30 – Radical-clock experiment

Optimized conditions applied to 2-allyloxyaniline **3-35** formed the cyclized 3-methylbenzofurane **3-36** as the main product. Only traces of coupling product **3-37** could be detected by GC-MS. This is consistent with previous results that showed that *ortho*-substituted arenediazonium salts failed to give efficient coupling (see Table 3.1). This means that, in addition to the radicals that can be generated from the decomposition of the triazene, one cannot exclude the existence of aryl radicals in the coordination sphere of copper, resulting of the reduction of the diazonium salt and subsequent oxidation of copper. This result led us to propose that $Cu^{(II)}$ constitutes a convenient pre-catalyst to enter the $Cu^{(I)}/Cu^{(III)}$ catalytic cycle (see Figure 3.31).

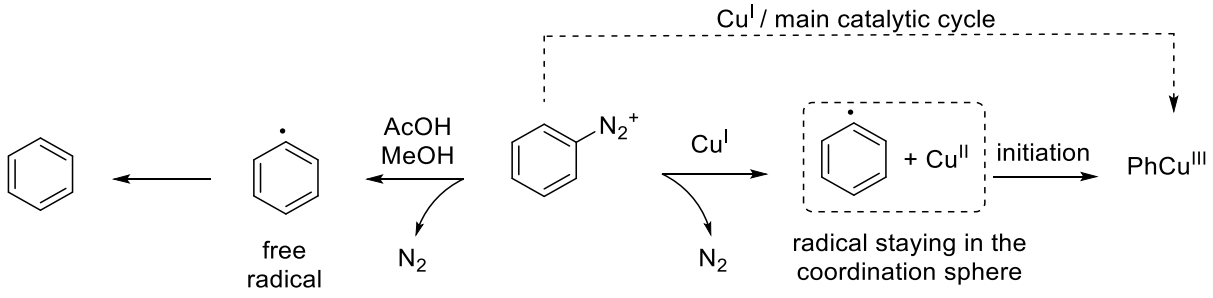

Figure 3.31 – Generation of aryl radicals from diazonium salts and their reactivity

Such a mechanism is proposed even if *t*BuONO is able to oxidize $Cu^{(I)}$ to $Cu^{(II)}$ in the reaction medium, as was evidenced by cyclic voltammetry experiments (see the Appendix page 202-203). Indeed, the radical by-path is able to regenerate the active form of the $Cu^{(I)}$ catalyst.

Existing mechanisms in the literature and proposition of a $Cu^{(I)}/Cu^{(III)}$ catalytic cycle

Thus, we postulated a mechanism consistent with those generally proposed for the activation of diazonium salts by transition metals (Figure 3.32). The $Cu^{(I)}$ catalyst reacts with the diazonium salt according to either an oxidative addition[6,140,146] (**a**) or a single electron transfer[157,158,196] (SET) (**b**), with departure of the N_2 group as a gas. A SET from another reductive agent source (for example the solvent), can also generate the arene radical. Then reductive elimination (**c**) can proceed, or $S_{RN}1$(**d**). Both routes are not completely independent since the aryl radical generated by **b** can interact with $Cu^{(II)}$ to generate $Cu^{(III)}$.

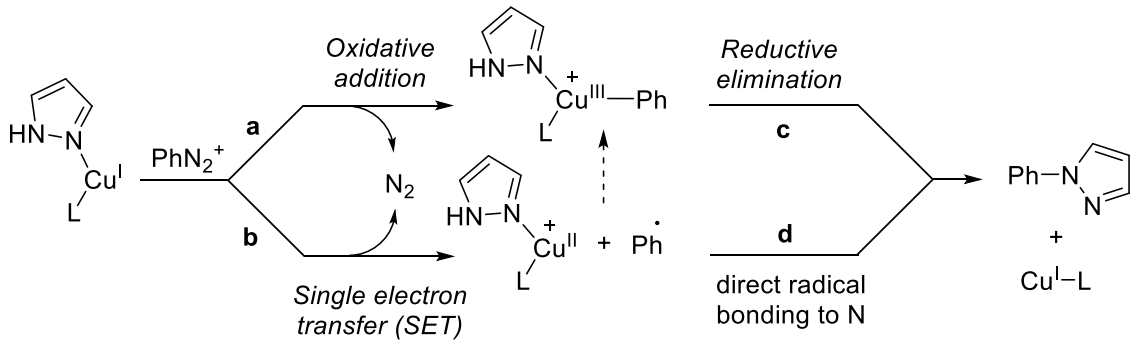

Figure 3.32 – Mechanisms of the activation of arenediazonium by $Cu^{(I)}$

The choice between **a** and **b** is usually motivated by a radical-clock experiment or by a control experiment in presence of a radical scavenger.[197–199] In our reaction, $Cu^{(II)}$ is used in the

optimized conditions, meaning that, according to Figure 3.32, radicals must be present in the reaction medium. They can initiate the reaction with $Cu^{(II)}$ and the formation of the coupling product along with $Cu^{(I)}$. $Cu^{(I)}$ is then involved in a $Cu^{(I)}/Cu^{(III)}$ catalytic cycle. On the basis of all these findings, a suitable catalytic cycle involving $Cu^{(I)}$ as active catalytic species can be postulated as depicted in Figure 3.33.

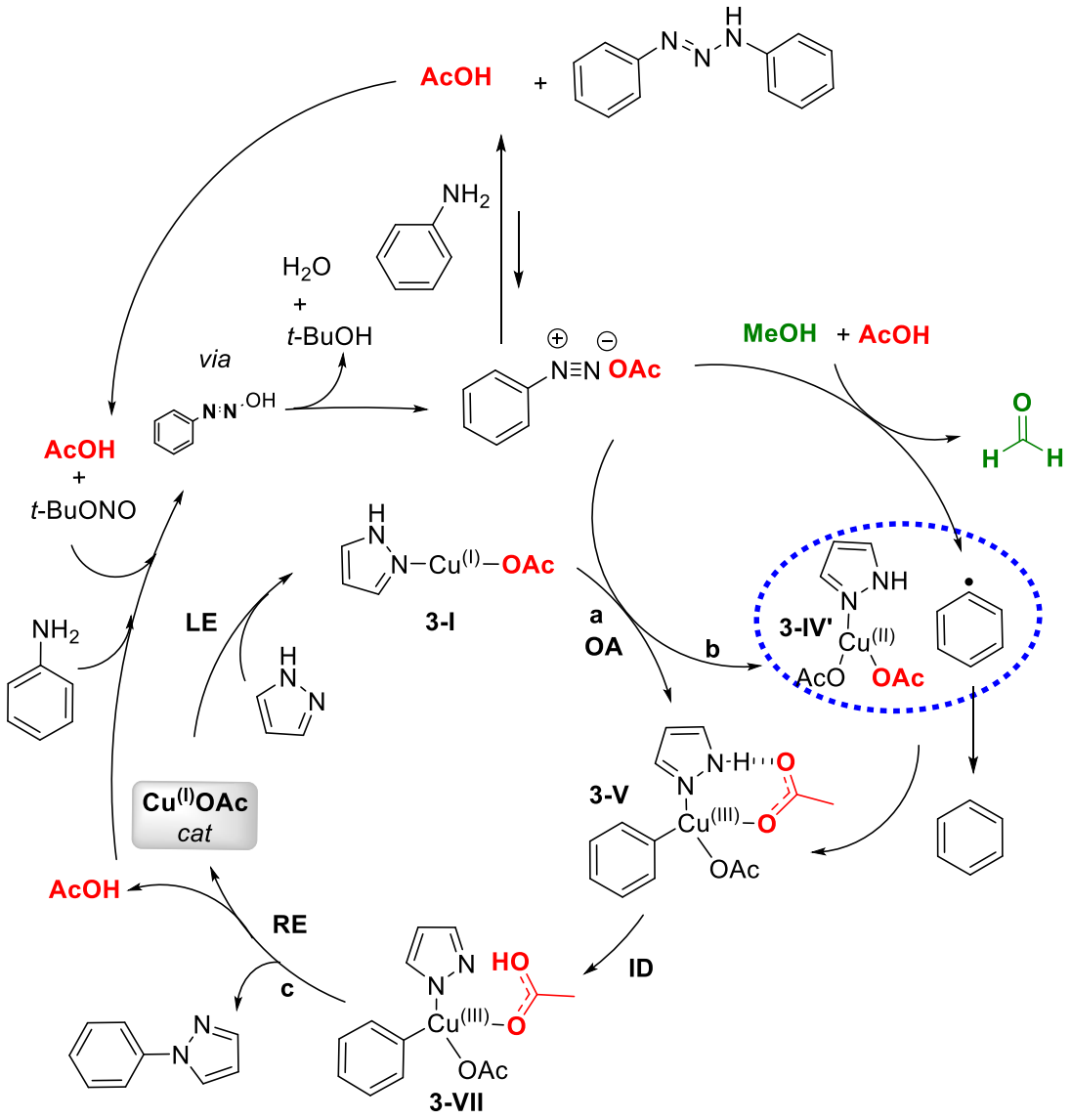

Figure 3.33 – Proposed catalytic cycle

In this rather complex catalytic cycle, all previously identified species play a role. The catalytic cycle for the reaction between the arenediazonium acetate and the $Cu^{(I)}$ active catalyst involve oxidative addition (OA), intramolecular deprotonation (ID) and reductive elimination (RE). Since this reaction proceeds without the addition of an external base, it is reasonable to

hypothesize that the nucleophile (pyrazole) is not deprotonated *before* its complexation on copper. The deprotonation more likely happens *on* the copper center by intramolecular deprotonation with an acetate ligand acting as a base. The excess of pyrazole in the reaction medium (with respect to the catalyst and to the diazonium acetate) and the affinity of this ligand for copper[200,201] and copper acetate[202] suggests its complexation to form the intermediate **3-I** prior to the complexation of the diazonium. In a next step, OA yields to the $Cu^{(III)}$ intermediate **3-V** with release of a molecule of nitrogen. Alternatively, **3-I** can reduce the diazonium by SET to form the $Cu^{(II)}$ intermediate **3-IV'**, along with arene radical, before the oxidative addition to form the intermediate **3-V**. Successive ID of a pyrazole by an acetate enables the formation of **3-VII** which can then undergo RE to regenerate the initial $Cu^{(I)}$ complex after ligand exchange (LE). Along with the cross-coupling product, a molecule of acetic acid is expelled from the coordination sphere of copper and can thus participate in the generation of the diazonium salt.

After reductive elimination, $Cu^{(I)}$ is formed which can directly undergo oxidative addition with the diazonium salt. This justifies the catalytic activity of CuOAc and CuI as copper sources (see Table 3.2). The lower yield for CuOAc can be explained by the fact that this copper complex is very moisture and air sensitive and decomposes, giving a green product.[203] Attempts to sublimate commercial CuOAc to access a purer $Cu^{(I)}$ source were unfruitful. Interestingly, the catalytic activity of metallic copper (Table 3.2, entry 1) comes from the *in situ* generation of $Cu^{(I)}$ as well: oxidation of metallic copper by arenediazonium salts is indeed known to promote the formation of $Cu^{(I)}$ species from $Cu^{(0)}$: [121,204]

$$ArN_2^+ + Cu^{(0)} \rightarrow Ar^{\cdot} + N_2 + Cu^{(I)+}$$

We then explored this catalytic cycle involving copper.

DFT for the study of the $Cu^{(I)}/Cu^{(III)}$ catalytic cycle

Computational details

All calculations were performed using the Gaussian 09 program[21]. The geometric structures of all minima and transition states of the reactions were fully optimized using 6-311+G(d,p)[22] basis sets on the main group elements (H, C, N, O). Copper atom was described with Los-Alamos double zeta basis and associated pseudo-potential[24–26]. Bulk solvent effects

(MeOH) were introduced using a Polarizable Continuum model (PCM)[30]. All stationary points were fully characterized via a subsequent analytical harmonic frequency calculation either as minima or as first order transition states (one imaginary frequency). Beside analysis of normal modes, IRC calculations[31,32] were used to confirm the minima linked by the most relevant transition states.

BLYP,[14,15] PBE0[16], M06[20], M062X[20], B3LYP[14,15,17], CAM-B3LYP[18], MPW91[19] functionals were considered as representative of currently applied global and range separated functionals. In order to evaluate the impact of dispersion interaction on barriers and reaction energies, the Grimme empirical dispersion correction was also applied to the B3LYP functional. This dispersion correction[205] has been previously applied for Ni and Pd catalyzed reactions[186] or in Schwartz hydrozirconation reactions[206] and improves the agreement with the experimental data.

Comparison of the functionals on the overall catalytic cycle

The whole catalytic cycle depicted in Figure 3.34 was computed with all above mentioned functionals. In the reaction medium, acetate and pyrazole can both coordinate to copper. The definition of the active catalytic species present in solution is therefore an important question to be addressed. We envisaged an interaction between an anionic copper complex, bearing two pyrazole ligands and two acetate ligands, and a cationic diazonium. One of the pyrazole and one of the acetate ligands are linked by hydrogen bonding. This choice will be justified in the next section with the study of the nature of the active catalyst. The results for the reaction energies and barriers are given under different representations. Table 3.5 gives the reaction energies, for each step of the reaction. Figure 3.35 gives the same information with more visual bar charts, whereas Figure 3.36 represents energy diagrams. Reaction energies were used to compare with MP2 calculations taken as a reference. Due to the relatively large size of the systems under analysis, MP2 single point energies (corrected for BSSE) were evaluated on B3LYP-D optimized structures. Corresponding values for the free energies computed at DFT level for standard conditions at 298.15 K are given in the Appendix (pages 203-204).

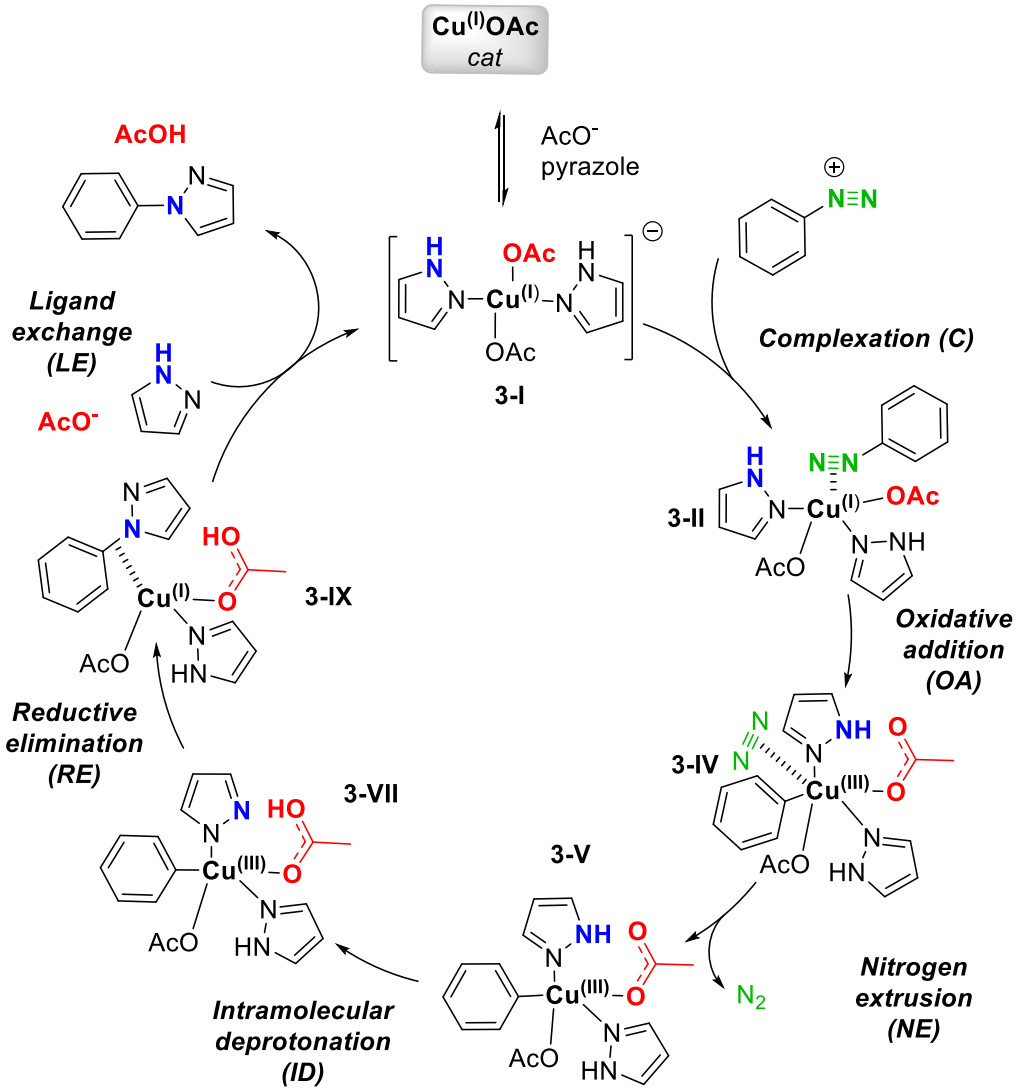

Figure 3.34 – Computed reaction mechanism

Table 3.5 - Reactions energies and barriers (in kcal.mol^{-1}) computed at different levels of theory for the catalytic cycle depicted in Figure 3.34.

	ΔE_C	Ea_{OA}	ΔE_{OA}	ΔE_{NE}	Ea_{ID}	ΔE_{ID}	Ea_{RE}	ΔE_{RE}	ΔE_{LE}
BLYP	- 9.66	+ 24.78	- 14.57	+ 0.07	+ 2.03	+ 1.91	+ 5.65	- 40.75	-5.75
PBE0	- 8.66	+ 25.46	- 15.15	+ 0.53	+1.72	+ 1.64	+ 2.86	- 49.02	- 6.59
B3LYP	- 5.20	+ 23.28	- 16.67	+ 0.08	+ 2.39	+ 2.07	+ 3.81	- 50.09	- 4.72
mPW91	- 6.42	+ 24.99	- 16.13	+ 0.35	+ 1.81	+ 1.70	+ 2.92	- 49.59	- 6.86
CAM-B3LYP	- 5.33	+ 22.94	- 17.54	+ 0.28	+ 2.57	+ 2.39	+ 3.37	- 52.87	- 5.49
B3LYP-D	- 17.58	+ 21.57	- 19.26	+ 3.09	+ 3.00	+ 2.74	+ 3.90	- 46.80	+ 1.36
M06	- 14.64	+ 21.50	- 15.45	+ 3.14	+ 2.27	+ 1.46	+ 2.19	- 51.19	- 0.93
M062X	- 14.60	+ 26.62	- 4.85	+3.67	+ 1.25	+ 0.80	+ 0.02	- 66.66	- 2.90
MP2	- 4.60	+ 17.84	- 42.17	+ 8.59	+ 0.27	- 0.04	+ 1.43	- 36.89	- 12.04

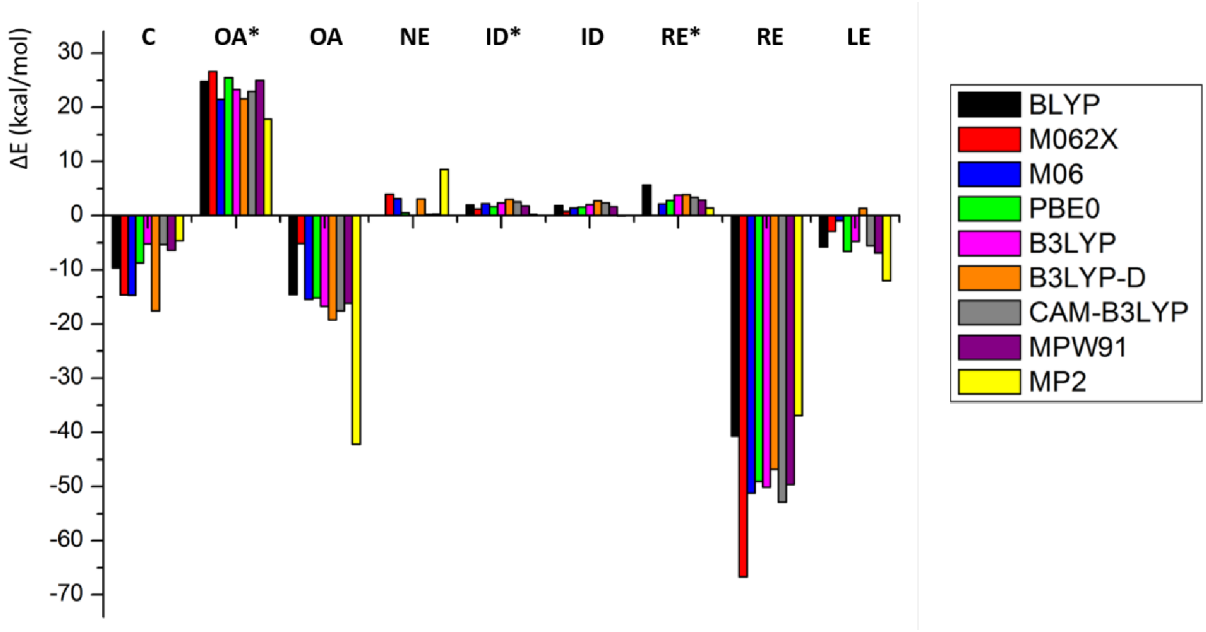

Figure 3.35 - Reactions energies and barriers (in kcal.mol^{-1}) computed at different levels of theory for the catalytic cycle depicted in Figure 3.34. The bars with a star represent activation energies.

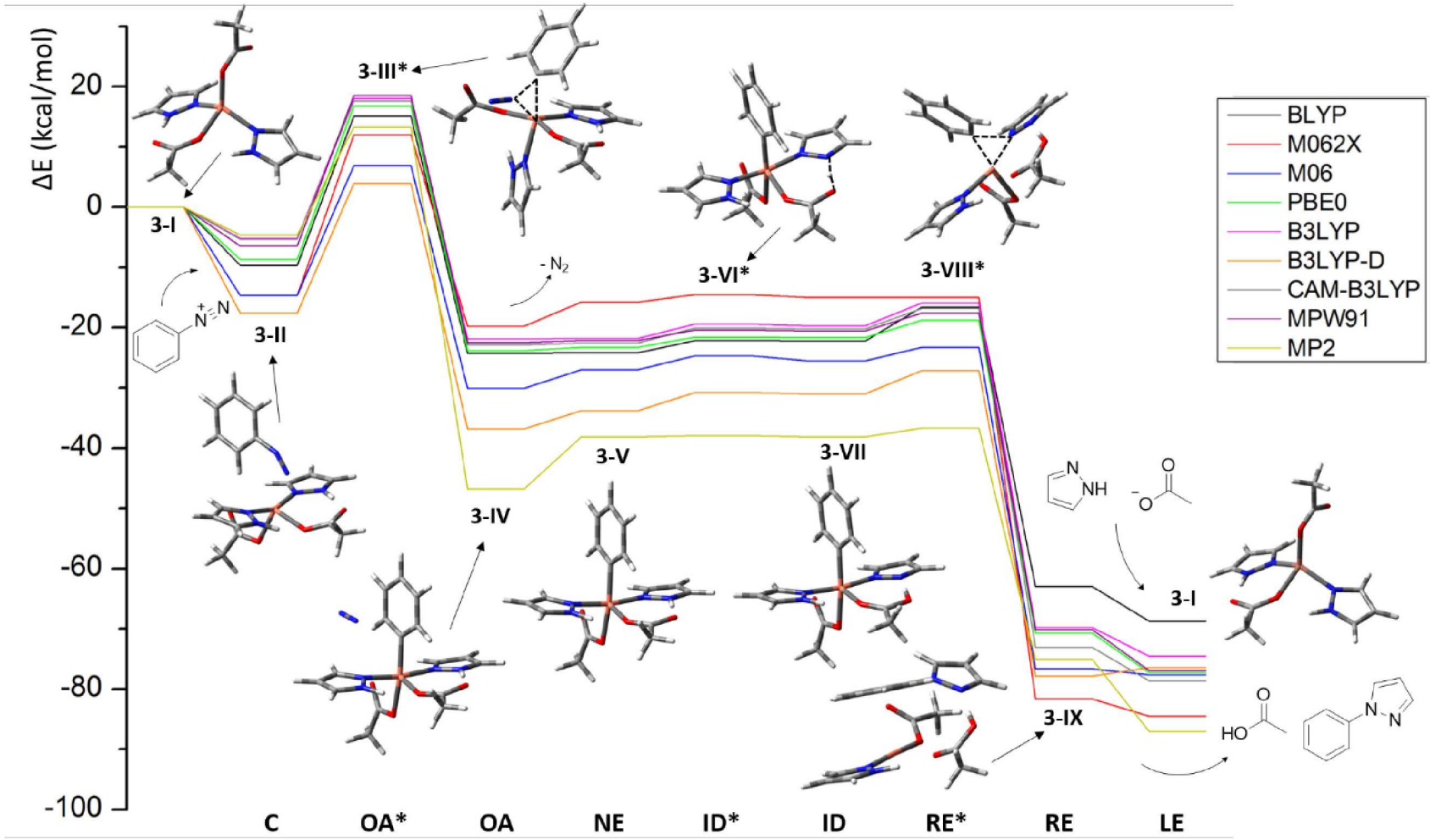

Figure 3.36 – Computed reactions energies and barriers (in kcal.mol^{-1}) computed at different levels of theory for the catalytic cycle depicted in Figure 3.34. The stars represent transition states. The complexes represented are the optimized structures with B3LYP-D.

Effect of the functionals on thermodynamics

The energy for the complexation is very dependent on the functionals (from -5 to -17 kcal.mol^{-1}) and, as expected, is significantly increased by applying dispersion correction (from -5.20 kcal.mol^{-1} to -17.58 kcal.mol^{-1}). All functionals show a slightly endergonic intramolecular deprotonation step, while the very favorable reductive elimination drives the reaction. Long-range corrected functionals (such as CAM-B3LYP) behave quite similarly to global hybrids. A poorly favored oxidative addition (from **3-II** to **3-V**) is observed with M062X: ΔE = -1.17 kcal.mol^{-1} when all other functionals give results between -12 and -17 kcal.mol^{-1}. This suggests that this functional may not be particularly adapted for the description of our system.

Effect of the functionals on kinetics

The effect of the functional on the kinetics of the reaction can be evaluated on the three energy barriers involved, the activation energy for: oxidative addition, intramolecular deprotonation and reductive elimination. Results show that the rate-determining step is the oxidative addition, which barrier is the lowest for M06 (among functionals without dispersion correction): Ea_{OA} = 21.50 kcal.mol^{-1}. Intramolecular deprotonation and reductive elimination can be easily achieved in all cases. BLYP gives a particularly high activation energy for the reductive elimination: Ea_{RE} = 5.65 kcal.mol^{-1}. As observed for the thermodynamics, M062X is the less performant functional for our reaction and has the highest activation energy for the oxidative addition: Ea_{OA} = 26.62 kcal.mol^{-1}. The introduction of dispersion correction shows a small effect on the activation energies and lowers the barrier for the OA (compare B3LYP, Ea_{OA} = 23.28 kcal.mol^{-1}. and B3LYP-D, Ea_{OA} = 21.57 kcal.mol^{-1}).

The relative stabilities of the reaction and products associated to the primary steps of the catalytic cycle depicted in Figure 3.34 were computed with and without Counterpoise[27–29] (CP) correction to highlight the impact of basis set superposition error.[207,208] Corrections are reported in Table 3.6 in the case of MP2 and B3LYP-D methods. MP2 is, as expected, more affected by BSSE than DFT based approaches. All results given are in the absence of BSSE correction for DFT methods and with BSSE correction for the MP2 method.

Table 3.6 - Computed relative stabilities (in kcal.mol^{-1}) in presence (-CP) and absence of BSSE corrections for the relevant steps of the reaction

	ΔE_c	ΔE_{NE}	ΔE_{LE}
B3LYP-D	- 17.58	+ 3.09	+ 1.36
B3LYP-D-CP	- 14.95	+ 4.55	- 2.73
MP2	-16.59	+ 4.99	+ 3.55
MP2-CP	- 4.60	+ 8.59	- 12.04

MP2 results give the smallest activation energy for the rate-determining step, the oxidative addition (17.84 kcal.mol^{-1}), in agreement with the small value obtained with B3LYP-D, confirming the choice of this functional for our system.

Comparaison of the geometries of complexes 3-I and 3-II obtained with different functionals

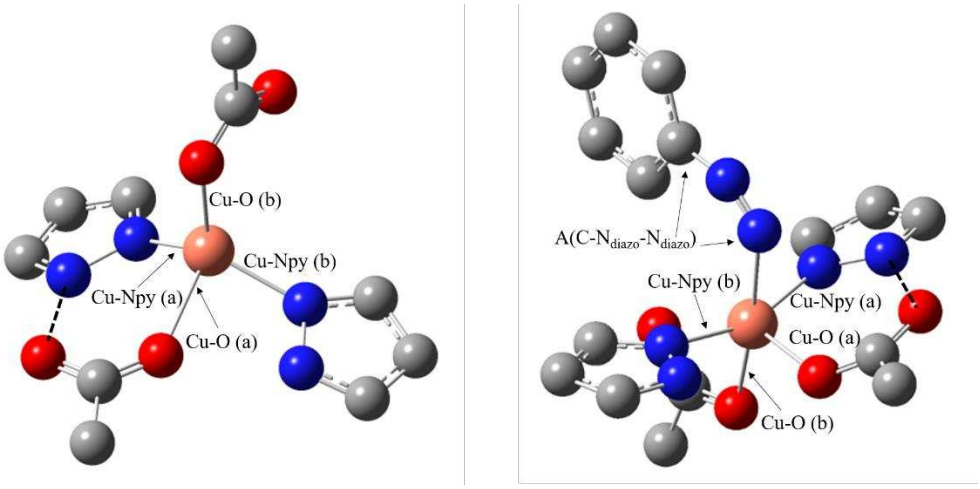

Figure 3.37 – Active catalytic species considered for the catalytic cycle (**3-I**, left) and complexation of the diazonium on copper (**3-II**, right) (hydrogen atoms were omitted for clarity, the H bond is represented with a dashed line)

The complexation step shows the most important variations with the functional used. In order to compare different functionals' behavior on this step, we compared the relative structures obtained for compounds **3-I**, the active copper complex, and **3-II**, the complex with the diazonium on copper, using different DFT approaches. We focused particularly on the Cu coordination sphere as well as on the deformation of the arenediazonium cation on the Cu coordination sphere (see Figure 3.37). The results are reported in Table 3.7.

Table 3.7 – Selected atom-atom distances in complexes **3-I** and **3-II** in Ångström, and bond-bond angles in degrees

	3-I		**3-II**			
	Cu-N_{py} (a)/ Cu-N_{py} (b)	**Cu-O (a)/ Cu-O (b)**	**Cu-N_{py} (a)/ Cu-N_{py} (b)**	**Cu-O (a)/ Cu-O (b)**	**Cu-N_{diazo}**	**A(C-N_{diazo}-N_{diazo})**
BLYP	2.00/1.99	4.21/2.12	2.01/2.03	2.46/2.11	2.14	145.15
PBE0	2.03/2.06	2.40/2.10	2.00/2.02	2.34/2.11	2.16	151.52
B3LYP	2.04/2.07	2.49/2.10	2.02/2.04	2.43/2.15	2.26	156.74
mPW91	2.04/2.07	2.40/2.09	2.00/2.02	2.35/2.12	2.19	153.15
CAM-B3LYP	2.04/2.07	2.37/2.09	2.02/2.04	2.47/2.13	3.08	178.11
B3LYP-D	2.03/2.07	2.40/2.11	1.99/2.01	2.30/2.10	2.18	148.55
M06	2.01/2.03	2.37/2.13	1.99/2.02	2.27/2.14	2.39	159.05
M062X	2.11/2.15	2.29/2.11	2.13/2.20	2.18/2.12	3.17	178.14

First value, a: ligand with H-bond; second value, b: ligand without H-bond

For the complex **3-I**, the largest variations are observed for Cu-N_{py} (b) and Cu-O (a). BLYP gives the shortest Cu-N_{py} (b) bond length when compared to the other functionals (1.99 Å against 2.03 to 2.07 Å) while M062X provides the longest one (2.15 Å). For Cu-O (a) the opposite holds, BLYP providing a much longer distance than the other functionals (4.21 Å, practically non coordinating, against 2.37 to 2.40 Å) and M062X a shorter one (2.29 Å against 2.37 to 2.40 Å). The behavior is more homogeneous for the hybrid-GGA functionals, and only B3LYP gives a longer Cu-O (a) than other hybrid-GGA. Inclusion of dispersion corrections yields, as expected, to shorter bonds (from 2.49 Å with B3LYP to 2.40 Å with B3LYP-D).

For the complex **3-II**, M062X exhibits the most important variations from the values obtained with other functionals. The Cu-N_{py} (a) (2.13 Å against 1.99 to 2.02 Å), Cu-N_{py} (b) (2.20 Å against 2.01 to 2.04 Å) and Cu-N_{diazo} (3.17 Å against 2.14 to 2.39 Å) bonds are longer and while Cu-O (a) bond is shorter (2.18 Å against 2.27 to 2.47 Å). The angle A(C-N_{diazo}-N_{diazo}) is larger (178.14 degrees against 148.55 to 159.05 degrees). Similarly, CAM-B3LYP gives a long Cu-N_{diazo} bond (3.08 Å against 2.14 to 2.39 Å) and a large A(C-N_{diazo}-N_{diazo}) angle (178.11 degrees against 145.15 degrees). The dispersion shortens all the selected bonds and disminishes the C-N_{diazo}-N_{diazo} angle from 156.74 degrees to 148.55 degrees.

All these observations can be summarized by computing the root mean square deviation (RMSD) between a structure computed at a given level of thoery and a reference one (here the structure obtained at B3LYP-D). The RMSD measures the average distance between the same atoms in the two superimposed complexes, and allows to evaluate their similarity. To compare two complexes a and b, with n atoms of spatial coordinates (x, y, z), the RMSD is calculated using the following expression:

$$RMSD\ (a,b) = \sqrt{\frac{1}{n}\sum_{i=1}^{n}(a_{ix} - b_{ix})^2 + \left(a_{iy} - b_{iy}\right)^2 + (a_{iz} - b_{iz})^2)}$$

The Kabsch algorithm was used.[209] It allows to first find the centroid for each complex, align their center of coordinates and then align the molecules by rotation to minimize the RMSD before its calculation. This allows to take all the distances into account. The results are given in Table 3.8.

Table 3.8 – RMSD (in Å) of the structures of **3-I** and **3-II** taking B3LYP-D as reference

RMSD (B3LYP-D as reference)	**3-I**	**3-II**
BLYP	1.404	0.246
PBE0	0.117	0.178
B3LYP	0.167	0.284
mPW91	0.116	0.197
CAM-B3LYP	0.117	0.765
M06	0.312	0.154
M062X	0.165	0.381

As already concluded from the previous analysis, for complex **3-I**, BLYP shows the largest variation from the reference B3LYP-D geometry, followed by M06 which is also much deviated with a RMSD of 0.312 Å. For complex **3-II**, CAM-B3LYP shows the most deviated structure, followed by M062X, B3LYP and BLYP, respectively.

Nonetheless, beside the structural and energetic quantitative difference provided by the different functionals, all of them agree in providing the same qualitative picture, which is that

the postulated catalytic cycle is energetically feasible, with the oxidative addition as the rate determining step. In the following sections the B3LYP-D will be used.

Evaluation of alternative mechanisms

Oxidative addition of the triazene

To further confirm the hypothesis of a diazonium salt as an active species, DFT calculations were performed to evaluate the reactivity of the triazene species on a $Cu^{(I)}$ complex bearing one pyrazole and one acetate ligand. The triazene can be stabilized by complexation to copper (-23.10 kcal.mol^{-1}), but direct oxidative addition to the C-N bond requires a much higher energy to be achieved under the reaction conditions (E_a = 54.00 kcal.mol^{-1}). These results further confirmed that the triazene is a stable reservoir for the diazonium compound, which is the active coupling partner in this reaction.

Pure radical pathway

The possibility of a pure radical pathway, already ruled out by the experiments in the presence or radical scavengers, was eliminated by computing the mechanism for the path **d** in Figure 3.32. A $Cu^{(II)}$ complex brings together the pyrazole and the acetate for the deprotonation, but there is no change in its oxidation state. The results are detailed in the Appendix (page 205). The formation of the aryl-nitrogen bond requires 35 kcal.mol^{-1} and cannot be envisaged in our reaction conditions.

Oxidative addition of the diazonium *vs* SET to form an aryl radical

We also evaluated the possibility to go through path **b** in Figure 3.32, with a $Cu^{(I)}/Cu^{(II)}/Cu^{(III)}$ catalytic cycle. In this mechanism, the $Cu^{(I)}$ complex **3-II** reduces the diazonium to generate a $Cu^{(II)}$ complex **3-IV'** and an aryl radical that stays in the coordination sphere of copper before its addition to form the $Cu^{(III)}$ complex **3-V** (Figure 3.38). After deprotonation and reductive elimination, a $Cu^{(I)}$ complex is regenerated like in the $Cu^{(I)}/Cu^{(III)}$ mechanism proposed initially.

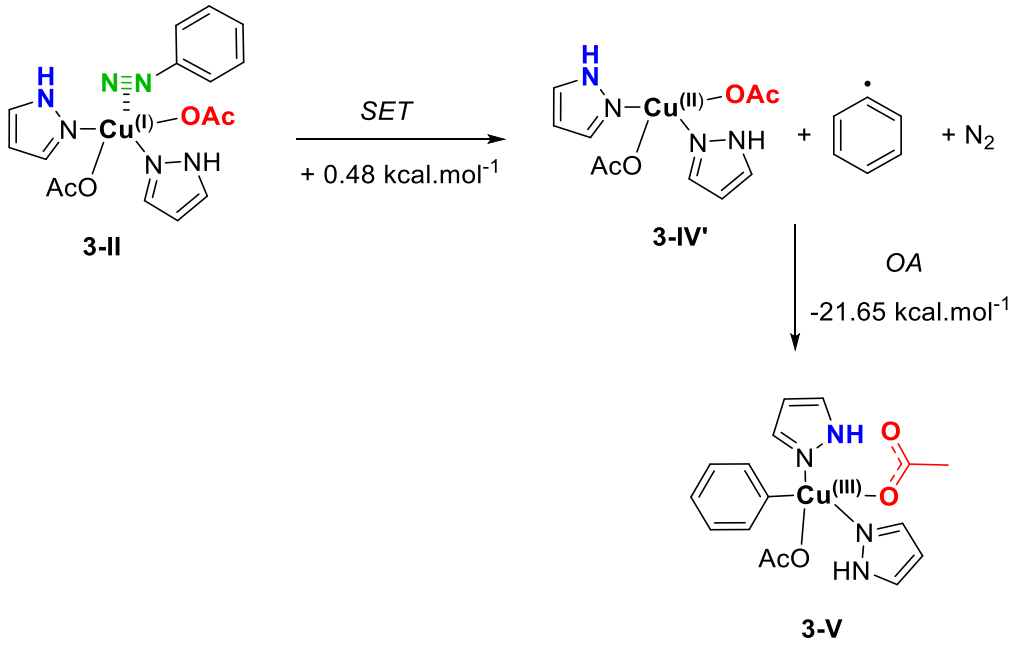

Figure 3.38 – Formation of a $Cu^{(III)}$ complex via a $Cu^{(I)}/Cu^{(II)}/Cu^{(III)}$ mechanism (reaction energies in kcal.mol^{-1})

The SET to form the radical and $Cu^{(II)}$ requires 0.48 kcal.mol^{-1}. The products of this reaction are almost isoenergetic to the reagents and this route can be envisaged. The results obtained with the radical-clock experiment suggest that at least part of the diazonium is reduced into aryl radical before its oxidative addition to copper. Nevertheless, we kept the two possible pathways as plausible hypotheses: $Cu^{(I)}/Cu^{(III)}$ or $Cu^{(I)}/Cu^{(II)}/Cu^{(III)}$.

The nature of the active copper species

NMR and cyclic voltammetry evidence for complexation of acetates and pyrazoles

Considering an active $Cu^{(I)}$ species, we investigated the stoichiometry of the active $Cu^{(I)}$ complex **3-I**, because acetate and pyrazole can both coordinate copper in the reaction medium.

The preferred formation of a complex was investigated by cyclic voltammetry (CV) performed in methanol with *tetrakis*acetonitrile copper$^{(I)}$ hexafluorophosphate ($Cu^{I}(CH_3CN)_4^+$ PF_6^-) as the copper source. The observation of the reduction wave of $Cu^{(I)}$ in $Cu^{(0)}$ showed the complexation of acetate (Figure 3.39). Addition of one to six equivalents of pyrazole formed several new copper species in equilibrium (Figure 3.40).

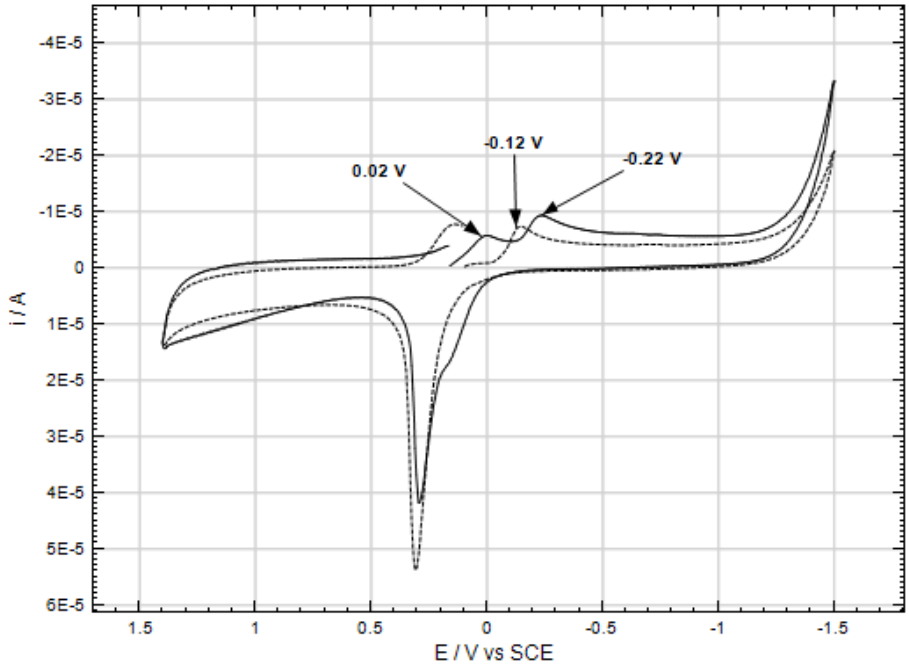

Figure 3.39 - CV performed in MeOH containing *n*-Bu_4NBF_4 (0.3 M) at a steady glassy carbon disk electrode (d = 1 mm), at a scan rate of 0.5 $V.s^{-1}$, at 20 °C, starting from the resting potential (a) Reduction of $Cu(CH_3CN)_4PF_6$ (2 mM) (dashed line); (b) Reduction of $Cu(CH_3CN)_4PF_6$ (2 mM) in the presence of *n*-Bu_4NOAc (2 mM) (solid line).

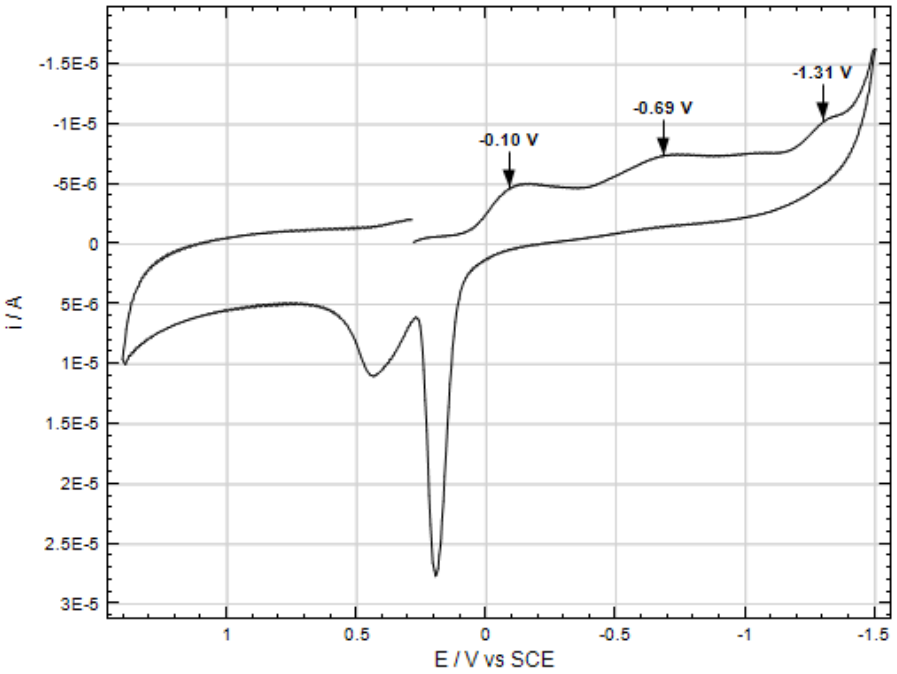

Figure 3.40 - CV performed in MeOH containing *n*-Bu_4NBF_4 (0.3 M) at a steady glassy carbon disk electrode (d = 1 mm), at a scan rate of 0.5 $V.s^{-1}$, at 20 °C, starting from the resting potential. Reduction of $Cu(CH_3CN)_4PF_6$ (2 mM) in the presence of *n*-Bu_4NOAc (2 mM) and 6 equivalents of pyrazole (12 mM). The voltammograms after addition of 1, 2, 3, 4 or 6 equivalents of pyrazole were identical.

The same experiment followed by NMR showed very broad peaks for the pyrazole protons, suggesting the coexistence of various complexes as well. In both cases, by electrochemistry or NMR, the copper complexes could be neither identified nor quantified experimentally.

Comparison of different possible $Cu^{(I)}$ species

To discriminate between different $Cu^{(I)}$ complexes, DFT was applied. The heat of formation for complexes with various numbers of ligands and various conformations was computed according to the following equation:

$$Cu^{+} + m\ AcO^{-} + n\ Pyrazole \rightarrow Cu(OAc)_m Pyrazole_n^{(m-1)-}$$ (see Table 3.9).

Table 3.9 – Computed heat of formation and structures of the complexes considered. Hydrogen atoms were removed for clarity; Intramolecular hydrogen bonds are highlighted with black dashed lines.

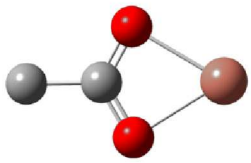 **3-Ia** m = 1, n = 0 ΔH_f = - 44.07 kcal.mol^{-1}	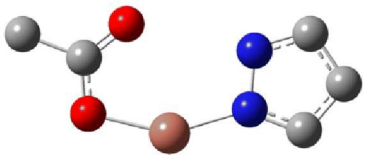 **3-Ib** m = 1, n = 1 ΔH_f = - 78.75 kcal.mol^{-1}
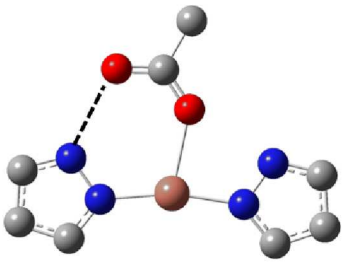 **3-Ic** m = 1, n = 2 ΔH_f = - 102.10 kcal.mol^{-1}	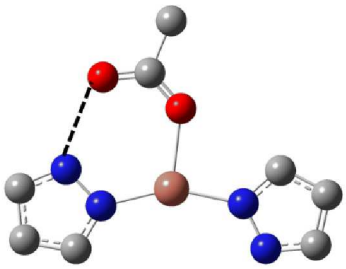 **3-Id** m = 1, n = 2 ΔH_f = - 97.72 kcal.mol^{-1}
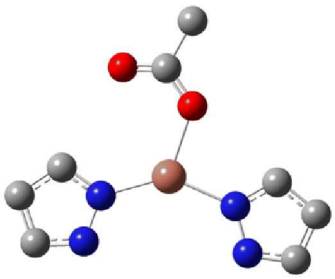 **3-Ie** m = 1, n = 2 ΔH_f = - 89.02 kcal.mol^{-1}	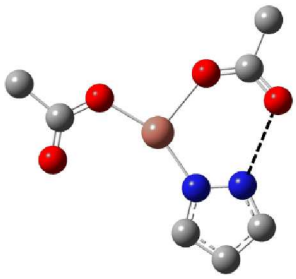 **3-If** m = 2, n = 1 ΔH_f = - 96.92 kcal.mol^{-1}
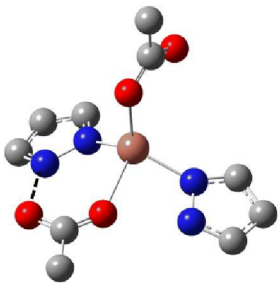 **3-Ig** m = 2, n = 2 ΔH_f = - 107.19 kcal.mol^{-1}	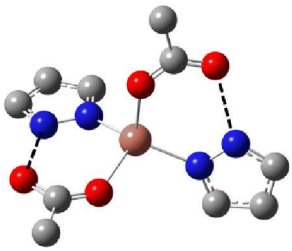 **3-Ih** m = 2, n = 2 ΔH_f = - 111.31 kcal.mol^{-1}

We assumed that in a first time a neutral $Cu^{(I)}Pyrazole_nOAc$ complex was formed (complexes **3-Ia** to **3-Ie**). When the diazonium acetate approaches, its acetate binds to the copper ion so that a favorable electrostatic interaction between the cationic arenediazonium and an anionic $Cu^{(I)}$ complex bearing two acetates (complexes **3-If** to **3-Ih**) can be envisaged. Results show that adding one pyrazole to CuOAc is very favorable (**3-Ia** → **3-Ib**, ΔE = - 34.68 kcal.mol^{-1}). Adding a second pyrazole is less stabilizing (**3-Ib** → **3-Ic**, **3-Id** or **3-Ie**, $\Delta E \approx$ - 10-20 kcal.mol^{-1}). When the external acetate from the diazonium complexes to copper, it is more stabilizing when only one pyrazole molecule is already ligated (**3-Ib** → **3-If**, ΔE = - 18.17 kcal.mol^{-1}) than when there are two (**3-Ic** → **3-Ig** or **3-Ic** → **3-Ih**, $\Delta E \approx$ - 10 kcal.mol^{-1}). This means that we do not necessarily have the complexation of two pyrazoles on copper before the oxidative addition.

The whole catalytic cycle was then computed starting from complexes **3-If**, **3-Ig** and **3-Ih** (see Figure 3.41). **3-Ig** is the one that was used for the benchmark of functionals.

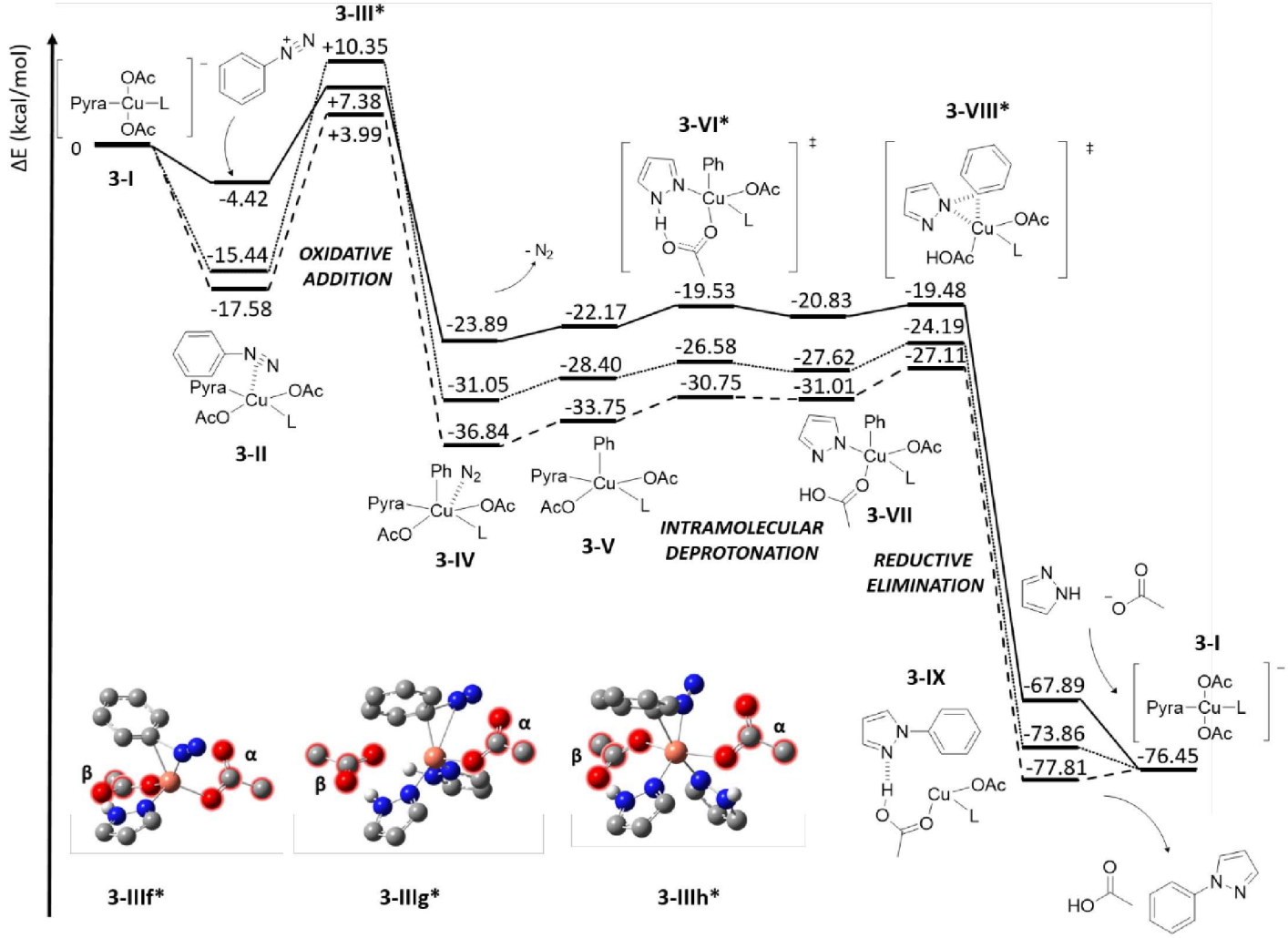

Figure 3.41 - Computed reaction path starting from the selected copper complexes **3-If** (solid line), **3-Ig** (dashed line), and **3-Ih** (dotted line). L = pyrazole ligand or free coordination site. Intermediates with asterisks are transition states. The transition-state structures **3-IIIf***, **3-IIIg*** and **3-IIIh*** are represented; α- and β-acetate ligands are highlighted in red and some hydrogen atoms have been removed for

The structural parameters have no significant influence on the reaction energies except for the complexation step, which is more favorable when two pyrazoles are present. They have an important effect on the energy barriers. Indeed, the copper complex bearing only one pyrazole molecule (**3-f**) exhibits significantly lower activation energies for the three key steps of the reaction, and especially for the most energy-demanding one: the oxidative addition (11.81 kcal.mol^{-1} for **3-f** against 21.57 kcal.mol^{-1} for **3-g** and 25.79 kcal.mol^{-1} for **3-h**) which appears to be the rate determining step. This can be related to the steric hindrance. Less space is left to the diazonium cation to approach the copper when increasing the number of pyrazoles. This forces the diazonium to adopt a twisted geometry to be able to undergo the oxidative addition, with a nitrogen atom further apart from the copper center (Cu-N bond of 2.97 Å for **3-IIIg*** against 1.98 Å for **3-IIIf***). It is reasonable to think that if **3-Ig** or **3-Ih** is formed, a pyrazole ligand is released to form **3-If** before the oxidative addition.

Analyzing the structure of the transition state **3-III*** (Figure 3.41), we can understand the role of each of the two acetates coordinated to the copper: one is stabilizing the approach of the diazonium cation through the oxygen not coordinated to copper (labelled α), while the other one is H-bonded to the pyrazole to allow the intramolecular deprotonation afterwards (labelled β). It would not be possible for a single acetate ligated to the copper cation to do both actions.

Overall, the proposed reaction mechanism allows to explain the observed reactivity in the case of pyrazole substrate.

Complementary results - the case of imidazole

Nonetheless, to further confirm its validity, it is important to see if the difference in the reactivity observed for imidazole substrates could also be justified by the same mechanism.

Indeed, initial experimental results showed that applying standard conditions to imidazole leads to a lower yield (42 %) and different conditions were applied. An explanation can be found by analyzing the structure of $Cu^{(III)}$ intermediates **3-Vg** for pyrazole and for imidazole (see Figure 3.42).

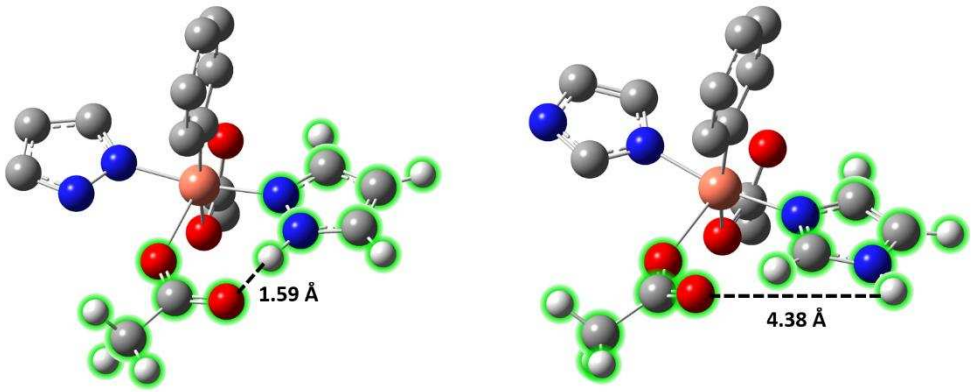

Figure 3.42 – $Cu^{(III)}$ intermediates **3-Vg** bearing pyrazole (left) or imidazole (right) ligands and distance for intramolecular deprotonation. The ligands involved in the deprotonation are highlighted in green, and hydrogen atoms on other ligands have been removed for clarity

In the case of a pyrazole substrate, a hydrogen bond between a copper ligated acetate and the acidic proton of the pyrazole can be formed, allowing a pre-oriented easy intramolecular deprotonation. However, in the case of imidazole such an interaction cannot exist (as depicted in Figure 3.42). The acidic proton of imidazole points outside the copper complex and is too far from the acetate ligand. An intermolecular deprotonation pathway was thus postulated with the participation of a free external acetate. We computed this intermolecular deprotonation starting with **3-Ig** for the imidazole substrate, but also for the pyrazole, as a validation of our intramolecular deprotonation mechanism (see Figure 3.43).

The first step of the mechanism is similar, with a complexation of the diazonium on the anionic $Cu^{(I)}$ complex, followed by a favorable oxidative addition with an activation energy Ea_{OA} = 23.82 kcal.mol^{-1} for imidazole (Ea_{OA} = 21.57 kcal.mol^{-1} for the pyrazole). In the case of pyrazole, the acidic proton is involved in an intramolecular hydrogen bond with the acetate. Twisting (**3-V → 3-XI**), allows to make this acidic proton available for another base. This is kinetically (Ea_{twist} = 10.44 kcal.mol^{-1}) and thermodynamically (ΔE_{twist} = 5.88 kcal.mol^{-1}) not favorable. For both substrates, this complex is then stabilized by the presence of an external acetate (**3-XII**) and intermolecular deprotonation is easily achieved (Ea_{ID} = 0.48 kcal.mol^{-1} for imidazole, Ea = 1.20 kcal.mol^{-1} for pyrazole). The departure of acetic acid (**3-XIV → 3-XV**) is energetically disfavored in both cases ($\Delta E \approx +$ 16 kcal.mol^{-1}). Reductive elimination can finally proceed easily.

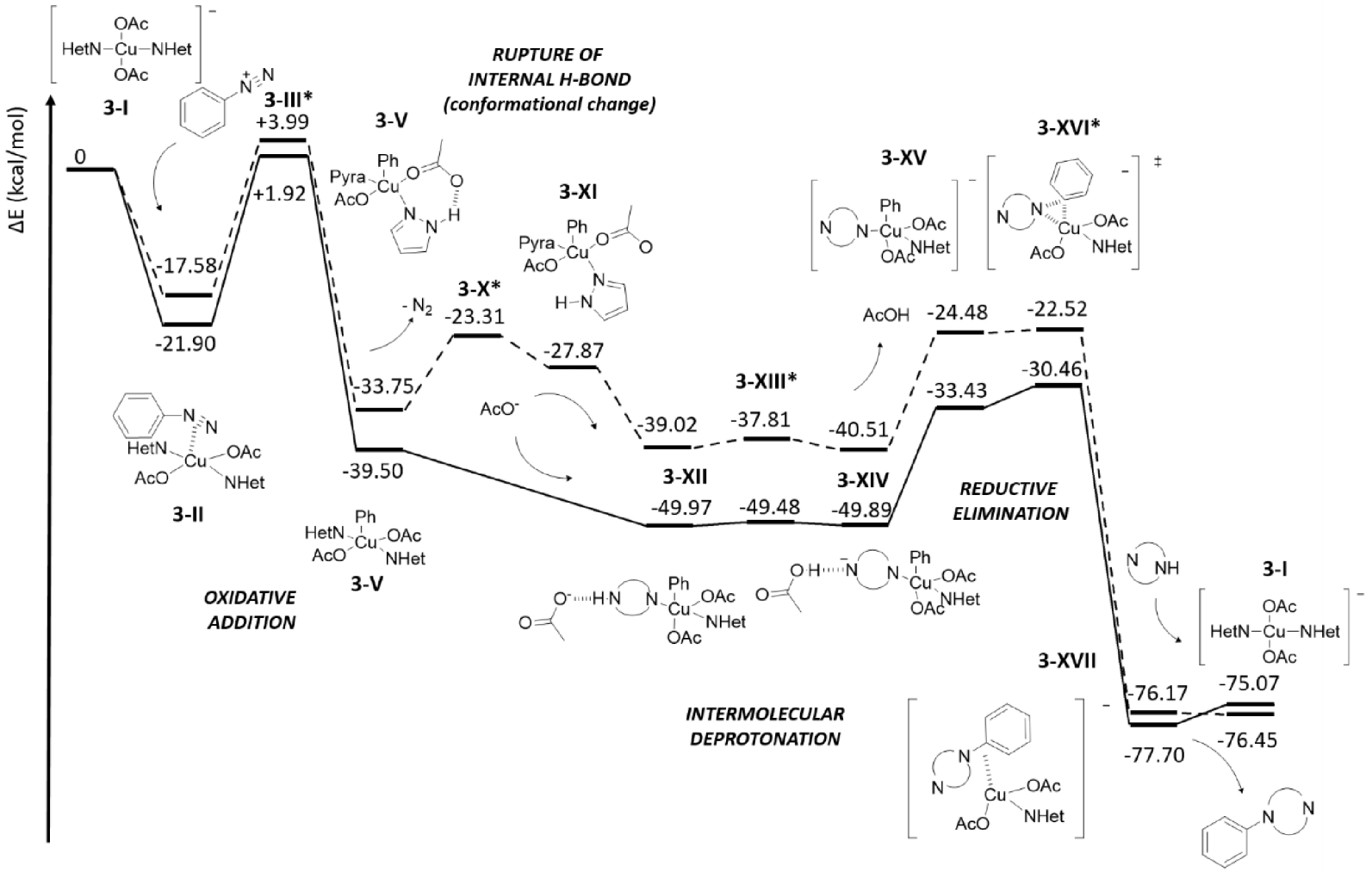

Figure 3.43 - Intermolecular deprotonation mechanism for pyrazole (dashed line) and imidazole (solid line) starting from **3-Ig**. The circles refer to any of the two nitrogen heterocycles. Intermediates with asterisks are transition states.

The lower yields obtained for imidazole can thus be explained by the fact that very few free acetate molecules are present in the reaction medium due to the quantitative formation of triazene at the beginning of the reaction. It can also be explained by the fact that acetic acid has to leave the coordination sphere of copper to enable the reductive elimination. This departure is energetically disfavored. Furthermore, if we consider an intermolecular deprotonation for the pyrazole, energy barriers for both deprotonation and reductive elimination are lower than for intramolecular deprotonation (1.20 and 1.93 kcal.mol^{-1}, respectively, with respect to 3.00 and 3.90 kcal.mol^{-1} for intramolecular deprotonation) but the intervention of an extra acetate introduces two new high barriers: one for the conformational twisting of the pyrazole and one for the departure of the acetic acid. These two steps and the entropy factor disfavor the intermolecular deprotonation mechanism.

We have here a clear indication that the intramolecular mechanism for the deprotonation is favored when possible (case of pyrazole) and that the intermolecular one is more challenging although achievable (explaining lower efficiency of the reaction with imidazole). With these conclusions in hand, we can postulate that better yields should be obtained for imidazole by adding external acetate. Unfortunately, acetate is also playing an important role in the formation of the starting active species, resulting in a slower formation of the triazene (due to the overall lower acidity of the reaction medium). The antagonistic effect of acetate and acetic acid in several steps of the reaction as well as in by-paths explains that their concentrations have to be finely tuned for each family of substrates employed.

Conclusion

Both experimental and computational approaches have been developed as complementary tools to investigate the reaction mechanism of the copper-catalyzed arylation of nitrogen heterocycles from *in situ* generated diazonium salts. In this reaction, a triazene species is quantitatively formed and acts as a dormant diazonium reservoir. It maintains a low concentration of active species in the reaction medium and thus limits the non-effective parallel formation of arene. The amount of acid is crucial for the reactivity of the diazonium: it is required to generate the diazonium salt, but it accelerates the decomposition of the triazene to arene if introduced at high concentration. The role of radical species is also relevant: they are involved in the initiation step, and we cannot exclude their presence in the coordination sphere of copper. As evidenced by computational outcomes used to investigate the various steps of the reaction, the acetate also plays an important role as a ligand. Indeed, it favors the complexation of the diazonium on copper and allows an easy intramolecular deprotonation of the pyrazole. The latter step can explain the difference of reactivity observed between pyrazole and imidazole. A DFT benchmark was performed and revealed that B3LYP with dispersion correction was a good candidate to describe our system.

Overall, our investigation allows to show that only a fine tuning of the antagonistic effect played by the AcOH/AcO^- couple in the complex reaction mechanism enables the optimization of the reaction conditions.[210]

Chapter 4 – Stereoselective access to trisubstituted fluorinated alkenyl thioethers

This chapter presents the development of a general strategy for the synthesis of fluorinated alkenyl thioethers. This method allows to combine the presence of sulfur and fluorine in the same small molecule, which can be of interest in the development of new pharmaceutical compounds. The methodology development is followed by a mechanistic study which reveals a radical mechanism that can be generalized to the difluoroacetylation of other molecules. Post-functionalization of the molecules obtained gives access to isotetronic acids, a core structure for natural and active molecules.

This work was done in collaboration with Dr. Thomas Poisson and Pr. Xavier Pannecoucke (INSA Rouen) and Pr. Isabelle Gillaizeau (Université d'Orléans).

This work was published: Stereoselective access to trisubstituted fluorinated alkenyl thioethers, I. Fabre, T. Poisson, X. Pannecoucke, I. Gillaizeau, I. Ciofini, L. Grimaud, *Catal. Sci. Technol.*, 2017, DOI:10.1039/C7CY00076F.

State of the art

Interest of fluorine and sulfur in drug development

Interest of fluorine

The presence of fluorine in already approved drugs or drug candidates entering clinical trials has been increasing since it first appeared in the 1950's.[211–214] This atom was found to have unique properties in the biological activity of active compounds, due to its high electronegativity and small size. The C-F bond is strong and exhibits metabolic stability.[215] Moreover, fluorine acts as a bioisostere of the hydrogen atom. Incorporation of fluorine generally changes the compounds lipophilicity, and modifies the physical and biological properties of a molecule. More than 25 % of the drugs on the market now contain fluorine. Some examples of these drugs are given in Figure 4.1. Fludrocortisone was the first fluorine-containing drug approved by the US Food and Drug Administration (FDA), in 1955. Fluoxetine, known as Prozac®, is a widely used antidepressant. Efavirenz and Emtricitabine are used in the triple combination therapy for the treatment of human immunodeficiency virus (HIV) infection. Tafluoprost is an eye treatment for open-angle glaucoma and ocular hypertension.

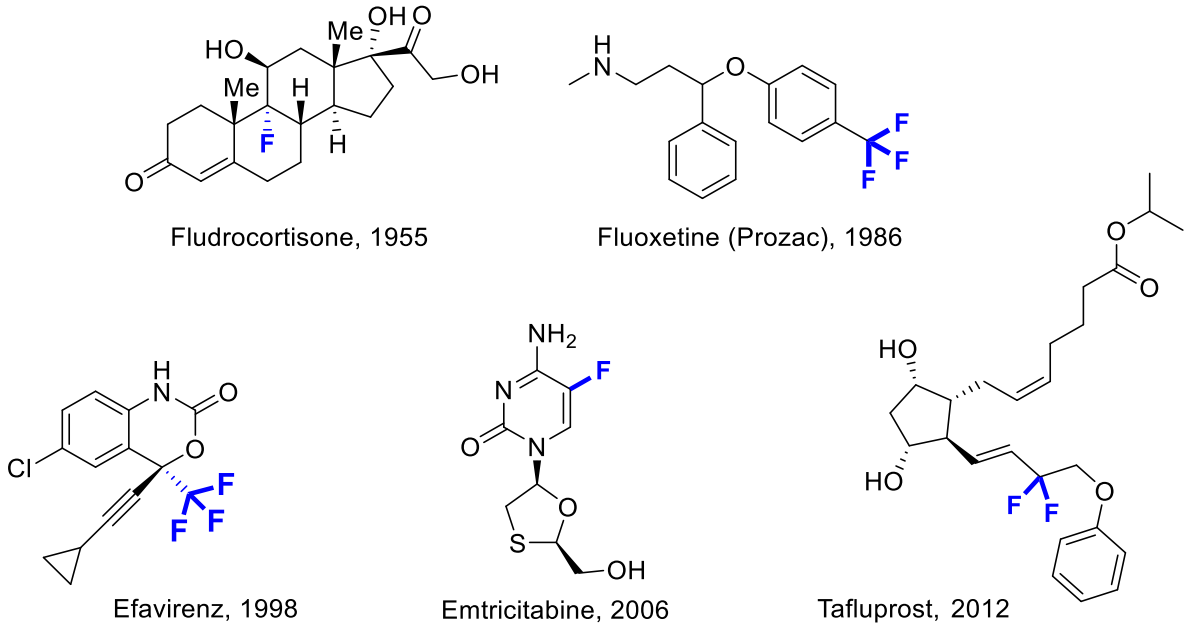

Figure 4.1 - Fluorine-containing drugs, with their names and FDA approval date

These compounds show the variety of fluorine-containing structures that can be encountered in pharmaceuticals, with –F, -CF_2 or -CF_3 groups. In that context, the development of new methodologies to access these strategic molecules is of high demand toward the discovery of new bioactive molecules, and since the last decade, organofluorine chemistry has known a very fast expansion. The direct C-H bond functionalization was recently recognized as an outstanding and efficient method for a straightforward access to the desired fluorine-containing molecules.[216]

Interest of sulfur

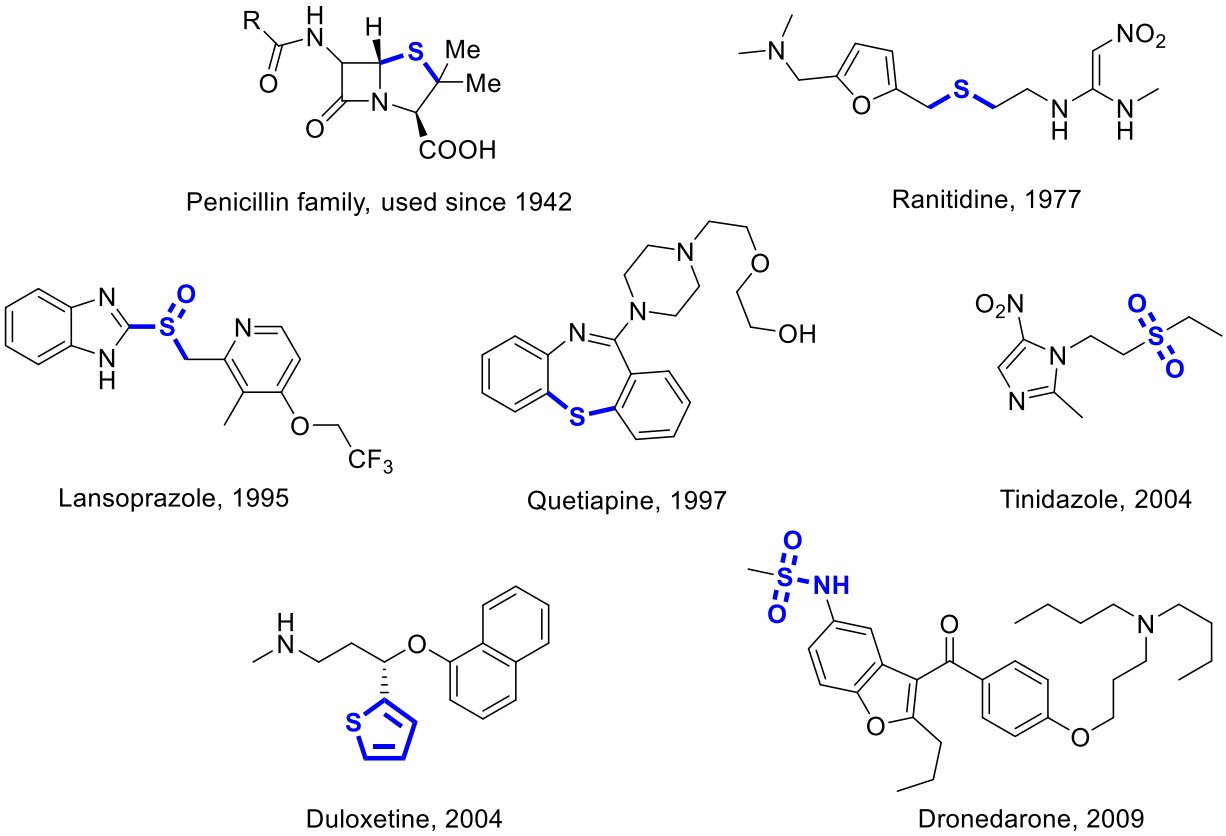

Figure 4.2 – Sulfur-containing drugs, with their names and FDA approval date

Sulfur is the fifth most prevalent element in drugs (after carbon, hydrogen, oxygen and nitrogen). Sulfur-containing molecules often display interesting biological activities. They are efficient in the treatment of various ailments, including cancer, acquired immune deficiency syndrome, depression, diabetes, arthritis.[217] Various sulfur-containing scaffolds exist in drugs

and natural products, including sulfonamides, thioethers, sulfoxides, sulfones, thiophenes, and penicillin derivatives.[218] A few examples of sulfur-containing drugs are given in Figure 4.2.

Penicillin is a group of antibiotics. It was discovered in 1928 and is still widely used today. Ranitidine and Lansoprazole are used to decrease stomach acid production. Quietiapine is used for the treatment of schizophrenia and depression. Tinidazole is used against parasitic infections. Duloxetine is mostly used for major depressive disorders. Dronedarone is indicated for the treatment of cardiac arrhythmias.

Among sulfur-containing molecules, alkenyl thioethers[219] are a versatile chemical platform and represent an interesting motif to access complex sulfur-containing molecules.

Methods of functionalization of alkenyl thioethers

There are only a few reactions developed for the C-H functionalization of alkenyl thioethers (Figure 4.3).

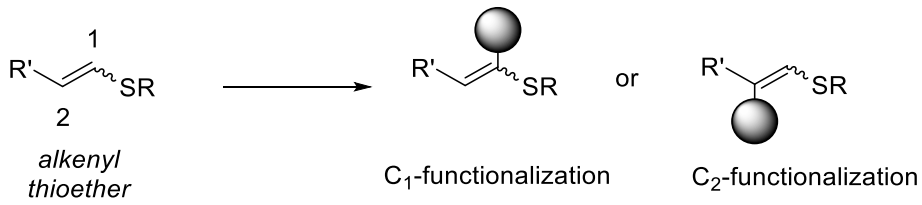

Figure 4.3 – C_1 and C_2 functionalization of alkenyl thioether

Anionic method

In the 80's, Julia and coworkers developed the introduction of alkyl, allyl or silyl groups on 1-*tert*-butylthio-3-methoxy-1-alkenes using metalating agents (Figure 4.4).[220] Two different sets of conditions allow a regioselective substitution either at the C_1 or at the C_2 position.

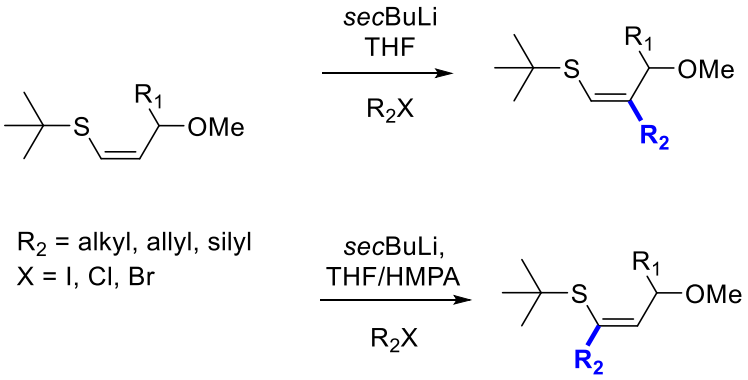

Figure 4.4 – Functionalization of 1-*tert*-butylthio-3-methoxy-1-alkenes using metalating agents

Heck-type reaction

Most efforts to functionalize alkenyl thioethers then focused on the development of palladium-catalyzed arylation of alkenyl thioethers.[221–223] Very good yields and high regio- and stereoselectivities can be obtained with these methods. The one developed by Gillingham and coworkers is depicted in Figure 4.5.[223]

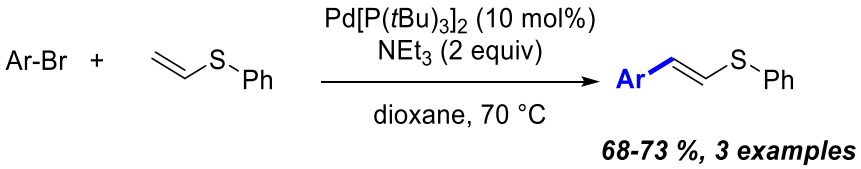

Figure 4.5 – Stereoselective Heck reaction with alkenyl thioethers

Electrolysis

Regarding the synthesis of fluorinated alkenyl thioethers, Marquet and coworkers described an approach based on the anodic functionalization of alkenyl thioethers allowing the introduction of a fluorine atom at the C_2 position (Figure 4.6).[224,225]

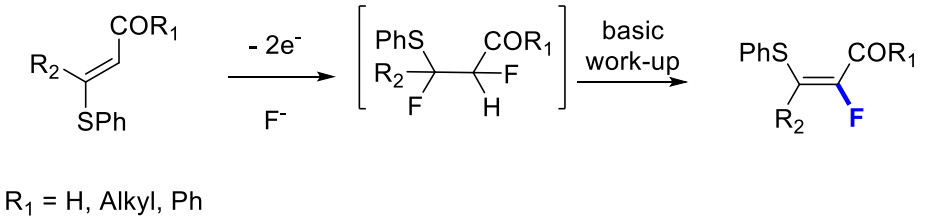

Figure 4.6 – Anodic fluorination of alkenyl thioethers

Functionalization of alkenyl thioethers bearing a CF_3 motif

More recently, β-trifluoromethyl-α-functionalized alkenyl thioethers were synthesized under anionic conditions by Hanamoto and coworkers (Figure 4.7).[226,227]

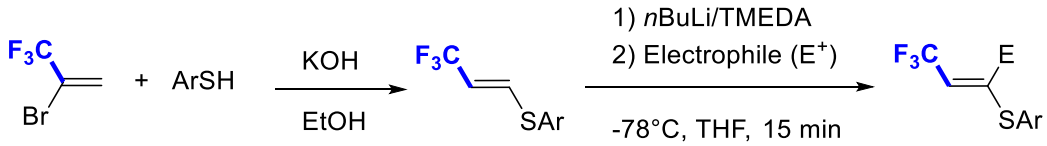

Figure 4.7 – Synthesis and C_1-functionalization of alkenyl thioethers bearing C_2-trifluoromethyl group

As a complementary approach, Zard and coworkers reported the synthesis of tri- and tetra-substituted functionalized alkenyl thioethers by radical allylation, including examples bearing a CF_3 motif (Figure 4.8).[228]

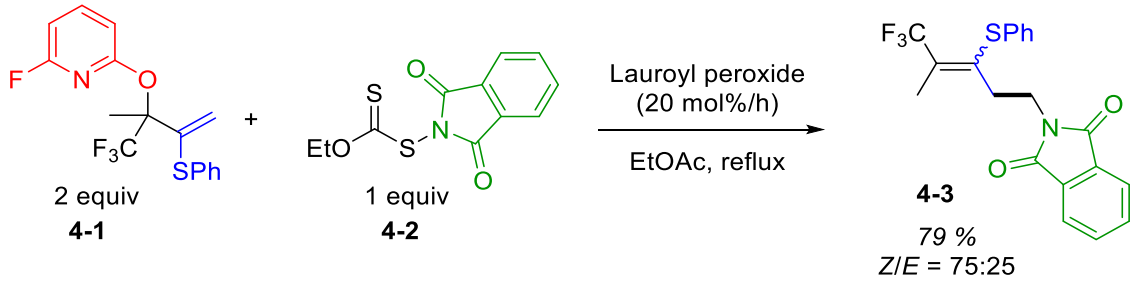

Figure 4.8 – Functionalization of alkenyl thioethers by radical allylation

In summary, there is no general method to introduce pre-functionalized fluorinated groups on alkenyl thioethers. Difluoroacetylation methods are nevertheless widely developed for other olefinic substrates and are detailed in the next section.

Difluoroacetylation methods by C-H functionalization

For the introduction of fluorinated methyl groups, efforts have first mainly focused on CF_3 and CF_2R groups. Then, the introduction of pre-functionalized fluorinated building blocks that can be used for further transformations has been developed. In the last few years, literature for fluorination methods has exploded. In this chapter, for clarity, only literature dealing with the introduction of pre-functionalized fluorinated building blocks by C-H functionalization will be developed, focusing on aryl, heteroaryl and olefinic substrates.

Radical methods

CF_2R building-blocks can be introduced via a radical pathway. $^{\bullet}CF_2R$ radicals can be generated from halogenated or selenium-based X-CF_2R reagents.

In 2006, Fuchigami and coworkers reported the photochemical substitution of olefins and aromatic compounds, with difluoromethyl radicals bearing ester and phosphonate groups (Figure 4.9).[229] α,α-difluoro-α-(phenylseleno)acetate **4-4** can be obtained by selenation of ethyl 2-bromoacetate followed by anodic fluorination.[230] Phenylselanyl difluorophosphonate **4-5** can be obtained from commercially available diethyl difluoromethylphosphonate after lithiation and quench by diphenyl diselenide or phenylselanyl chloride.[231]

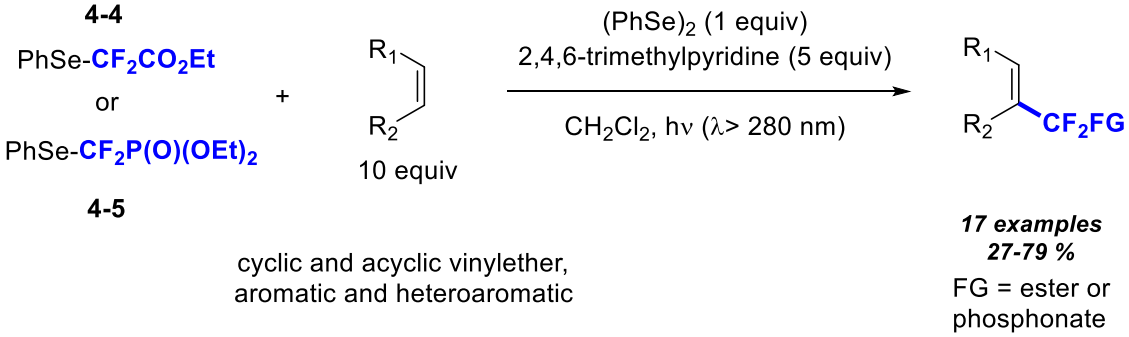

Figure 4.9 – Photochemical substitution of olefins and aromatic compounds with difluoromethyl radicals

In this reaction, the light irradiation allows a homolytic cleavage of the Se-C bond. The two radicals formed add to the double bond before elimination of PhSeH. Addition of $(PhSe)_2$ and 2,4,6-trimethylpyridine limits the formation of the saturated by-product. A wide variety of

substrates is tolerated: benzene, vinyl ethers, dihydropyrane, furane, dihydrofurane, thiophene and pyrroles.

In 2007, Hu and coworkers reported the radical (phenylsulfonyl)difluoromethylation of terminal alkenes.[232] The readily available $PhSO_2CF_2I$ **4-6**, prepared from $PhSO_2CF_2H$ and I_2 in the presence of *t*BuOK,[233] is used as a $PhSO_2CF_2^{\bullet}$ precursor, with Et_3B/air as initiating system for the reaction (Figure 4.10). DBU allows the dehydroiodination to give the alkene with a good stereoselectivity.

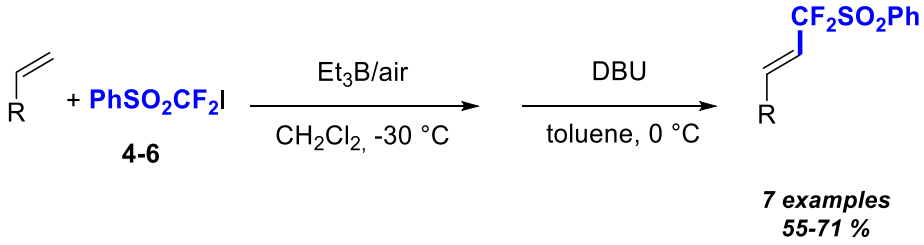

Figure 4.10 – Radical (phenylsulfonyl)difluoromethylation of terminal alkenes

In 2011, Yamakawa and coworkers reported the direct ethoxycarbonyldifluoromethylation of aromatic compounds using Fenton reagent and the commercially available $BrCF_2CO_2Et$ **4-8** (Figure 4.11).[234] The reaction is initiated by the generation of a hydroxyl radical from H_2O_2 by $Fe^{(II)}$.

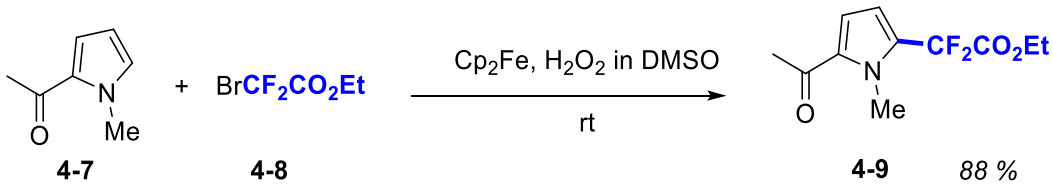

Figure 4.11 – Ethoxycarbonyldifluoromethylation using Fenton reagent

The scope of the reaction is wide and includes benzene, pyrrole, thiophene, benzothiophene, furane, benzofurane, imidazole and pyrazole derivatives. When *para*-substituted anilines like **4-10** are used, the functionalization can be followed by an intramolecular amidation to form the fluorinated oxindole **4-12** (Figure 4.12).

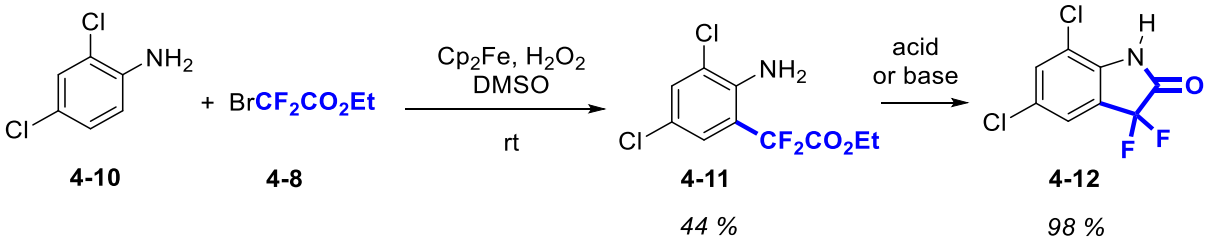

Figure 4.12 – Ethoxycarbonyldifluoromethylation of anilines using Fenton reagent followed by intramolecular amidation

Silver-mediated reaction

In 2016, Hao and coworkers reported the silver-mediated C-H difluoromethylation of arenes using ethyl(trimethylsilyl)difluoroacetate **4-13**.[235] The reaction can also proceed with thiophene. Successful capture of the $^{\bullet}CF_2CO_2Et$ radical by TEMPO led the authors to propose a radical mechanism in which a $AgCF_2CO_2Et$ intermediate generates a $^{\bullet}CF_2CO_2Et$ radical before its addition to the aromatic ring.

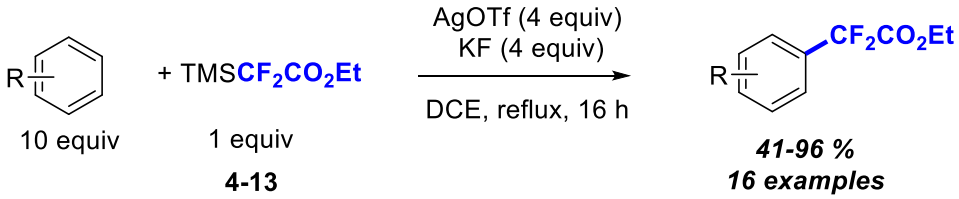

Figure 4.13 – Silver-mediated C-H difluoromethylation of arenes

Methods with visible-light photocatalysis

The introduction of pre-functionalized fluorinated groups by C-H functionalization was also developed under visible-light photocatalysis. In 2013, Qing and coworkers reported the direct introduction of ethoxycarbonyldifluoromethyl group to heteroarenes with a ruthenium catalyst (Figure 4.14).[236]

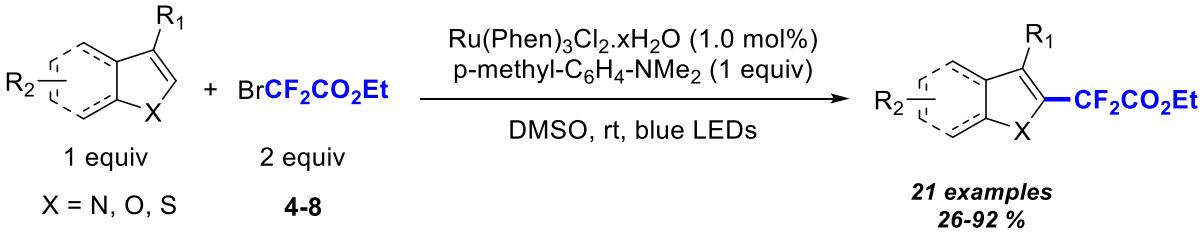

Figure 4.14 - Direct introduction of ethoxycarbonyldifluoromethyl group with a ruthenium catalyst under visible-light photocatalysis

Under irradiation, the $Ru^{(II)}$ complex is excited and quenched by the amine which plays the role of sacrificial reductant to generate a $Ru^{(I)}$ species, able to reduce $BrCF_2CO_2Et$ and to form $^{\bullet}CF_2CO_2Et$.

In 2014, Wang and coworkers developed a similar methodology for the C-H difluoromethylation of electron-rich heteroarenes (Figure 4.15).[237] The reaction was inhibited by radical scavengers and the authors proposed a $Ru^{(II)}/Ru^{(III)}$ catalytic cycle involving a $PhSO_2CF_2^{\bullet}$ radical.

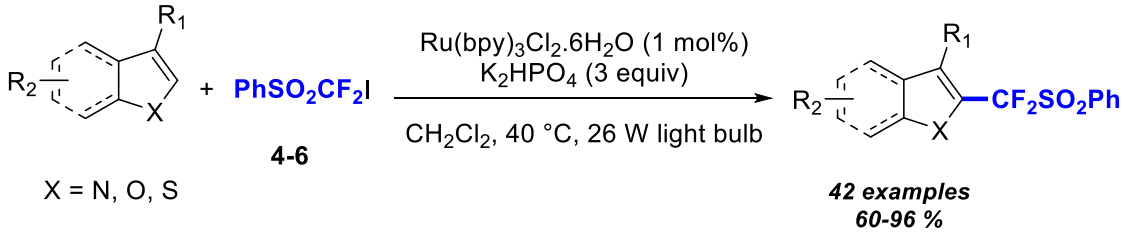

Figure 4.15 - Visible light-mediated C-H difluoromethylation of electron-rich heteroarenes

Several iridium-based catalytic systems were also developed. In 2012, Yu and coworkers reported the direct C-H functionalization of enamides and enecarbamates by using visible-light photoredox catalysis (Figure 4.16).[238]

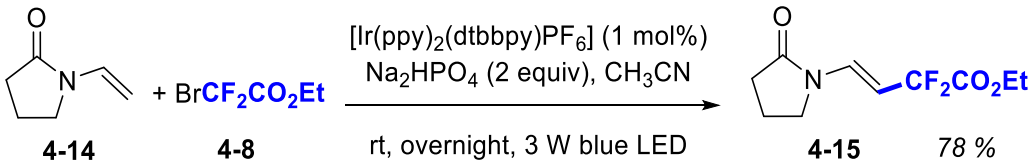

Figure 4.16 – C-H functionalization of enamides using visible-light photoredox catalysis

In 2014, Cho and coworkers reported a similar reaction on aromatics and heteroaromatics (Figure 4.17).[239] The scope includes benzene, pyrrole, furane, and thiophene derivatives.

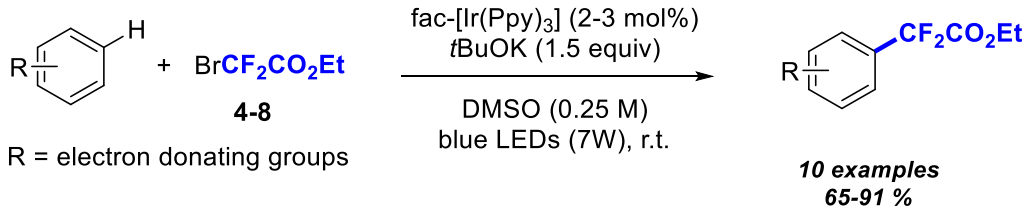

Figure 4.17 – Visible light-induced aromatic difluoroalkylation

In very similar conditions, they also reported the difluoroalkylation of alkenes (Figure 4.18).[240]

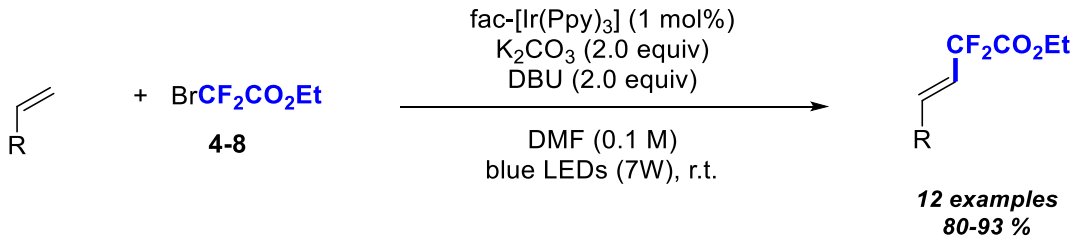

Figure 4.18 – Difluoroalkylation of alkenes by using visible light photoredox catalysis

With $Ir^{(III)}$ catalysts, photoexcitation by visible light produces $Ir^{(IV)+}ligand^{\bullet -}$ through a metal to ligand charge transfer. This transient species is oxidatively quenched by one-electron transfer to $BrCF_2CO_2Et$, producing $Ir^{(IV)+}$ and $^{\bullet}CF_2CO_2Et$.

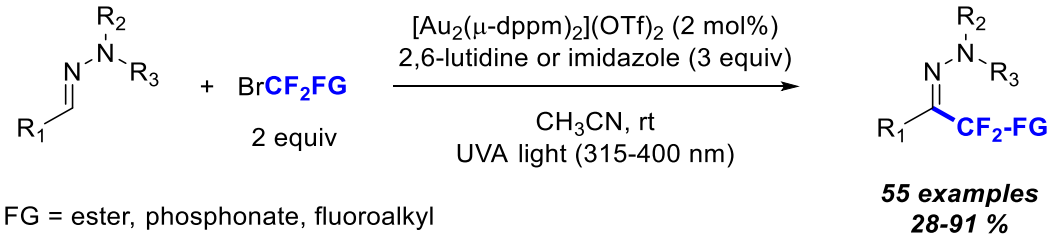

Figure 4.19 – Gold-catalyzed photoredox difluoroalkylation and perfluoroalkylation of hydrazones

In 2016, Hashmi and coworkers developed a gold-catalyzed $C(sp^2)$-H difluoroalkylation and perfluoroalkylation of hydrazones (Figure 4.19).[241] The proposed mechanism involves the

generation of a long-lived photoexcited state of the $Au^{(I)}$ complex, able to reduce $BrCF_2FG$ to deliver the $^{\bullet}CF_2FG$ radical.

Palladium-catalyzed methods

A few palladium-catalyzed methods allow the difluoroalkylation of styrene derivatives and heteroarenes.

In 2012, Reutrakul and coworkers reported the palladium-mediated Heck-type reaction of [(bromodifluoromethyl)-sulfonyl]benzene.[242] This reagent is obtained from the reaction between thiophenol and dibromodifluoromethane followed by oxidation. The reaction can be performed on styrene derivatives and heteroaromatic compounds. It is limited by the important amount of Pd-catalyst needed: 35 mol%. In this reaction, initial mechanistic studies tend to rule out a radical mechanism.

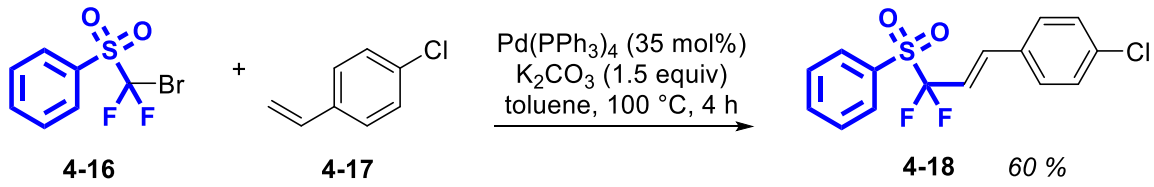

Figure 4.20 – Palladium-mediated synthesis of α-alkenyl α,α-difluoromethyl sulfones

These conditions were improved in 2015 by Zhang and coworkers who reported a general synthesis of fluoroalkylated alkenes by palladium-catalyzed Heck-type reaction (Figure 4.21).[243] This reaction is suggested to proceed via a radical mechanism, in which fluoroalkyl radicals are initiated by a [Pd^0/Xantphos] complex through a SET pathway.

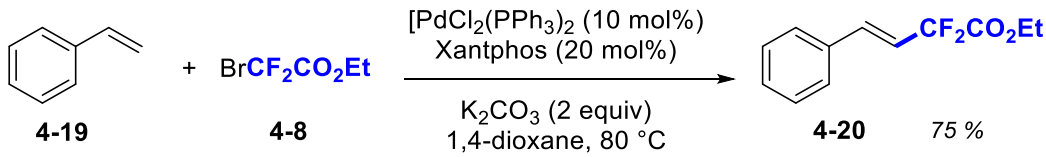

Figure 4.21 – Palladium-catalyzed Heck-type reaction of bromodifluoroacetate with styrene

This methodology is also amenable to electron-rich heteroarenes, as reported by Guan and coworkers (Figure 4.22).[244]

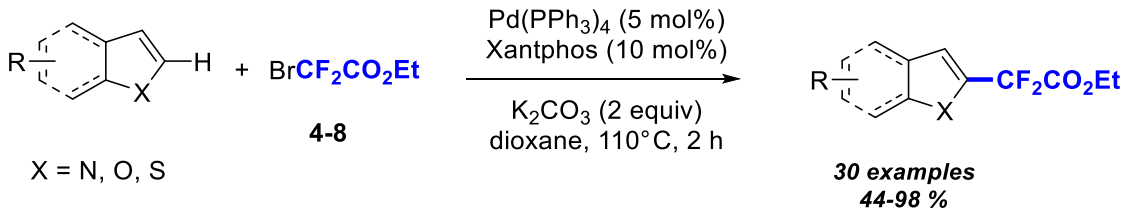

Figure 4.22 - Pd-catalyzed difluoroalkylation of electron-rich heteroarenes

In 2016, Skrydstrup reported a palladium-catalyzed carbonylative coupling of aryl and heteroaryl boronic acid derivatives with carbon monoxide and bromodifluoroacetamides (Figure 4.23).[245]

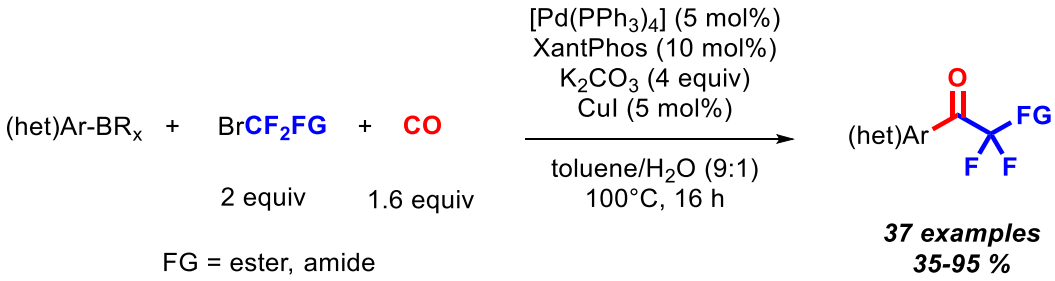

Figure 4.23 – Palladium-catalyzed carbonylation of (hetero)aryl boronic acid derivatives to access difluoroacylated arenes

In a recent mechanistic study,[246] they proposed a pathway proceeding through single-electron elementary steps, to form carbon-centered alkyl radicals from the alkyl bromide.

Copper-catalyzed methods

The C-H functionalization of electron-rich olefins and hydrazones has been developed under copper catalysis.

The first developments of this methodology were made by Belhomme and coworkers, our collaborators from the INSA de Rouen. In 2013, they reported the first introduction of -CF_2CO_2Et by means of C-H bond functionalization on dihydropyrans and glycals (Figure 4.24).[247]

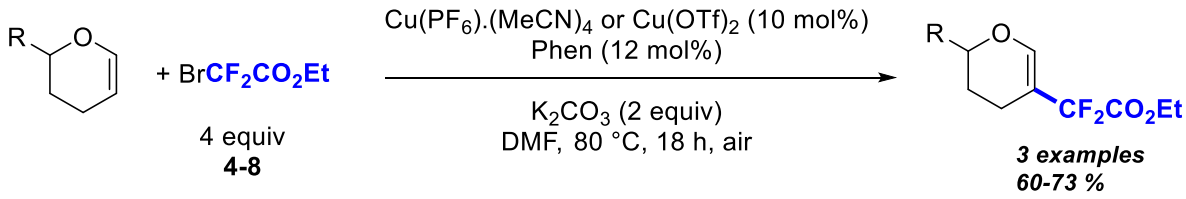

Figure 4.24 – Copper-catalyzed β-difluoroacetylation of dihydropyrans and glycals

They then generalized this approach to the difluoromethylation of furans and benzofurans (Figure 4.25),[248] and to the difluoroacetylation of cyclic and acyclic enamides bearing an electron withdrawing group. This latter was done in collaboration with Gillaizeau and coworkers (Figure 4.26).[249]

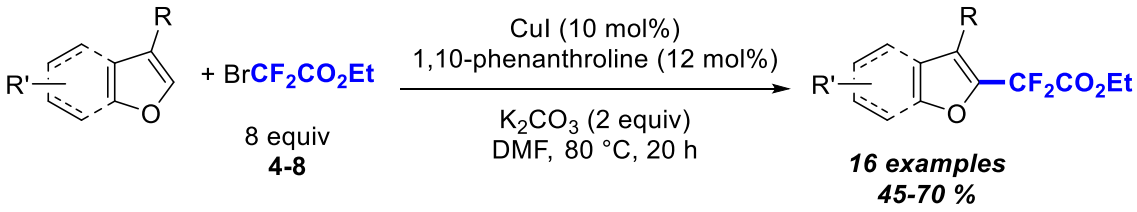

Figure 4.25 – Copper-catalyzed direct C_2-difluoromethylation of furans and benzofurans

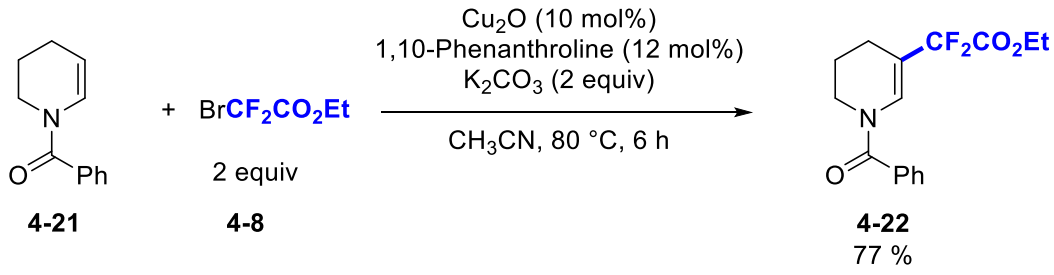

Figure 4.26 – Copper-catalyzed olefinic C-H difluoroacetylation of enamides

This strategy could also be applied to the ethoxycarbonyldifluoromethylation of electron-rich arenes (Figure 4.27).[250] The reaction works with both difluorinated esters and difluorinated amides.

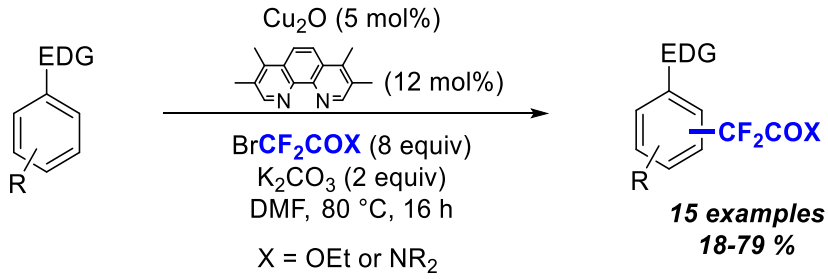

Figure 4.27 – Copper-catalyzed ethoxycarbonyldifluoromethylation of electron-rich arenes

In 2016, Hajra and coworkers reported the use of a similar catalytic system for the C-H ethoxycarbonyldifluoromethylation of imidazoheterocycles (Figure 4.28).[251]

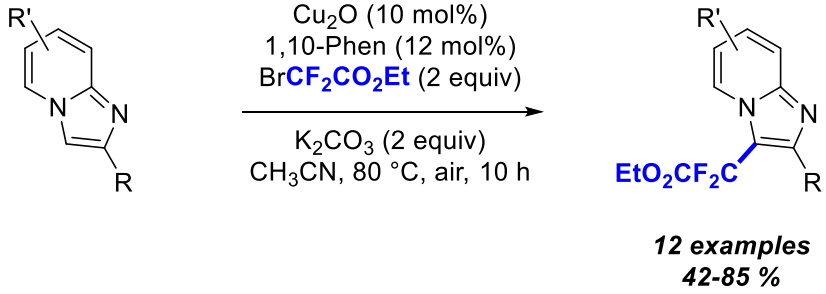

Figure 4.28 – Copper-catalyzed C-H ethoxycarbonyldifluoromethylation of imidazoheterocycles

For all these catalytic systems, a $Cu^{(I)}/Cu^{(III)}$ catalytic cycle was proposed. A radical pathway was ruled out because radical scavengers did not inhibit the reaction. The catalytic cycle proposed is depicted in Figure 4.29 in the case of the difluoroacetylation of enamides.[249] Cyclic voltammetry experiments and mass spectroscopy evidenced the complexation of the enamide on the copper to form **4-23**, but completely ruled out a direct oxidative addition of the bromo compound on a copper complex. A deprotonation step is then proposed, before the oxidative addition of $BrCF_2CO_2Et$ to form a $Cu^{(III)}$ complex. Finally, reductive elimination would provide the product, regenerating the $Cu^{(I)}$ catalyst.

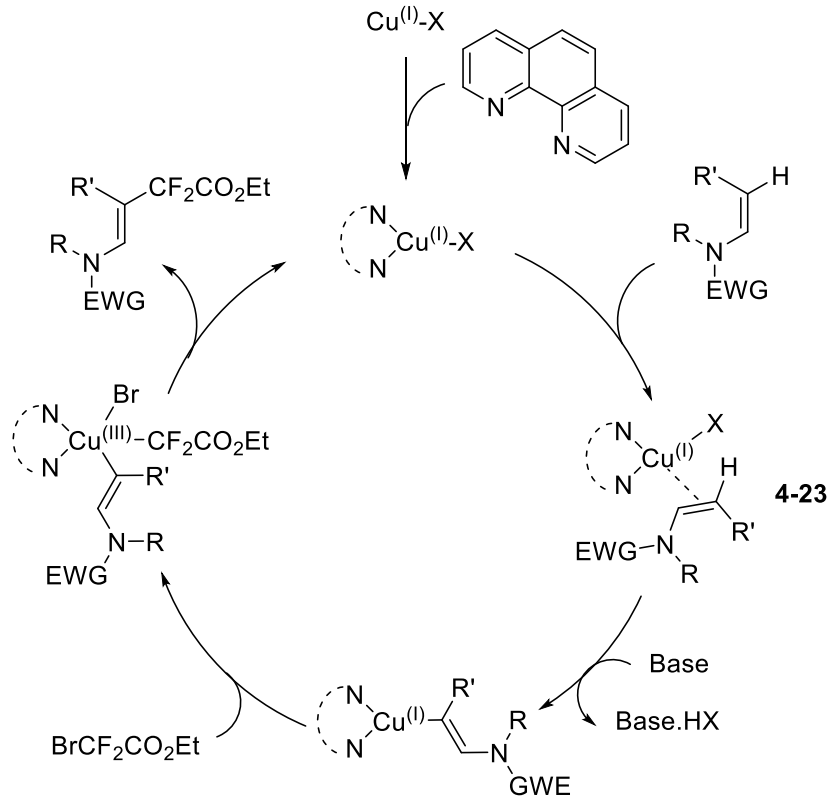

Figure 4.29 – Proposed reaction mechanism for the copper-catalyzed difluoroacetylation of enamides

In 2016, two closely related studies were reported for the C-H difluoroalkylation of aldehyde-derived hydrazones. Song and coworkers reported a catalytic system with a $Cu^{(II)}$ catalyst and diboron as reductant (Figure 4.30).[252]

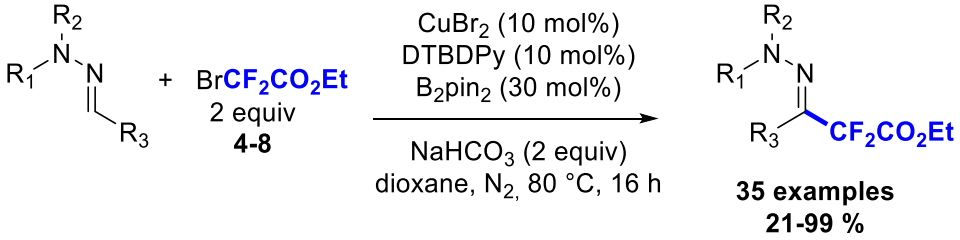

Figure 4.30 – Copper-catalyzed C-H difluoroalkylation of aldehyde derived hydrazones with diboron as reductant

Monteiro and coworkers reported a catalytic system with $Cu^{(I)}$ and 1,10-phenanthroline that proceeds smoothly with both bromodifluoroacetates and bromodifluoroacetamides (Figure 4.31).[253] Recently, Jiang and coworkers reported the copper-catalyzed gem-difluoromehylenation of alkenes (Figure 4.32).[254]

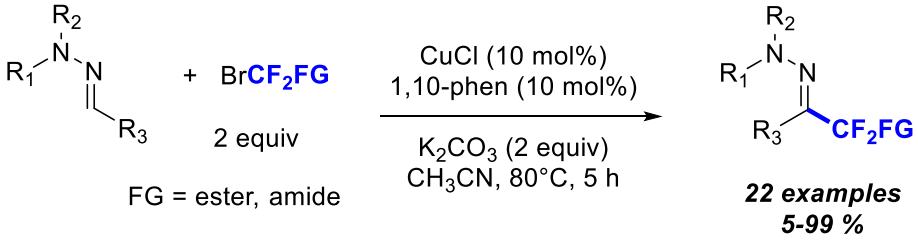

Figure 4.31 – Copper-catalyzed C-H difluoroalkylation of aldehyde-derived from hydrazine

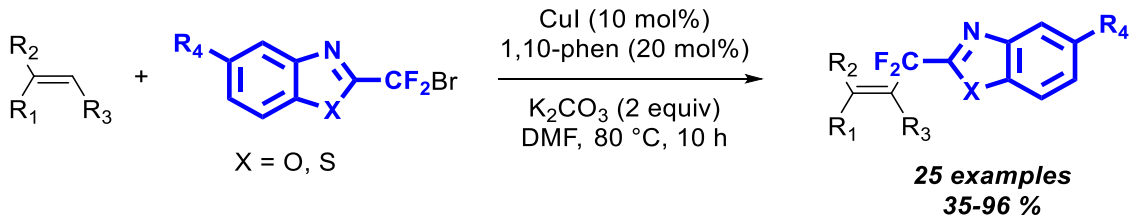

Figure 4.32 – Copper-catalyzed gem-difluoromethylenation of alkenes

For these three catalytic systems, the reactions were inhibited by the presence of radical scavengers and, in some cases, the TEMPO-CF_2R adduct could be identified. For this reason, a $Cu^{(I)}/Cu^{(II)}$ catalytic cycle involving radical species was proposed as depicted in Figure 4.33.[253] A $^{\bullet}CF_2R$ radical is formed by single electron transfer (SET) from $Cu^{(I)}$, along with $Cu^{(II)}$. The radical can add to the substrate to form a new radical species, which is able to reduce $Cu^{(II)}$ in $Cu^{(I)}$ to regenerate the catalyst. The resulting cation further evolves through deprotonation to give the desired product.

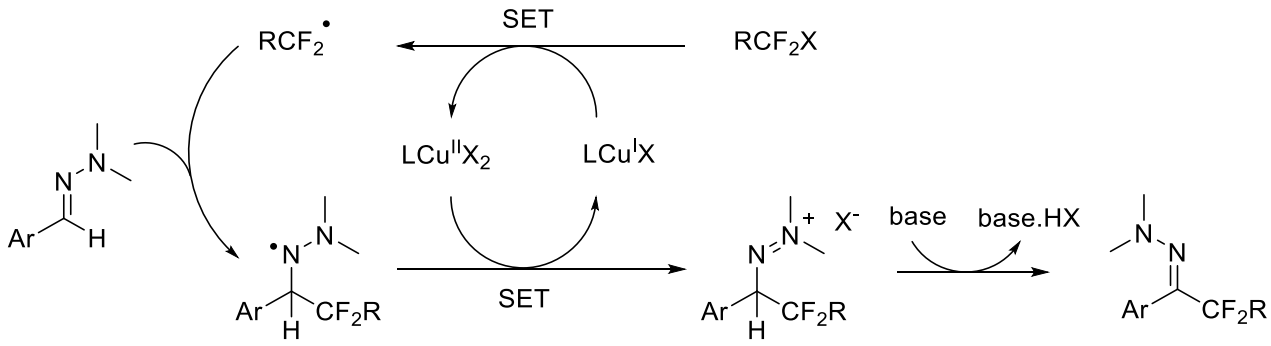

Figure 4.33 – Proposed mechanism for the copper-catalyzed C-H difluoroalkylation of hydrazones

Methodology for the copper–catalyzed difluoroacetylation of alkenyl thioethers

Stimulated by the previous works of our collaborators, the Pannecoucke and the Gillaizeau groups, dealing with the copper-catalyzed ethoxy carbonyl difluoromethylation of various scaffolds through a direct C-H functionalization, we extended the methodology to the functionalization of alkenyl thioethers. In addition, significant insights regarding the mechanism of this reaction are disclosed, establishing a radical pathway.

Optimization of the conditions

The reaction conditions were first optimized using *n*-hexyl(styryl)sulfane **4-24a** as a model substrate. Standard screening of solvent, catalysts, bases, ligands, temperature and reagent stoichiometries were performed and are detailed below.

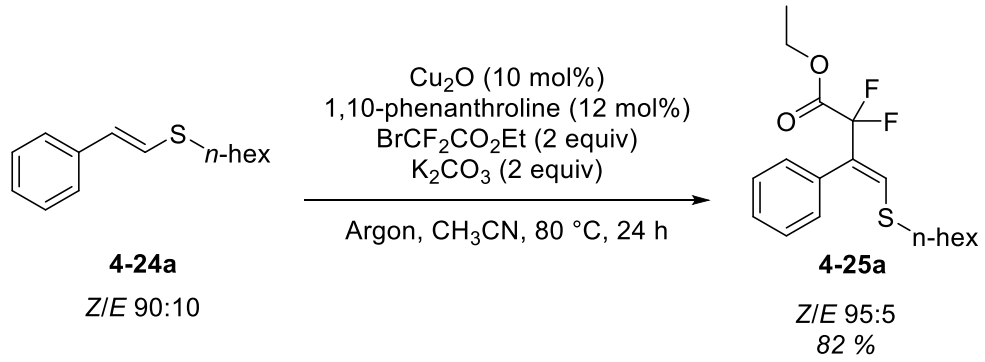

Figure 4.34 – Standard conditions for the difluoroacetylation of alkenyl thioethers

The desired product **4-25a** was isolated in 82 % yield (Figure 4.34) when using Cu_2O (10 mol%), 1,10-phenanthroline (12 mol%) as a ligand in the presence of K_2CO_3 (2 equiv) and $BrCF_2CO_2Et$ (2 equiv), in acetonitrile at 80 °C for 24 h.

Several copper sources were also found to be efficient: CuI, $Cu(CH_3CN)_4PF_6$, and $Cu(OTf)_2$ catalyzed the reaction but gave lower yields than Cu_2O (Table 4.1, entries 2-4). A control experiment clearly showed the absence of reactivity without any catalyst (Table 4.1, entry 5).

Table 4.1 – Screening of catalysts

Entry	Deviation from the standard conditions	Yield of 4-25a (%)
1	None	82 [a]
2	Catalyst: $Cu(OTf)_2$	60 [a]
3	Catalyst: CuI	59 [a]
4	Catalyst: $Cu(CH_3CN)_4PF_6$	70 [a]
5	No catalyst	0

a. Isolated yield

Table 4.2 – Screening of ligands

Entry	Deviation from the standard conditions	Yield of 4-25a (%)
1	None	82 [a]
2	Ligand: Neocuproine 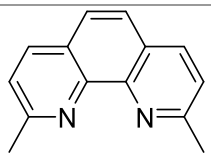	0
3	Ligand: TMEDA 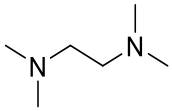	0
4	Ligand: TMHD 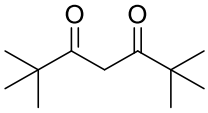	0
5	Ligand: 2,2'-bipyridine 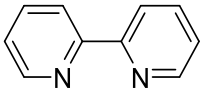	35 [a]
6	No ligand	0
7	No ligand and catalyst: $Cu(CH_3CN)_4PF_6$	0
8	No ligand and catalyst: CuI	0

a. Isolated yield

Different bidentate ligands were then tested (Table 4.2). The 2,2,6,6-tetramethyl-3,5-heptanedione (TMHD) gave no conversion (Table 4.2, entry 4). Tetramethylethylenediamine (TMEDA) failed to give any product (Table 4.2, entry 3). Neocuproine, whose structure is very

similar to 1,10-phenanthroline, gave no conversion (Table 4.2, entry 2), probably due to the steric hindrance of the methyl groups. 2,2'-bipyridine was the only other ligand exhibiting reactivity, with 35 % yield of **4-25a** (Table 4.2, entry 5). A control experiment established the lack of reactivity without added ligand (Table 4.2, entry 6). To confirm that the ligand had an impact on the reactivity and did not only help the solubilization of the catalyst Cu_2O, the control experiments were also performed with the reactive $Cu(CH_3CN)_4PF_6$ and CuI and confirmed the former results (Table 4.2, entry 7 and 8).

Table 4.3 – Screening of bases

Entry	Deviation from the standard conditions	Yield of 4-25a (%)
1	None	82 [a]
2	Base: Cs_2CO_3	28 [b]
3	Base: Na_2CO_3	12 [b]
4	Base: Et_3N	< 5 [b]
5	Base: 2,6-lutidine 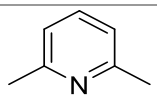	0
6	Base: nBu$_4$NOAc	0
7	No base	0

a. Isolated yield b. ^{19}F NMR yield. α,α,α-trifluorotoluene was used as internal standard.

Table 4.4 – Screening of solvents

Entry	Deviation from the standard conditions	Yield of 4-25a (%)
1	None	82 [a]
2	Solvent: DMF	< 5 [b]
3	Solvent: NMP	10 [b]

a. Isolated yield b. ^{19}F NMR yield. α,α,α-trifluorotoluene was used as internal standard.

Among the other bases tested, low conversions were observed with other carbonates: Cs_2CO_3 and Na_2CO_3 (Table 4.3, entries 2 and 3), and organic bases (Et_3N and 2,6-lutidine,

nBu_4NOAc) failed to give any adduct (Table 4.3, entries 4-6). A control experiment showed no reactivity in the absence of base (Table 4.3, entry 7).

Several polar solvents were tested since these are usually efficient for this type of reactions.[247,249,250] Only low yields were obtained in DMF and NMP (Table 4.4, entries 2 and 3).

Additional optimization tests were then done by changing the temperature, the reaction time or the reagents loadings (Table 4.5). No conversion occurred at room temperature after prolonged reaction time (Table 4.5, entry 2). Shortening the reaction time cut down the yield of the reaction (46 % yield after 6 h of reaction, Table 4.5, entry 3). The reaction could proceed under an air atmosphere, albeit with lower yields (65 %, Table 4.5, entry 4). Lowering the amount of substrate ($BrCF_2CO_2Et$) from 2 equiv to 1.3 equiv greatly impacted the reaction yield (Table 4.5, entry 5). The catalyst loading could not be reduced since the yield significantly dropped off when using 2 mol% of copper salt (Table 4.5, entry 6).

Table 4.5 – Screening of reaction conditions

Entry	Deviation from the standard conditions	Yield of 4-25a (%)
1	none	82 [a]
2	RT, 40 h	0
3	6 h	46 [a]
4	Air atmosphere	65 [b]
5	1.3 equiv of $BrCF_2CO_2Et$	30 [b]
6	2 % Cu_2O	24 [b]

a. Isolated yield b. ^{19}F NMR yield. α,α,α-trifluorotoluene was used as internal standard.

Overall, the optimization of the reaction conditions confirmed that the best yields were obtained using the conditions previously settled for the ethoxy carbonyl difluoromethylation of enamides,[249] with longer reaction time.

Under this optimized set of experimental conditions, the reaction turned out to be highly regio- and stereoselective. Indeed, the trisubstituted alkene **4-25a** was isolated as the major compound with a 5:95 *Z*/*E* ratio starting from alkenyl thioether **4-24a** as a *Z*/*E* (10:90).

Scope of the reaction

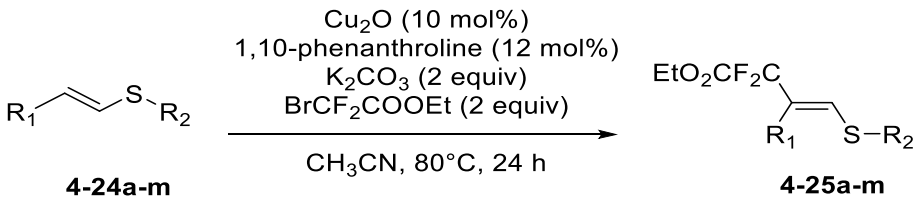

Figure 4.35 – Optimized reaction conditions used for the development of the scope of the reaction

Table 4.6 – Scope of the reaction

Name	Structure of 4-24	4-24 (*Z*/*E*)	Structure of 4-25	4-25 (*Z*/*E*)	Yield[a] of 4-25 (%)
a	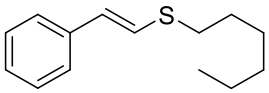	10 : 90	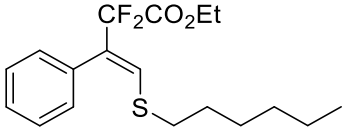	5 : 95	82
b	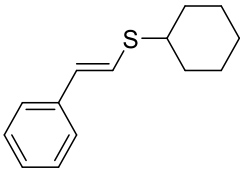	48 : 52	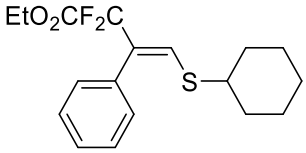	7 : 93	83
c	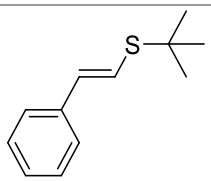	64 : 36	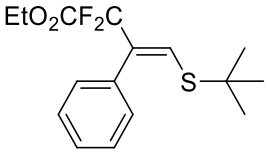	5 : 95	81
d	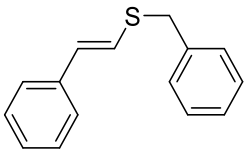	20 : 80	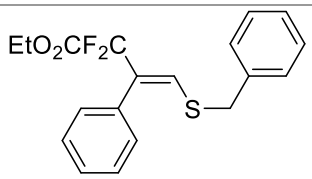	6 : 94	75
e	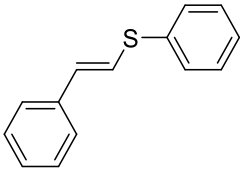	10 : 90	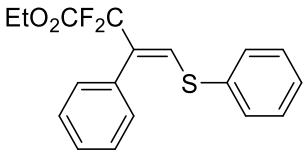	8 : 92	53

f	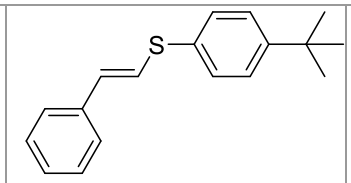	26 : 74	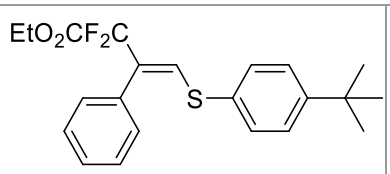	9 : 91	73
g	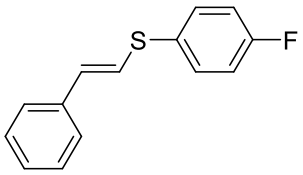	35 : 65	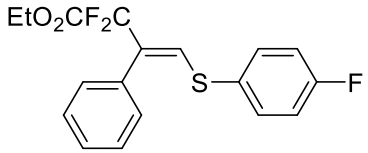	8 : 92	60
h	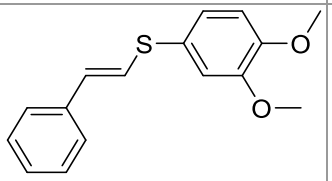	35 : 65	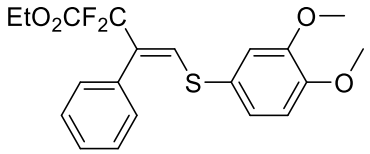	6 : 94	41
i	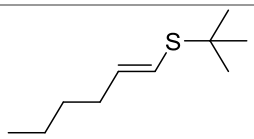	> 1 : 99	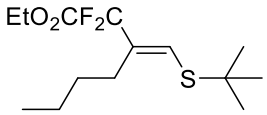	> 1 : 99	81
j	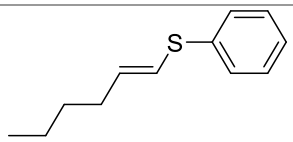	> 1 : 99	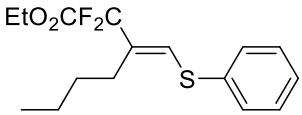	> 1 : 99	81
k	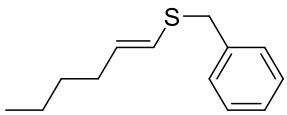	> 1 : 99	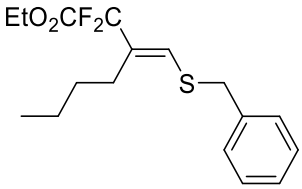	> 1 : 99	71
l	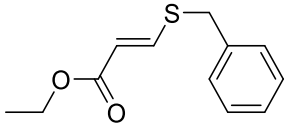	17 : 83	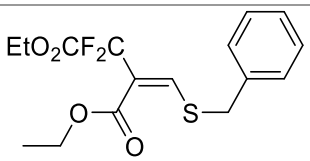	42 : 58	20
m	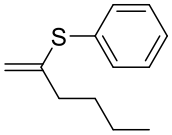	Single isomer	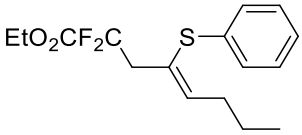	81 : 19	55

a. Isolated yields

Having established the optimal reaction conditions (Figure 4.35), the scope of the reaction was further examined with a wide array of alkenyl thioether derivatives (see Table 4.6, the major isomer is represented). Different styryl thioethers were successfully functionalized

under these conditions. The reaction turned out to be of similar efficiency when performed with *S*-secondary (**4-25b**) or *S*-tertiary (**4-25c**) alkyl substituents as well as with benzyl groups (**4-25d**). Aryl styryl thioethers gave slightly lower yields of isolated adducts (**4-25e** to **4-25h**) whatever the nature of the substituent on the aromatic ring. When replacing the styryl moiety with an alkyl-substituted olefin, the reaction behaved similarly affording excellent yields of the trisubstituted alkenes **4-25i** to **4-25k**. However, the electron-deficient sulfanyl acrylate **4-24l** was poorly reactive giving **4-25l** in a modest 20 % yield. When the *gem*-disubstituted alkenyl thioether **4-24m** was used, traces of the expected product were obtained (yield about 8 %) along with the product **4-25m** (55 % yield) resulting from a subsequent isomerization.

Selectivity of the reaction

The reaction turned out to be highly regio- and stereoselective.

Stereoselectivity

In order to determine the configuration of the trifunctionalized thioethers, Heteronuclear NOESY experiments (HOESY) were performed. They clearly demonstrated a correlation between the fluorine atom and the olefinic proton on **4-25j** and **4-25k**, enabling us to establish the *E* selectivity of the reaction (Figure 4.36). All other configurations were assigned by analogy.

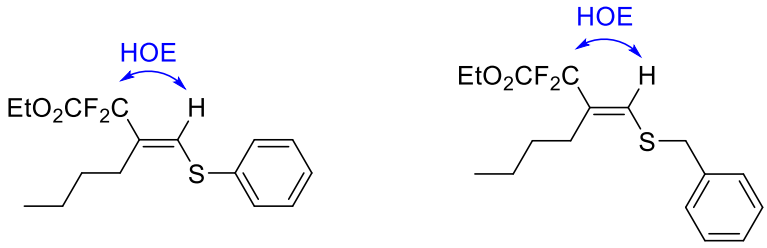

Figure 4.36 - HOE observed on compounds **4-25j** and **4-25k**

When starting with a nearly equimolar *Z*/*E* mixture of alkenyl thioether (eg. **4-24b** or **4-24c**), the trisubstituted alkenes **4-25b** and **4-25c** were isolated in a diastereomeric ratio greater than 90:10 in favor of the *E* isomer. Except for **4-25l**, no isomerization was observed when starting with pure *E* substrates as observed for **4-24i** to **4-24k**.

Regioselectivity

Small amounts of by-product were obtained in up to 15 % yield with **4-24a** to **4-24l**. This by-product **4-26** was identified as the product that could result from an addition-desulfitation at the C_1 position (Figure 4.37).

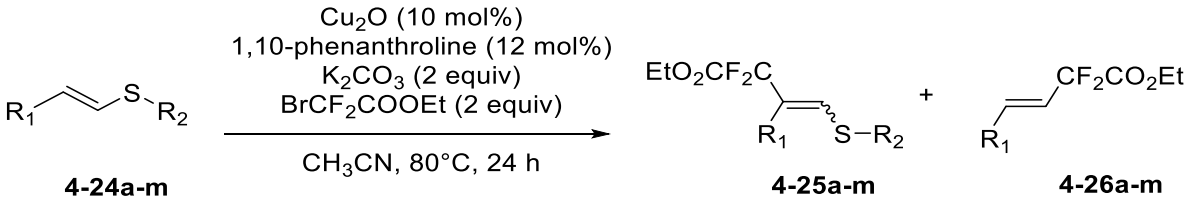

Figure 4.37 – Mixture of products obtained in the optimized conditions

The ^{19}F NMR yields for this by-product are detailed in Table 4.7.

Table 4.7 – Yield for the main by-product

Starting material	Structure of 4-26	^{19}F NMR yield of 4-26 (%)[a]
4-24a	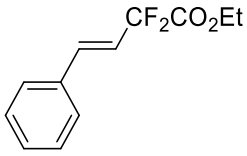	10
4-24b		4
4-24c		7
4-24d		12
4-24e		8
4-24f		12
4-24g		9
4-24h		16
4-24i	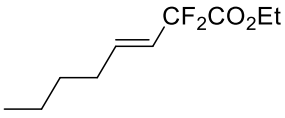	6
4-24j		7
4-24k		6
4-24l	-	0

a. α,α,α-trifluorotoluene was used as internal standard.

The regioselectivity of the reaction and the structure of the by-product was further confirmed using the C_2-disubstituted styryl thioether **4-24n**. In this case, the compound **4-26n** was isolated in a modest 30 % yield along with diphenyldisulfide. This confirms that substitution at the C_1 position results in desulfitation.

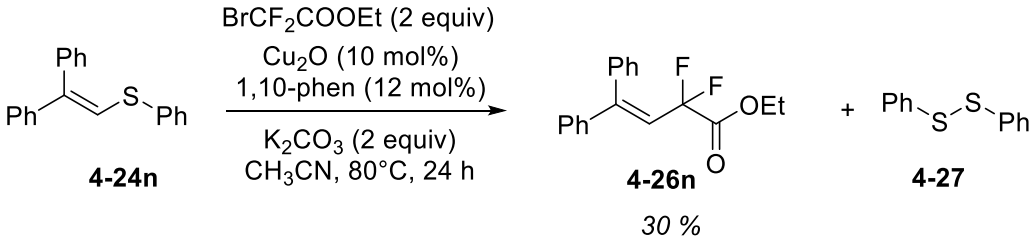

Figure 4.38 - Copper-catalyzed difluoroacetylation of **4-24n**

The regioselectivity of the reaction was also confirmed by NOESY experiments on the substrates **4-25a** and **4-25i**. A NOE was obtained between the vinylic proton and the alkyl chain on the sulfur atom, meaning that they are both on the same side of the double bond (Figure 4.39).

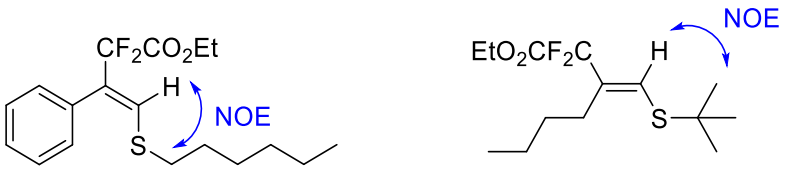

Figure 4.39 – NOE observed on compounds **4-25a** and **4-25i**

Reactivity with other substrates and post-functionalization

Reactivity of other alkylbromides

In an attempt to vary the structure of the obtained products, $BrCF_2CO_2Et$ was replaced by other alkyl bromides. All the fluorinated and non-fluorinated partners tested under the same conditions are represented in Figure 4.40. All of them failed to react.

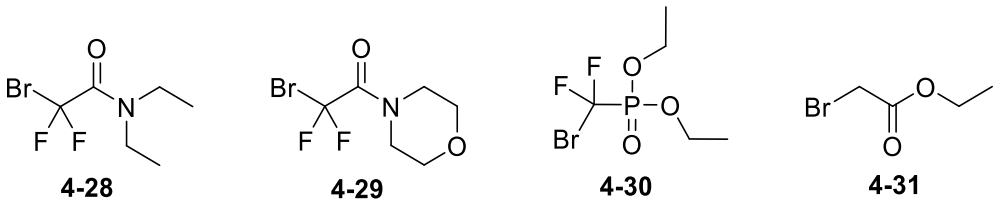

Figure 4.40 – Unreactive alkyl bromides

Post-functionalization

However, the post-functionalization of product **4-25e** turned out to be very efficient as shown in Scheme 3. The ester residue can be readily converted into the corresponding amide by treating compound **4-25e** with an excess of benzylamine (Figure 4.41). This transformation enlarges the molecular diversity accessible with this protocol.

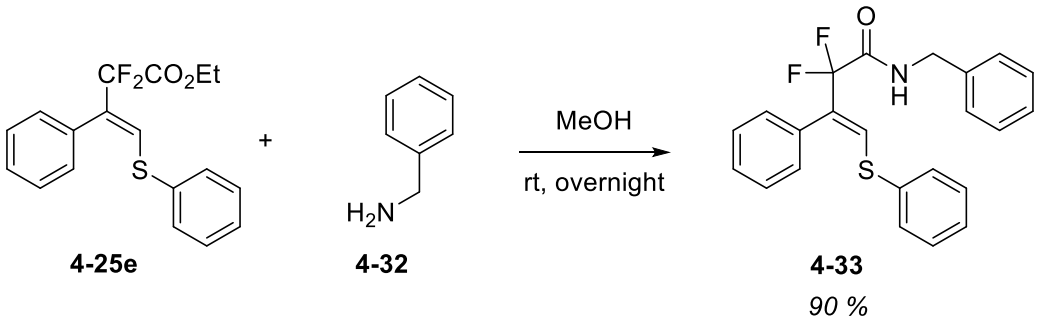

Figure 4.41 – Transformation of the fluorinated alkenyl thioether **4-25e**

Reactivity of alkenes

Since the reaction works in similar conditions with various types of electron-rich alkenes (enamides, dihydropyranes, alkenyl thioethers), we tested our conditions on unactivated alkenes.

Starting from 1,1-diphenylethylene **4-34**, the trisubstituted product **4-26n** was obtained in 48 % yield along with 21 % of the saturated product **4-35**. These two products could not be easily separated by column chromatography (Figure 4.42) and any attempt to improve the yield failed.

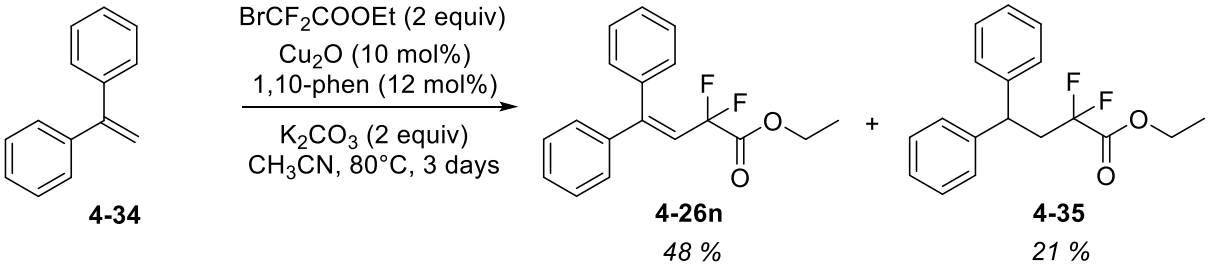

Figure 4.42 – Reactivity of the 1,1-diphenylethylene **4-34** (^{19}F NMR yields are given)

The reaction was then performed on styrene **4-36** and cyclooctene **4-37**. In both cases, polymerization products were obtained (Figure 4.43).

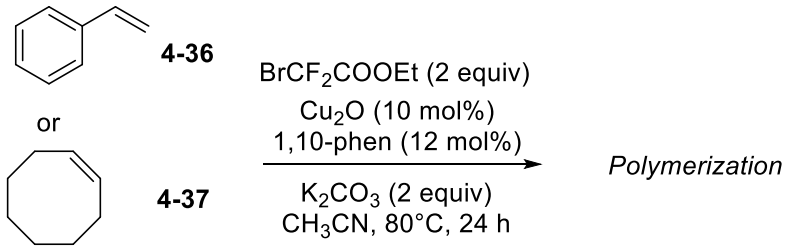

Figure 4.43 – Reactivity of styrene and cyclooctene

The functionalization of unactivated alkenes was not explored further. We developed a copper-catalyzed reaction of fluorination of alkenyl thioethers with direct C-H bond functionalization using $BrCF_2CO_2Et$. This methodology allows the preparation of trisubstituted olefins with controlled regio- and stereoselectivities. We then turned our attention to the mechanism of this reaction.

Mechanistic study of the copper-catalyzed difluoroacetylation of alkenyl thioethers

Experimental evidence for a radical process

To get more insights into the reaction mechanism, selected reactions were performed in the presence of radical scavengers. When **4-24a** was reacted under standard reaction conditions in the presence of Galvinoxyl (1 equiv), no product was formed, while in the presence of TEMPO (1 equiv, Table 4.8, entry 1), traces of product **4-25a** were obtained along with 53 % of the TEMPO-adduct **4-38**, characterized both by ^{19}F NMR and Mass Spectrometry. These experimental observations, along with the formation of diphenyldisulfide **4-27** as by-product and the reactivity on 1,1-diphenylethylene **4-34** described in the previous section, suggest that a radical mechanism is involved in the process. These conclusions are consistent with the recent studies of fluorination of hydrazones with analogous copper systems[252,253] and with similar radical reactions mediated by copper[255–257] as presented above.

Table 4.8 – Mechanistic experiments performed in the presence of TEMPO

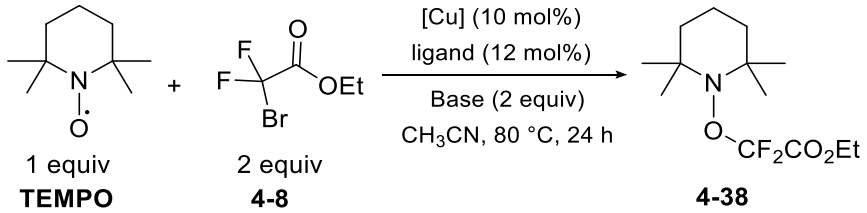

1 equiv **TEMPO** 2 equiv **4-8** **4-38**

Entry	[Cu]	Base	Ligand	Yield of 4-38 (%)
1[a]	Cu_2O	K_2CO_3	1,10-Phen	53
2	Cu_2O	K_2CO_3	1,10-Phen	44
3[b]	$Cu(CH_3CN)_4PF_6$	K_2CO_3	-	0
4	$Cu(CH_3CN)_4PF_6$	K_2CO_3	1,10-Phen	61
5	Cu_2O	-	1,10-Phen	15
6	-	K_2CO_3	1,10-Phen	0

Yields were evaluated by ^{19}F NMR using α,α,α-trifluorotoluene as an internal standard.
a. In the presence of 1 equiv of **4-24a**. 2 % of **4-25a** was formed.
b. The copper source was changed for solubility issues in the absence of ligand.

To identify the key players in the radical formation, the trapping by TEMPO was further examined under various conditions (Table 4.8). The yield of **4-38** is only slightly lower (44 %, Table 4.8, entry 2) when the reaction is performed in the absence of the alkenyl thioether **4-**

24a, suggesting that **4-24a** is not essential for the formation of the difluoroacetate radical. In the absence of copper, no radical was generated (Table 4.8, entry 6). As already observed during the optimization process, *tetrakis*(acetonitrile)copper(I) hexafluorophosphate behaved similarly (Table 4.8, entry 4). This copper source allowed to test the effect of the ligand toward the formation of **4-38**. Indeed, the use of Cu_2O without ligand was not conclusive due to solubility issues. In the absence of 1,10-phenanthroline, no traces of **4-38** were detected (Table 4.8, entry 3), revealing its crucial role for the generation of the radical species, and explaining the failure of the reaction without any ligand. The formation of **4-38** dropped significantly without base (Table 4.8, entry 5), unveiling its contribution in the generation of the reactive species. These experimental observations suggested that the combination of copper, 1,10-phenanthroline and K_2CO_3 might be responsible for the formation of a radical species in the previously settled reaction conditions.

Study of the initiation of the reaction

For a better understanding of the elementary steps involved in this transformation, further investigations on the $Cu^{(I)}$ complex involved in the reduction of $BrCF_2CO_2Et$ were performed at the theoretical level using density functional theory (DFT). All geometric structures were fully optimized using the B3LYP functional. The 6-311+G(d,p) basis sets was used for all main group atoms. Copper atom was described using a double zeta basis set (Lanl2dz) and associated pseudo potential. Bulk solvent effects for acetonitrile were included by means of a polarizable continuum model (PCM). Though the approach used here cannot provide a good description of the entropic effects that can play a role in the present case, the energetic - ie enthalpies - associated to these reactions can be trustfully estimated and are discussed herein. An estimate of the associated reaction free energies is reported in the Appendix (page 226-228). Enthalpies and free energies were calculated for standard conditions at 298.15 K.

Starting complex

Evaluation of the starting complexes by DFT calculations

As starting complexes models, **4-I** to **4-V** were considered, with solvent molecules, alkenyl thioether **4-24b**, 1,10-phenanthroline and hydroxide anion (the base formed in the

reaction medium) included as possible ligands. We chose $Cu(CH_3CN)_4PF_6$ as a simpler starting complex whose observed reactivity was similar to Cu_2O (see Table 4.1). The relative stability of complexes **4-I** to **4-V** is represented in Figure 4.44, and their optimized structure is represented in Figure 4.45. 1,10-Phenanthroline stabilizes the copper complex (**4-I → 4-II**, ΔH = -8.0 kcal.mol^{-1}). The replacement of a solvent molecule by the thioether **4-24b** has no stabilizing effect (**4-II → 4-IV** ΔH = +2.6 kcal.mol^{-1}), whereas the complexation by a hydroxide, resulting in a neutral complex, is very favorable (**4-II → 4-III** ΔH = -11.8 kcal.mol^{-1}). From complex **4-III**, replacement of the solvent molecule by the thioether **4-24b** in the coordination sphere of copper has almost no effect (**4-III → 4-V** ΔH = +0.6 kcal.mol^{-1}), as **4-III** and **4-V** are quasi isoenergetic.

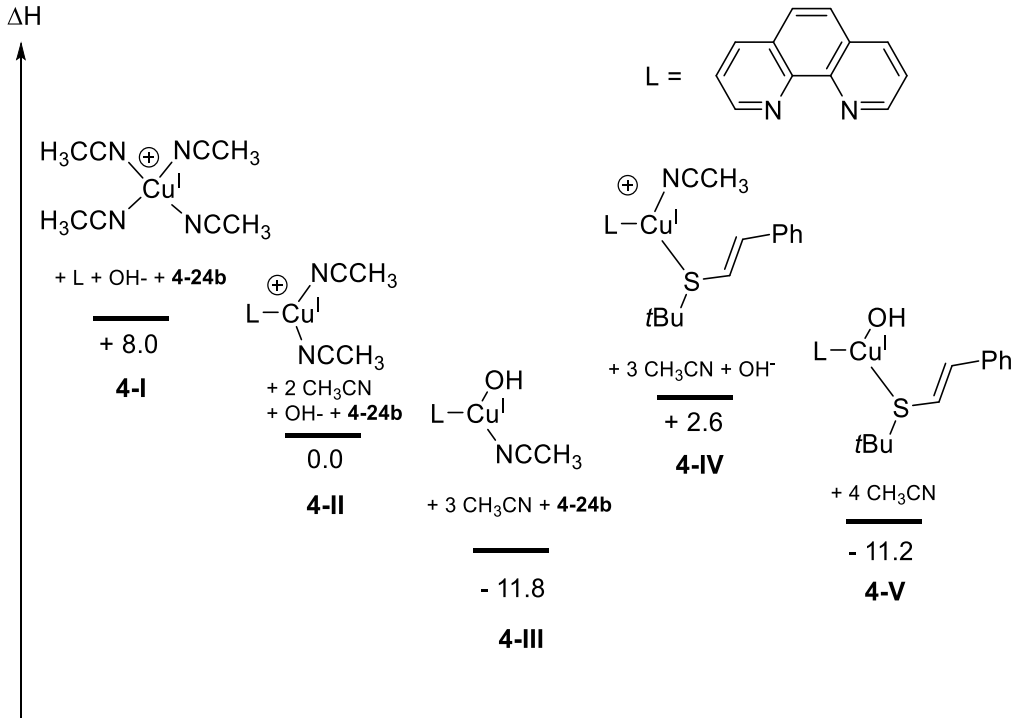

Figure 4.44 – Relative stability of possible starting complexes (in kcal.mol^{-1})

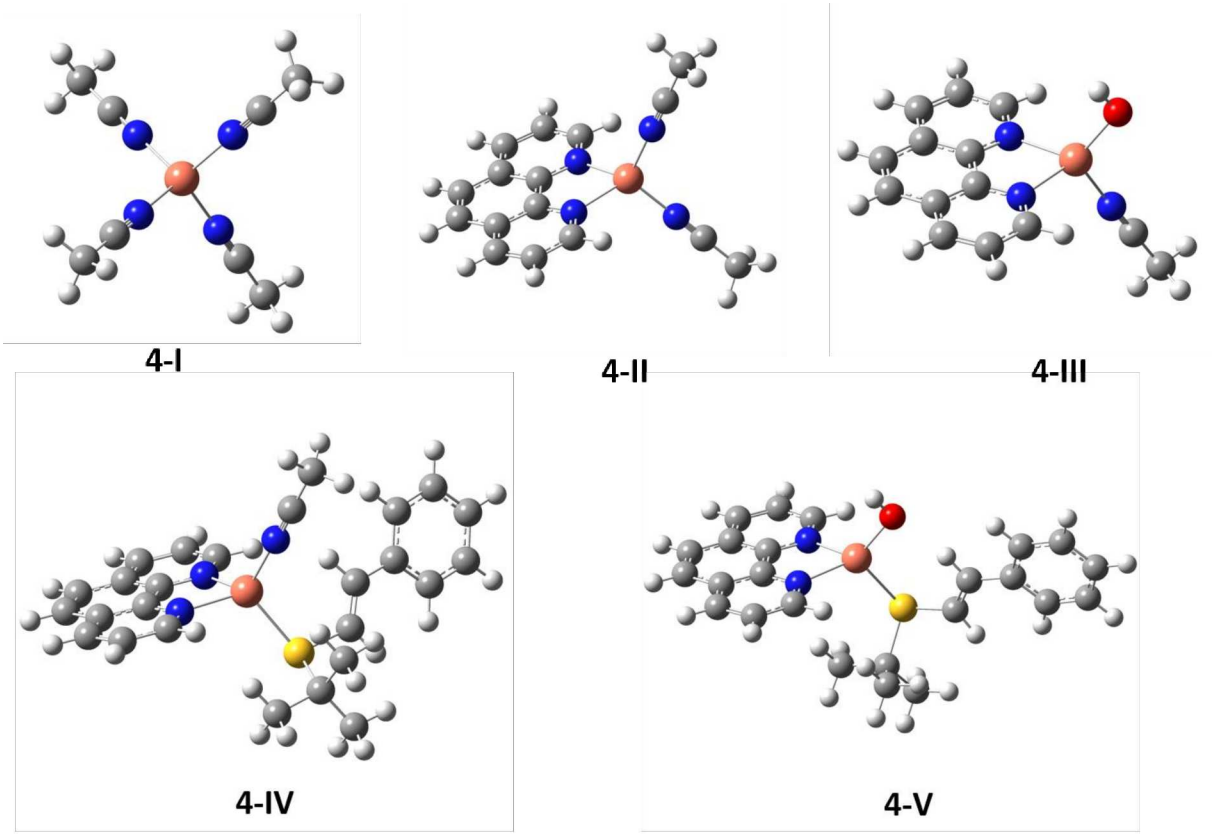

Figure 4.45 – Optimized structures of complexes **4-I** to **4-V**

Experimental investigation of the structure of the starting complex

Because this exchange between acetonitrile and **4-24b** results in small energy differences, the complexation of **4-24a** to the copper/phenanthroline complex in the absence and in the presence of base was investigated experimentally.

Tetrakis(acetonitrile)copper(I) hexafluorophosphate (1 equiv) and 1,10-phenanthroline (1 equiv) were dissolved in CD_3CN. 1,2-dichloroethane was used as an internal standard. Increasing amounts of **4-24a** were added and ^1H NMR spectra were recorded. The same experiment was then performed adding nBu$_4$NOH (1 equiv, solution in water). The chemical shifts for the two vinylic protons were plotted against the amount of **4-24a** added, noted as n (Figure 4.46 and Figure 4.47).

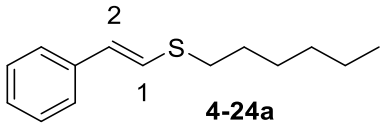

4-24a

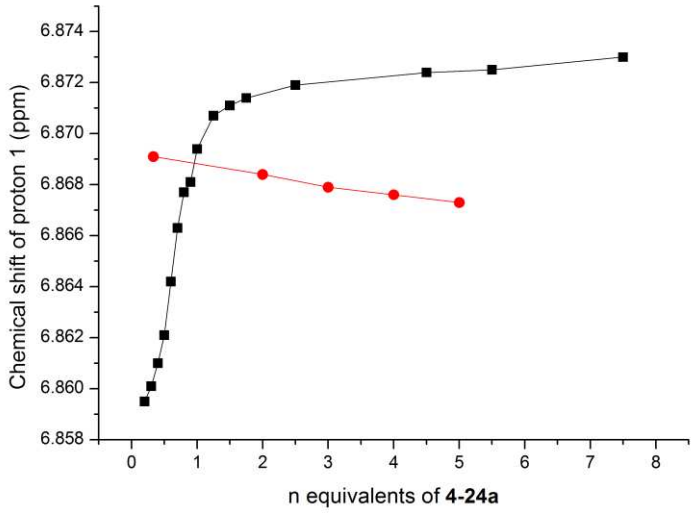

Figure 4.46 - NMR ^{1}H chemical shift of proton 1 of **4-24a** as a function of n, equivalents of **4-24a** added, in the absence (black curve) and presence (red curve) of hydroxide.

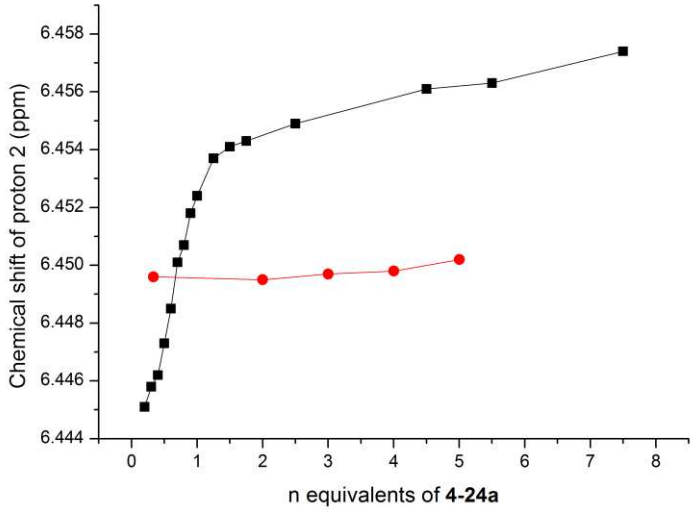

Figure 4.47 - NMR ^{1}H chemical shift of proton 2 of **4-24a** as a function of n, equivalents of **4-24a** added, in the absence (black curve) and presence (red curve) of hydroxide.

^{1}H NMR revealed a displacement of the two vinylic protons upon addition of 0.2 to 8 equivalents of vinylsulfide to CuPhen$(CH_3CN)_4^+PF_6^-$ attesting of the complexation. Proton 1 is more affected by the complexation than proton 2, suggesting that the complexation occurs *via* the sulfur atom. For both positions, the overall shift is very small (around 0.013 ppm) making the fitting difficult. The data obtained could not be fitted to the partial complexation of one thioether to a copper center, with fast equilibration on the NMR timescale but fitted reasonably

well with a simpler model of a complete 1:1 complexation between 1 and 5 equivalents of alkenyl thioether, as described in Figure 4.48.

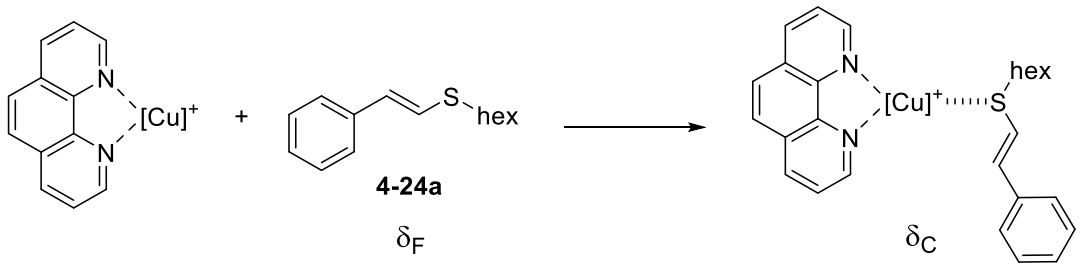

Figure 4.48 – Complete complexation of one molecule of **4-24a** to the Cu/Phen complex

The measured chemical shift δ_{obs} results from the coexistence of the free **4-24a** and of the complexed **4-24a**, with respective chemical shifts δ_F and δ_C. The following equation can be written:

$$\delta_{obs} = \frac{(n-1)\delta_F + \delta_C}{n} = \delta_F + \frac{\delta_C - \delta_F}{n}$$

If this hypothesis is valid, $\delta_{obs} = f\left(\frac{1}{n}\right)$ should be linear. It is the case between 1 and 5 equivalents of **4-24a**, as represented in Figure 4.49.

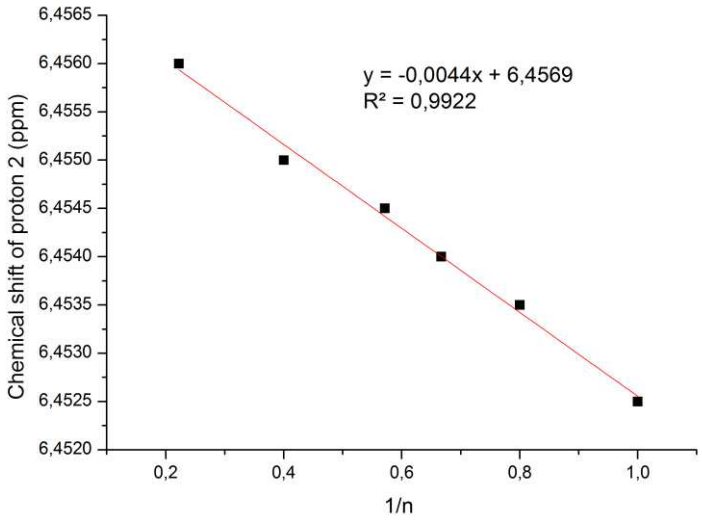

Figure 4.49 – Linear regression for the chemical shift of proton 2 between 1 and 5 equivalents of **4-24a**

Above 5 equivalents, linearity is lost and we cannot exclude the complexation of two substrates on some copper centers. Below 1 equivalent, there might be several copper centers for one thioether molecule. The values obtained from the linear regression are $\delta_F = 6.4569\ ppm$ (consistent with the ^{1}H NMR measured value) and $\delta_c = 6.4526\ ppm$.

In the presence of a base (red curves in Figure 4.46 and Figure 4.47), there is no obvious influence of the addition of increasing amounts of **4-24a** on the chemical shift, and the complexation cannot be proven by ^{1}H NMR.

Overall, experimentally, in the absence of base, complex **4-IV** is formed, but ^{1}H NMR did not allow to evidence the formation of **4-V**.

Mechanism of initiation

To generate radicals from a $Cu^{(I)}$ species and $BrCF_2CO_2Et$ **4-8**, two different mechanisms are possible: a single electron transfer (SET) from the $Cu^{(I)}$ to **4-8** can form a $Cu^{(II)}$ complex and the radical anion $[BrCF_2CO_2Et]^{\bullet -}$ and a halogen atom transfer (HAT) would result in the formation of a $Cu^{(II)}$ complex bearing the bromine, along with the free radical $^{\bullet}CF_2CO_2Et$. For comparison purposes, an oxidative addition (OA), which does not involve the generation of free radicals, proposed in previous studies,[247–251] was also calculated (Figure 4.50, Table 4.9 and Appendix pages 224-226).

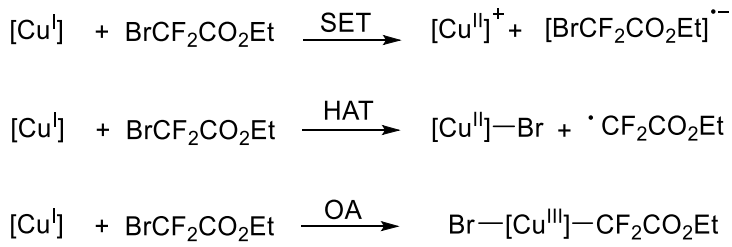

Figure 4.50 – Possible mechanisms for the initiation of the reaction

Table 4.9 – Computed reaction energies for the different complexes (in kcal.mol^{-1})

	4-I	**4-II**	**4-III**	**4-IV**	**4-V**
ΔH SET	55.2	39.9	11.7	39.1	16.7
ΔH HAT	-	28.4	4.7	25.8	4.1
ΔH OA	-	30.4	16.4	27.2	-
ΔH$_a$ OA	-	35.7	36.5	36.1	-

SET, HAT and OA were all computed to be endothermic processes ($\Delta H > 0$). In the absence of the ligand (**4-I**), the energy required for the SET is very high ($\Delta H = 55.2$ kcal.mol^{-1}). This energy is lowered by complexation with 1,10-phenanthroline (**4-II**: $\Delta H = 39.9$ kcal.mol^{-1} and **4-IV**: $\Delta H = 39.1$ kcal.mol^{-1}), and even more favorable when copper is bound to a hydroxide anion (**4-III**: $\Delta H = 11.7$ kcal.mol^{-1} and **4-V**: $\Delta H = 16.7$ kcal.mol^{-1}). The presence of alkenyl thioether **4-24b** has only a tiny effect, as one can see by comparison of the energies computed for **4-II** with the ones for **4-IV** and of the energies computed for **4-III** with the ones for **4-V**. In all cases, the reaction energies for HAT reactions were lower than those calculated for SET. For the OA, both activation energies (ΔH_a) and reaction energies (ΔH) were computed. The reaction energies are always higher than the ones for the HAT, and the activation energies are above 30 kcal.mol^{-1}.

These findings are consistent with the experimental data from Table 4.8, and allow to rule out the OA pathway. In the presence or in the absence of the alkenyl thioether, the same behavior is observed. In the absence of 1,10-phenanthroline, no radical can be formed. The absence of base significantly impacts the radical formation. Overall, complexes **4-III** and **4-V** are the most likely to initiate the formation of the difluoroacetate radical by HAT (**4-III**: $\Delta H = 4.7$ kcal.mol^{-1} and **4-V**: $\Delta H = 4.1$ kcal.mol^{-1}).

After HAT, both **4-III** and **4-V** formed a $Cu^{(II)}$ complex **4-III$_{HAT}$** (identical to **4-V$_{HAT}$**), bearing a phenanthroline ligand, a hydroxide and a bromide (see Figure 4.51). Surprisingly, the alkenyl thioether has low affinity for the copper complex and, if present, it is expelled from the coordination sphere of copper at this step for **4-V**. This highlights the fact that the presence of the alkenyl thioether does not really affect the reactivity of the copper complex.

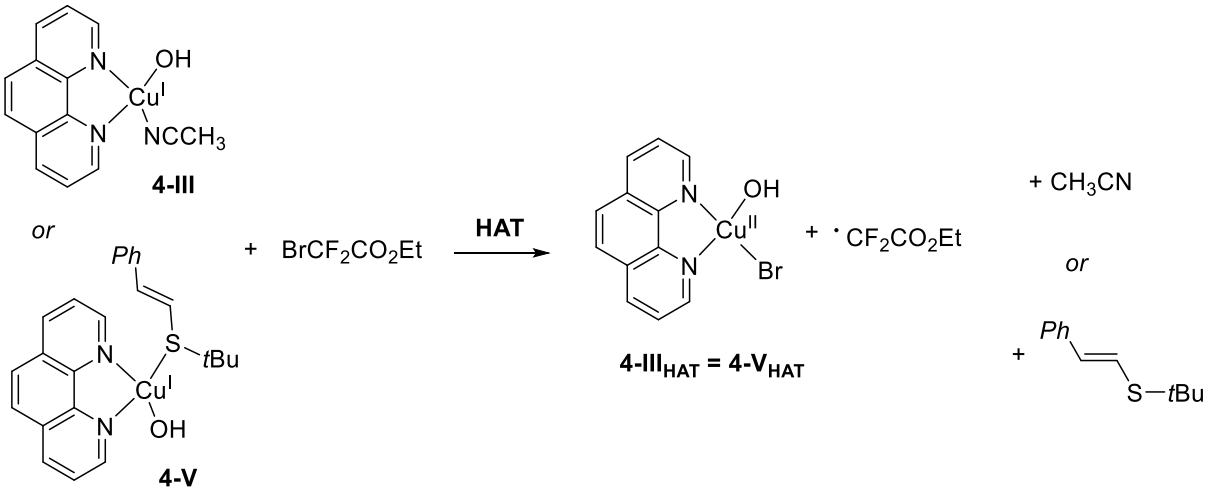

Figure 4.51 – Formation of a $Cu^{(II)}$ complex after the most favored HAT

Unreactive substrates

Table 4.10 - Reduction potentials and reaction energies for reactive and unreactive alkylhalides

Entry	Substrate	Reactivity	Measured reduction potential peak (vs ECS)	ΔH (kcal.mol^{-1})
1	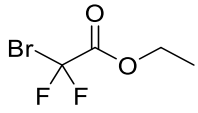 **4-8**	Yes	-1.50 V	4.7
2	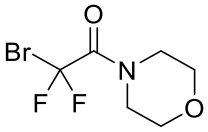 **4-29**	No	-1.61 V	5.5
3	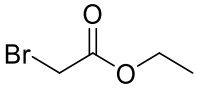 **4-31**	No	-1.68 V	6.1
4	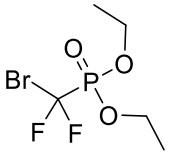 **4-30**	No	-1.97 V	7.9

For this initiation step, we could rationalize the absence of reactivity of $BrCF_2CONR_2$ **4-29**, $BrCF_2P(O)(OEt)_2$ **4-30** and $BrCH_2CO_2Et$ **4-31** with the higher reactions energies computed for the HAT from complex **4-III** as well as with their higher reduction potential

measured by cyclic voltammetry (CV). CV were performed in CH_3CN containing *n*-Bu_4NBF_4 (0.3 M) at a steady glassy carbon disk electrode (d = 1 mm), at a scan rate of 0.5 $V.s^{-1}$, at 20 °C.

Addition on the alkenyl thioether

Complete mechanism

The formed $^{\bullet}CF_2CO_2Et$ radical can then add to the alkenyl thioether **4-24b**. The addition at the C_1 position with regards to the sulfur atom (ΔH_a = 7.6 $kcal.mol^{-1}$, **TS-1'**) had a higher activation barrier than the addition at the C_2 position (ΔH_a = 5.1 $kcal.mol^{-1}$, **TS-1**), but appeared achievable under the reaction conditions (Table 4.11 and Figure 4.52). This small difference allowed us to explain the observed regioselectivity with the formation of the disulfide as by-product. The addition of the $^{\bullet}CF_2CO_2Et$ radical on the alkenyl thioether **4-24b** on the $Cu^{(I)}$ complex **4-IV** has a higher energy barrier (ΔH_a = 8.2 $kcal.mol^{-1}$, Table 4.11), and is thus less favorable.

Table 4.11 - Comparison of the reaction energies computed for the addition of the difluoroacetate radical on **4-24b** (in $kcal.mol^{-1}$)

	Ha addition	**ΔH addition**
Free substrate –C_1	+7.6	-18.3
Free substrate –C_2	+5.1	-15.0
4-IV-C_2	+8.2	-13.8

The radical **I-1** formed can reduce the $Cu^{(II)}$ complex to regenerate $Cu^{(I)}$ (ΔH = 12.9 $kcal.mol^{-1}$ to regenerate **4-III**, ΔH = 13.5 $kcal.mol^{-1}$ to regenerate **4-V**). The resulting carbocation **I-2** can then be deprotonated by the base to form the final product **4-25b**. The different conformations of the carbocation **I-2** are very close in energy (ΔH = 0.8 $kcal.mol^{-1}$) and are in equilibrium. These conformers are similar whatever the configuration of the starting alkenyl thioether (*Z* or *E*). Both can undergo a deprotonation step: after interaction with the base (OH^-) leading to two stable and closely lying intermediates **(*E*)-I-3** and **(*Z*)-I-3** (ΔH = 1.4 $kcal.mol^{-1}$), the *E* and *Z* products can be formed. In agreement with the experiments, the transition state corresponding to the deprotonation step for the *E* form (that is **(*E*)-TS-3**) and leading to the most stable **(*E*)-4-25b** product is computed to be lower in energy than the one of the corresponding *Z* form (Figure 4.52).

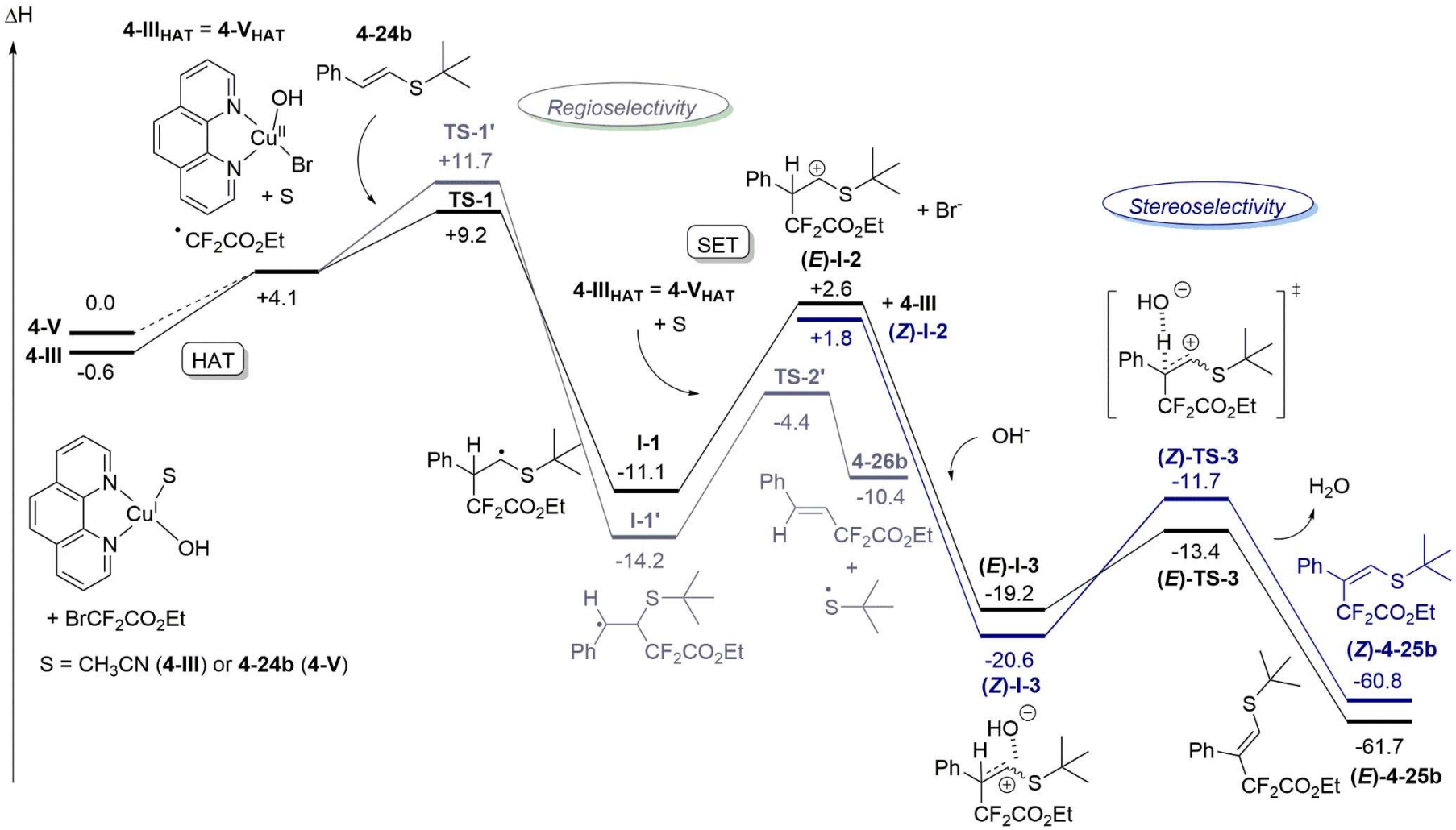

Figure 4.52 - Computed reaction pathways (in kcal.mol^{-1}). Solid line: initiation with **4-III**. Dashed line: initiation with **4-V**. The last part of the reaction path after regeneration of **4-V** by SET is omitted for clarity. This part is the same as for **4-III**. Grey: path for the formation of the main by-product. Blue: path for the formation of the minor stereoisomer.

Generalization of the mechanism to other substrates

The fact that the radical initiation did not depend on the presence of the alkenyl thioether led us to surmise that this method is broadly applicable to the generation of $^{\bullet}CF_2CO_2Et$ radicals using copper catalyst. This hypothesis was confirmed by performing a radical trapping experiment with TEMPO in the presence of enamides (Table 4.12, entry 1) and benzofuranes (Table 4.12, entries 2 and 3) under previously reported conditions.[248,249] For example the adduct **4-38** was isolated in 30 % yield in the case of enamide **4-21** without traces of the desired addition product, revealing a similar mechanism for these substrates. When benzofuranes **4-39** or **4-40** were used, 10 % of **4-38** were obtained.

Table 4.12 - Experiments in the presence of TEMPO for other substrates

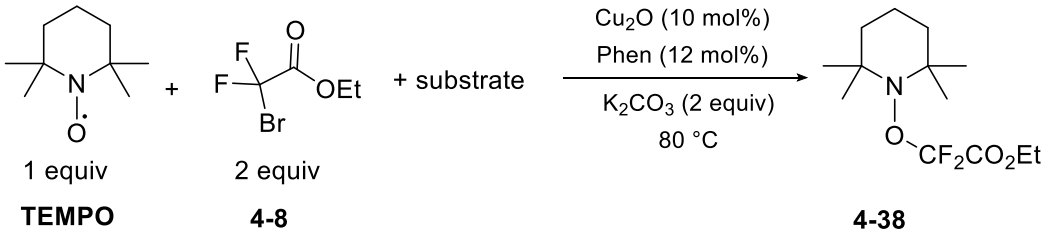

Entry	Substrate	Solvent, time	Yield of 4-38 (%)
1	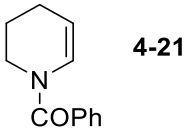 **4-21**	CH_3CN, 6 h	30
2	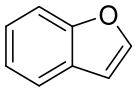 **4-39**	DMF, 20 h	10
3	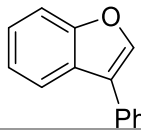 **4-40**	DMF, 20 h	10

a. ^{19}F NMR yield, α,α,α-trifluorotoluene was used as an internal standard

In the initial studies, some reactions were already performed in the presence of radical scavengers. In the case of benzofuranes, TEMPO and *tert*-butylhydroxytoluene (BHT) were used, in substoichiometric or stoichiometric amount (Table 4.13). The yield dropped from 50 % to 40 % but this small decrease was not considered crucial, the TEMPO-CF_2CO_2Et adduct **4-38** was not identified and a $Cu^{(I)}/Cu^{(III)}$ catalytic cycle was proposed. Nevertheless, in this reaction, 8 equivalents of $BrCF_2CO_2Et$ **4-8** were used. It means that if one equivalent of $^{\bullet}CF_2CO_2Et$ is trapped by the radical scavenger, 7 equivalents can still react in the reaction medium.

Table 4.13 – Mechanistic experiments initially performed with benzofuranes[248]

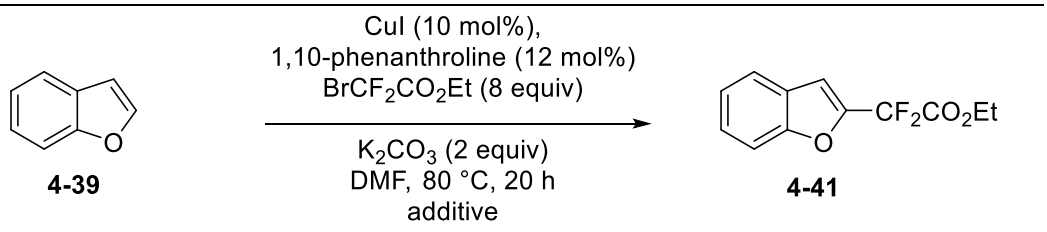

Entry	Additive	Quantity	Yield of 4-41 (%)
1	None	-	50
2	TEMPO	20 mol%	49
3	TEMPO	100 mol%	40
4	BHT	100 mol%	42

In the case of enamides,[249] the reaction was optimized with 2 equivalents of $BrCF_2CO_2Et$. In the initial study, when a catalytic amount (20 mol%) of radical inhibitors was added (TEMPO, benzoquinone or BHT), no inhibition of the reaction was observed, and with 1 equivalent of TEMPO the reaction required a much longer reaction time. For this reaction, a more complete mechanistic study was performed. A non-radical mechanism was proposed based on stoichiometric reactions performed in the absence of the base. After ruling out the direct oxidative addition of $BrCF_2CO_2Et$ with the cationic $Cu^{(I)}$ complex (by both NMR and electrochemistry performed at RT), a pre-complexation of the latter with enamide was established via cyclic voltammetry as was evidenced here earlier by ^1H NMR in the case of the alkenyl thioether (in the absence of the base).

In this initial study on enamides, the cationic copper complex was considered, whereas here the complete experimental conditions are taken into account, in particular the base. Finally, these results are not contradictory and the radical mechanism established herein turns out to be quite general for these systems.

Based on these findings, we proposed the mechanism depicted in Figure 4.53. In the presence of 1,10-phenanthroline and a base, the $Cu^{(I)}$ hydroxo complex reduced $BrCF_2CO_2Et$ to form a $Cu^{(II)}$ complex and an ethoxy carbonyl difluoromethyl radical. Then, the addition of this radical on the alkenyl thioether **4-24** proceeded according to an outer sphere process and the observed stereoselectivity is related to the relative stability of the two possible isomers after the deprotonation step.

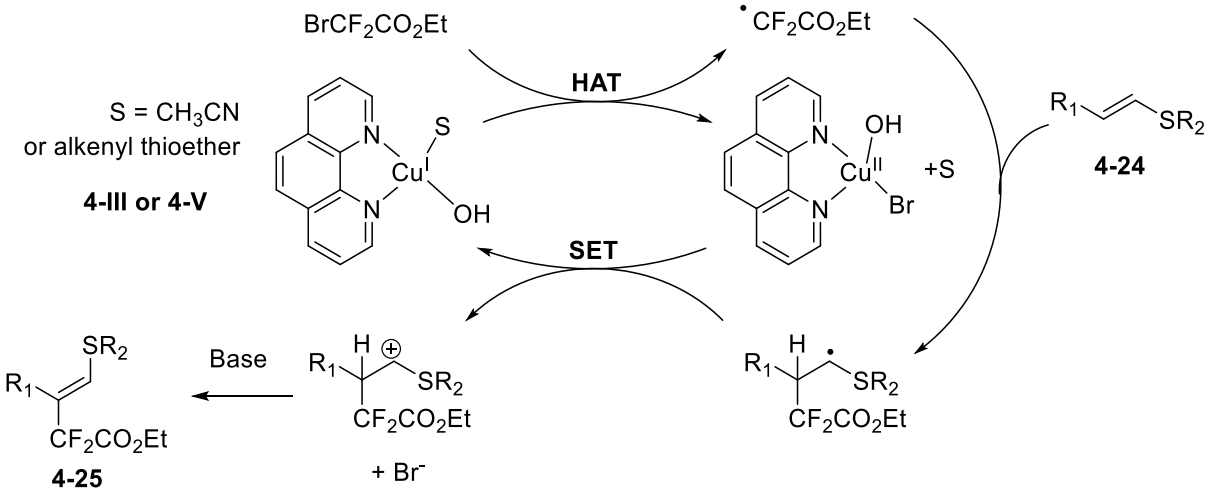

Figure 4.53 – Proposed reaction mechanism for the difluoroacetylation of alkenyl thioethers

Perspectives

Reactivity of fluorinated alkenyl thioethers

In an attempt to post-functionalize the fluorinated products, a saponification of **4-25a** was performed with aqueous lithium hydroxide. Surprisingly, the carboxylic acid was not obtained, but two new cyclic compounds **4-42a** and **4-43a** were isolated. The reaction was performed on a few substrates in these unoptimized conditions to evaluate its scope (Table 4.14). This reaction turned out to be quite general on our substrates, with the formation of either one or two cyclic products. Increasing the reaction time and the temperature allowed to obtain compound **4-43a** only from **4-25a** in 70 % yield.

To understand the origin of the product **4-43**, the fluorinated cyclized product **4-42a** was isolated and treated with aqueous lithium hydroxide. In these same reaction conditions, it was completely converted into **4-43a** (Figure 4.54). This is an evidence that **4-42a** is most probably an intermediate for the formation of **4-43a**, and explains why increasing the reaction time and temperature only gives **4-43a**.

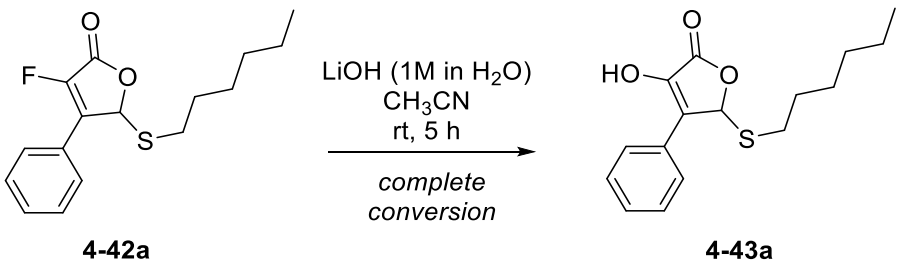

Figure 4.54 – Reactivity of **4-42a** in basic medium

A proposed mechanism for the reaction is depicted in Figure 4.55. After saponification, a carboxylate **4-44** is formed. The formation of the thiocarbenium **4-45** can result in the elimination of fluoride. From there, ring closure can form **4-42** or, addition of hydroxide can form **4-46.** Cyclisation and fluoride elimination can finally form **4-43**. Cyclisation and hydroxide elimination of **4-46** can also form **4-42**. The conversion of **4-42** into **4-43** can be explained by the reversibility of the ring closure from **4-45**.

Table 4.14 – Reactivity of various fluorinated alkenyl thioethers

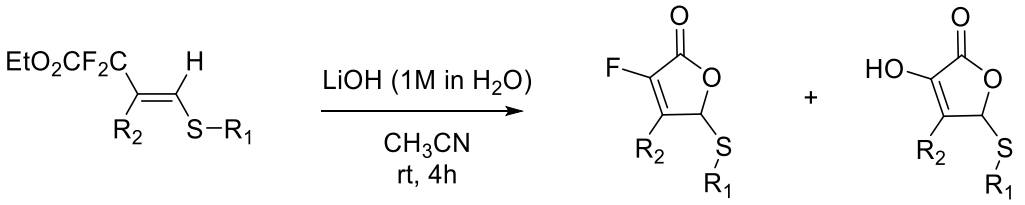

4-25 **4-42** **4-43**

Entry	Starting material	Product 4-42	Isolated yield of 4-42	Product 4-43	Isolated yield of 4-43
1	4-25a	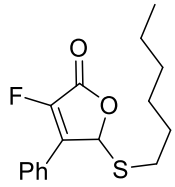 4-42a	30 %	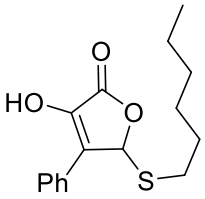 4-43a	24 %
2	4-25b	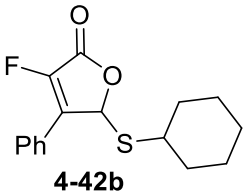 4-42b	-	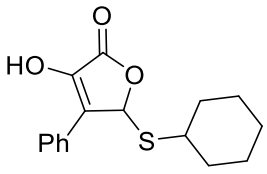 4-43b	42 %
3	4-25c	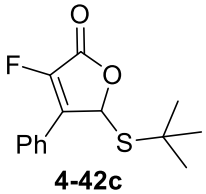 4-42c	-	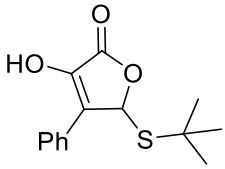 4-43c	31 %
4	4-25g	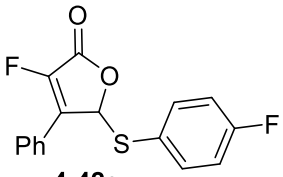 4-42g	19 %	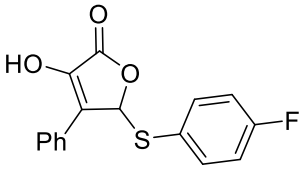 4-43g	-
5	4-25j	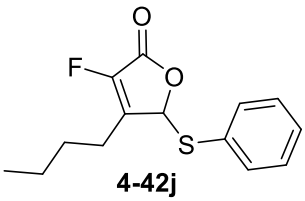 4-42j	19 %	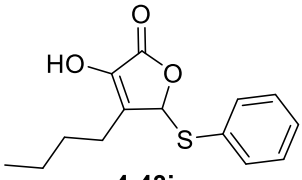 4-43j	26 %

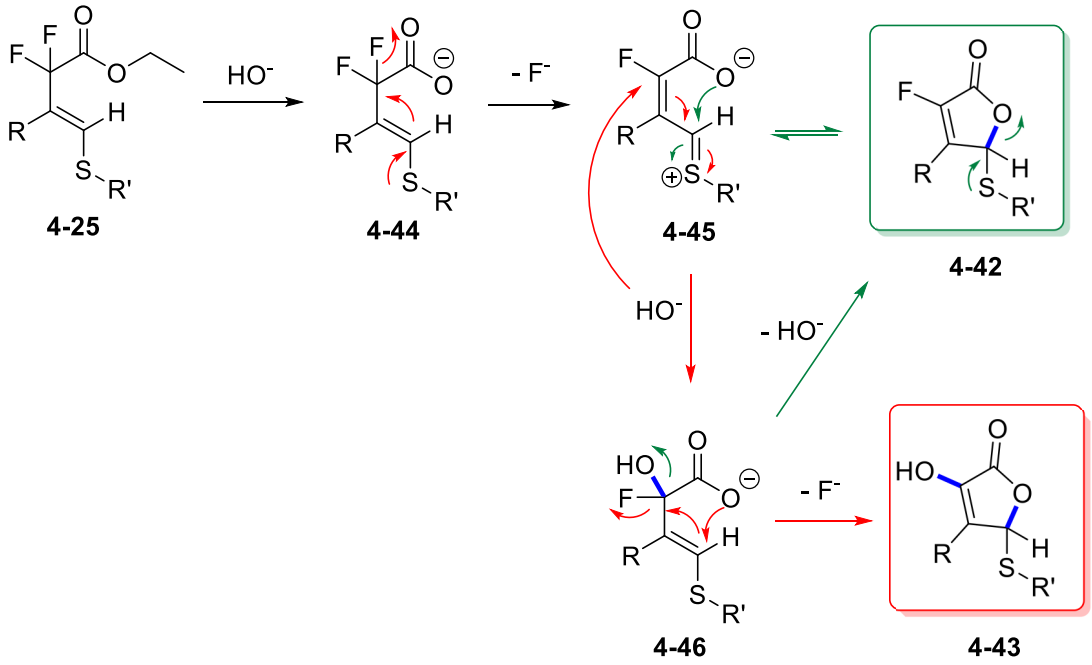

Figure 4.55 – Proposed mechanism for the reaction

Isotetronic acids

The cyclic compounds obtained are called isotetronic acids (or 2-hydroxybutenolides) and are five-membered lactones. Their general structure is depicted in Figure 4.56.

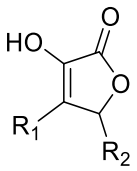

Figure 4.56 – General structure of isotetronic acids

This structural motif is present in various natural products. For example (+)-leptosphaerin is a metabolite of the marine ascomycete *Leptosphaeria oreamaris*,[258] and butyrolactone I was a metabolite isolated from *Aspergillus terreus* var. *africanus*[259] (Figure 4.57).

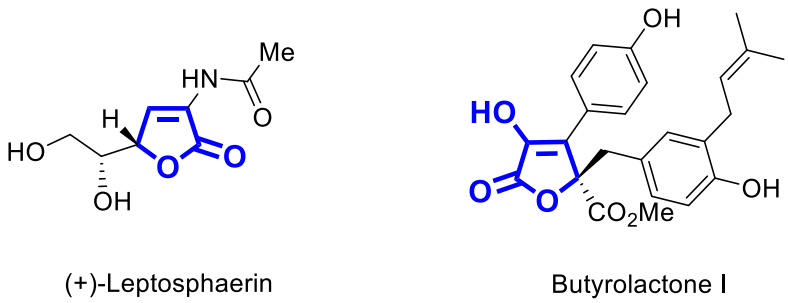

(+)-Leptosphaerin Butyrolactone I

Figure 4.57 –Natural products with isotetronic acid structure

Functionalized isotetronic acids are also key intermediates for the synthesis of natural products.[260–262] This structure has useful pharmacological activities. For example butyrolactone I (Figure 4.57) is a potent inhibitor of CDK1 and CDK2 kinases with an antiproliferative activity, and this molecule has been of interest for antitumoral strategies.[263]

A number of synthetic approaches to isotetronic acids are already known.[264–267] The interest of our reaction mainly lies in the formation of the compound **4-42**, which has the structure of an isotetronic acid, with a fluorine atom instead of hydroxide and could have interesting biological activities. Moreover, to our knowledge, this type of isotetronic acids are not known yet and the presence of a mixed acetal on these compounds allows further reactivity. Efforts are now focused on the optimization of the conditions for its formation only.

Conclusion

We report herein a general regio- and stereoselective method for the ethoxy carbonyl difluoromethylation of alkenyl thioethers. The developed methodology was applied to a broad range of substrates with good yields and excellent selectivities in favor of *E* isomers. Mechanistic studies supported by experimental observations and theoretical calculations gave evidences for a radical mechanism. The generation of a difluoroacetate radical promoted by a well-defined copper complex was established by these studies. Compared to other strategies to introduce a fluorine atom or a fluorinated group, this method allowed the generation of a radical under mild conditions, without requirement of light irradiation, expensive metal or radical initiator, which constitutes a real asset. It allows an easy access to fluorinated chemical platform of interest, since post-functionalizations of these substrates are possible thanks to the versatility of the ester moiety.[268] An easy access to fluorinated isotetronic acid is now under study for further optimization.

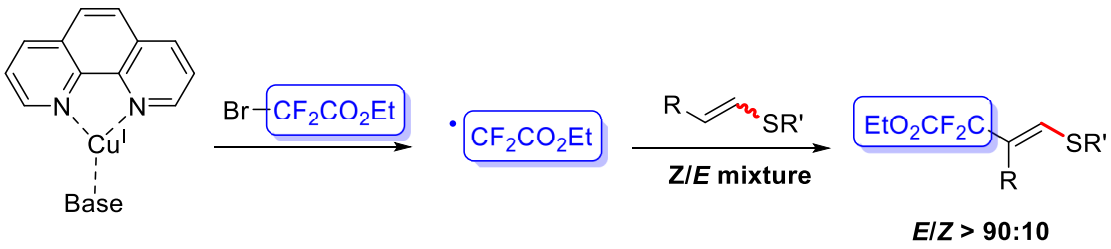

General conclusion

This thesis aimed at combining synthetic methodology developments and mechanistic studies to improve and rationalize the way reactions are designed. For this purpose, a complementary approach with both experimental and theoretical work was used.

The first study was the *t*BuOK/DMF mediated alpha-arylation of aryl ketones. The advantage of this reaction lies in the absence of transition metal catalyst. We managed to show why DMF, as a solvent, and *t*BuOK, as a base, are both necessary for this reaction. Indeed, the radical chain reaction is initiated by an electron-rich species generated by the deprotonation of DMF by *t*BuOK. This species can reduce iodobenzene to give an aryl radical which initiates the reaction. This deprotonation could be evidenced experimentally by NMR. DFT calculations confirmed the feasibility of this step and also allowed, to some extent, the explanation of why *t*BuOLi is inefficient in this reaction. One of the benefits taken from this mechanistic study is the possibility to generalize the initiation mechanism of this reaction to other reactions starting with a one-electron reduction of an aryl iodide. Other reducing agents can be replaced by the combination of DMF and *t*BuOK, and new reactions, for example with a nucleophile different from an enolate, can be imagined.

The second study is the copper-catalyzed arylation of nitrogen heterocycles, starting from anilines. This reaction uses a cheap catalyst of low toxicity and does not require the presence of ligands. Harmless by-products are generated (N_2, water, *t*BuOH). More interestingly, a diazonium is generated *in situ* with a catalytic amount of acid. This allows to overcome the safety-related issues that are associated with the use of these compounds. The mechanistic study revealed that the formed diazonium is immediately converted into a triazene, which plays the role of safe diazonium reservoir. The regeneration of the diazonium is modulated by the acidity of the medium, due to the presence of acetic acid and acetate. Experimental data and computational results showed that this diazonium could react with copper, in a $Cu^{(I)}/Cu^{(III)}$ catalytic cycle. The formation of $Cu^{(II)}$ and aryl radical during the catalytic cycle could not be ruled out. The mechanistic study also allowed to understand the different reactivity observed between pyrazole and imidazole substrates. The former undergoes intramolecular deprotonation whereas the latter undergoes intermolecular deprotonation, which is less efficient. A more extensive study of the performance of different DFT approaches was performed and allowed to evidence the quantitative difference that can be found. This study

allows one to fully show the complementarity of experiments and calculations and how it helps to have a complete picture of such a complex mechanism. The DFT methodology developed can be applied to other similar systems. This method for the slow generation of diazonium salts can be used for other reactions, even with other catalysts.

The third study is the copper-catalyzed difluoroacetylation of alkenyl thioethers. In this case, the methodology itself was developed in this thesis. Strategies for the introduction of functionalized fluorinated groups are of great interest for pharmaceutical applications, and very few methods exist for the functionalization of alkenyl thioethers. Our method forms trisubstituted alkenyl thioethers with controlled stereoselectivity in mild conditions. We gave access to a new family of compounds. In basic medium, they can cyclize and form unprecedented structures of isotetronic acids. The mechanism of the reaction was studied and revealed a radical pathway. The $Cu^{(I)}$ species which is able to reduce $BrCF_2CO_2Et$ to form the active radical was identified. Experimental and theoretical results are consistent, and show that this first step does not depend on the substrate. For this reason, we could generalize this mechanism to the difluoroacetylation of enamides and benzofuranes that is achievable in analogous conditions.

With these three studies, we successfully achieved the challenge of extending the methods to design reactions. With this innovative combined work (combination of synthetic methodology development and mechanistic study, and combination of experimental and computational results), which is becoming more and more popular, we believe that great achievements can be done and that a faster development of new reactions will be possible. Understanding the mechanism of a reaction will not be made only by specialists a posteriori, but will become a real tool in the design of new reactions.

Appendix

General considerations

All reagents and solvents were obtained from commercial suppliers and used without further purification, unless otherwise stated. Reactions were monitored by thin-layer chromatography (TLC) analysis using silica gel plates (60 F254). Compounds were visualized by UV irradiation. Column chromatography was performed on silica gel 60 (230-400 mesh, 0.040-0.063 mm).

^{1}H (300 MHz), ^{13}C (75.5 MHz) and ^{19}F (282 MHz) NMR spectra were recorded on a Bruker spectrometer. ^{13}C NMR spectra were obtained with complete proton decoupling. For ^{19}F NMR spectra, relaxation delay *d1* was adjusted to 10 s for accurate integration, and signals were decoupled from ^{1}H. ^{1}H and ^{13}C chemical shifts (δ) are given in parts per million (ppm) relative to tetramethylsilane (TMS) using the ^{1}H (residual) and ^{13}C chemical shifts of the solvent as secondary standard. NMR data are reported as follows: chemical shift (in ppm), multiplicity (s = singlet, d = doublet, t = triplet, q = quartet, m = multiplet, br = broad, dd = doublet of doublets, dt = doublet of triplets, ddt = doublet of doublets of triplets), coupling constant (in Hz), integration, attribution.

HRMS Spectra were recorded on a JEOL JMS-GC Mate II apparatus. GLC analyses were performed on a Varian 3900 instrument with H_2 as a carrier gas and a FID detector. A Varian VF-1ms (15 m x 0.25 mm i.d.) capillary column was used.

Cyclic voltammetry was performed with a Metrohm Autolab PGSTAT101 potentiostat connected to a Nova software interface. Cyclic Voltammetry (CV) was performed in a three-electrode cell connected to a Schlenk line under argon at 20 °C. The working electrode was a gold disk (*d* = 0.5 mm) or glassy carbon (d = 1 mm) electrode, the counter electrode a platinum wire of *ca*. 0.2 cm apparent area. The reference was a saturated calomel electrode (SCE) separated from the solution by a bridge filled with 3 mL of solvent (containing nBu$_4$NBF$_4$ 0.3 M).

All calculations were performed using the Gaussian 09 program (Revision A.02). Bulk solvent effects were introduced using a Polarizable Continuum model (PCM). All stationary points were fully characterized via a subsequent analytical frequency calculation either as

minima or as first order transition states (one imaginary frequency). IRC calculations were used to confirm the minima linked by each transition state. Enthalpies and free energies were calculated for standard conditions at 298.15 K.

Appendix to chapter 2

General procedure for the α-arylation of aryl ketones

To a flame-dried Schlenk flask was added, under argon, *t*BuOK (561.1 mg, 5.0 mmol, 5.0 equiv). The flask was evacuated and backfilled with argon 3 times, then dry DMF (3 mL) was added by syringe, and the mixture was allowed to stir for 10 minutes at room temperature. Then, iodobenzene (1.0 mmol, 1.0 equiv), and propiophenone (2.0 mmol, 2.0 equiv or 4.0 mmol, 4.0 equiv), were successively added. The reaction mixture was stirred and heated at 60 °C for 13 h. After allowing the reaction to cool to room temperature, 1N HCl (2 mL) was added and the mixture was allowed to stir for 10 minutes at room temperature. Then, 1,3,5-trimethoxybenzene (56.1 mg, 0.33 mmol, 0.33 equiv) was added as internal standard. The resulting mixture was diluted with diethyl ether (10 mL) and washed with water (3 x 2 mL) and brine (1 x 2 mL). The organic layer was dried over anhydrous $MgSO_4$ and diethyl ether was evaporated under reduced pressure (rotary evaporator). The residue was purified by column chromatography to give the desired α-aryl ketone.

General procedure for the kinetics of the proton exchange of DMF-d_7 in presence of base

An oven-dried NMR tube was charged with *t*BuOK (100 mg, 0.9 mmol). 0.5 mL DMF-d_7 were added and the NMR tube was vigorously shaken. ^{1}H NMR (300 MHz) and ^{13}C NMR (75 MHz) were then performed at 24 °C immediately after and then from time to time.

Cyclic voltammetry experiments

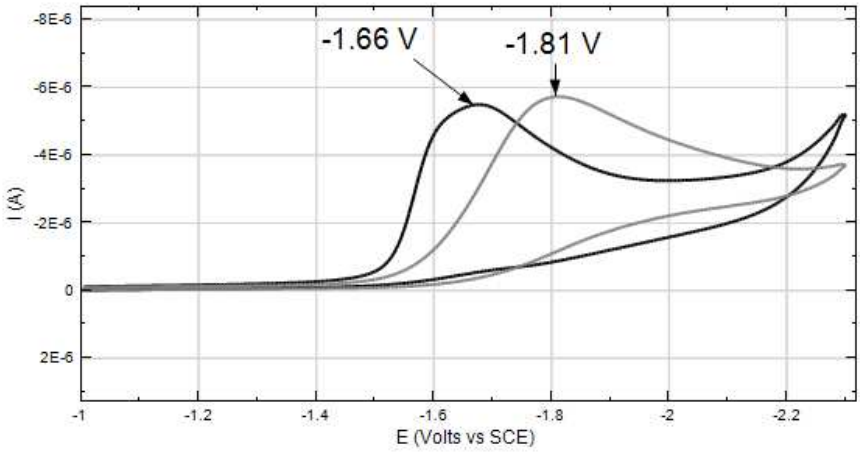

Figure A1- Cyclic voltammetry: reduction of PhI (2 mM) in DMF containing nBu$_4$NBF$_4$ (0.3 M) at a steady gold-disk electrode (d = 0.5 mm) at a scan rate of 0.5 V.s^{-1} at 20 °C (in grey) and after addition of KCl (6 mM) (in black)

Appendix to chapter 3

General considerations

Dry methanol was used for NMR and Schlenk reactions and it was distilled on Mg(OMe)$_2$ and degassed for cyclic voltammetry experiments. Kinetics performed under argon or under an air atmosphere gave the same results. This was confirmed on one example and other experiments were done under air. GCL calibration curves were done for 1-(4-fluorophenyl)-1*H*-pyrazole and 1-phenyl-1*H*-pyrazole using *n*-tetradecane as an internal standard.

Synthesis of the reference coupling product 1-phenyl-1*H*-pyrazole using the general procedure for the arylation of pyrazole from aniline:

After standard cycles of evacuation and back-filling with argon, a Schlenk tube equipped with a magnetic stirring bar was charged with Cu(OAc)$_2$ anhydrous (0.2 mmol, 36.3 mg), pyrazole (1 mmol, 68.1 mg), MeOH (1.5 mL), cooled down to 0 °C and, under stirring, *t*BuONO (1.65 mmol, 197 L) and AcOH (0.3 mmol, 17.2 L) were added. A solution of aniline (1.5 mmol, 205 L) in MeOH (3 mL), was slowly added using a syringe pump over 2 h. The mixture was then allowed to warm up to room temperature and stirred for 48 h. The crude reaction mixture was diluted with EtOAc (20 mL), and washed with a 10 % ammonia solution (5 mL) and brine (5 mL). Volatiles were removed in vacuo and the residue was purified by flash chromatography on silica gel (eluent: cyclohexane / ethyl acetate 100:0 to 95:5) to give

the title compound as a light yellow oil (110 mg, 76 %). Spectral data are in agreement with the literature.[109]

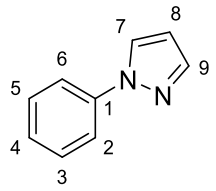

^{1}H NMR (300 MHz, $CDCl_3$): δ 7.90 (d, *J* = 2.4 Hz, 1H, H_7), 7.75-7.64 (m, 3H, H_{ar}), 7.47-7.37 (m, 2H, H_{ar}), 7.30-7.22 (m, 1H, H_9), 6.46-6.43 (m, 1H, H_8). ^{13}C NMR (75.5 MHz, $CDCl_3$): δ 141.1 (C_9), 140.3 (C_1), 129.5 (C_{ar}), 126.8 (C_7), 126.5 (C_{ar}), 119.3 (C_{ar}), 107.7 (C_8).

Synthesis of the reference coupling product 1-(4-Fluorophenyl)-1H-pyrazole

This compound was synthesized using an independent procedure.[269]

A flask was charged with pyrazole (68.1 mg, 1.0 mmol), CuI (9.5 mg, 0.05 mmol) and K_2CO_3 (290 mg, 2.1 mmol), closed by a rubber septum and conditioned under argon. Deoxygenated toluene (1 mL), 4-fluoroiodobenzene (138.4 µL, 1.2 mmol) and N,N'-dimethylethylenediamine (21.5 L, 0.2 mmol) were added sequentially by syringe. The mixture was stirred at 110 °C for 24 h. The cooled reaction mixture was diluted with EtOAc (20 mL), and washed with a 10 % ammonia solution (5 mL) and brine (5 mL). Volatiles were removed in vacuo and the residue was purified by flash chromatography on a short column of silica gel (eluent: petroleum ether / ethyl acetate 95:5) to give the title compound as an off-white solid (148 mg, 91 %). Spectral data are in agreement with the literature.[270]

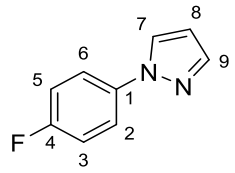

^{1}H NMR (300 MHz, $CDCl_3$): δ 7.86 (d, *J* = 2.2 Hz, 1 H, H_7), 7.71 (d, *J* = 2.2 Hz, 1 H, H_9), 7.68-7.60 (m, 2 H, H_{ar}), 7.17-7.11 (m, 2 H, H_{ar}), 6.46 (t, *J* = 2.2 Hz, 1 H, H_8). ^{13}C NMR (75.5 MHz, $CDCl_3$): δ 161.1 (d, $^{1}J_{CF}$ = 245.7 Hz, C_4), 141.1 (C_9), 136.6 (C_1), 126.9 (C_7), 121.0 (d, $^{3}J_{CF}$ = 8.3 Hz, C_{ar}), 116.2 (d, $^{2}J_{CF}$ = 22.9 Hz, C_{ar}), 107.7 (C_8). ^{19}F NMR (282 MHz, $CDCl_3$): δ -116.1.

Synthesis of the triazenes

The aryltriazenes were synthesized according to a reported procedure.[271] In a 25 mL flask were placed water (3 mL) concentrated hydrochloric acid (0.75 mL) and the aniline derivative (5 mmol). After dissolution of the amine, crushed ice (1.5 g) was added. A solution of sodium nitrite (2.5 mmol) in 0.5 mL of water was introduced with constant stirring during a period of 5 minutes. A solution of sodium acetate trihydrate (5.2 mmol) in 1.5 mL of water was added during 5 minutes and the mixture was stirred for 45 min at 5-10 °C. The yellow precipitate 1,3-diaryltriaz-1-ene was filtered off, washed with water (3 x 5 mL) and dried on the filter. The solid was dried under vacuum overnight and used without further purification.

- 1,3-diphenyltriaz-1-ene

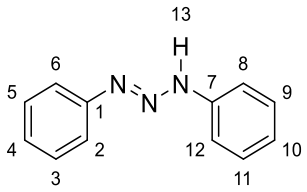

^{1}H NMR (300 MHz, $CDCl_3$): δ 9.55 (br s, 1H, H_{13}), 7.44-7.35 (m, 8H, H_{ar}), 7.20-7.14 (m, 2H, H_{ar}).

- 1,3-bis(4-fluorophenyl)triaz-1-ene

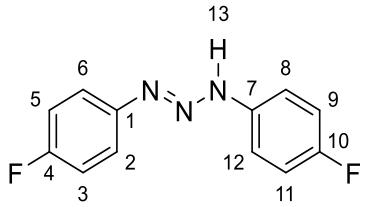

^{1}H NMR (300 MHz, $CDCl_3$): δ 7.39-7.35 (m, 4H, H_{ar}), 7.11-7.05 (m, 4H, H_{ar}), 4.98 (br s, 1H, H_{13}). ^{19}F NMR (282 MHz, $CDCl_3$): δ -117.5.

CuOAc mediated formation of 1-phenyl-1H-pyrazole from 1,3-diphenyltriaz-1-ene

After standard cycles of evacuation and back-filling with argon, a Schlenk tube equipped with a magnetic stirring bar was charged with Cu(OAc) (0.15 mmol, 18.5 mg), pyrazole (0.15 mmol, 10 mg), MeOH (1 mL), cooled down to 0 °C and, under stirring, AcOH

(0.15 mmol, 9 L) was added. The mixture was then allowed to warm up to room temperature and stirred for 24 h. The crude reaction mixture was diluted with diethyl ether (10 mL), and *n*-tetradecane was added as an internal standard. GC yield was evaluated to 20 % using calibration curve.

General procedure for the kinetics of the formation and decomposition of the triazene species in the absence of copper under stoichiometric conditions

An oven-dried NMR tube equipped with a DMSO-d_6 insert was charged with dry MeOH (0.5 mL), followed by para-fluoroaniline (0.5 mmol, 47 µL), α,α,α-trifluorotoluene as internal standard (5 L, 0.041 mmol), *t*BuONO (0.55 mmol, 66 L) and AcOH (0.5 mmol, 29 L). The NMR tube was vigorously shaken. ^{19}F NMR was recorded immediately after and at selected times.

The same procedure was applied with different amounts of reagents for the experiments described in Figure 3.25.

General procedure for the kinetics of arylation of pyrazole with 1,3-bis(4-fluorophenyl)triaz-1-ene mediated by $Cu(OAc)_2$ under stoichiometric conditions:

An oven-dried NMR tube equipped with a DMSO-d_6 insert was charged with $Cu(OAc)_2$ (36.3 mg, 0.2 mmol), 1,3-bis(4-fluorophenyl)triaz-1-ene (47 mg, 0.2 mmol) and pyrazole (18 mg, 0.26 mmol). The tube was introduced in a Schlenk and three cycles of vacuum and argon filling were applied. Dry MeOH (0.5 mL) was added, followed by α,α,α-trifluorotoluene as internal standard (5 L, 0.041 mmol), and AcOH (11.4 L, 0.2 mmol). The NMR tube was vigorously shaken until complete dissolution. ^{19}F NMR was recorded immediately after and the evolution was then followed with time.

The same procedure was applied with different amounts of acid or with K_2CO_3 for the experiments described in Figure 3.27.

General procedure for the kinetics of arylation of pyrazole with para-fluoroaniline catalyzed by $Cu(OAc)_2$ under catalytic conditions:

An oven-dried NMR tube equipped with a DMSO-d_6 insert was charged with $Cu(OAc)_2$ (12 mg, 0.066 mmol) and pyrazole (23 mg, 0.33 mmol). The tube was introduced in a Schlenk and three cycles of vacuum and argon filling were applied. Dry MeOH (0.5 mL) was added, followed by α,α,α-trifluorotoluene as internal standard (5 L, 0.041 mmol), para-fluoroaniline (47.4 L, 0.5 mmol), *t*BuONO (66 L, 0.55 mmol) and AcOH (5.7 L, 0.1 mmol). The NMR tube was vigorously shaken until complete dissolution. ^{19}F NMR was performed immediately after and the evolution was then followed with time.

Reduction of diazonium salt by benzyl alcohol

An oven-dried NMR tube equipped with a DMSO-d_6 insert was charged with benzyl alcohol (0.5 mL), para-fluoroarenediazonium tetrafluoroborate (0.1 mmol, 21 mg) and tetrabutyl ammonium benzoate (0.1 mmol, 36 mg). Once the gas evolution was finished, ^1H NMR (300 MHz), ^{19}F NMR (282 MHz) and gas chromatography were performed. Observed signals were compared to authentic samples.

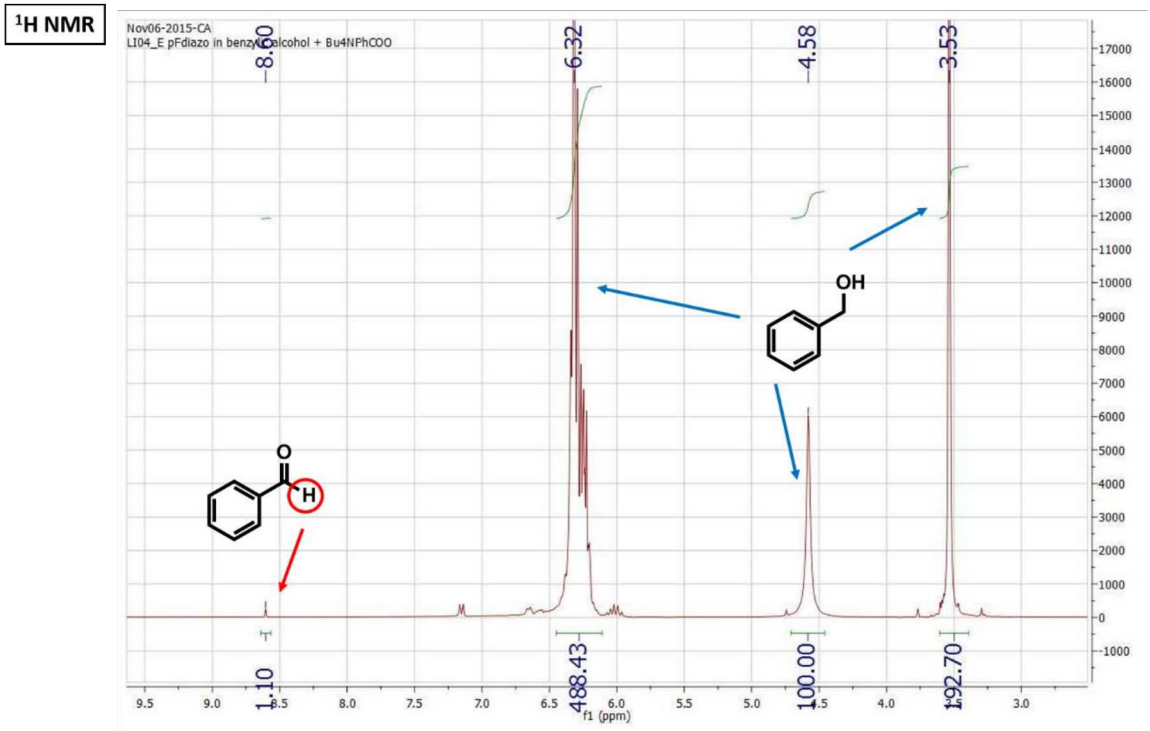

Figure A2 – ^1H NMR spectrum of the reduction of diazonium salt by benzyl alcohol

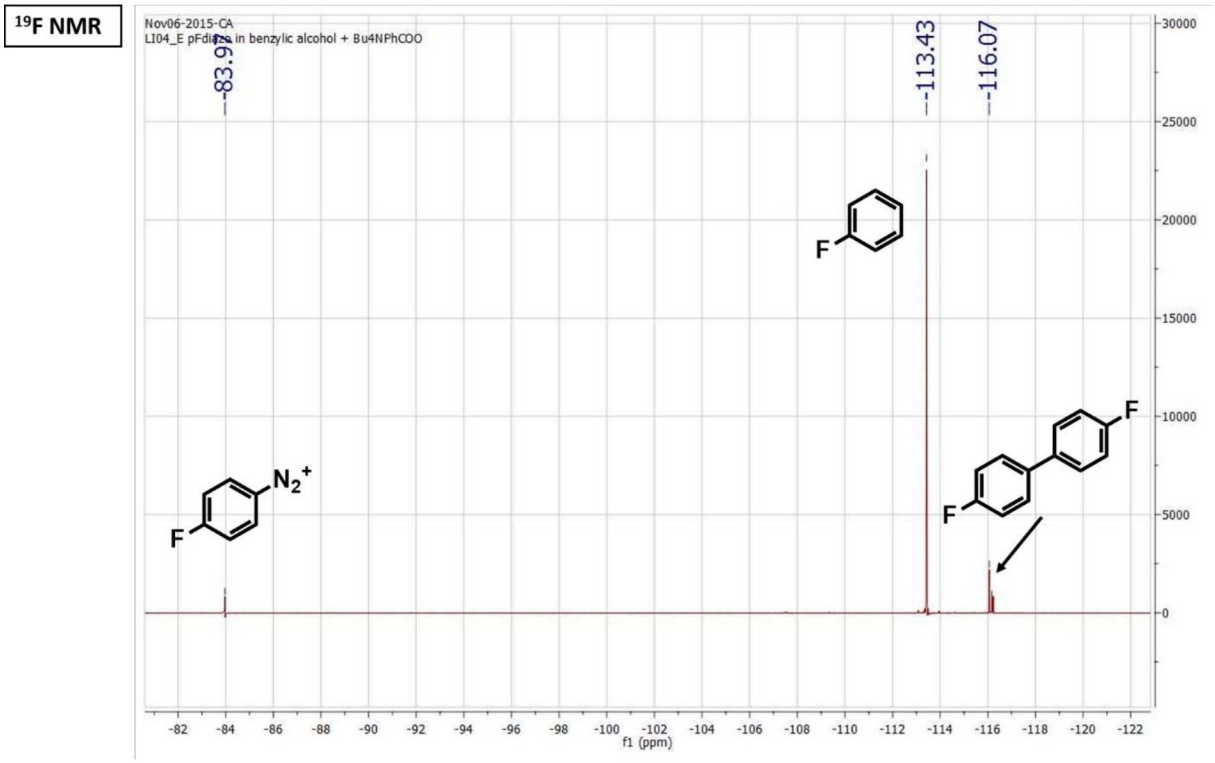

Figure A3 – ^{19}F NMR spectrum of the reduction of diazonium salt by benzyl alcohol

Radical clock experiment

2-(Allyloxy)aniline was synthesized in three steps according to reported procedures.[272–274]

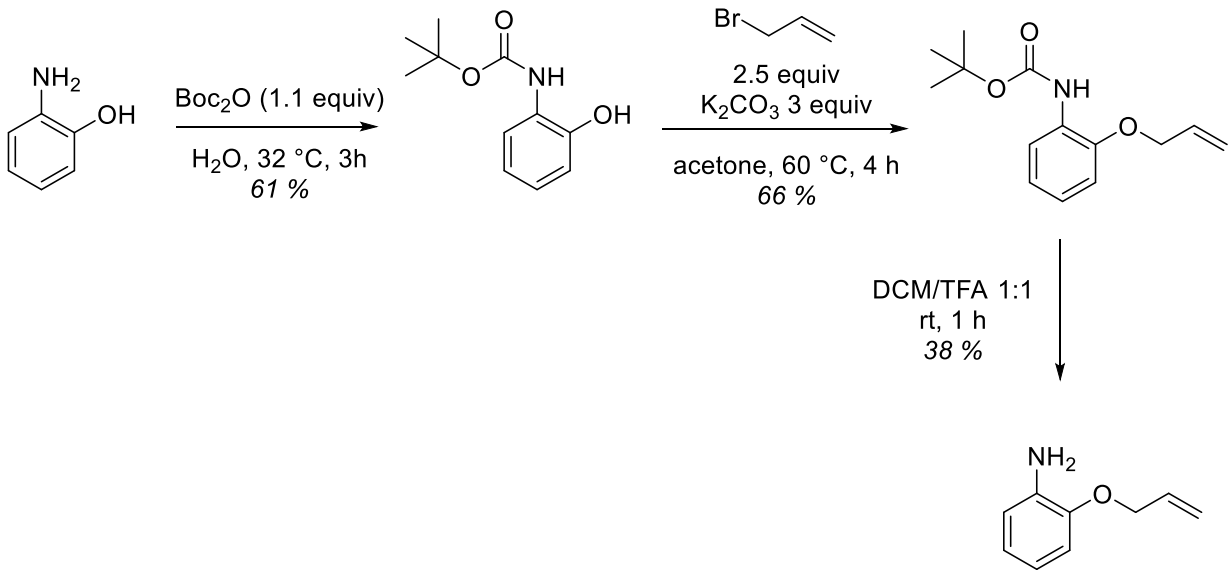

Figure A4 – Synthetic route for the synthesis of 2-(allyloxy)aniline

- 2-(allyloxy)aniline

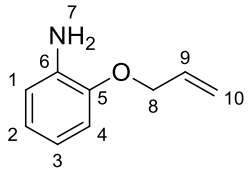

^{1}H NMR (300 MHz, $CDCl_3$): 6.72-6.63 (m, 2H, H_{ar}), 6.62-6.53 (m, 2H, H_{ar}), 5.94 (ddt, *J* = 17.2, 10.5, 5.3 Hz, 1H, H_9), 5.27 (ddt, *J* = 17.2, 3.0, 1.5 Hz, 1H, H_{10}), 5.15 (ddt, *J* = 10.5, 3.0, 1.5 Hz, 1H, H_{10}), 4.40 (dt, *J* = 5.3, 1.5 Hz, 2H, H_8) 3.66 (br s, 2H, H_7). ^{13}C NMR (75.5 MHz, $CDCl_3$): δ 146.2 (C_5), 136.5 (C_6), 133.6 (C_9), 121.3 (C_{ar}), 118.2 (C_{ar}), 117.3 (C_{10}), 115.1 (C_{ar}), 112.0 (C_{ar}), 69.1 (C_8).

The general procedure for the arylation of pyrazole from aniline was then applied to 2-(allyloxy)aniline and gave the cyclized compound 3-methylbenzofurane as major product.

- 3-methylbenzofurane

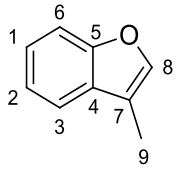

^{1}H NMR (300 MHz, $CDCl_3$): δ 7.44 (d, *J* = 7.2 Hz, 1H, H_{ar}), 7.37 (d, *J* = 7.8 Hz, 1H, H_{ar}), 7.32 (s, 1H, H_8), 7.18 (m, 2H, H_{ar}), 2.16 (s, 3H, H_9). ^{13}C NMR (75.5 MHz, $CDCl_3$): δ 155.4 (C_5), 141.5 (C_8), 129.1 (C_4), 124.2 (C_{ar}), 122.3 (C_{ar}), 119.5 (C_{ar}), 115.7 (C_7), 111.4 (C_{ar}), 8.0 (C_9).

Cyclic voltammetry: oxidation of Cu$^{(I)}$ by *t*BuONO:

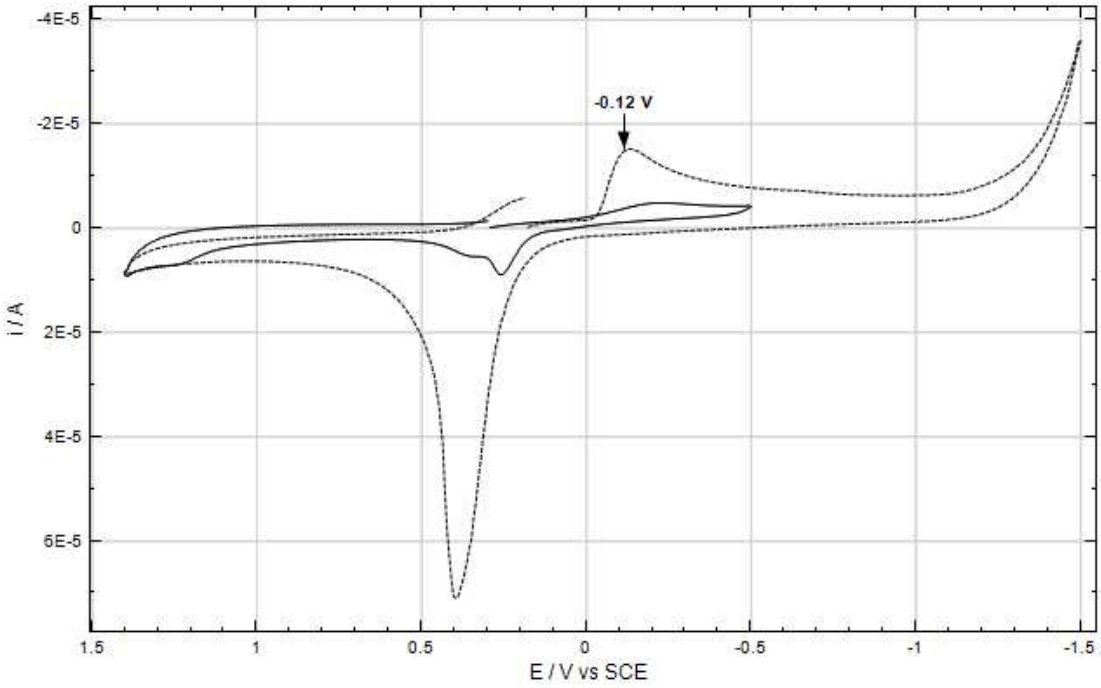

Figure A5 - CV performed in MeOH containing n-Bu_4NBF_4 (0.3 M) at a steady glassy carbon disk electrode (d = 1 mm), at a scan rate of 0.5 V.s^{-1}, at 20 °C, starting from the resting potential (a) Reduction of $Cu(CH_3CN)_4PF_6$ (2 mM) (dashed line); (b) Reduction of $Cu(CH_3CN)_4PF_6$ (2 mM) in the presence of *t*BuONO (2 mM) (solid line).

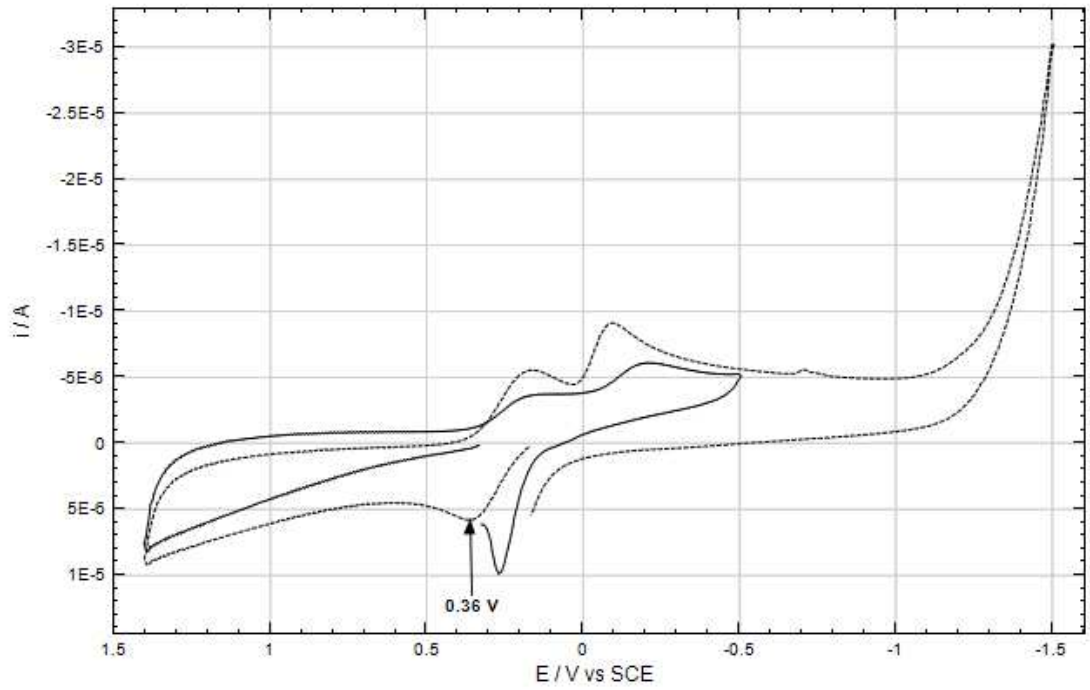

Figure A6 - CV performed in MeOH containing *n*-Bu_4NBF_4 (0.3 M) at a steady glassy carbon disk electrode (d = 1 mm), at a scan rate of 0.5 $V.s^{-1}$, at 20 °C, starting from the resting potential (a) Oxidation of $Cu(CH_3CN)_4PF_6$ (2 mM) (dashed line); (b) Oxidation of $Cu(CH_3CN)_4PF_6$ (2 mM) in the presence of *t*BuONO (2 mM) (solid line).

Complementary computational results

Table A1 - Reactions free energies and barriers (in $kcal.mol^{-1}$) computed at different levels of theory for the catalytic cycle depicted in Figure 3.34.

	ΔG_C	Ga_{OA}	ΔG_{OA}	ΔG_{NE}	Ga_{ID}	ΔG_{ID}	Ga_{RE}	ΔG_{RE}	ΔG_{LE}
BLYP	+ 6.76	+ 19.64	- 24.15	- 2.31	+ 0.64	+ 1.71	+5.01	- 43.82	- 4.30
PBE0	+ 7.13	+ 21.08	- 20.49	- 4.57	+ 0.16	+ 0.86	+ 3.56	- 50.23	- 7.23
B3LYP	+ 9.34	+19.96	- 22.97	- 2.91	- 0.95	+ 1.11	+ 2.82	- 52.37	- 3.94
mPW91	+ 7.99	+ 21.15	- 22.79	- 3.34	+ 0.72	+ 1.62	+ 3.13	- 52.92	- 4.84
CAM-B3LYP	+ 5.52	+ 23.09	- 17.98	- 4.52	+ 0.28	+ 1.69	+ 3.03	- 55.24	- 5.19
B3LYP-D	- 0.94	+ 16.86	- 20.60	- 6.25	+ 1.13	+ 2.62	+ 3.72	- 46.77	- 1.53
M06	+ 1.93	+ 17.59	- 14.71	- 6.92	- 0.50	+ 0.51	+ 0.73	- 47.13	- 8.24
M062X	+ 0.00	+ 18.77	- 4.40	- 5.80	-1.71	- 0.83	+ 0.50	- 63.18	- 7.19

No free energies are given for the MP2 method because the structures were not optimized at this level of theory.

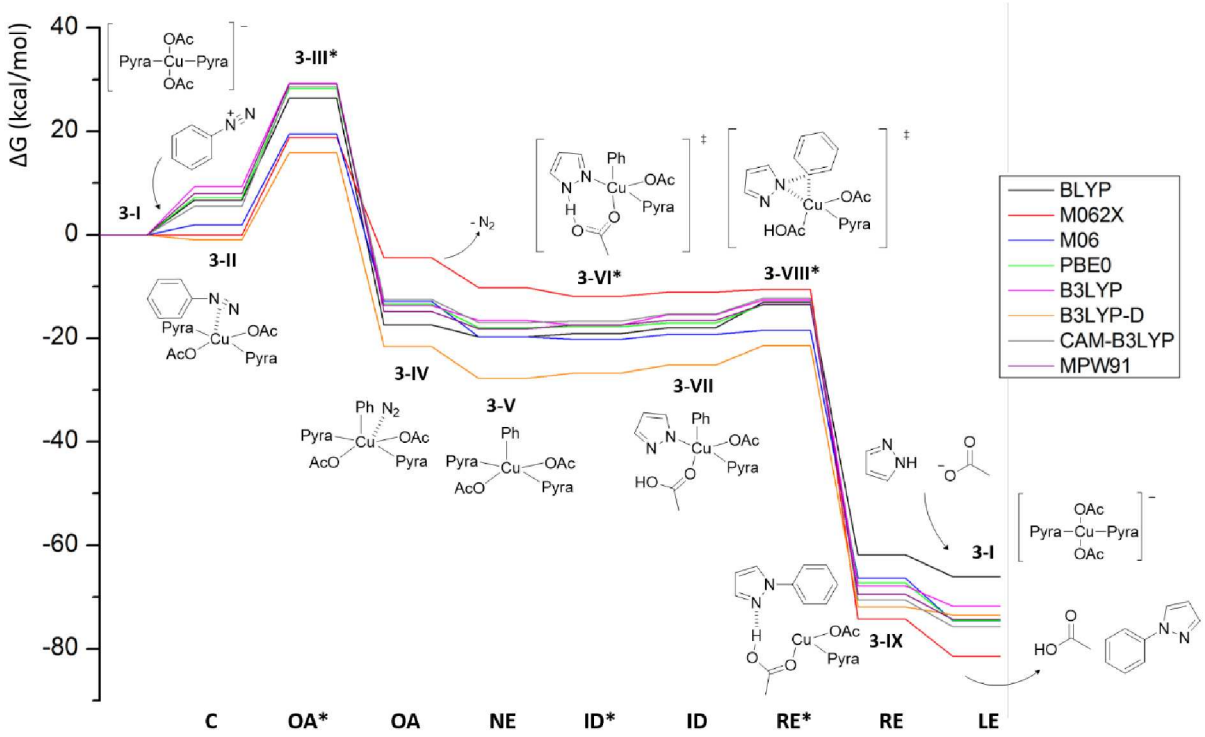

Figure A7 - Reactions free energies and barriers (in kcal.mol^{-1}) computed at different levels of theory for the catalytic cycle depicted in Figure 3.34. The stars represent transition states.

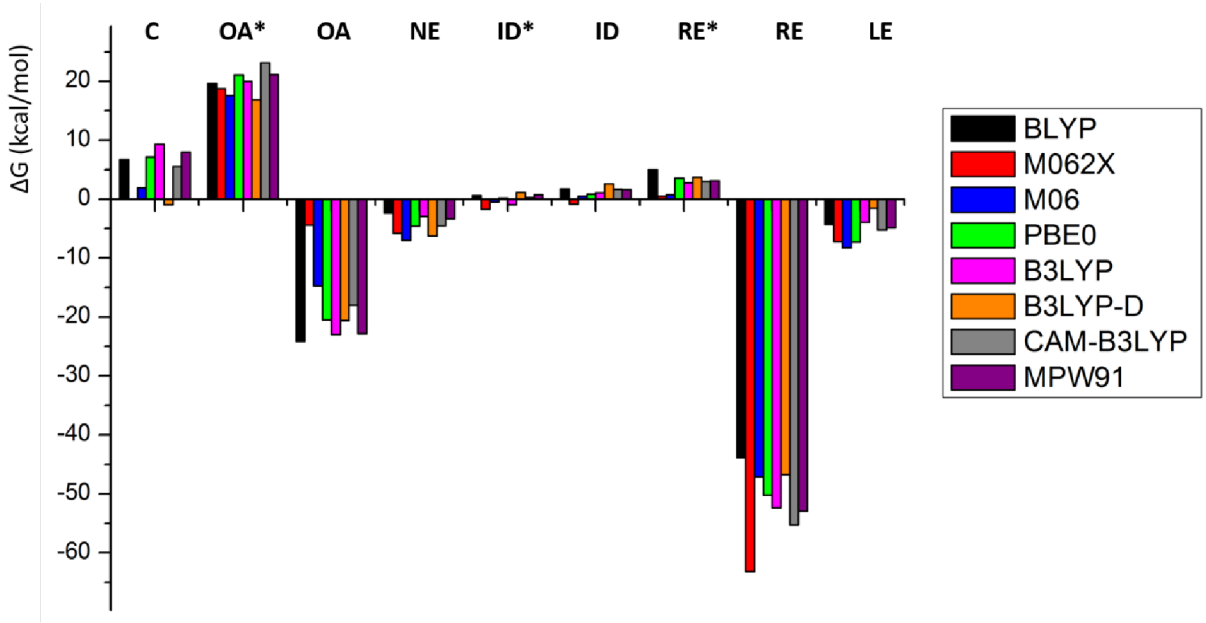

Figure A8 - Reactions free energies and barriers (in kcal.mol^{-1}) computed at different levels of theory for the catalytic cycle depicted in Figure 3.34. The bars with a star represent activation energies.

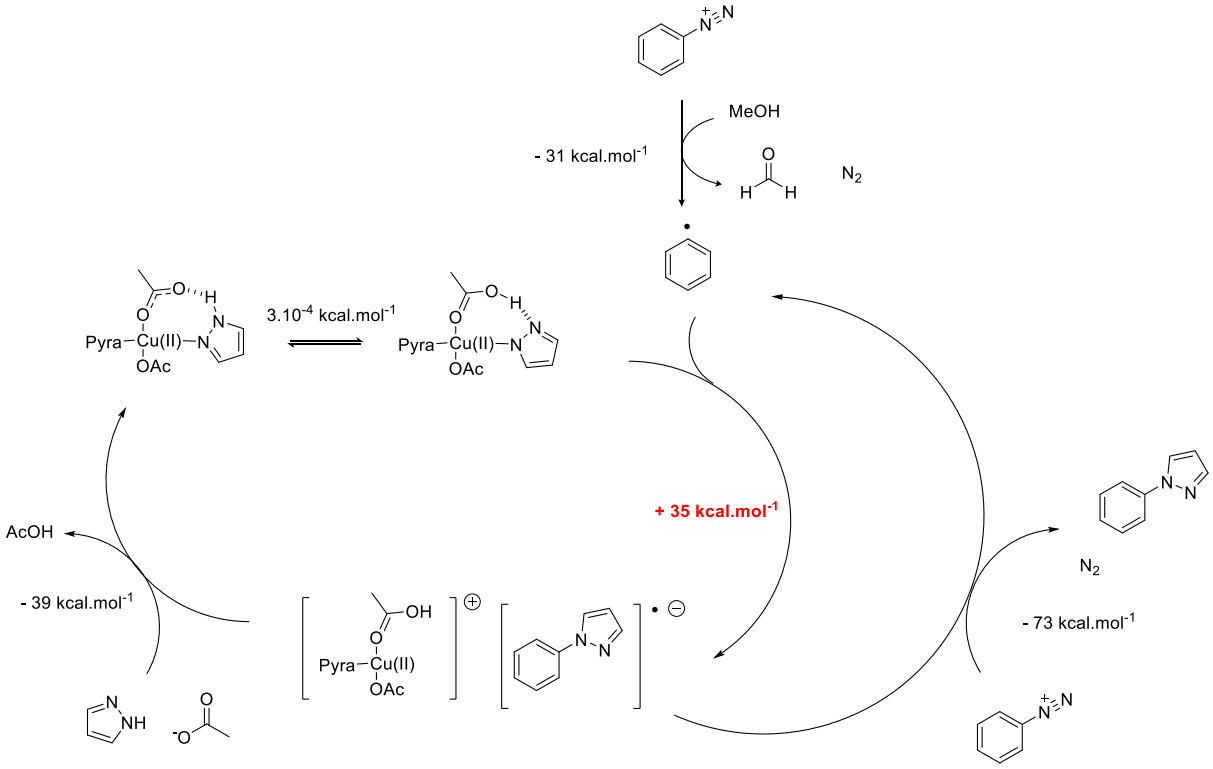

Figure A9 – Reaction energies (in kcal.mol^{-1}) for the hypothesis of a pure radical mechanism

Appendix to chapter 4

α,α,α-trifluorotoluene was used as an internal standard for ^{19}F NMR spectra for the determination of the crude yield of coupling and the ratio of isomers and by-products.

General procedure A for the synthesis of alkenyl thioethers 4-24a to 4-24l:

Alkenyl thioethers **4-24a** to **4-24l** were synthesized according to a reported procedure.[275]

An argon flushed schlenk was charged with KOH (10 mmol) and Cu_2O (0.25 mmol). Then distilled dioxane (2.5 mL) was added, followed by bromostyrene (6 mmol) and then hexanethiol (5 mmol). The schlenk was sealed and heated at 110 °C in a sand bath. After stirring at this temperature for 24 to 72 h, the heterogeneous mixture was cooled to room temperature and diluted with ethyl acetate (100 mL). The resulting solution was filtered through a pad of celite, washed with ethyl acetate (150 mL) and concentrated in vacuo to give the crude material which was then purified by column chromatography (SiO_2, EtOAc in cyclohexane 0 to 5 %) to afford the desired product.

The *Z* or *E* configuration of the products was established with the coupling constant of the vinyl protons.

- Hexyl(styryl)sulfane (**4-24a**)[276] *Z/E* (90:10)

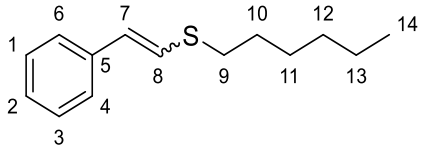

Following the general procedure A, **4-24a** was synthesized on a 10 mmol scale in 74 % yield. <u>*E isomer*</u>*:* ^{1}H NMR (300 MHz, $CDCl_3$): δ 7.41-7.18 (m, 5H, H_{ar}), 6.77 (d, *J* = 15.6 Hz, 1H, H_7), 6.50 (d, *J* = 15.6 Hz, 1H, H_8), 2.83 (t, *J* = 7.2 Hz, 2H, H_9), 1.81-1.64 (m, 2H, H_{10}), 1.53-1.43 (m, 2H, H_{11}), 1.40-1.30 (m, 4H, H_{12} and H_{13}), 0.97-0.92 (m, 3H, H_{14}). ^{13}C NMR (75 MHz, $CDCl_3$): δ 137.3 (C_5), 128.8 (C_{ar}), 126.8 (C_{ar}), 126.8 (C_8), 125.6 (C_{ar}), 125.5 (C_7), 32.8 (C_9), 31.5 (C_{10}), 29.6 (C_{11}), 28.6 (C_{12}), 22.7 (C_{13}), 14.2 (C_{14}). <u>*Characteristic peaks for the Z isomer*</u>*:* ^{1}H NMR (300 MHz, $CDCl_3$): δ 7.54-7.52 (m, 2H, H_{ar}), 6.47 (d, *J* = 10.9 Hz, 1H, H_7), 6.28 (d, *J* = 10.9 Hz, 1H, H_8).^{13}C NMR (75 MHz, $CDCl_3$): δ 137.2 (C_5), 128.3 (C_{ar}), 127.8 (C_8), 126.7 (C_{ar}), 125.4 (C_7).

- Cyclohexyl(styryl)sulfane (**4-24b**)[277] *Z/E* (48:52)

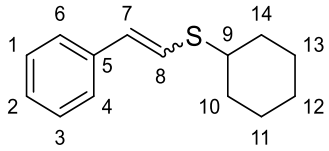

Following the general procedure A, **4-24b** was synthesized on a 5 mmol scale in 36 % yield. <u>*E isomer*</u>*:* ^{1}H NMR (300 MHz, $CDCl_3$): δ 7.50 (d, *J* = 7.2, 1H, H_{ar}), 7.38-7.30 (m, 3H, H_{ar}), 7.23-7.18 (m, 1H, H_{ar}), 6.78 (d, *J* = 15.6 Hz, 1H, H_7), 6.58 (d, *J* = 15.6 Hz, 1H, H_8), 2.99-2.89 (m, 1H, H_9), 2.10-2.06 (m, 2H, H_{cy}), 1.84-1.80 (m, 2H, H_{cy}), 1.67-1.30 (m, 6H, H_{cy}). ^{13}C NMR (75 MHz, $CDCl_3$): δ 137.3 (C_5), 128.8 (C_8), 128.7 (C_{ar}), 127.0 (C_{ar}), 125.7 (C_{ar}), 124.2 (C_7), 45.5 (C_9), 33.7 (C_{cy}), 26.1 (C_{cy}), 25.8 (C_{cy}). <u>*Z isomer*</u>*:* ^{1}H NMR (300 MHz, $CDCl_3$): δ 7.50 (d, *J* = 7.2, 1H, H_{ar}), 7.38-7.30 (m, 3H, H_{ar}), 7.23-7.18 (m, 1H, H_{ar}), 6.44 (d, *J* = 11.1 Hz, 1H, H_7), 6.34 (d, *J* = 11.1 Hz, 1H, H_8), 2.99-2.89 (m, 1H, H_9), 2.10-2.06 (m, 2H, H_{cy}), 1.84-1.80 (m, 2H, H_{cy}), 1.67-1.30 (m, 6H, H_{cy}). ^{13}C NMR (75 MHz, $CDCl_3$): δ 137.3 (C_5), 128.8 (C_{ar}),

128.3 (C_{ar}), 126.6 (C_8), 126.0 (C_{ar}), 125.2 (C_7), 47.9 (C_9), 33.8 (C_{cy}), 26.1 (C_{cy}), 25.7 (C_{cy}). HRMS (EI, m/z) [M] calcd. for $C_{14}H_{18}S$: 218.1129, found: 218,1135.

- *Tert*-butyl(styryl)sulfane (**4-24c**)[276] *Z/E* (64:36)

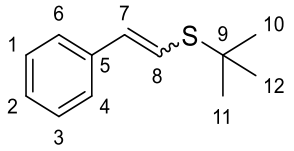

Following the general procedure A, **4-24c** was synthesized on a 5 mmol scale in 55 % yield. <u>*E isomer*</u>*:* ^{1}H NMR (300 MHz, $CDCl_3$): δ 7.49 (d, *J* = 6.0 Hz, 1H, H_{ar}), 7.39-7.29 (m, 3H, H_{ar}), 7.25-7.18 (m, 1H, H_{ar}), 6.89 (d, *J* = 15.6 Hz, 1H, H_7), 6.72 (d, *J* = 15.6 Hz, 1H, H_8), 1.42 (s, 9H, H_{10}, H_{11} and H_{12}). ^{13}C NMR (75 MHz, $CDCl_3$): δ 137.2 (C_5), 132.2 (C_8), 128.8 (C_{ar}), 127.4 (C_{ar}), 126.0 (C_{ar}), 122.2 (C_7), 44.5 (C_9), 31.2 (C_{10}, C_{11} and C_{12}). <u>*Z isomer*</u>*:* ^{1}H NMR (300 MHz, $CDCl_3$): δ 7.49 (d, *J* = 6.0 Hz, 1H, H_{ar}), 7.39-7.29 (m, 3H, H_{ar}), 7.25-7.18 (m, 1H, H_{ar}), 6.50 (d, *J* = 11.4 Hz, 1H, H_7), 6.45 (d, *J* = 11.4 Hz, 1H, H_8), 1.44 (s, 9H, H_{10}, H_{11} and H_{12}). ^{13}C NMR (75 MHz, $CDCl_3$): δ 137.3 (C_5), 128.9 (C_{ar}), 128.3 (C_{ar}), 126.7 (C_8), 125.5 (C_{ar}), 123.6 (C_7), 44.6 (C_9), 30.9 (C_{10}, C_{11} and C_{12}). HRMS (EI, m/z) [M] calcd. for $C_{12}H_{16}S$: 192.0973, found: 192,0980.

- Benzyl(styryl)sulfane (**4-24d**)[278] *Z/E* (20:80)

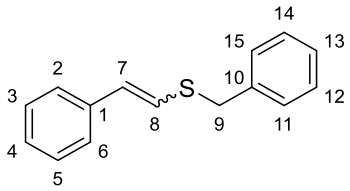

Following the general procedure A, **4-24d** was synthesized on a 5 mmol scale in 89 % yield. <u>*E isomer*</u>*:* ^{1}H NMR (300 MHz, $CDCl_3$): δ 7.50-7.22 (m, 10H, H_{ar}), 6.75 (d, *J* = 15.6 Hz, 1H, H_7), 6.56 (d, *J* = 15.6 Hz, 1H, H_8), 4.05 (s, 2H, H_9). ^{13}C NMR (75 MHz, $CDCl_3$): δ 137.4 (C_1 or C_{10}), 137.1 (C_{10} or C_1), 129.0 (C_{ar}), 128.8 (C_{ar}), 128.7 (C_{ar}), 128.1 (C_{ar}), 127.5 (C_8), 127.1 (C_{ar}), 125.7 (C_{ar}), 124.5 (C_7), 37.5 (C_9). <u>*Z isomer*</u>*:* ^{1}H NMR (300 MHz, $CDCl_3$): δ 7.50-7.22 (m, 10H, H_{ar}), 6.46 (d, *J* = 10.8 Hz, 1H, H_7), 6.29 (d, *J* = 10.8 Hz, 1H, H_8), 4.03 (s, 2H, H_9). ^{13}C NMR (75 MHz, $CDCl_3$): δ 137.5 (C_1 or C_{10}), 137.0 (C_{10} or C_1), 129.1 (C_{ar}), 128.8 (C_{ar}), 128.7

(C_{ar}), 128.4 (C_{ar}), 127.5 (C_8), 126.9 (C_{ar}), 126.1 (C_7), 126.0 (C_{ar}), 39.7 (C_9). HRMS (EI, m/z) [M] calcd. for $C_{15}H_{14}S$: 226.0816, found: 226.0820.

- Phenyl(styryl)sulfane (**4-24e**)[279] *Z/E* (10:90)

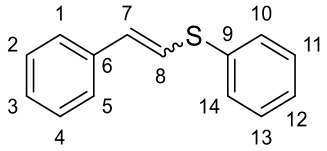

Following the general procedure A, **4-24e** was synthesized on a 5 mmol scale in 26 % yield. *E isomer:* ^{1}H NMR (300 MHz, $CDCl_3$): δ 7.37-7.12 (m, 10H, H_{ar}), 6.80 (d, *J* = 15.5 Hz, 1H, H_7), 6.65 (d, *J* = 15.5 Hz, 1H, H_8). ^{13}C NMR (75 MHz, $CDCl_3$): δ 136.7 (C_6 or C_9), 135.4 (C_9 or C_6), 131.9 (C_8), 130.0 (C_{ar}), 129.3 (C_{ar}), 128.8 (C_{ar}), 127.7 (C_{ar}), 127.1 (C_{ar}), 126.2 (C_{ar}), 123.5 (C_7). *Characteristic peaks for the Z isomer:* ^{1}H NMR (300 MHz, $CDCl_3$): δ 7.48-7.36 (m, 5H, H_{ar}), 6.51 (d, *J* = 10.8 Hz, 1H, H_7), 6.42 (d, *J* = 10.8 Hz, 1H, H_8). ^{13}C NMR (75 MHz, $CDCl_3$): δ 130.2 (C_{ar}), 128.9 (C_{ar}), 128.5 (C_{ar}), 127.4 (C_{ar}), 127.3 (C_{ar}). HRMS (EI, m/z) [M] calcd. for $C_{14}H_{12}S$: 212.0660, found: 212.0659.

- (4-(tert-butyl)phenyl)(styryl)sulfane (**4-24f**) *Z/E* (26:74)

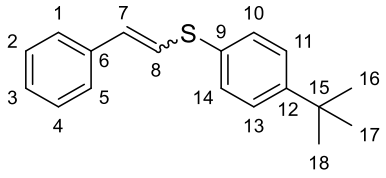

Following the general procedure A, **4-24f** was synthesized on a 5 mmol scale in 43 % yield. *E isomer:* ^{1}H NMR (300 MHz, $CDCl_3$): δ 7.44-7.08 (m, 9H, H_{ar}), 6.79 (d, *J* = 15.6 Hz, 1H, H_7), 6.57 (d, *J* = 15.6 Hz, 1H, H_8), 1.21 (s, 9H, H_{16}, H_{17} and H_{18}). ^{13}C NMR (75 MHz, $CDCl_3$): δ 150.5 (C_{12}), 136.8 (C_6), 131.6 (C_9), 130.8 (C_8), 130.2 (C_{ar}), 128.7 (C_{ar}), 127.5 (C_{ar}), 126.3 (C_{ar}), 126.0 (C_{ar}), 124.5 (C_7), 34.7 (C_{15}), 31.4 (C_{16}, C_{17} and C_{18}). *Z isomer:* ^{1}H NMR (300 MHz, $CDCl_3$): δ 7.44-7.08 (m, 9H, H_{ar}), 6.42 (d, *J* = 10.8 Hz, 1H, H_7), 6.37 (d, *J* = 10.8 Hz, 1H, H_8), 1.21 (s, 9H, H_{16}, H_{17} and H_{18}). ^{13}C NMR (75 MHz, $CDCl_3$): δ 150.7 (C_{12}), 136.7 (C_6), 132.8 (C_9), 130.3 (C_{ar}), 128.8 (C_{ar}), 128.4 (C_{ar}), 127.1 (C_{ar}), 127.0 (C_{ar}), 126.6 (C_8), 126.3 (C_7), 31.4 (C_{16}, C_{17} and C_{18}), 29.8 (C_{15}). HRMS (EI, m/z) [M] calcd. for $C_{18}H_{20}S$: 268.1286, found: 268.1282.

- (4-Fluorophenyl)(styryl)sulfane (**4-24g**)[280] *Z/E* (35:65)

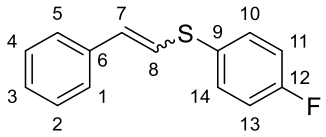

Following the general procedure A, **4-24g** was synthesized on a 4 mmol scale in 35 % yield. <u>*E isomer:*</u> ^{1}H NMR (300 MHz, $CDCl_3$): δ 7.57-7.27 (m, 7H, H_{ar}), 7.09 (t, *J* = 9 Hz, 2H, H_{11} and H_{13}), 6.86 (d, *J* = 15.3 Hz, 1H, H_7), 6.69 (d, *J* = 15.3 Hz, 1H, H_8). ^{13}C NMR (75 MHz, $CDCl_3$): δ 162.4 (d, J = 245 Hz, C_{12}), 136.5 (C_6), 132.8 (d, *J* = 8.0 Hz, C_{10} and C_{14}), 131.3 (C_8), 130.0 (d, *J* = 3 Hz, C_9), 128.8 (C_{ar}), 127.7 (C_{ar}), 126.1 (C_{ar}), 124.0 (C_7), 116.5 (d, *J* = 22 Hz, C_{11} and C_{13}). ^{19}F NMR (282 MHz, $CDCl_3$): δ -114.27. <u>*Z isomer:*</u> ^{1}H NMR (300 MHz, $CDCl_3$): δ 7.57-7.27 (m, 7H, H_{ar}), 7.09 (t, *J* = 9 Hz, 2H, H_{11} and H_{13}), 6.61 (d, *J* = 10.8 Hz, 1H, H_7), 6.44 (d, *J* = 10.8 Hz, 1H, H_8). ^{13}C NMR (75 MHz, $CDCl_3$): δ 162.5 (d, J = 245 Hz, C_{12}), 136.5 (C_6), 132.8 (d, *J* = 8.0 Hz, C_{10} and C_{14}), 131.5 (d, *J* = 3 Hz, C_9), 128.9 (C_{ar}), 128.5 (C_{ar}), 127.3 (C_8), 127.2 (C_7), 126.7 (C_{ar}), 116.4 (d, *J* = 22 Hz, C_{11} and C_{13}). ^{19}F NMR (282 MHz, $CDCl_3$): δ -114.03. HRMS (EI, m/z) [M] calcd. for $C_{15}H_{11}FS$: 230.0565, found: 230.0564.

- (3,4-dimethoxyphenyl)(styryl)sulfane (**4-24h**) *Z/E* (10:90)

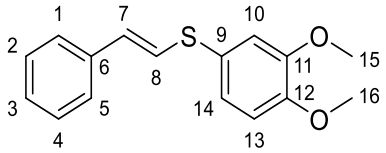

Following the general procedure A, **4-24h** was synthesized on a 1 mmol scale in 52 % yield. <u>*E isomer:*</u> ^{1}H NMR (300 MHz, $CDCl_3$): δ 7.20-7.10 (m, 5H, H_{ar}), 6.95 (dd, *J* = 8.4, 2.1 Hz, 1H, H_{ar}), 6.89 (d, *J* = 2.1 Hz, 1H, H_{ar}), 6.75 (d, *J* = 8.4 Hz, 1H, H_{ar}), 6.75 (d, *J* = 15.6 Hz, 1H, H_7), 6.44 (d, *J* = 15.6 Hz, 1H, H_8), 3.77 (s, 3H, H_{15} or H_{16}), 3.78 (s, 3H, H_{16} or H_{15}).^{13}C NMR (75 MHz, $CDCl_3$): δ 149.4 (C_{11} or C_{12}), 149.1 (C_{12} or C_{11}), 136.7 (C_6), 129.2 (C_8), 128.7 (C_{ar}), 127.3 (C_{ar}), 125.9 (C_{ar}), 125.4 (C_{ar}), 124.9 (C_9), 124.7 (C_7), 115.0 (C_{ar}), 111.8 (C_{ar}), 56.0 (C_{15} or C_{16}), 56.0 (C_{16} or C_{15}). <u>*Characteristic peaks for the Z isomer:*</u> ^{1}H NMR (300 MHz, $CDCl_3$): δ 6.41 (d, *J* = 10.8 Hz, 1H, H_7), 6.34 (d, *J* = 10.8 Hz, 1H, H_8). ^{13}C NMR (75 MHz, $CDCl_3$): δ 135.2 (C_6), 128.4 (C_{ar}), 128.1 (C_{ar}), 127.0 (C_{ar}), 124.2 (C_9), 114.6 (C_{ar}), 111.7 (C_{ar}). HRMS (EI, m/z) [M] calcd. for $C_{16}H_{16}O_2S$: 272.0871, found: 272.0864.

- (*E*)-*tert*-butyl(hex-1-en-1-yl)sulfane (**4-24i**) *Z/E* > (1:99)

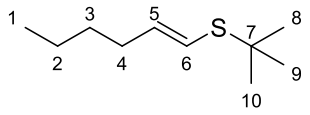

Following the general procedure A, **4-24i** was synthesized on a 2 mmol scale in 46 % yield. <u>*E isomer*</u>*:* ^{1}H NMR (300 MHz, $CDCl_3$): δ 6.02 (d, *J* = 14.7 Hz, 1H, H_6), 5.86 (dt, *J* = 14.7, 6.9 Hz, 1H, H_5), 2.08 (dt, *J* = 6.9, 6.6 Hz, 2H, H_4), 1.37-1.28 (m, 13H, H_2, H_3, H_8, H_9 and H_{10}), 0.87 (t, *J* = 7.2, 3H, H_1). ^{13}C NMR (75 MHz, $CDCl_3$): δ 138.1 (C_5), 119.8 (C_6), 43.5 (C_7), 33.0 (C_4), 31.4 (C_3), 30.8 (C_8, C_9 and C_{10}), 22.2 (C_2), 13.9 (C_1).

- (*E*)-hex-1-en-1-yl(phenyl)sulfane (**4-24j**)[281] *Z/E* > (1:99)

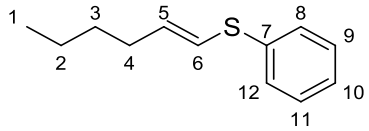

Following the general procedure A, **4-24j** was synthesized on a 3 mmol scale in 84 % yield. <u>*E isomer*</u>*:* ^{1}H NMR (300 MHz, $CDCl_3$): δ 7.24-7.20 (m, 4H, H_{ar}), 7.12-7.07 (m, 1H, H_{ar}), 6.06 (d, *J* = 14.9 Hz, 1H, H_6), 5.92 (dt, *J* = 14.9, 6.7 Hz, 1H, H_5), 2.13-2.06 (m, 2H, H_4), 1.41 – 1.05 (m, 4H, H_2 and H_3), 0.84 (t, *J* = 7.1 Hz, 3H, H_1). ^{13}C NMR (75 MHz, $CDCl_3$): δ 137.9 (C_5), 136.8 (C_7), 129.0 (C_{ar}) 128.5 (C_{ar}), 126.1 (C_{ar}), 120.7 (C_6), 32.9 (C_4), 31.3 (C_3), 22.3 (C_2), 14.0 (C_1).

- (*E*)-benzyl(hex-1-en-1-yl)sulfane (**4-24k**)[278] *Z/E* > (1:99)

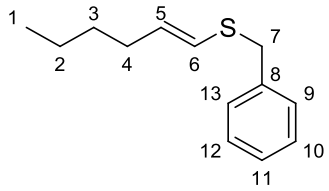

Following the general procedure A, **4-24k** was synthesized on a 1 mmol scale in 44 % yield. <u>*E isomer*</u>*:* ^{1}H NMR (300 MHz, $CDCl_3$): δ 7.23-7.13 (m, 5H, H_{ar}), 5.81 (dt, *J* = 15.0, 1.2 Hz, 1H, H_6), 5.58 (dt, *J* = 15.0, 6.9 Hz, 1H, H_5), 3.74 (s, 2H, H_7), 1.95 (dt, *J* = 6.9, 6.1 Hz, 2H, H_4), 1.27-1.13 (m, 4H, H_2 and H_3), 0.78 (t, *J* = 6.9 Hz, 3H, H_1). ^{13}C NMR (75 MHz, $CDCl_3$): δ

138.0 (C_8), 132.7 (C_5), 128.9 (C_{ar}), 128.6 (C_{ar}), 127.1 (C_{ar}), 122.0 (C_6), 37.7 (C_7), 32.9 (C_4), 31.4 (C_3), 22.1 (C_2), 14.0 (C_1).

- Benzyl(2-ethyl carbonovinyl)sulfane (**4-24l**)[282] *Z/E* (17:83)

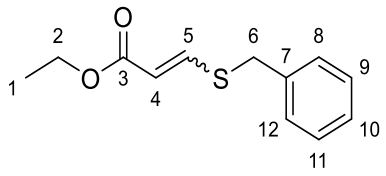

Following the general procedure A, **4-24l** was synthesized on a 2.5 mmol scale in 58 % yield. <u>*E isomer:*</u> ^{1}H NMR (300 MHz, $CDCl_3$): δ 7.62 (d, *J* = 15.1 Hz, 1H, H_5), 7.33 – 7.14 (m, 5H, H_{ar}), 5.72 (d, *J* = 15.1 Hz, 1H, H_4), 4.09 (q, *J* = 7.1 Hz, 2H, H_2), 3.94 (s, 2H, H_6), 1.19 (t, *J* = 7.1 Hz, 3H, H_1). ^{13}C NMR (75 MHz, $CDCl_3$): δ 165.3 (C_3), 146.0 (C_5), 135.6 (C_7), 128.9 (C_{ar}), 128.8 (C_{ar}), 127.9 (C_{ar}), 114.5 (C_4), 60.3 (C_2), 36.6 (C_6), 14.4 (C_1). <u>*Characteristic peaks for the Z isomer:*</u> ^{1}H NMR (300 MHz, $CDCl_3$): δ 6.97 (d, *J* = 10.2 Hz, 1H, H_4), 3.87 (s, 2H, H_6). ^{13}C NMR (75 MHz, $CDCl_3$): δ 166.7 (C_3), 148.6 (C_5), 137.3 (C_7), 113.7 (C_4), 60.2 (C_2), 39.5 (C_6), 14.4 (C_1). HRMS (EI, m/z) [M] calcd. for $C_{12}H_{14}O_2S$: 222.0715, found: 222.0716.

- hex-1-en-2-yl(phenyl)sulfane (**4-24m**)[283]

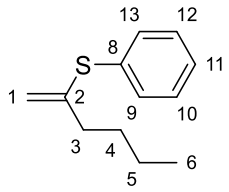

Following a reported procedure[284], **4-24m** was synthesized on a 6 mmol scale in 27 % yield. ^{1}H NMR (300 MHz, $CDCl_3$): δ 7.55-7.49 (m, 2H, H_{ar}), 7.43-7.31 (m, 3H, H_{ar}), 5.23 (t, *J* = 1.1 Hz, 1 H, H_1), 4.96 (s, 1H, H_1), 2.38-2.28 (m, 2H, H_3), 1.69-1.57 (m, 2H, H_4), 1.50-1.32 (m, 2H, H_5), 0.98 (t, *J* = 7.3 Hz, 3H, H_6). ^{13}C NMR (75 MHz, $CDCl_3$): δ 146.1 (C_2), 133.3 (C_8), 133.2 (C_{ar}), 129.0 (C_{ar}), 127.7 (C_{ar}), 112.4 (C_1), 36.3 (C_3), 30.6 (C_4), 22.0 (C_5), 13.9 (C_6). HRMS (EI, m/z) [M] calcd. for $C_{12}H_{16}S$: 192.0973, found: 192.0964.

- (2,2-diphenylvinyl)(phenyl)sulfane (**4-24n**)[285]

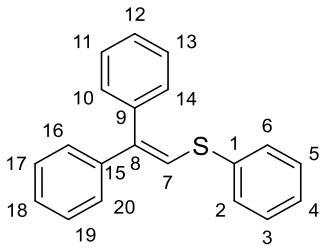

Following a reported procedure,[285] **4-24n** was synthesized on a 6 mmol scale in 47 % yield. ^{1}H NMR (300 MHz, $CDCl_3$): δ 7.53-7.23 (m, 15H, H_{ar}), 6.90 (s, 1H, H_7). ^{13}C NMR (75 MHz, $CDCl_3$): δ 141.6 (C_9 or C_{15}), 141.3 (C_{15} or C_9), 139.4 (C_1), 136.7 (C_8), 129.9 (C_{ar}), 129.7 (C_{ar}), 129.3 (C_{ar}), 128.5 (C_{ar}), 128.5 (C_{ar}), 128.0 (C_{ar}), 127.4 (C_{ar}), 127.4 (C_{ar}), 126.9 (C_{ar}), 124.3 (C_7). HRMS (EI, m/z) [M] calcd. for $C_{20}H_{16}S$: 288.0973, found: 288.0979.

General procedure B for the difluoroalkylation

An argon flushed schlenk was charged with the starting alkenyl thioether **4-24** (1 mmol, 1.0 equiv). Anhydrous acetonitrile (5 mL) was added, then Cu_2O (14.4 mg, 0.1 mmol, 0.10 equiv), 1,10-phenanthroline monohydrate (23.8 mg, 0.12 mmol, 0.12 equiv) and oven-dried potassium carbonate (276.4 mg, 2 mmol, 2 equiv). The mixture was stirred under argon for a few seconds and ethylbromodifluoroacetate (256 µL, 2 mmol, 2 equiv) was added. The Schlenk was sealed and placed in a sand bath at 80 °C, and the mixture was stirred at this temperature for 24 h. The mixture was then cooled to room temperature. Ethyl acetate and water were added; the aqueous layer was separated and extracted with ethyl acetate. The organic layers were gathered, dried over magnesium sulfate and the solvents were evaporated at room temperature. The residue was then purified by column chromatography (SiO_2, EtOAc in cyclohexane 0 to 20%) to afford the corresponding fluorine-containing alkenyl thioether **4-25**.

- Ethyl-2,2-difluoro-4-(hexylthio)-3-phenylbut-3-enoate (**4-25a**) *Z/E* (5:95)

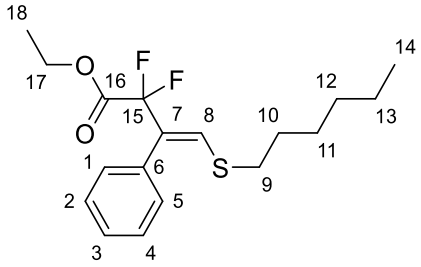

Following the general procedure B, **4-25a** was synthesized on a 1 mmol scale in 82 % yield. *E isomer:* ^{1}H NMR (300 MHz, $CDCl_3$): δ 7.38 – 7.15 (m, 5H, H_{ar}), 6.94 (t, *J* = 1.7 Hz, 1H, H_8), 4.09 (q, *J* = 7.1 Hz, 2H, H_{17}), 2.64 (t, *J* = 7.4 Hz, 2H, H_9), 1.62 – 1.45 (m, 2H, H_{10}), 1.36 – 1.13 (m, 6H, H_{11}, H_{12} and H_{13}), 1.05 (t, *J* = 7.2 Hz, 3H, H_{18}), 0.79 (t, *J* = 6.7 Hz, 3H, H_{14}). ^{13}C NMR (75 MHz, $CDCl_3$): δ 163.7 (t, *J* = 35.1 Hz, C_{16}), 135.6 (t, *J* = 9.0 Hz, C_8), 133.2 (C_6), 129.5 (C_{ar}), 128.6 (C_{ar}), 128.5 (C_{ar}), 127.4 (t, *J* = 21.8 Hz, C_7), 112.9 (t, *J* = 252.6 Hz, C_{15}), 62.8 (C_{17}), 34.6 (C_9), 31.3 (C_{10}), 30.3 (C_{11}), 28.1 (C_{12}), 22.5 (C_{13}), 14.0 (C_{14}), 13.8 (C_{18}). ^{19}F NMR (282 MHz, $CDCl_3$): δ -100.7. HRMS (EI, m/z) [M] calcd. for $C_{18}H_{24}F_2O_2S$: 342.1465, found: 342.1465. *Characteristic peak for the Z isomer:* ^{19}F NMR (282 MHz, $CDCl_3$): δ -97.6. *Characteristic peak for the major by-product*: ^{19}F NMR (282 MHz, $CDCl_3$): δ -103.1.

- Ethyl-4-(cyclohexylthio)-2,2-difluoro-3-phenylbut-3-enoate (**4-25b**) *Z/E* (7:93)

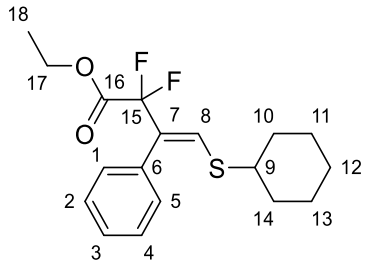

Following the general procedure B, **4-25b** was synthesized on a 1 mmol scale in 83 % yield. *E isomer:* ^{1}H NMR (300 MHz, $CDCl_3$): δ 7.27-7.17 (m, 5H, H_{ar}), 7.02 (t, *J* = 1.8 Hz, 1H, H_8), 4.05 (q, *J* = 7.1 Hz, 2H, H_{17}), 2.86 – 2.74 (m, 1H, H_9), 1.89-1.86 (m, 2H, H_{cy}), 1.64-1.62 (m, 2H, H_{cy}), 1.55 – 1.06 (m, 6H, H_{cy}), 1.02 (t, *J* = 7.1 Hz, 3H, H_{18}). ^{13}C NMR (75 MHz, $CDCl_3$): δ 163.6 (t, *J* = 35.4 Hz, C_{16}), 133.7 (t, *J* = 8.9 Hz, C_8), 133.3 (t, *J* = 1.6 Hz, C_6), 129.4 (C_{ar}), 128.4 (C_{ar}), 128.3 (C_{ar}), 127.1 (t, *J* = 21.3 Hz, C_7), 113.0 (t, *J* = 251.3 Hz, C_{15}), 62.7 (C_{17}), 46.6 (C_9), 33.7 (C_{cy}), 25.8 (C_{cy}), 25.3 (C_{cy}), 13.7 (C_{18}). ^{19}F NMR (282 MHz, $CDCl_3$): δ -100.4. HRMS (EI, m/z) [M] calcd. for $C_{18}H_{22}F_2O_2S$: 340.1309, found: 340.1319. *Characteristic peak for the E isomer*: ^{19}F NMR (282 MHz, $CDCl_3$): δ -97.3. *Characteristic peak for the major by-product*: ^{19}F NMR (282 MHz, $CDCl_3$): δ -103.0.

- Ethyl-4-(tert-butylthio)-2,2-difluoro-3-phenylbut-3-enoate (**4-25c**) *Z/E* (5:95)

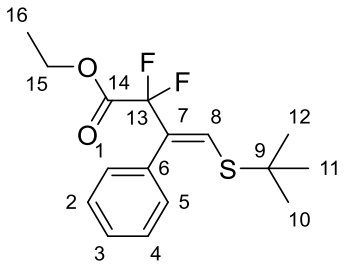

Following the general procedure B, **4-25c** was synthesized on a 1 mmol scale in 81 % yield. *E isomer:* ^{1}H NMR (300 MHz, $CDCl_3$): δ 7.26-7.18 (m, 5H, H_{ar}), 7.11 (t, *J* = 1.9 Hz, 1H, H_8), 4.09 (q, *J* = 7.1 Hz, 2H, H_{15}), 1.29 (s, 9H, H_{10}, H_{11} and H_{12}), 1.05 (t, *J* = 7.1 Hz, 3H, H_{16}). ^{13}C NMR (75 MHz, $CDCl_3$): δ 163.7 (t, *J* = 35.4 Hz, C_{14}), 133.4 (t, *J* = 1.6 Hz, C_6), 131.5 (t, *J* = 8.9 Hz, C_8), 129.6 (C_{ar}), 128.5 (C_{ar}), 128.4 (C_{ar}), 127.5 (t, *J* = 22.8 Hz, C_7), 113.1 (t, *J* = 252.4 Hz, C_{13}), 62.8 (C_{15}), 44.7 (C_9), 31.0 (C_{10}, C_{11} and C_{12}), 13.8 (C_{16}). ^{19}F NMR (282 MHz, $CDCl_3$): δ -100.4. HRMS (EI, m/z) [M] calcd. for $C_{16}H_{20}F_2O_2S$: 314.1152, found: 314.1152. *Characteristic peak for the Z isomer*: ^{19}F NMR (282 MHz, $CDCl_3$): δ -96.9. *Characteristic peak for the major by-product*: ^{19}F NMR (282 MHz, $CDCl_3$): δ -103.1.

- Ethyl-4-(benzylthio)-2,2-difluoro-3-phenylbut-3-enoate **(4-25d)** *Z/E* (6:94)

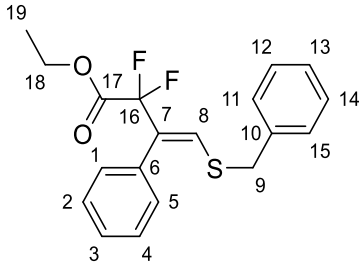

Following the general procedure B, **4-25d** was synthesized on a 1 mmol scale in 75 % yield. *E isomer:* ^{1}H NMR (300 MHz, $CDCl_3$): δ 7.30 – 7.15 (m, 10H, H_{ar}), 6.94 (t, *J* = 1.9 Hz, 1H, H_8), 4.08 (q, *J* = 7.1 Hz, 2H, H_{18}), 3.87 (s, 2H, H_9), 1.05 (t, *J* = 7.2 Hz, 3H, H_{19}). ^{13}C NMR (75 MHz, $CDCl_3$): δ 163.7 (t, *J* = 34.9 Hz, C_{17}), 136.9 (C_{10}), 134.2 (t, *J* = 9.0 Hz, C_8), 133.1 (t, *J* = 1.6 Hz, C_6), 129.6 (C_{ar}), 129.0 (C_{ar}), 128.9 (C_{ar}), 128.8 (C_{ar}), 128.6 (C_{ar}), 128.3 (C_7), 127.7 (C_{ar}), 112.9 (t, *J* = 252.5 Hz, C_{16}), 63.0 (C_{18}), 38.5 (C_9), 13.9 (C_{19}). ^{19}F NMR (282 MHz, $CDCl_3$): -100.8. HRMS (EI, m/z) [M] calcd. for $C_{19}H_{18}F_2O_2S$: 348.0996, found: 348.0995. *Characteristic peak for the Z isomer*: ^{19}F NMR (282 MHz, $CDCl_3$): δ -97.4. *Characteristic peak for the major by-product*: ^{19}F NMR (282 MHz, $CDCl_3$): δ -103.0.

- Ethyl-2,2-difluoro-3-phenyl-4-(phenylthio)but-3-enoate **(4-25e)** Z/E (8:92)

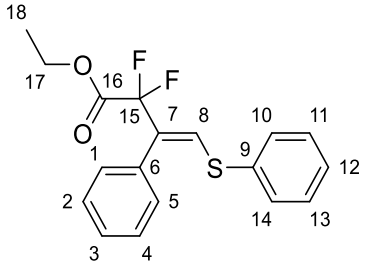

Following the general procedure B, **4-25e** was synthesized on a 1 mmol scale in 53 % yield. *Z isomer:* ^{1}H NMR (300 MHz, $CDCl_3$): δ 7.36 – 7.17 (m, 10H, H_{ar}), 7.15 (t, *J* = 1.7 Hz, 1H, H_8), 4.09 (q, *J* = 7.1 Hz, 2H, H_{17}), 1.05 (t, *J* = 7.1 Hz, 3H, H_{18}). ^{13}C NMR (75 MHz, $CDCl_3$): δ 163.5 (t, *J* = 35.0 Hz, C_{16}), 134.8 (t, *J* = 9.1 Hz, C_8), 134.2 (C_9), 132.8 (t, *J* = 1.6 Hz, C_6), 130.7 (C_{ar}), 129.6 (C_{ar}), 129.4 (C_{ar}), 129.1 (C_7), 129.0 (C_{ar}), 128.7 (C_{ar}), 128.0 (C_{ar}), 112.9 (t, *J* = 253.1 Hz, C_{15}), 63.0 (C_{17}), 13.8 (C_{18}). ^{19}F NMR (282 MHz, $CDCl_3$): δ -101.1. HRMS (EI, m/z) [M] calcd. for $C_{18}H_{16}F_2O_2S$: 334.0839, found: 334.0840. *Characteristic peak for the E isomer:* ^{19}F NMR (282 MHz, $CDCl_3$): δ -96.8. *Characteristic peak for the major by-product:* ^{19}F NMR (282 MHz, $CDCl_3$): δ -103.1.

- Ethyl-4-((4-(tert-butyl)phenyl)thio)-2,2-difluoro-3-phenylbut-3-enoate **(4-25f)** *Z/E* (9:91)

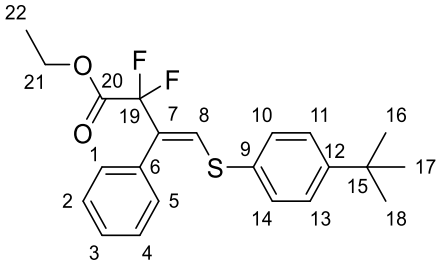

Following the general procedure B, **4-25f** was synthesized on a 1 mmol scale in 73 % yield. *E isomer:* ^{1}H NMR (300 MHz, $CDCl_3$): δ 7.33 – 7.21 (m, 9H, H_{ar}), 7.13 (t, *J* = 1.8 Hz, 1H, H_8), 4.08 (q, *J* = 7.1 Hz, 2H, H_{21}), 1.20 (s, 9H, H_{16}, H_{17} and H_{18}), 1.04 (t, *J* = 7.1 Hz, 3H, H_{22}). ^{13}C NMR (75 MHz, $CDCl_3$): δ 163.5 (t, *J* = 35.1 Hz, C_{20}), 151.4 (C_{12}), 135.7 (t, *J* = 9.0 Hz, C_8), 132.9 (t, *J* = 1.6 Hz, C_6), 130.9 (C_{ar}), 130.7 (C_9), 129.6 (C_{ar}), 128.9 (C_{ar}), 128.7 (C_{ar}), 128.4 (C_7), 126.5 (C_{ar}), 112.9 (t, *J* = 255.7 Hz, C_{19}), 63.0 (C_{21}), 34.7 (C_{15}), 31.3 (C_{16}, C_{17} and C_{18}), 13.8 (C_{22}). ^{19}F NMR (282 MHz, $CDCl_3$): δ -100.9. HRMS (EI, m/z) [M] calcd. for $C_{22}H_{24}F_2O_2S$: 390.1465, found: 390.1479. *Characteristic peak for the Z isomer:* ^{19}F NMR (282

MHz, $CDCl_3$): δ -96.8. <u>*Characteristic peak for the major by-product*</u>: ^{19}F NMR (282 MHz, $CDCl_3$): δ -103.1.

- Ethyl-2,2-difluoro-4-((4-fluorophenyl)thio)-3-phenylbut-3-enoate **(4-25g)** Z/E (8:92)

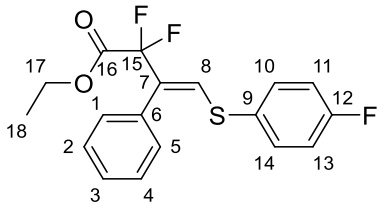

Following the general procedure B, **4-25g** was synthesized on a 1 mmol scale in 60 % yield. <u>*E isomer:*</u> ^1H NMR (300 MHz, $CDCl_3$): δ 7.34-7.21 (m, 7H, H_{ar}), 7.04 (t, *J* = 1.8 Hz, 1H, H_8), 6.92 (t, *J* = 8.6 Hz, 2H, H_{ar}), 4.09 (q, *J* = 7.1 Hz, 2H, H_{17}), 1.04 (t, *J* = 7.1 Hz, 3H, H_{18}). ^{13}C NMR (75 MHz, $CDCl_3$): δ 163.4 (t, *J* = 35.0 Hz, C_{16}), 162.8 (d, *J* = 247.5 Hz, C_{12}), 135.2 (t, *J* = 9.1 Hz, C_8), 133.3 (d, *J* = 8.3 Hz, C_{ar}), 132.6 (t, *J* = 1.7 Hz, C_6), 129.5 (C_{ar}), 129.3 (d, *J* = 3 Hz, C_9), 129.1 (C_{ar}), 128.9 (C_7), 128.7 (C_{ar}), 116.6 (d, *J* = 22.5 Hz, C_{ar}), 112.8 (t, *J* = 253.2 Hz, C_{15}), 63.0 (C_{17}), 13.8 (C_{18}). ^{19}F NMR (282 MHz, $CDCl_3$): -101.2, -112.8. HRMS (EI, m/z) [M] calcd. for $C_{18}H_{15}F_3O_2S$: 352.0745, found: 352.0749.<u>*Characteristic peaks for the Z isomer:*</u> ^{19}F NMR (282 MHz, $CDCl_3$): δ -97.0, -112.7. <u>*Characteristic peak for the major by-product*</u>: ^{19}F NMR (282 MHz, $CDCl_3$): δ -103.1.

- Ethyl-4-((3,4-dimethoxyphenyl)thio)-2,2-difluoro-3-phenylbut-3-enoate **(4-25h)** *Z/E* (6:94)

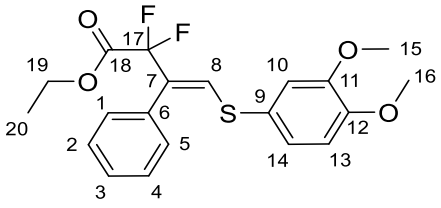

Following the general procedure B, **4-25h** was synthesized on a 0.25 mmol scale in 41 % yield. <u>*E isomer:*</u> ^1H NMR (300 MHz, $CDCl_3$): δ 7.36-7.28 (m, 5H, H_{ar}), 7.08 (t, *J* = 1.8 Hz, 1H, H_8), 6.96 (dd, *J* = 8.3, 2.1 Hz, 1H, H_{14}), 6.87 (d, *J* = 2.1 Hz, 1H, H_{10}), 6.76 (d, *J* = 8.4 Hz, 1H, H_{13}), 4.12 (q, *J* = 7.1 Hz, 2H, H_{19}), 3.80 (s, 6H, H_{15} and H_{16}), 1.08 (t, *J* = 7.1 Hz, 3H, H_{20}). ^{13}C NMR (75 MHz, $CDCl_3$): δ 163.6 (C_{18}), 149.7 (C_{11} or C_{12}), 149.4 (C_{11} or C_{12}), 136.7 (t, *J* = 9.0 Hz, C_8), 132.8 (C_6), 129.6 (C_{ar}), 128.9 (C_{ar}), 128.7 (C_{ar}), 127.8 (t, *J* = 22.5 Hz, C_7),

125.0 (C_{ar}), 124.8 (C_9), 115.1 (C_{ar}), 112.9 (t, J = 251.3 Hz, C_{17}), 111.9 (C_{ar}), 63.0 (C_{19}), 56.2 (C_{15} or C_{16}), 56.1 (C_{16} or C_{15}), 13.9 (C_{20}). ^{19}F NMR (282 MHz, $CDCl_3$): δ -101.0. HRMS (EI, m/z) [M] calcd. for $C_{20}H_{20}F_2O_4S$: 394.1050, found: 394.1041. *Characteristic peak for the Z isomer*: ^{19}F NMR (282 MHz, $CDCl_3$): δ -97.1. *Characteristic peak for the major by-product*: ^{19}F NMR (282 MHz, $CDCl_3$): δ -103.2.

- Ethyl-3-((tert-butylthio)methylene)-2,2-difluoroheptanoate **(4-25i)** *Z/E* (> 1:99)

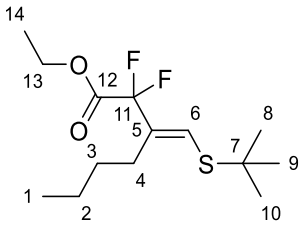

Following the general procedure B **4-25i** was synthesized on a 1 mmol scale in 81 % yield. *E isomer:* ^{1}H NMR (300 MHz, $CDCl_3$): δ 6.75 (t, J = 2.0 Hz, 1H, H_6), 4.28 (q, J = 7.1 Hz, 2H, H_{13}), 2.24 – 2.09 (m, 2H, H_4), 1.54 – 1.15 (m, 16H, H_2, H_3, H_8, H_9, H_{10} and H_{14}), 0.88 (t, J = 7.1 Hz, 3H, H_1). ^{13}C NMR (75 MHz, $CDCl_3$): δ 164.2 (t, J = 35.9 Hz, C_{12}), 128.6 (t, J = 21.8 Hz, C_5), 128.2 (t, J = 9.8 Hz, C_6), 114.1 (t, J = 251.7 Hz, C_{11}), 62.9 (C_{13}), 44.5 (C_7), 31.1 (C_8, C_9 and C_{10}), 30.0 (C_4), 27.9 (C_3), 22.9 (C_2), 14.0 (C_1 or C_{14}), 13.9 (C_{14} or C_1). ^{19}F NMR (282 MHz, $CDCl_3$): δ -103.5. HRMS (EI, m/z) [M] calcd. for $C_{14}H_{24}F_2O_2S$: 294.1465, found: 294.1461. *Characteristic peak for the major by-product*: ^{19}F NMR (282 MHz, $CDCl_3$): δ -100.1.

- Ethyl-2,2-difluoro-3-((phenylthio)methylene)heptanoate **(4-25j)** *Z/E* (> 1:99)

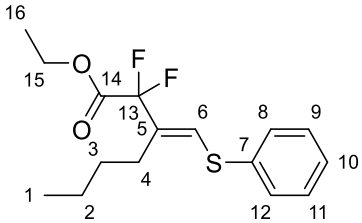

Following the general procedure B **4-25j** was synthesized on a 1 mmol scale in 81 % yield, *E isomer:* ^{1}H NMR (300 MHz, $CDCl_3$): δ 7.30-7.15 (m, 5H, H_{ar}), 6.75 (t, J = 1.9 Hz, 1H, H_6), 4.22 (q, J = 7.1 Hz, 2H, H_{15}), 2.22 (m, 2H, H_4), 1.48-1.36 (m, 2H, H_3), 1.33-1.28 (m, 2H, H_2), 1.23 (t, J = 7.1 Hz, 3H, H_{16}), 0.85 (t, J = 7.2 Hz, 3H, H_1). ^{13}C NMR (75 MHz, $CDCl_3$): δ 163.9 (t, J = 35.6 Hz, C_{14}), 134.4 (C_7), 131.1 (t, J = 10.1 Hz, C_6), 130.3 (C_{ar}), 130.2 (t, J = 22.5

Hz, C_5), 129.4 (C_{ar}), 127.7 (C_{ar}), 113.8 (t, *J* = 252.3 Hz, C_{13}), 63.1 (C_{15}), 30.1 (C_4), 28.0 (C_3), 22.9 (C_2), 14.0 (C_1 or C_{16}), 13.9 (C_{16} or C_1). ^{19}F NMR (282 MHz, $CDCl_3$): δ -103.8. HRMS (EI, m/z) [M] calcd. for $C_{16}H_{20}F_2O_2S$: 314.1152, found: 314.1155. *Characteristic peak for the major by-product*: ^{19}F NMR (282 MHz, $CDCl_3$): δ -99.7.

- Ethyl-3-((benzylthio)methylene)-2,2-difluoroheptanoate **(4-25k)** *Z/E* (> 1:99)

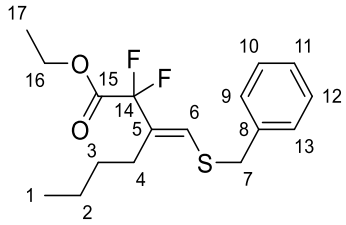

Following the general procedure B, **4-25k** was synthesized on a 0.5 mmol scale in 71 % yield. *E isomer:* ^{1}H NMR (300 MHz, $CDCl_3$): δ 7.27-7.16 (m, 5H, H_{ar}), 6.52 (t, *J* = 2.0 Hz, 1H, H_6), 4.16 (q, *J* = 7.1 Hz, 2H, H_{16}), 3.86 (s, 2H, H_7), 2.15 – 2.05 (m, 2H, H_4), 1.33-1.24 (m, 4H, H_2 and H_3), 1.19 (t, *J* = 7.1 Hz, 3H, H_{17}), 0.81 (t, *J* = 7.2 Hz, 3H, H_1). ^{13}C NMR (75 MHz, $CDCl_3$): δ 164.0 (t, *J* = 35.6 Hz, C_{15}), 137.2 (C_8), 131.0 (t, *J* = 10.1 Hz, C_6), 129.0 (t, *J* = 18.0 Hz, C_5), 128.9 (C_{ar}), 128.8 (C_{ar}), 127.6 (C_{ar}), 113.9 (t, *J* = 251.7 Hz, C_{14}), 63.0 (C_{16}), 38.2 (C_7), 29.8 (C_3), 28.0 (t, *J* = 1.8 Hz, C_4), 22.9 (C_2), 14.0 (C_{17}), 13.9 (C_1). ^{19}F NMR (282 MHz, $CDCl_3$): δ -103.6. HRMS (EI, m/z) [M] calcd. for $C_{17}H_{22}F_2O_2S$: 314.1309, found: 328.1314. *Characteristic peak for the major by-product*: ^{19}F NMR (282 MHz, $CDCl_3$): δ -101.0.

- Diethyl 3-((benzylthio)methylene)-2,2-difluorosuccinate **(4-25l)** *Z/E* (42:58)

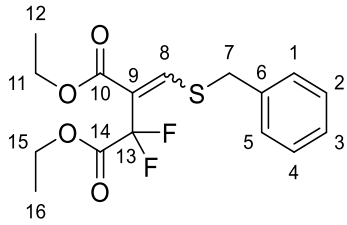

Following the general procedure B, **4-25l** was synthesized on a 1 mmol scale in 20 % yield. *E isomer:* ^{1}H NMR (300 MHz, $CDCl_3$): δ 7.76 (t, J = 1.4 Hz, 1H, H_8), 7.36 – 7.15 (m, 5H, H_{ar}), 4.22 (q, *J* = 7.0 Hz, 2H, H_{11} or H_{15}), 4.15 (q, *J* = 7.1 Hz, 2H, H_{15} or H_{11}), 3.99 (s, 2H, H_7), 1.24 (t, *J* = 7.1 Hz, 3H, H_{12} or H_{16}), 1.18 (t, *J* = 7.0 Hz, 3H, H_{16} or H_{12}). ^{13}C NMR (75 MHz, $CDCl_3$): δ 163.3 (t, *J* = 33.8 Hz, C_{14}), 163.3 (t, *J* = 3.8 Hz, C_{10}), 152.3 (t, *J* = 8.5 Hz, C_8),

136.2 (C_6), 129.1 (C_{ar}), 129.1 (C_{ar}), 128.0 (C_{ar}), 117.3 (t, *J* = 23.1 Hz, C_9), 111.3 (t, *J* = 250.4 Hz, C_{13}), 63.1 (C_{11} or C_{15}), 61.4 (C_{15} or C_{11}), 40.5 (C_7), 14.2 (C_{12} or C_{16}), 14.0 (C_{16} or C_{12}). ^{19}F NMR (282 MHz, $CDCl_3$): δ -101.2. HRMS (EI, m/z) [M] calcd. for $C_{16}H_{18}F_2O_4S$: 344.0894, found: 344.0905. <u>*Z isomer:*</u> ^{1}H NMR (300 MHz, $CDCl_3$): δ 8.06 (t, J = 2.4 Hz, 1H, H_8), 7.33 – 7.22 (m, 5H, H_{ar}), 4.24 (q, *J* = 7.0 Hz, 2H, H_{11} or H_{15}), 4.09 (q, *J* = 7.1 Hz, 2H, H_{15} or H_{11}), 4.00 (s, 2H, H_7), 1.25 (t, *J* = 7.1 Hz, 3H, H_{12} or H_{16}), 1.16 (t, *J* = 7.0 Hz, 3H, H_{16} or H_{12}). ^{13}C NMR (75 MHz, $CDCl_3$): δ 163.0 (t, *J* = 33.4 Hz, C_{14}), 162.5 (t, *J* = 5.9 Hz, C_{10}), 152.4 (C_8), 135.8 (C_6), 129.2 (C_{ar}), 129.2 (C_{ar}), 128.2 (C_{ar}), 118.4 (t, *J* = 24.9 Hz, C_9), 113.4 (t, *J* = 250.9 Hz, C_{13}), 63.1 (C_{11} or C_{15}), 61.4 (C_{15} or C_{11}), 40.4 (C_7), 14.1 (C_{12} or C_{16}), 14.0 (C_{16} or C_{12}). ^{19}F NMR (282 MHz, $CDCl_3$): δ -100.0.

- Ethyl-2,2-difluoro-4-(phenylthio)oct-4-enoate **(4-25m)** *Z/E* (81:19)

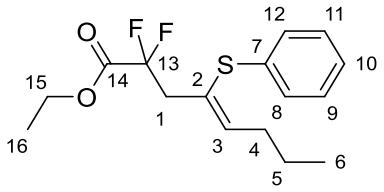

Following the general procedure B (during 12 h to avoid decomposition), **4-25m** was synthesized on a 1 mmol scale in 55 % yield. <u>*Z isomer:*</u> ^{1}H NMR (300 MHz, $CDCl_3$): δ 7.41-7.05 (m, 5H, H_{ar}), 6.07 (t, *J* = 7.3 Hz, 1H, H_3), 4.24 – 4.15 (m, 2H, H_{15}), 2.98 – 2.75 (m, 2H, H_1), 2.35 – 2.20 (m, 2H, H_4), 1.47 – 1.29 (m, 2H, H_5), 1.28 – 1.07 (m, 3H, H_{16}), 0.91 – 0.77 (t, *J* = 7.3 Hz, 3H, H_6).^{13}C NMR (75 MHz, $CDCl_3$): δ 163.9 (t, *J* = 32.4 Hz, C_{14}), 144.3 (C_3), 134.6 (C_7), 129.4 (C_{ar}), 129.2 (C_{ar}), 126.5 (C_{ar}), 123.0 (t, *J* = 5.1 Hz, C_2), 115.0 (t, *J* = 252.4 Hz, C_{13}), 62.9 (C_{15}), 42.1 (t, *J* = 24.5 Hz, C_1), 32.3 (C_4), 22.3 (C_5), 13.9 (C_{16}), 13.7 (C_6). ^{19}F NMR (282 MHz, $CDCl_3$): δ -104.1. HRMS (EI, m/z) [M] calcd. for $C_{16}H_{20}F_2O_2S$: 314.1152, found: 314.1151. <u>*Characteristic peak for the E isomer:*</u> ^{19}F NMR (282 MHz, $CDCl_3$): δ -103.5.<u>*Characteristic peaks for the major by-products:*</u> ^{19}F NMR (282 MHz, $CDCl_3$): δ -92.7, -92.3.

- Ethyl 2,2-difluoro-4,4-diphenylbut-3-enoate (**4-26n**)[230]

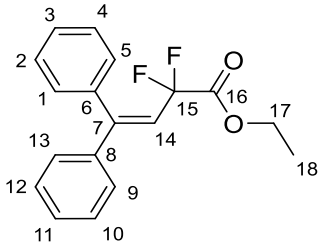

Following the general procedure B starting from **4-24n**, **4-26n** was synthesized on a 0.6 mmol scale in 30 % yield. ^{1}H NMR (300 MHz, $CDCl_3$): δ 7.45 – 6.98 (m, 10H, H_{ar}), 6.19 (t, *J* = 11.8 Hz, 1H, H_{14}), 3.82 (q, *J* = 7.1 Hz, 2H, H_{17}), 1.08 (t, *J* = 7.1 Hz, 3H, H_{18}). ^{13}C NMR (75 MHz, $CDCl_3$): δ 163.6 (t, *J* = 33.9 Hz, C_{16}), 151.1 (t, *J* = 9.5 Hz, C_7), 140.6 (C_6 or C_8), 137.2 (C_8 or C_6), 130.0 (C_{ar}), 129.2 (C_{ar}), 128.7 (C_{ar}), 128.5 (C_{ar}), 128.1 (C_{ar}), 128.0 (C_{ar}), 119.6 (t, *J* = 28.4 Hz, C_{14}), 112.7 (t, *J* = 245.0 Hz, C_{15}), 62.8 (C_{17}), 13.8 (C_{18}). ^{19}F NMR (282 MHz, $CDCl_3$): δ -90.9. HRMS (EI, m/z) [M] calcd. for $C_{18}H_{16}F_2O_2$: 302.1118, found: 302.1127.

Aminolysis of fluorinated alkenyl thioether 4-25e

4-25e (167 mg, 0.5 mmol, 1 equiv) was dissolved in methanol (5 mL) and benzylamine (110 µL, 1 mmol, 2 equiv) was added dropwise at room temperature. After 20 hours, the mixture was diluted with dichloromethane (20 mL) and successively washed with 1N HCl (20 mL), water (20 mL) and brine (20 mL), then dried over magnesium sulfate and evaporated to dryness. The amide **4-33** was obtained sufficiently pure as a white solid (178 mg, 90 %).

- *N*-benzyl-2,2-difluoro-3-phenyl-4-(phenylthio)but-3-enamide **(4-33),** *Z/E* (> 1:99)

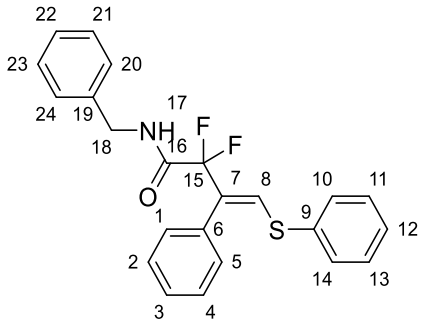

^{1}H NMR (300 MHz, $CDCl_3$): δ 7.49-7.25 (m, 14H, H_{ar} and H_8), 7.06-7.00 (m, 2H, H_{ar}), 6.55 (br s, 1H, H_{17}), 4.42 (d, *J* = 5.9 Hz, 2H, H_{18}). ^{13}C NMR (75 MHz, $CDCl_3$): δ 163.3 (t, *J* = 30.9 Hz, C_{16}), 136.7 (C_9 or C_{19}), 135.4 (t, *J* = 9.2 Hz, C_8), 134.2 (C_{19} or C_9), 133.0 (t, *J* = 1.6 Hz, C_6), 130.8 (C_{ar}), 129.8 (C_{ar}), 129.4 (C_{ar}), 129.0 (C_{ar}), 128.9 (C_{ar}), 128.8 (C_{ar}), 128.5 (C_7),

127.9 (C_{ar}), 127.9 (C_{ar}), 127.7 (C_{ar}), 114.6 (t, J = 254.3 Hz, C_{15}), 43.6 (C_{18}). ^{19}F NMR (282 MHz, $CDCl_3$): δ -102.2. HRMS (EI, m/z) [M] calcd. for $C_{23}H_{19}F_2NOS$: 395.1155, found: 395.1168.

Synthesis of bromodifluoroacetamides

2-bromo-N,N-diethyl-2,2-difluoroacetamide **4-28** and 2-bromo-2,2-difluoro-1-morpholinoethan-1-one **4-29** were synthesized according to a reported procedure.[253]

- 2-bromo-N,N-diethyl-2,2-difluoroacetamide **4-28**

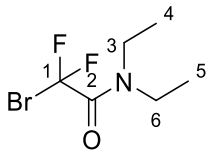

^{1}H NMR (300 MHz, $CDCl_3$): δ 3.50 (qt, J = 7.1, 1.3 Hz, 2H, H_3 or H_6), 3.41 (q, J = 7.1 Hz, 2H, H_6 or H_3), 1.23 (t, J = 7.1 Hz, 3H, H_5 or H_4), 1.17 (t, J = 7.1 Hz, 3H, H_5 or H_4). ^{13}C NMR (75 MHz, $CDCl_3$): δ 158.8 (t, J = 26.2 Hz, C_2), 111.3 (t, J = 314.7 Hz, C_1), 43.0 (t, J = 3.8 Hz, C_3 or C_6), 42.2 (C_6 or C_3). 13.9 (C_4 or C_5), 12.0 (C_5 or C_4). ^{19}F NMR (282 MHz): δ -54.4. HRMS (EI, m/z) [M] calcd. for $C_6H_{10}BrF_2NO$: 228.9914, found: 228.9917.

- 2-bromo-2,2-difluoro-1-morpholinoethan-1-one **4-29**

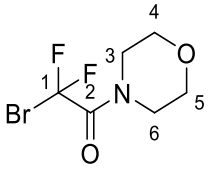

^{1}H NMR (300 MHz, $CDCl_3$): δ 3.76-3.66 (m, 8H, H_3, H_4, H_5 and H_6). ^{13}C NMR (75 MHz, $CDCl_3$): δ 158.01 (t, J = 26.6 Hz, C_2), 110.60 (t, J = 314.4 Hz, C_1), 66.63 (C_4 or C_5), 66.21 (C_5 or C_4), 47.39 (t, J = 3.9 Hz, C_3 or C_6), 43.99 (C_6 or C_3). ^{19}F NMR (282 MHz): δ -54.5. . HRMS (EI, m/z) [M] calcd. for $C_6H_8BrF_2NO_2$: 242.9706, found: 242.9710.

Radical trapping experiments

Experiments described in Table 4.8 in the presence of TEMPO were conducted according to the general procedure B, with the addition of TEMPO (1 equiv) after the other reagents. The substrate **1a**, the ligand or the base, were omitted according to Table 4.8. After concentration in vacuo, α,α,α trifluorotoluene was added as internal standard, the mixture was diluted with DCM and analyzed by ^{19}F NMR with a DMSO-d_6 insert.

- Ethyl 2,2-difluoro-2-((2,2,6,6-tetramethylpiperidin-1-yl)oxy)acetate **(4-38)**

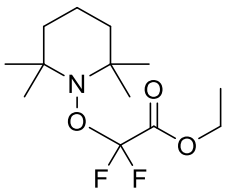

^{19}F NMR (282 MHz, DMSO-d_6): δ -73.9. MS (GC/CI-NH3) [M+H^+]: 280.13.

Cyclic voltammetry experiments

CV were performed in CH_3CN containing *n*-Bu_4NBF_4 (0.3 M) at a steady glassy carbon disk electrode (d = 1 mm), at a scan rate of 0.5 $V.s^{-1}$, at 20 °C, starting from the resting potential.

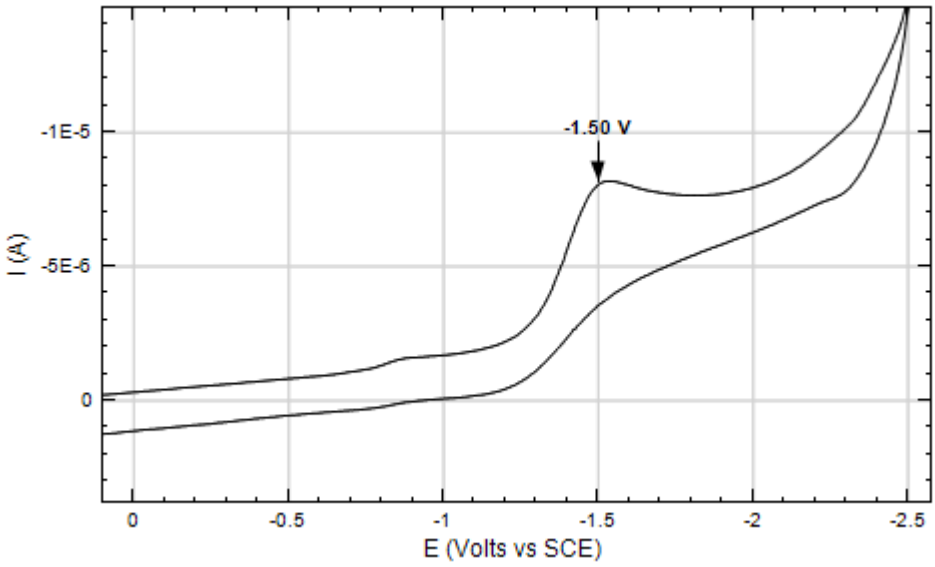

Figure A10 - Reduction of $BrCF_2CO_2Et$ **4-8** (2 mM)

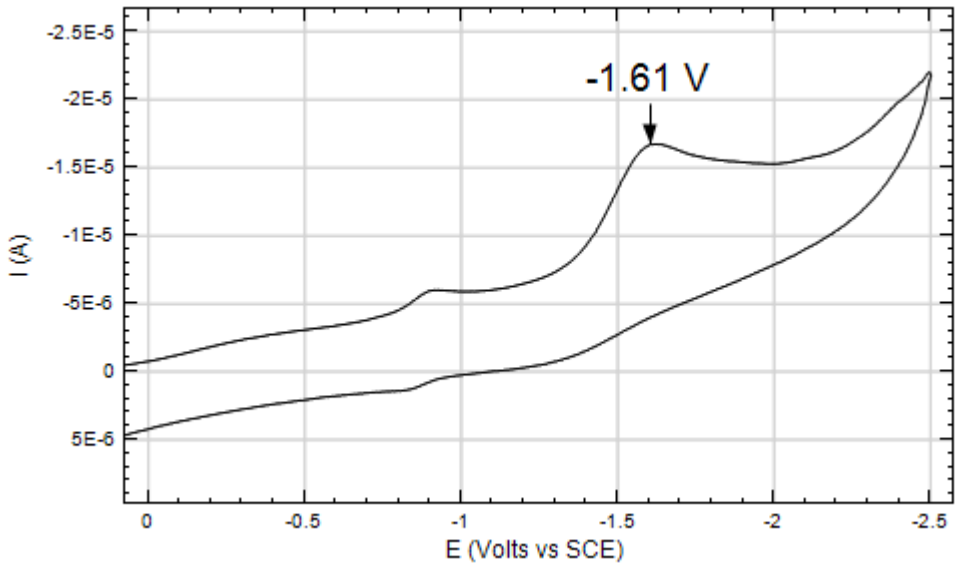

Figure A11 - Reduction of 2-bromo-2,2-difluoro-1-morpholinoethan-1-one **4-29** (2mM)

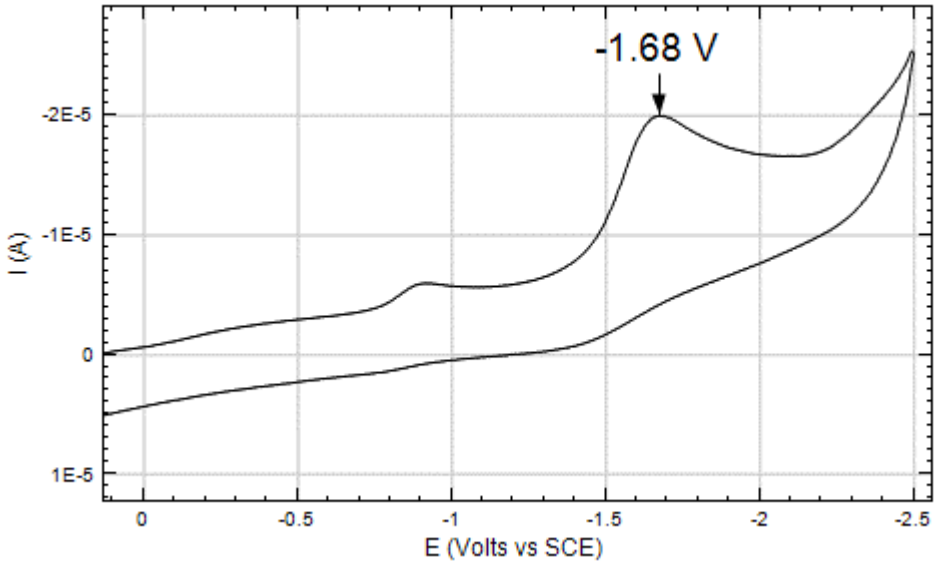

Figure A12 - Reduction of $BrCH_2CO_2Et$ **4-31** (2mM)

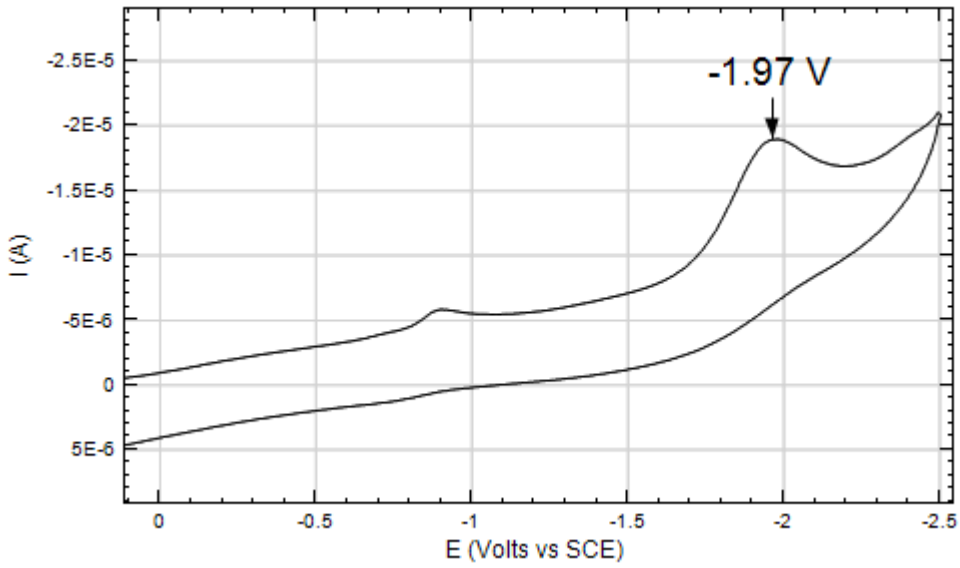

Figure A13 - Reduction of $BrCF_2PO(OEt)_2$ **4-30** (2mM)

Complexation in the presence of copper and base measured by ^{1}H NMR

An oven-dried NMR tube was charged under argon with tetrakis(acetonitrile)copper(I) hexafluorophosphate (9.3 mg, 0.025mmol), 1,10-phenanthroline monohydrate (5.0 mg, 0.025 mmol), 0.5 mL CD_3CN, and 2 L 1,2-dichloroethane as an internal standard. Increasing amounts of vinylsulfide **4-24a** in solution in CD_3CN were added and ^{1}H NMR spectra were recorded at 23 °C. The same experiment was then performed with the addition of nBu$_4$NOH (0.025 mmol, 16 L of a 1.54 M solution in water,).

Computational details

Reactions related to energies reported in Table 4.9, Table ES2 and Table ES3:

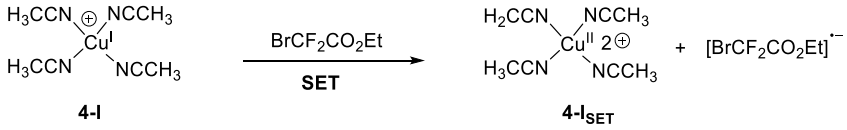

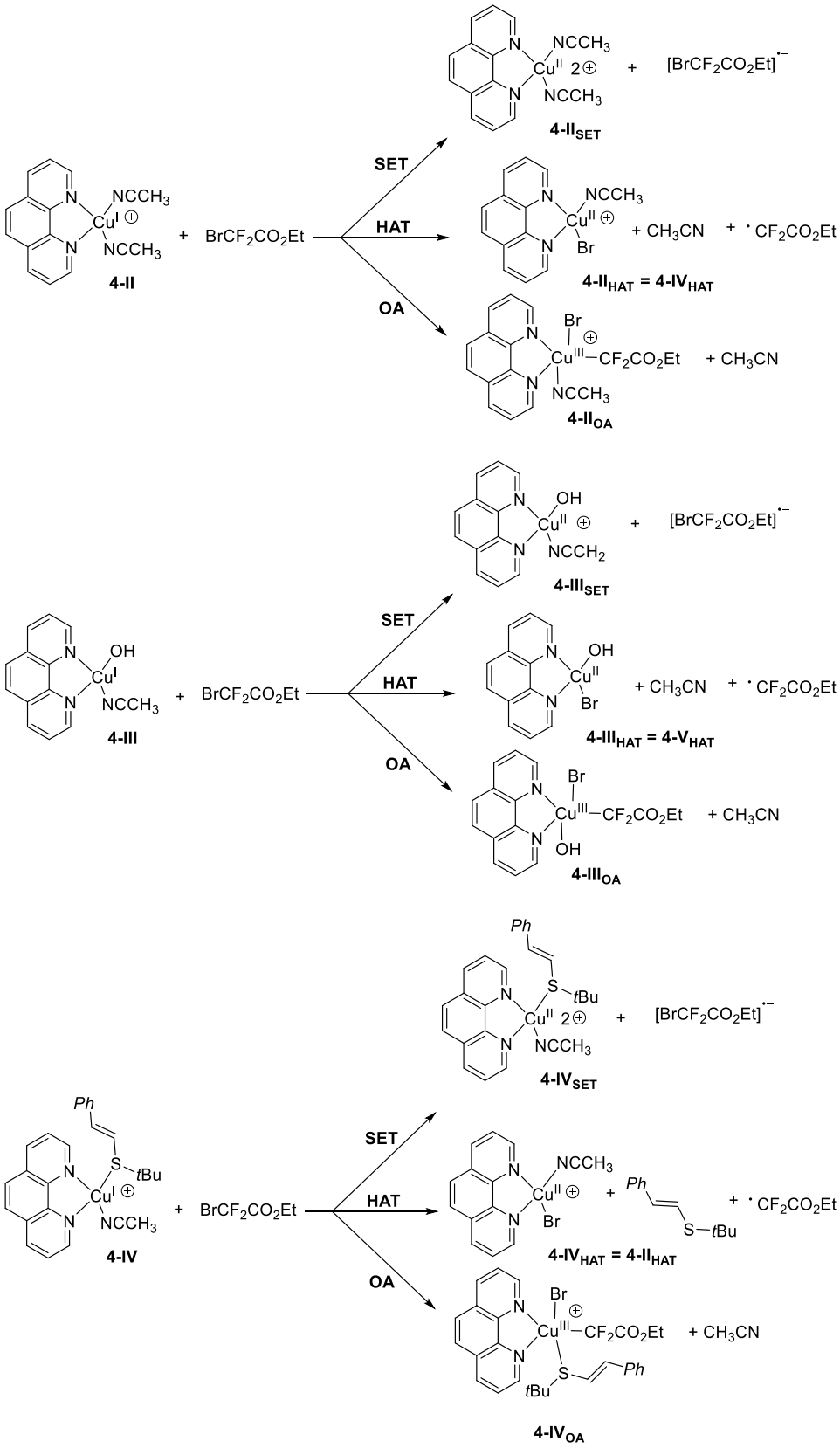
4-II
BrCF2CO2Et
SET
HAT
OA
4-IISET
4-IIHAT = 4-IVHAT
4-IIOA
4-III
4-IIISET
4-IIIHAT = 4-VHAT
4-IIIOA
4-IV
4-IVSET
4-IVHAT = 4-IIHAT
4-IVOA
CH3CN
[BrCF2CO2Et]•−
•CF2CO2Et

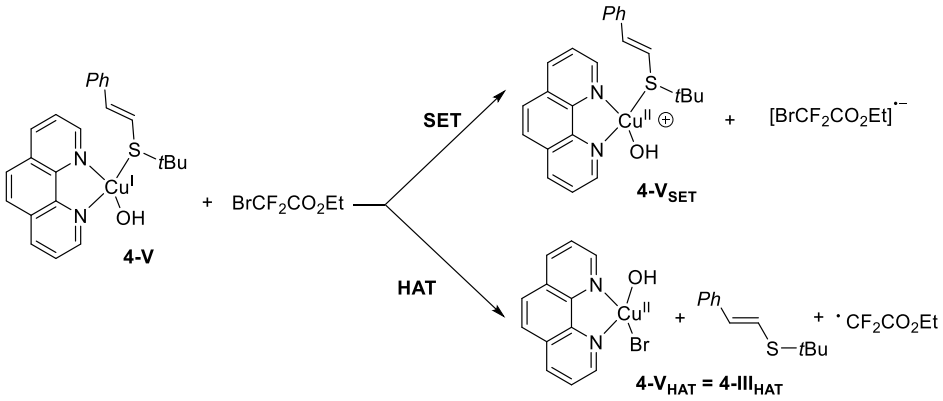

Table A2 - Compared reactivity of different complexes (energies in kcal mol^{-1})

	4-I	**4-II**	**4-III**	**4-IV**	**4-V**
ΔE SET	55.0	39.2	10.7	38.7	16.0
ΔE HAT	-	29.3	5.2	26.9	4.9
ΔE OA	-	30.3	16.1	27.1	-
ΔE_a OA	-	36.6	37.5	36.9	-

Table A3- Compared reactivity of different complexes (free energies in kcal mol^{-1})

	4-I	**4-II**	**4-III**	**4-IV**	**4-V**
ΔG SET	57.1	39.9	10.2	38.1	14.6
ΔG HAT	-	18.6	-5.1	13.5	-8.6
ΔG OA	-	37.9	21.5	34.6	-
ΔG_a OA	-	41.9	40.0	41.7	-

Addition of the CF_2CO_2Et radical on **4-24a**:

Table A4 – Comparison of the addition of the difluoroacetate radical on **4-24a** (energies in kcal.mol^{-1})

	Ea addition	**ΔE addition**
Free substrate –C_1	+7.29	-20.01
Free substrate –C_2	+4.68	-16.76
4-IV-C_2	+ 7.9	-15.48

Table A5 - Comparison of the addition of the difluoroacetate radical on **4-24a** (free energies in kcal.mol^{-1})

	Ga addition	**ΔG addition**
Free substrate –C_1	+20.96	-3.76
Free substrate –C_2	+18.11	-1.45
4-IV-C_2	+21.65	+0.62

Computed reaction energies for non-reactive alkyl halides:

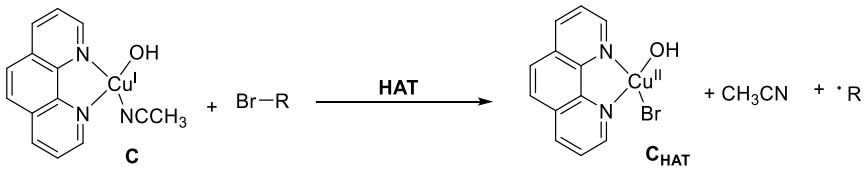

Table A6 - Computed reaction energies for the non-reactive alkyl halides (in kcal.mol^{-1})

Entry	**Substrate**	**ΔE**	**ΔG**
1	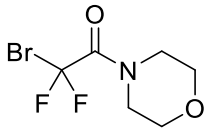	6.1	-3.8
2	$BrCH_2CO_2Et$	8.2	-1.7
3	$BrCF_2PO(OEt)_2$	8.3	-1.5

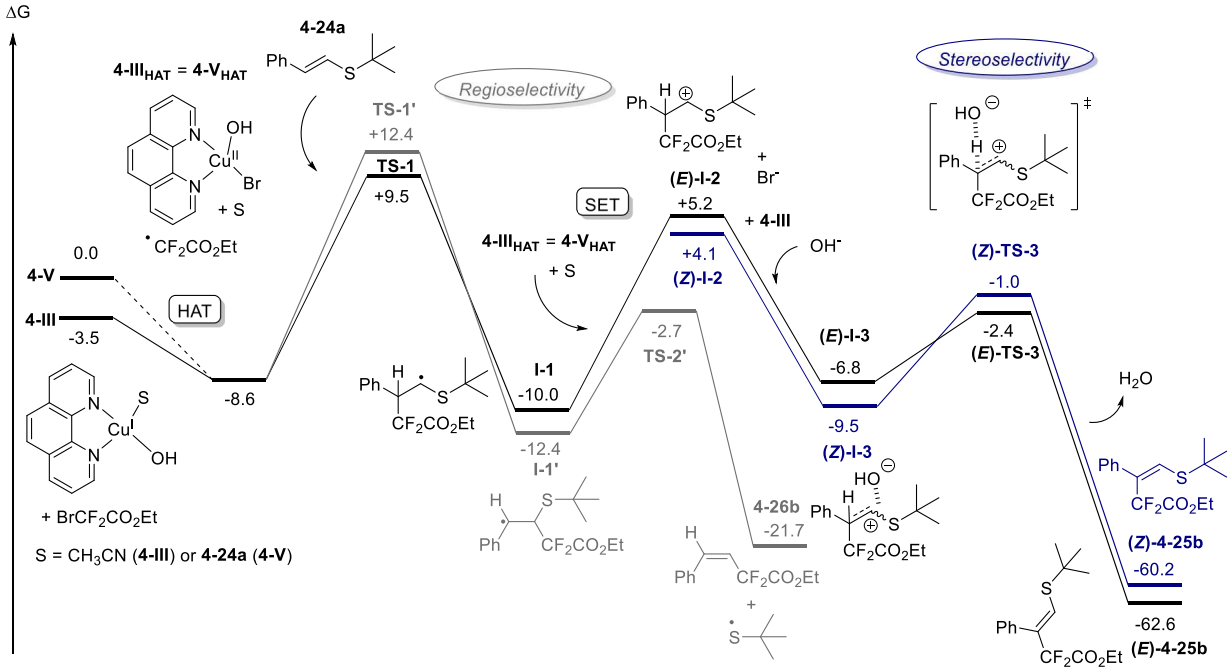

Figure A14 - Computed reaction pathways (free energies in kcal.mol^{-1}). Solid line: initiation with **4-III**. Dashed line: initiation with **4-V**. The last part of the reaction path after regeneration of **4-V** by SET is omitted for clarity. This part is the same as for **4-III**. Grey: path for the formation of the main by-product. Blue: path for the formation of the minor stereoisomer.

General procedure C for the preparation of isotetronic acids

0.7 mmol of **4-25** were dissolved in 3 mL acetonitrile. 3 mL of 1 M aqueous LiOH were added and the biphasic mixture was vigorously shaken at room temperature for 4 h. After completion of the reaction, 1 M HCl was added until pH=1, and the reaction mixture was extracted with EtOAc. The organic layers were gathered and dried over magnesium sulfate and the solvents were evaporated. The residue was then purified by column chromatography (SiO_2, EtOAc in cyclohexane 5 to 20%) to afford the corresponding cyclized products **4-42** and **4-43**.

- 3-fluoro-5-(hexylthio)-4-phenylfuran-2(5*H*)-one (**4-42a**)

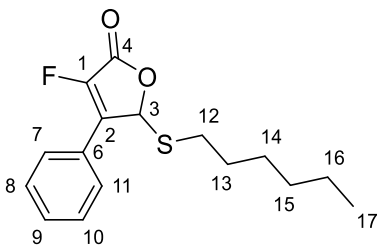

Following the general procedure C, **4-42a** was synthesized on a 0.6 mmol scale in 30 % yield.

^{1}H NMR (300 MHz, $CDCl_3$): δ 7.73-7.70 (m, 2H, H_{ar}), 7.50-7.48 (m, 3H, H_{ar}), 6.36 (d, *J* = 5.2 Hz, 1H, H_3), 2.73 (dt, *J* = 12.3, 7.4 Hz, 1H, H_{12}), 2.62 (dt, *J* = 12.3, 7.5 Hz, 1H, H_{12}), 1.66-1.54 (m, 2H, H_{13}), 1.37-1.13 (m, 6H, H_{14}, H_{15} and H_{16}), 0.92-0.84 (m, 3H, H_{17}). ^{13}C NMR (75 MHz, $CDCl_3$): δ 163.7 (d, *J* = 31.1 Hz, C_4), 143.7 (d, *J* = 281.8 Hz, C_1), 134.8 (d, *J* = 1.2 Hz, C_6), 131.4 (d, *J* = 1.8 Hz, C_{ar}), 129.1 (C_{ar}), 128.5 (d, *J* = 6.2 Hz, C_{ar}), 126.8 (d, *J* = 5.8 Hz, C_2), 81.8 (d, *J* = 7.4 Hz, C_3), 31.3 (C_{12}), 30.2 (C_{13}), 29.3 (C_{14}), 28.5 (C_{15}), 22.5 (C_{16}), 14.1 (C_{17}). ^{19}F NMR (282 MHz): δ -141.8. HRMS (EI, m/z) [M] calcd. for $C_{16}H_{19}FO_2S$: 294.1090, found: 294.1102.

- 3-fluoro-5-((4-fluorophenyl)thio)-4-phenylfuran-2(5*H*)-one (**4-42g**)

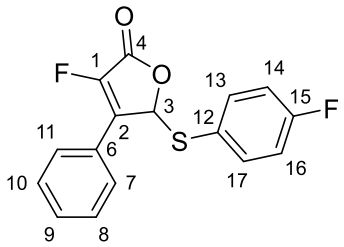

Following the general procedure C, **4-42g** was synthesized on a 0.5 mmol scale in 19 % yield.

^{1}H NMR (300 MHz, $CDCl_3$): δ 7.59-7.56 (m, 2H, H_{ar}), 7.47-7.44 (m, 3H, H_{ar}), 7.23-7.18 (m, 2H, H_{ar}), 6.94-6.88 (m, 2H, H_{ar}), 6.35 (d, *J* = 5.2 Hz, 1H, H_3). ^{13}C NMR (75 MHz, $CDCl_3$): δ 164.1 (d, *J* = 250.0 Hz, C_{15}), 163.2 (d, *J* = 31.3 Hz, C_4), 143.9 (d, *J* = 283.1 Hz, C_1), 138.0 (d, *J* = 8.7 Hz, C_{ar}), 133.9 (C_6), 131.5 (d, *J* = 1.8 Hz, C_{ar}), 129.3 (C_{ar}), 128.54 (d, *J* = 6.1 Hz, C_{ar}), 126.80 (d, *J* = 5.8 Hz, C_2), 122.33 (d, *J* = 3.4 Hz, C_{12}) 116.61 (d, *J* = 22.0 Hz, C_{ar}), 82.76 (dd, *J* = 7.5, 1.5 Hz, C_3). ^{19}F NMR (282 MHz): δ -109.5, -141.8. HRMS (EI, m/z) [M] calcd. for $C_{16}H_{10}F_2O_2S$: 304.0370, found: 304.0359.

- 4-butyl-3-fluoro-5-(phenylthio)furan-2(5*H*)-one (**4-42j**)

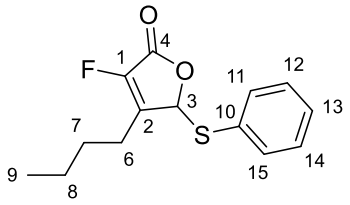

Following the general procedure C, **4.42j** was synthesized on a 0.5 mmol scale in 19 % % yield.

^{1}H NMR (300 MHz, $CDCl_3$): δ 7.53-7.50 (m, 2H, H_{ar}), 7.39-7.33 (m, 3H, H_{ar}), 5.98 (d, *J* = 5.1 Hz, 1H, H_3), 2.63-2.49 (m, 1H, H_6), 2.42-2.29 (m, 1H, H_6), 1.69-1.49 (m, 2H, H_7), 1.45-1.33 (m, 2H, H_8), 0.95 (t, *J* = 7.3 Hz, 3H, H_9). ^{13}C NMR (75 MHz, $CDCl_3$): δ 163.5 (d, *J* = 31.4 Hz, C_4), 145.4 (d, *J* = 275.8 Hz, C_1), 138.8 (d, *J* = 6.5 Hz, C_2), 134.5 (C_{ar}), 129.8 (C_{ar}), 129.5 (C_{ar}), 128.7 (C_{10}), 84.9 (d, *J* = 8.7 Hz, C_3), 28.7 (d, *J* = 2.2 Hz, C_6), 24.8 (d, *J* = 3.2 Hz, C_7), 22.7 (C_8), 13.7 (C_9). ^{19}F NMR (282 MHz): δ -147.4. HRMS (EI, m/z) [M] calcd. for $C_{14}H_{15}FO_2S$: 266.0777, found: 266.0788.

- 5-(hexylthio)-3-hydroxy-4-phenylfuran-2(5*H*)-one (**4-43a**)

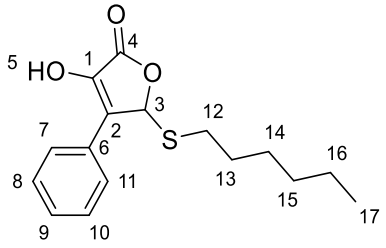

Following the general procedure C, **4-43a** was synthesized on a 0.6 mmol scale in 24 % yield.

^{1}H NMR (300 MHz, $CDCl_3$): δ 7.87-7.83 (m, 2H, H_{ar}), 7.51-7.44 (m, 3H, H_{ar}), 6.48 (s, 1H, H_3), 4.74 (br s, 1H, H_5), 3.19 (dt, *J* = 12.6, 7.5 Hz, 1H, H_{12}), 3.09 (dt, *J* = 12.6, 7.5 Hz, 1H, H_{12}), 1.60-1.50 (m, 2H, H_{13}), 1.37-1.21 (m, 6H, H_{14}, H_{15} and H_{16}), 0.86-0.82 (t, *J* = 6.9 Hz, 3H, H_{17}). ^{13}C NMR (75 MHz, $CDCl_3$): δ 169.5 (C_4), 154.7 (C_1), 130.7 (C_{ar}), 130.3 (C_6), 129.1 (C_{ar}), 128.8 (C_{ar}), 124.5 (C_2), 97.3 (C_3), 31.89 (C_{12}), 31.4 (C_{13}), 30.2 (C_{14}), 28.3 (C_{15}), 22.6 (C_{16}), 14.1 (C_{17}). HRMS (EI, m/z) [M] calcd. for $C_{16}H_{20}O_3S$: 292.1133, found: 292.1143.

- 5-(cyclohexylthio)-3-hydroxy-4-phenylfuran-2(5*H*)-one (**4-43b**)

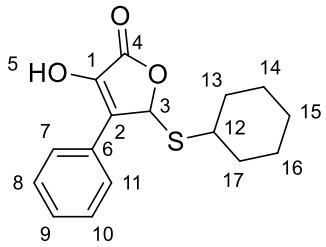

Following the general procedure C, **4-43b** was synthesized on a 0.7 mmol scale in 42 % yield.

^{1}H NMR (300 MHz, $CDCl_3$): δ 7.91-7.88 (m, 2H, H_{ar}), 7.47-7.44 (m, 3H, H_{ar}), 6.50 (s, 1H, H_3), 5.24 (br s, 1H, H_5), 3.89-3.82 (m, 1H, H_{12}), 1.96-1.86 (m, 2H, H_{cy}), 1.68-1.54 (m, 4H, H_{cy}), 1.36-1.24 (m, 4H, H_{cy}). ^{13}C NMR (75 MHz, $CDCl_3$): δ 170.2 (C_4), 156.4 (C_1), 130.7 (C_{ar}), 130.4 (C_6), 129.2 (C_{ar}), 128.7 (C_{ar}), 123.7 (C_2), 97.5 (C_3), 44.3 (C_{12}), 34.2 (C_{cy}), 33.5 (C_{cy}), 25.9 (C_{cy}), 25.8 (C_{cy}), 25.6 (C_{cy}). HRMS (EI, m/z) [M] calcd. for $C_{16}H_{18}O_3S$: 290.0977, found: 290.0981.

- 5-(tert-butylthio)-3-hydroxy-4-phenylfuran-2(5*H*)-one (**4-43c**)

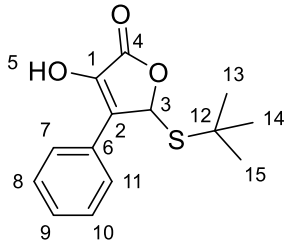

Following the general procedure C, **4-43c** was synthesized on a 0.7 mmol scale in 31 % yield.

^{1}H NMR (300 MHz, MeOD-d_4): δ 7.82-7.78 (m, 2H, H_{ar}), 7.45-7.34 (m, 3H, H_{ar}), 6.75 (s, 1H, H_3), 1.53 (s, 9H, H_{13}, H_{14} and H_{15}). H_5 not visible in MeOD-d_4. ^{13}C NMR (75 MHz, MeOD-d_4): δ 170.3 (C_4), 140.5 (C_1), 131.6 (C_6), 129.6 (C_{ar}), 129.2 (C_{ar}), 129.1 (C_{ar}), 127.7 (C_2), 83.5 (C_3), 45.9 (C_{12}), 31.9 ($C_{t13,}$ C_{14} and C_{15}). HRMS (EI, m/z) [M] calcd. for $C_{14}H_{16}O_3S$: 264.0820, found: 264.0824.

- 4-butyl-3-hydroxy-5-(phenylthio)furan-2(5*H*)-one (**4-43j**)

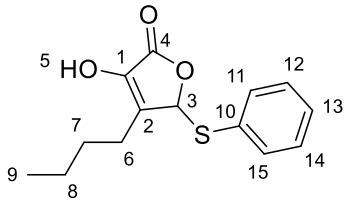

Following the general procedure C, **4-43j** was synthesized on a 0.5 mmol scale in 26 % yield.

^{1}H NMR (300 MHz, $CDCl_3$): δ 7.27-715 (m, 5H, H_{ar}), 5.98 (s, 1H, H_3), 5.20 (br s, 1H, H_5), 2.57-2.33 (m, 2H, H_6), 1.50-1.36 (m, 2H, H_7), 1.28-1.08 (m, 2H, H_8), 0.82 (t, *J* = 7.2 Hz, 3H, H_9). ^{13}C NMR (75 MHz, $CDCl_3$): δ 169.9 (C_4), 169.5 (C_1), 132.2 (C_{10}), 130.3 (C_{ar}), 129.3 (C_{ar}), 127.6 (C_{ar}), 124.2 (C_2), 98.0 (C_3), 29.4 (C_6), 27.3 (C_7), 22.9 (C_8), 13.8 (C_9). HRMS (EI, m/z) [M] calcd. for $C_{14}H_{16}O_3S$: 264.0820, found: 264.0822.

References

1 T. R. Hoye, B. M. Eklov, T. D. Ryba, M. Voloshin and L. J. Yao, *Org. Lett.*, 2004, **6**, 953–956.

2 A. Jutand, *Chem. Rev.*, 2008, **108**, 2300–2347.

3 S. Mahouche-Chergui, S. Gam-Derouich, C. Mangeney and M. M. Chehimi, *Chem. Soc. Rev.*, 2011, **40**, 4143.

4 D. Bélanger and J. Pinson, *Chem. Soc. Rev.*, 2011, **40**, 3995.

5 P. Renaud and M. P. Sibi, *Radicals in Organic Synthesis*, pages 317-336, Wiley-VCH., 2001, vol. 1 & 2.

6 R. Cai, M. Lu, E. Y. Aguilera, Y. Xi, N. G. Akhmedov, J. L. Petersen, H. Chen and X. Shi, *Angew. Chem. Int. Ed.*, 2015, **54**, 8772–8776.

7 W. Koch and M. C. Holthausen, *A Chemist's Guide to Density Functional Theory (2nd Edition)*, Wiley-VCH, Weinheim, 2001.

8 C. J. Cramer, *Essentials of Computational Chemistry - Theories and Models (2nd Edition)*, John Wiley & Sons, Ltd, Chichester, 2004.

9 F. Jensen, *Introduction to Computational Chemistry (2nd Edition)*, John Wiley & Sons, Ltd, Chichester, 2007.

10 E. Schrödinger, *Phys. Rev.*, 1926, **28**, 1049–1070.

11 E. Fermi, *Rend Accad Naz Lincei*, 1927, **6**, 602–607.

12 L. H. Thomas, *Math. Proc. Camb. Philos. Soc.*, 1927, **23**, 542–548.

13 P. Hohenberg and W. Kohn, *Phys. Rev. B*, 1964, **136**, 864–871.

14 A. D. Becke, *Phys. Rev. A*, 1988, **38**, 3098–3100.

15 C. Lee, W. Yang and R. G. Parr, *Phys. Rev. B*, 1988, **37**, 785–789.

16 C. Adamo and V. Barone, *J. Chem. Phys.*, 1999, **110**, 6158–6170.

17 A. D. Becke, *J. Chem. Phys.*, 1993, **98**, 5648–5652.

18 T. Yanai, D. P. Tew and N. C. Handy, *Chem. Phys. Lett.*, 2004, **393**, 51–57.

19 C. Adamo and V. Barone, *J. Chem. Phys.*, 1998, **108**, 664–675.

20 Y. Zhao and D. G. Truhlar, *Theor. Chem. Acc.*, 2008, **120**, 215–241.

21 M. J. Frisch, G. W. Trucks, H. B. Schlegel, G. E. Scuseria, M. A. Robb, J. R. Cheeseman, G. Scalmani, V. Barone, G. A. Petersson, H. Nakatsuji, X. Li, M. Caricato, A. Marenich, J. Bloino, B. G. Janesko, R. Gomperts, B. Mennucci, H. P. Hratchian, J. V. Ortiz, A. F. Izmaylov, J. L. Sonnenberg, D. Williams-Young, F. Ding, F. Lipparini, F. Egidi, J. Goings, B. Peng, A. Petrone, T. Henderson, D. Ranasinghe, V. G. Zakrzewski, J. Gao, N. Rega, G. Zheng, W. Liang, M. Hada, M. Ehara, K. Toyota, R. Fukuda, J. Hasegawa, M. Ishida, T. Nakajima, Y. Honda, O. Kitao, H. Nakai, T. Vreven, K. Throssell, J. A. Montgomery, J. E. Peralta, F. Ogliaro, M. Bearpark, J. J. Heyd, E. Brothers, K. N. Kudin, V. N. Staroverov, T. Keith, R. Kobayashi, J. Normand, K. Raghavachari, A. Rendell, J. C. Burant, S. S. Iyengar, J. Tomasi, M. Cossi, J. M. Millam, M. Klene, C. Adamo, R. Cammi, J. W. Ochterski, R. L. Martin, K. Morokuma, O. Farkas, J. B. Foresman and D. J. Fox, *Gaussian 09, Revision A.02*, Gaussian, Inc., Wallingford CT, 2016.

22 R. Krishnan, J. S. Binkley, R. Seeger and J. A. Pople, *J. Chem. Phys.*, 1980, **72**, 650–654.

23 A. D. McLean and G. S. Chandler, *J. Chem. Phys.*, 1980, **72**, 5639–5648.

24 P. J. Hay and W. R. Wadt, *J. Chem. Phys.*, 1985, **82**, 270–283.

25 W. R. Wadt and P. J. Hay, *J. Chem. Phys.*, 1985, **82**, 284–298.

26 P. J. Hay and W. R. Wadt, *J. Chem. Phys.*, 1985, **82**, 299–310.

27 S. F. Boys and F. Bernardi, *Mol. Phys.*, 1970, **19**, 553–566.

28 B. Liu and A. D. McLean, *J. Chem. Phys.*, 1980, **72**, 3418–3419.
29 B. Liu and A. D. McLean, *J. Chem. Phys.*, 1989, **91**, 2348–2359.
30 J. Tomasi, B. Mennucci and R. Cammi, *Chem. Rev.*, 2005, **105**, 2999–3093.
31 K. Fukui, *Acc. Chem. Res.*, 1981, **14**, 363–368.
32 H. P. Hratchian and H. B. Schlegel, *Theory and Applications of Computational Chemistry: The First 40 Years*, Elsevier: Amsterdam, Amsterdam, Ed. C. E. Dykstra, G. Frenking, K. S. Kim, and G. Scuseria., 2005.
33 A. A. C. Braga, G. Ujaque and F. Maseras, *Organometallics*, 2006, **25**, 3647–3658.
34 S. Sakaki, T. Takayama, M. Sumimoto and M. Sugimoto, *J. Am. Chem. Soc.*, 2004, **126**, 3332–3348.
35 M. Sumimoto, N. Iwane, T. Takahama and S. Sakaki, *J. Am. Chem. Soc.*, 2004, **126**, 10457–10471.
36 F. Bellina and R. Rossi, *Chem. Rev.*, 2010, **110**, 1082–1146.
37 C. C. C. Johansson and T. J. Colacot, *Angew. Chem. Int. Ed.*, 2010, **49**, 676–707.
38 M. Palucki and S. L. Buchwald, *J. Am. Chem. Soc.*, 1997, **119**, 11108–11109.
39 B. C. Hamann and J. F. Hartwig, *J. Am. Chem. Soc.*, 1997, **119**, 12382–12383.
40 T. Satoh, Y. Kawamura, M. Miura and M. Nomura, *Angew. Chem. Int. Ed. Engl.*, 1997, **36**, 1740–1742.
41 G. A. Grasa and T. J. Colacot, *Org. Lett.*, 2007, **9**, 5489–5492.
42 C. Cao, L. Wang, Z. Cai, L. Zhang, J. Guo, G. Pang and Y. Shi, *Eur. J. Org. Chem.*, 2011, 1570–1574.
43 K. Matsubara, K. Ueno, Y. Koga and K. Hara, *J. Org. Chem.*, 2007, **72**, 5069–5076.
44 M. Henrion, M. J. Chetcuti and V. Ritleng, *Chem. Commun.*, 2014, **50**, 4624–4627.
45 R. Takise, K. Muto, J. Yamaguchi and K. Itami, *Angew. Chem. Int. Ed.*, 2014, **53**, 6791–6794.
46 S. M. Crawford, P. G. Alsabeh and M. Stradiotto, *Eur. J. Org. Chem.*, 2012, **2012**, 6042–6050.
47 P. Li, B. Lü, C. Fu and S. Ma, *Adv. Synth. Catal.*, 2013, **355**, 1255–1259.
48 K. D. Hesp, R. J. Lundgren and M. Stradiotto, *J. Am. Chem. Soc.*, 2011, **133**, 5194–5197.
49 L. Ackermann and V. P. Mehta, *Chem. – Eur. J.*, 2012, **18**, 10230–10233.
50 P. G. Alsabeh and M. Stradiotto, *Angew. Chem. Int. Ed.*, 2013, **52**, 7242–7246.
51 G. Danoun, A. Tlili, F. Monnier and M. Taillefer, *Angew. Chem. Int. Ed.*, 2012, **51**, 12815–12819.
52 FR 2012-055275, PCT/EP 2013-061697, .
53 R. A. Rossi, A. B. Pierini and A. B. Peñéñory, *Chem. Rev.*, 2003, **103**, 71–168.
54 R. A. Rossi and J. F. Bunnett, *J. Am. Chem. Soc.*, 1972, **94**, 683–684.
55 J. K. Kim and J. F. Bunnett, *J. Am. Chem. Soc.*, 1970, **92**, 7463–7464.
56 J.-M. Savéant, *Acc. Chem. Res.*, 1980, **13**, 323–329.
57 C. Amatore, J. Pinson, J.-M. Savéant and A. Thiébault, *J. Am. Chem. Soc.*, 1981, **103**, 6930–6937.
58 C. Amatore, J. Pinson, J.-M. Savéant and A. Thiébault, *J. Am. Chem. Soc.*, 1982, **104**, 817–826.
59 C. Amatore, M. A. Oturan, J. Pinson, J.-M. Savéant and A. Thiébault, *J. Am. Chem. Soc.*, 1984, **106**, 6318–6321.
60 C. Amatore, M. A. Oturan, J. Pinson, J.-M. Savéant and A. Thiébault, *J. Am. Chem. Soc.*, 1985, **107**, 3451–3459.
61 R. A. Rossi and J. F. Bunnett, *J. Org. Chem.*, 1973, **38**, 3020–3025.
62 R. A. Rossi, R. H. de Rossi and A. F. Lopez, *J. Am. Chem. Soc.*, 1976, **98**, 1252–1257.

63 E. Austin, C. G. Ferrayoli, R. A. Alonso and R. A. Rossi, *Tetrahedron*, 1993, **49**, 4495–4502.
64 J. F. Bunnett and J. E. Sundberg, *J. Org. Chem.*, 1976, **41**, 1702–1706.
65 M. T. Baumgartner, M. H. Gallego and A. B. Pierini, *J. Org. Chem.*, 1998, **63**, 6394–6397.
66 M. T. Baumgartner, L. B. Jiménez, A. B. Pierini and R. A. Rossi, *J. Chem. Soc. Perkin Trans. 2*, 2002, 1092–1097.
67 J. F. Guastavino and R. A. Rossi, *J. Org. Chem.*, 2012, **77**, 460–472.
68 D. R. Carver, A. P. Komin, J. S. Hubbard and J. F. Wolfe, *J. Org. Chem.*, 1981, **46**, 294–299.
69 S. M. Soria-Castro, D. A. Caminos and A. B. Peñéñory, *RSC Adv.*, 2014, **4**, 17490–17497.
70 D. A. Caminos, A. D. Garro, S. M. Soria-Castro and A. B. Peñéñory, *RSC Adv*, 2015, **5**, 20058–20065.
71 J. F. Bunnett, R. G. Scamehorn and R. P. Traber, *J. Org. Chem.*, 1976, **41**, 3677–3682.
72 M. P. Moon and J. F. Wolfe, *J. Org. Chem.*, 1979, **44**, 4081–4085.
73 I. Thomé, A. Nijs and C. Bolm, *Chem. Soc. Rev.*, 2012, **41**, 979–987.
74 S. Yanagisawa, K. Ueda, T. Taniguchi and K. Itami, *Org. Lett.*, 2008, **10**, 4673–4676.
75 C.-L. Sun, H. Li, D.-G. Yu, M. Yu, X. Zhou, X.-Y. Lu, K. Huang, S.-F. Zheng, B.-J. Li and Z.-J. Shi, *Nat. Chem.*, 2010, **2**, 1044–1049.
76 M. Rueping, M. Leiendecker, A. Das, T. Poisson and L. Bui, *Chem. Commun.*, 2011, **47**, 10629–10631.
77 C.-L. Sun, Y.-F. Gu, B. Wang and Z.-J. Shi, *Chem. - Eur. J.*, 2011, **17**, 10844–10847.
78 W. Liu, H. Cao, H. Zhang, H. Zhang, K. H. Chung, C. He, H. Wang, F. Y. Kwong and A. Lei, *J. Am. Chem. Soc.*, 2010, **132**, 16737–16740.
79 E. Shirakawa, X. Zhang and T. Hayashi, *Angew. Chem. Int. Ed.*, 2011, **50**, 4671–4674.
80 W. Liu, F. Tian, X. Wang, H. Yu and Y. Bi, *Chem. Commun.*, 2013, **49**, 2983–2985.
81 Y. Wu, S. M. Wong, F. Mao, T. L. Chan and F. Y. Kwong, *Org. Lett.*, 2012, **14**, 5306–5309.
82 Y. Qiu, Y. Liu, K. Yang, W. Hong, Z. Li, Z. Wang, Z. Yao and S. Jiang, *Org. Lett.*, 2011, **13**, 3556–3559.
83 K. Tanimoro, M. Ueno, K. Takeda, M. Kirihata and S. Tanimori, *J. Org. Chem.*, 2012, **77**, 7844–7849.
84 A. Dewanji, S. Murarka, D. P. Curran and A. Studer, *Org. Lett.*, 2013, **15**, 6102–6105.
85 Q. Song, D. Zhang, Q. Zhu and Y. Xu, *Org. Lett.*, 2014, **16**, 5272–5274.
86 W.-C. Chen, Y.-C. Hsu, W.-C. Shih, C.-Y. Lee, W.-H. Chuang, Y.-F. Tsai, P. P.-Y. Chen and T.-G. Ong, *Chem. Commun.*, 2012, **48**, 6702–6704.
87 D. Sustac Roman, Y. Takahashi and A. B. Charette, *Org. Lett.*, 2011, **13**, 3242–3245.
88 Y. Chen, X. Zhang, H. Yuan, W. Wei and M. Yan, *Chem. Commun.*, 2013, **49**, 10974–10976.
89 W. Wei, X. Dong, S. Nie, Y. Chen, X. Zhang and M. Yan, *Org. Lett.*, 2013, **15**, 6018–6021.
90 W. Wang, X. Zhao, L. Tong, J. Chen, X. Zhang and M. Yan, *J. Org. Chem.*, 2014, **79**, 8557–8565.
91 A. Studer and D. P. Curran, *Nat. Chem.*, 2014, **6**, 765–773.
92 S. Zhou, E. Doni, G. M. Anderson, R. G. Kane, S. W. MacDougall, V. M. Ironmonger, T. Tuttle and J. A. Murphy, *J. Am. Chem. Soc.*, 2014, **136**, 17818–17826.
93 L. Zhang, H. Yang and L. Jiao, *J. Am. Chem. Soc.*, 2016, **138**, 7151–7160.
94 J. Cuthbertson, V. J. Gray and J. D. Wilden, *Chem. Commun.*, 2014, **50**, 2575–2578.

95 H. Yi, A. Jutand and A. Lei, *Chem Commun*, 2015, **51**, 545–548.
96 S. Zhou, G. M. Anderson, B. Mondal, E. Doni, V. Ironmonger, M. Kranz, T. Tuttle and J. A. Murphy, *Chem. Sci.*, 2014, **5**, 476–482.
97 J. Muzart, *Tetrahedron*, 2009, **65**, 8313–8323.
98 C. L. Øpstad, T.-B. Melø, H.-R. Sliwka and V. Partali, *Tetrahedron*, 2009, **65**, 7616–7619.
99 G. B. Bajracharya and O. Daugulis, *Org. Lett.*, 2008, **10**, 4625–4628.
100 G. Cavallo, P. Metrangolo, R. Milani, T. Pilati, A. Priimagi, G. Resnati and G. Terraneo, *Chem. Rev.*, 2016, **116**, 2478–2601.
101 U. Schöllkopf and F. Gerhart, *Angew. Chem. Int. Ed. Engl.*, 1967, **6**, 805.
102 B. Bánhidai and U. Schöllkopf, *Angew. Chem. Int. Ed. Engl.*, 1973, **12**, 836–837.
103 K. Smith and K. Swaminathan, *J. Chem. Soc. Chem. Commun.*, 1976, **11**, 387–388.
104 J. T. Reeves, Z. Tan, M. A. Herbage, Z. S. Han, M. A. Marsini, Z. Li, G. Li, Y. Xu, K. R. Fandrick, N. C. Gonnella, S. Campbell, S. Ma, N. Grinberg, H. Lee, B. Z. Lu and C. H. Senanayake, *J. Am. Chem. Soc.*, 2013, **135**, 5565–5568.
105 R. J. Enemærke, T. B. Christensen, H. Jensen and K. Daasbjerg, *J. Chem. Soc. Perkin Trans. 2*, 2001, 1620–1630.
106 M. Pichette Drapeau, I. Fabre, L. Grimaud, I. Ciofini, T. Ollevier and M. Taillefer, *Angew. Chem. Int. Ed.*, 2015, **54**, 10587–10591.
107 J. P. Barham, G. Coulthard, K. J. Emery, E. Doni, F. Cumine, G. Nocera, M. P. John, L. E. A. Berlouis, T. McGuire, T. Tuttle and J. A. Murphy, *J. Am. Chem. Soc.*, 2016, **138**, 7402–7410.
108 N. S. Nudelman and G. E. García Liñares, *J. Org. Chem.*, 2000, **65**, 1629–1635.
109 D. Toummini, A. Tlili, J. Bergès, F. Ouazzani and M. Taillefer, *Chem. - Eur. J.*, 2014, **20**, 14619–14623.
110 J. F. Bunnett and R. E. Zahler, *Chem. Rev.*, 1951, **49**, 273–412.
111 H. Heaney, *Chem. Rev.*, 1962, **62**, 81–97.
112 S. Patai, *The chemistry of diazonium and diazo groups*, John Wiley & Sons, Ltd, Chichester, 1978, vol. 1.
113 G. Balz and G. Schiemann, *Berichte Dtsch. Chem. Ges. B Ser.*, 1927, **60**, 1186–1190.
114 M. Gomberg and W. E. Bachmann, *J. Am. Chem. Soc.*, 1924, **46**, 2339–2343.
115 H. T. Clarke and W. R. Kirner, *Org. Synth.*, 1922, **2**, 47–49.
116 J. L. Hartwell and L. F. Fieser, *Org. Synth.*, 1936, **16**, 12–15.
117 H. Zollinger, *Color Chemistry : Syntheses, Properties and Applications of Organic Dyes and Pigments*, Wiley-VCH, Weinheim, 3rd revised edition., 2003.
118 W. W. Hartman and J. B. Dickey, *Org. Synth.*, 1934, **14**, 24–25.
119 R. Huisgen and R. Lux, *Chem. Ber.*, 1960, **93**, 540–544.
120 J. E. Packer, C. J. Heighway, H. M. Miller and B. C. Dobson, *Aust. J. Chem.*, 1980, **33**, 965–977.
121 C. Galli, *Chem. Rev.*, 1988, **88**, 765–792.
122 F. W. Wassmundt and W. F. Kiesman, *J. Org. Chem.*, 1997, **62**, 8304–8308.
123 P. S. J. Canning, K. McCrudden, H. Maskill and B. Sexton, *Chem. Commun.*, 1998, 1971–1972.
124 P. S. J. Canning, K. McCrudden, H. Maskill and B. Sexton, *J. Chem. Soc. Perkin Trans. 2*, 1999, 2735–2740.
125 D. F. DeTar and M. N. Turetzky, *J. Am. Chem. Soc.*, 1955, **77**, 1745–1750.
126 D. F. DeTar and M. N. Turetzky, *J. Am. Chem. Soc.*, 1956, **78**, 3925–3928.
127 J. F. Bunnett and H. Takayama, *J. Org. Chem.*, 1968, **33**, 1924–1928.
128 T. J. Broxton and D. L. Roper, *J. Org. Chem.*, 1976, **41**, 2157–2162.

129 D. F. DeTar and T. Kosuge, *J. Am. Chem. Soc.*, 1958, **80**, 6072–6077.
130 J. F. Bunnett and C. Yijima, *J. Org. Chem.*, 1977, **42**, 639–643.
131 T. J. Broxton, J. F. Bunnett and C. H. Paik, *J. Org. Chem.*, 1977, **42**, 643–649.
132 C. Bravo-Díaz, L. S. Romsted, M. Harbowy, M. E. Romero-Nieto and E. Gonzalez-Romero, *J. Phys. Org. Chem.*, 1999, **12**, 130–140.
133 R. Pazo-Llorente, E. Gonzalez-Romero and C. Bravo-Diaz, *Int. J. Chem. Kinet.*, 2000, **32**, 210–220.
134 U. Costas-Costas, E. Gonzalez-Romero and C. Bravo-Diaz, *Helv. Chim. Acta*, 2001, **84**, 632–648.
135 R. Pazo-Llorente, H. Maskill, C. Bravo-Diaz and E. Gonzalez-Romero, *Eur. J. Org. Chem.*, 2006, 2201–2209.
136 F. Mo, G. Dong, Y. Zhang and J. Wang, *Org. Biomol. Chem.*, 2013, **11**, 1582–1593.
137 X.-F. Wu, H. Neumann and M. Beller, *Angew. Chem. Int. Ed.*, 2011, **50**, 11142–11146.
138 A. Roglans, A. Pla-Quintana and M. Moreno-Mañas, *Chem. Rev.*, 2006, **106**, 4622–4643.
139 H.-U. Blaser, A. Indolese, F. Naud, U. Nettekoven and A. Schnyder, *Adv. Synth. Catal.*, 2004, **346**, 1583–1598.
140 K. Shin, S.-W. Park and S. Chang, *J. Am. Chem. Soc.*, 2015, **137**, 8584–8592.
141 B. Schmidt and R. Berger, *Adv. Synth. Catal.*, 2013, **355**, 463–476.
142 S. Bhattacharya, S. Majee, R. Mukherjee and S. Sengupta, *Synth. Commun.*, 1995, **25**, 651–657.
143 N. H. Park, T. J. Senter and S. L. Buchwald, *Angew. Chem. Int. Ed.*, 2016, **55**, 11907–11911.
144 N. Oger, M. d'Halluin, E. Le Grognec and F.-X. Felpin, *Org. Process Res. Dev.*, 2014, **18**, 1786–1801.
145 F. Le Callonnec, E. Fouquet and F.-X. Felpin, *Org. Lett.*, 2011, **13**, 2646–2649.
146 N. Susperregui, K. Miqueu, J.-M. Sotiropoulos, F. Le Callonnec, E. Fouquet and F.-X. Felpin, *Chem. - Eur. J.*, 2012, **18**, 7210–7218.
147 N. Oger, F. Le Callonnec, D. Jacquemin, E. Fouquet, E. Le Grognec and F.-X. Felpin, *Adv. Synth. Catal.*, 2014, **356**, 1065–1071.
148 T. Sandmeyer, *Berichte Dtsch. Chem. Ges.*, 1884, **17**, 1633–1635.
149 H. Meerwein, E. Büchner and K. van Emster, *J. Für Prakt. Chem.*, 1939, **152**, 237–266.
150 T. Sandmeyer, *Berichte Dtsch. Chem. Ges.*, 1884, **17**, 2650–2653.
151 W. A. Cowdrey and D. S. Davies, *J. Chem. Soc. Resumed*, 1949, S48–S59.
152 J. K. Kochi, *J. Am. Chem. Soc.*, 1957, **79**, 2942–2948.
153 C. Galli, *J. Chem. Soc. Perkin Trans. 2*, 1981, 1459–1461.
154 I. P. Beletskaya, A. S. Sigeev, A. S. Peregudov and P. V. Petrovskii, *Synthesis*, 2007, 2534–2538.
155 I. P. Beletskaya, A. S. Sigeev, A. S. Peregudov and P. V. Petrovskii, *J. Organomet. Chem.*, 2004, **689**, 3810–3812.
156 I. P. Beletskaya, A. S. Sigeev, A. S. Peregudov and P. V. Petrovskii, *Mendeleev Commun.*, 2006, **16**, 250–251.
157 G. Danoun, B. Bayarmagnai, M. F. Grünberg and L. J. Gooßen, *Angew. Chem. Int. Ed.*, 2013, **52**, 7972–7975.
158 G. Danoun, B. Bayarmagnai, M. F. Gruenberg and L. J. Goossen, *Chem. Sci.*, 2014, **5**, 1312–1316.

159 A. Honraedt, F. Le Callonnec, E. Le Grognec, V. Fernandez and F.-X. Felpin, *J. Org. Chem.*, 2013, **78**, 4604–4609.
160 A. Honraedt, M.-A. Raux, E. Le Grognec, D. Jacquemin and F.-X. Felpin, *Chem Commun*, 2014, **50**, 5236–5238.
161 F. Ullmann, *Berichte Dtsch. Chem. Ges.*, 1903, **36**, 2382–2384.
162 I. Goldberg, *Berichte Dtsch. Chem. Ges.*, 1906, **39**, 1691–1692.
163 I. Goldberg, *Berichte Dtsch. Chem. Ges.*, 1907, **40**, 4541–4546.
164 F. Ullmann and E. Illgen, *Berichte Dtsch. Chem. Ges.*, 1914, **47**, 380–383.
165 J.-P. Corbet and G. Mignani, *Chem. Rev.*, 2006, **106**, 2651–2710.
166 G. Evano, N. Blanchard and M. Toumi, *Chem. Rev.*, 2008, **108**, 3054–3131.
167 F. Monnier and M. Taillefer, *Angew. Chem. Int. Ed.*, 2009, **48**, 6954–6971.
168 E. Sperotto, G. P. M. van Klink, G. van Koten and J. G. de Vries, *Dalton Trans.*, 2010, **39**, 10338–10351.
169 I. P. Beletskaya and A. V. Cheprakov, *Organometallics*, 2012, **31**, 7753–7808.
170 A. C. Tsipis, *Coord. Chem. Rev.*, 2014, **272**, 1–29.
171 D. Lupp, N. J. Christensen and P. Fristrup, *Dalton Trans.*, 2014, **43**, 11093–11105.
172 T. Sperger, I. A. Sanhueza, I. Kalvet and F. Schoenebeck, *Chem. Rev.*, 2015, **115**, 9532–9586.
173 S.-L. Zhang, L. Liu, Y. Fu and Q.-X. Guo, *Organometallics*, 2007, **26**, 4546–4554.
174 H. Guo and Y. Xue, *J. Theor. Comput. Chem.*, 2012, **11**, 1135–1147.
175 G. O. Jones, P. Liu, K. N. Houk and S. L. Buchwald, *J. Am. Chem. Soc.*, 2010, **132**, 6205–6213.
176 H.-Z. Yu, Y.-Y. Jiang, Y. Fu and L. Liu, *J. Am. Chem. Soc.*, 2010, **132**, 18078–18091.
177 L. Goerigk and S. Grimme, *Phys. Chem. Chem. Phys.*, 2011, **13**, 6670–6688.
178 D. Jacquemin, V. Wathelet, E. A. Perpète and C. Adamo, *J. Chem. Theory Comput.*, 2009, **5**, 2420–2435.
179 M. R. A. Blomberg, U. Brandemark and P. E. M. Siegbahn, *J. Am. Chem. Soc.*, 1983, **105**, 5557–5563.
180 M. R. A. Blomberg, P. E. M. Siegbahn, U. Nagashima and J. Wennerberg, *J. Am. Chem. Soc.*, 1991, **113**, 424–433.
181 P. E. M. Siegbahn, M. R. A. Blomberg and M. Svensson, *J. Phys. Chem.*, 1993, **97**, 2564–2570.
182 G. T. De Jong, D. P. Geerke, A. Diefenbach, M. Solà and F. M. Bickelhaupt, *J. Comput. Chem.*, 2005, **26**, 1006–1020.
183 G. T. de Jong and F. M. Bickelhaupt, *J. Phys. Chem. A*, 2005, **109**, 9685–9699.
184 G. T. de Jong and F. M. Bickelhaupt, *J. Chem. Theory Comput.*, 2006, **2**, 322–335.
185 W. Lai, J. Yao, S. Shaik and H. Chen, *J. Chem. Theory Comput.*, 2012, **8**, 2991–2996.
186 M. Steinmetz and S. Grimme, *ChemistryOpen*, 2013, **2**, 115–124.
187 M. K. Kesharwani and J. M. L. Martin, *Theor. Chem. Acc.*, 2014, **133**, 1452–1465.
188 X. Sun, X. Sun, C. Geng, H. Zhao and J. Li, *J. Phys. Chem. A*, 2014, **118**, 7146–7158.
189 Griess P., *Liebigs Ann. Chem.*, 1858, **106**, 123–125.
190 M. P. Doyle, W. Wierenga and M. A. Zaleta, *J. Org. Chem.*, 1972, **37**, 1597–1601.
191 M. P. Doyle and W. J. Bryker, *J. Org. Chem.*, 1979, **44**, 1572–1574.
192 S. Dahmen and S. Bräse, *Angew. Chem. Int. Ed.*, 2000, **39**, 3681–3683.
193 D. B. Kimball and M. M. Haley, *Angew. Chem. Int. Ed.*, 2002, **41**, 3338–3351.
194 S. Bräse, *Acc. Chem. Res.*, 2004, **37**, 805–816.
195 F. P. Dwyer, *J. Am. Chem. Soc.*, 1941, **63**, 78–81.
196 J. Wu, Y. Gu, X. Leng and Q. Shen, *Angew. Chem.*, 2015, **127**, 7758–7762.
197 L. He, G. Qiu, Y. Gao and J. Wu, *Org. Biomol. Chem.*, 2014, **12**, 6965–6971.

198 Y. Li, J. Pu and X. Jiang, *Org. Lett.*, 2014, **16**, 2692–2695.
199 X. Wang, Y. Xu, F. Mo, G. Ji, D. Qiu, J. Feng, Y. Ye, S. Zhang, Y. Zhang and J. Wang, *J. Am. Chem. Soc.*, 2013, **135**, 10330–10333.
200 J. Goslar, P. B. Sczaniecki, M. M. Strawiak and J. Mroziński, *Transit. Met. Chem.*, 1988, **13**, 81–86.
201 T. Chavez-Gil, J. Lugo, D. L. Cedeño and C. G. Hamaker, *J. Chem. Crystallogr.*, 2015, **45**, 189–192.
202 S.-W. Jin, X.-H. Ye, L. Jin, L. Zheng, J.-W. Li, B.-P. Jin and D.-Q. Wang, *Polyhedron*, 2014, **81**, 382–395.
203 D. H. Busch, *Inorganic Syntheses*, Chichester, John Wiley & Sons, Ltd., 2009, vol. 20.
204 E. P. Koval'chuk, O. V. Reshetnyak, V. Y. Smetanets'kyj and J. Błażejowski, *Chem. Met. Alloys*, 2009, **2**, 123–139.
205 S. Grimme, J. Antony, S. Ehrlich and H. Krieg, *J. Chem. Phys.*, 2010, **132**, 154104–154122.
206 Y. Sun and H. Chen, *J. Chem. Theory Comput.*, 2013, **9**, 4735–4743.
207 D. Asturiol, M. Duran and P. Salvador, *J. Chem. Phys.*, 2008, **128**, 144108–144112.
208 H. Valdés, V. Klusák, M. Pitoňák, O. Exner, I. Starý, P. Hobza and L. Rulíšek, *J. Comput. Chem.*, 2008, **29**, 861–870.
209 W. Kabsch, *Acta Crystallogr. A*, 1976, **32**, 922–923.
210 I. Fabre, L. A. Perego, J. Bergès, I. Ciofini, L. Grimaud and M. Taillefer, *Eur. J. Org. Chem.*, 2016, 5887–5896.
211 S. Purser, P. R. Moore, S. Swallow and V. Gouverneur, *Chem Soc Rev*, 2008, **37**, 320–330.
212 J. Wang, M. Sánchez-Roselló, J. L. Aceña, C. del Pozo, A. E. Sorochinsky, S. Fustero, V. A. Soloshonok and H. Liu, *Chem. Rev.*, 2014, **114**, 2432–2506.
213 E. P. Gillis, K. J. Eastman, M. D. Hill, D. J. Donnelly and N. A. Meanwell, *J. Med. Chem.*, 2015, **58**, 8315–8359.
214 Y. Zhou, J. Wang, Z. Gu, S. Wang, W. Zhu, J. L. Aceña, V. A. Soloshonok, K. Izawa and H. Liu, *Chem. Rev.*, 2016, **116**, 422–518.
215 D. O'Hagan, *Chem Soc Rev*, 2008, **37**, 308–319.
216 M.-C. Belhomme, T. Besset, T. Poisson and X. Pannecoucke, *Chem. - Eur. J.*, 2015, **21**, 12836–12865.
217 E. A. Ilardi, E. Vitaku and J. T. Njardarson, *J. Med. Chem.*, 2014, **57**, 2832–2842.
218 M. Feng, B. Tang, S. H. Liang and X. Jiang, *Curr. Top. Med. Chem.*, 2016, **16**, 1200–1216.
219 P. Johannesson, G. Lindeberg, A. Johansson, G. V. Nikiforovich, A. Gogoll, B. Synnergren, M. Le Grèves, F. Nyberg, A. Karlén and A. Hallberg, *J. Med. Chem.*, 2002, **45**, 1767–1777.
220 C. Bibang Bi Ekogha, O. Ruel and S. A. Julia, *Tetrahedron Lett.*, 1983, **24**, 4825–4828.
221 B. M. Trost and Y. Tanigawa, *J. Am. Chem. Soc.*, 1979, **101**, 4743–4745.
222 K. Itami, M. Mineno, N. Muraoka and J. Yoshida, *J. Am. Chem. Soc.*, 2004, **126**, 11778–11779.
223 D. G. Bachmann, C. C. Wittwer and D. G. Gillingham, *Adv. Synth. Catal.*, 2013, **355**, 3703–3707.
224 D. F. Andrès, E. G. Laurent, B. S. Marquet, H. Benotmane and A. Bensadat, *Tetrahedron*, 1995, **51**, 2605–2618.
225 D. F. Andrès, E. G. Laurent and B. S. Marquet, *Tetrahedron Lett.*, 1997, **38**, 1049–1052.

226 T. Hanamoto, R. Anno, K. Yamada and K. Ryu, *Tetrahedron Lett.*, 2007, **48**, 3727–3730.
227 T. Hanamoto, R. Anno, K. Yamada, K. Ryu, R. Maeda, K. Aoi and H. Furuno, *Tetrahedron*, 2009, **65**, 2757–2765.
228 L. Debien, M.-G. Braun, B. Quiclet-Sire and S. Z. Zard, *Org. Lett.*, 2013, **15**, 6250–6253.
229 S. Murakami, H. Ishii, T. Tajima and T. Fuchigami, *Tetrahedron*, 2006, **62**, 3761–3769.
230 S. Murakami, H. Ishii and T. Fuchigami, *J. Fluor. Chem.*, 2004, **125**, 609–614.
231 T. Lequeux, F. Lebouc, C. Lopin, H. Yang, G. Gouhier and S. R. Piettre, *Org. Lett.*, 2001, **3**, 185–188.
232 Y. Li, J. Liu, L. Zhang, L. Zhu and J. Hu, *J. Org. Chem.*, 2007, **72**, 5824–5827.
233 G. K. S. Prakash, J. Hu, Y. Wang and G. A. Olah, *Org. Lett.*, 2004, **6**, 4315–4317.
234 Y. Ohtsuka and T. Yamakawa, *Tetrahedron*, 2011, **67**, 2323–2331.
235 J. Li, W. Wan, G. Ma, Y. Chen, Q. Hu, K. Kang, H. Jiang and J. Hao, *Eur. J. Org. Chem.*, 2016, 4916–4921.
236 Q. Lin, L. Chu and F.-L. Qing, *Chin. J. Chem.*, 2013, **31**, 885–891.
237 Y.-M. Su, Y. Hou, F. Yin, Y.-M. Xu, Y. Li, X. Zheng and X.-S. Wang, *Org. Lett.*, 2014, **16**, 2958–2961.
238 H. Jiang, C. Huang, J. Guo, C. Zeng, Y. Zhang and S. Yu, *Chem. – Eur. J.*, 2012, **18**, 15158–15166.
239 J. Jung, E. Kim, Y. You and E. J. Cho, *Adv. Synth. Catal.*, 2014, **356**, 2741–2748.
240 C. Yu, N. Iqbal, S. Park and E. J. Cho, *Chem Commun*, 2014, **50**, 12884–12887.
241 J. Xie, T. Zhang, F. Chen, N. Mehrkens, F. Rominger, M. Rudolph and A. S. K. Hashmi, *Angew. Chem. Int. Ed.*, 2016, **55**, 2934–2938.
242 N. Surapanich, C. Kuhakarn, M. Pohmakotr and V. Reutrakul, *Eur. J. Org. Chem.*, 2012, 5943–5952.
243 Z. Feng, Q.-Q. Min, H.-Y. Zhao, J.-W. Gu and X. Zhang, *Angew. Chem. Int. Ed.*, 2015, **54**, 1270–1274.
244 C. Shao, G. Shi, Y. Zhang, S. Pan and X. Guan, *Org. Lett.*, 2015, **17**, 2652–2655.
245 T. L. Andersen, M. W. Frederiksen, K. Domino and T. Skrydstrup, *Angew. Chem. Int. Ed.*, 2016, **55**, 10396–10400.
246 T. L. Andersen, S. Kramer, J. Overgaard and T. Skrydstrup, *Organometallics*, , DOI:10.1021/acs.organomet.6b00893.
247 M.-C. Belhomme, T. Poisson and X. Pannecoucke, *Org. Lett.*, 2013, **15**, 3428–3431.
248 M.-C. Belhomme, T. Poisson and X. Pannecoucke, *J. Org. Chem.*, 2014, **79**, 7205–7211.
249 G. Caillot, J. Dufour, M.-C. Belhomme, T. Poisson, L. Grimaud, X. Pannecoucke and I. Gillaizeau, *Chem. Commun.*, 2014, **50**, 5887–5890.
250 M.-C. Belhomme, A. Bayle, T. Poisson and X. Pannecoucke, *Eur. J. Org. Chem.*, 2015, 1719–1726.
251 S. Mishra, P. Mondal, M. Ghosh, S. Mondal and A. Hajra, *Org Biomol Chem*, 2016, **14**, 1432–1436.
252 M. Ke and Q. Song, *J. Org. Chem.*, 2016, **81**, 3654–3664.
253 A. Prieto, R. Melot, D. Bouyssi and N. Monteiro, *ACS Catal.*, 2016, **6**, 1093–1096.
254 H. Xu, D. Wang, Y. Chen, W. Wan, H. Deng, K. Ma, S. Wu, J. Hao and H. Jiang, *Org Chem Front*, , DOI:10.1039/C7QO00119C.
255 L. Forti, F. Ghelfi, M. L. Lancellotti and U. M. Pagnoni, *Synth. Commun.*, 1996, **26**, 1699–1710.

256 A. J. Clark, *Chem. Soc. Rev.*, 2002, **31**, 1–11.
257 N. Zhang, S. R. Samanta, B. M. Rosen and V. Percec, *Chem. Rev.*, 2014, **114**, 5848–5958.
258 A. J. Pallenberg and J. D. White, *Tetrahedron Lett.*, 1986, **27**, 5591–5594.
259 N. Kiriyama, K. Nitta, Y. Sakaguchi, Y. Taguchi and Y. Yamamoto, *Chem. Pharm. Bull. (Tokyo)*, 1977, **25**, 2593–2601.
260 A. G. M. Barrett and H. G. Sheth, *J. Org. Chem.*, 1983, **48**, 5017–5022.
261 A. Hinman and J. Du Bois, *J. Am. Chem. Soc.*, 2003, **125**, 11510–11511.
262 P. Lu and T. Bach, *Angew. Chem. Int. Ed.*, 2012, **51**, 1261–1264.
263 M. F. Braña, M. L. García, B. López, B. de Pascual-Teresa, A. Ramos, J. M. Pozuelo and M. T. Domínguez, *Org. Biomol. Chem.*, 2004, **2**, 1864–1871.
264 R. Dede, L. Michaelis and P. Langer, *Tetrahedron Lett.*, 2005, **46**, 8129–8131.
265 P. Dambruoso, A. Massi and A. Dondoni, *Org. Lett.*, 2005, **7**, 4657–4660.
266 D. Lee, S. G. Newman and M. S. Taylor, *Org. Lett.*, 2009, **11**, 5486–5489.
267 Z. Zhou, P. M. Walleser and M. A. Tius, *Chem Commun*, 2015, **51**, 10858–10860.
268 I. Fabre, T. Poisson, X. Pannecoucke, I. Gillaizeau, I. Ciofini and L. Grimaud, *Catal Sci Technol*, , DOI:10.1039/C7CY00076F.
269 J. C. Antilla, J. M. Baskin, T. E. Barder and S. L. Buchwald, *J. Org. Chem.*, 2004, **69**, 5578–5587.
270 A. Correa and C. Bolm, *Angew. Chem. Int. Ed.*, 2007, **46**, 8862–8865.
271 A. I. Vogel, B. S. Furniss and A. I. Vogel, *Vogel's Textbook of practical organic chemistry*, Longman Scientific & Technical ; Wiley, London : New York, 5th ed., 1989.
272 D. M. Shendage, R. Fröhlich and G. Haufe, *Org. Lett.*, 2004, **6**, 3675–3678.
273 S. V. Chankeshwara and A. K. Chakraborti, *Org. Lett.*, 2006, **8**, 3259–3262.
274 E. Kumarasamy, R. Raghunathan, S. Jockusch, A. Ugrinov and J. Sivaguru, *J. Am. Chem. Soc.*, 2014, **136**, 8729–8737.
275 H.-L. Kao and C.-F. Lee, *Org. Lett.*, 2011, **13**, 5204–5207.
276 C.-M. Chu, Z. Tu, P. Wu, C.-C. Wang, J.-T. Liu, C.-W. Kuo, Y.-H. Shin and C.-F. Yao, *Tetrahedron*, 2009, **65**, 3878–3885.
277 C. G. Bates, P. Saejueng, M. Q. Doherty and D. Venkataraman, *Org. Lett.*, 2004, **6**, 5005–5008.
278 P. Zhong and X. Huang, *J. Serbian Chem. Soc.*, 2004, **69**, 175–178.
279 A. A. Oswald, K. Griesbaum, B. E. Hudson and J. M. Bregman, *J. Am. Chem. Soc.*, 1964, **86**, 2877–2884.
280 Z.-L. Wang, R.-Y. Tang, P.-S. Luo, C.-L. Deng, P. Zhong and J.-H. Li, *Tetrahedron*, 2008, **64**, 10670–10675.
281 M.-Z. Cai, M.-H. Jiang and H.-G. Li, *J. Chem. Res.*, 2006, 702–704.
282 J. Yang, A. Sabarre, L. R. Fraser, B. O. Patrick and J. A. Love, *J. Org. Chem.*, 2009, **74**, 182–187.
283 V. Fiandanese, G. Marchese, F. Naso and L. Ronzini, *Synthesis*, 1987, **11**, 1034–1036.
284 V. P. Ananikov, N. V. Orlov and I. P. Beletskaya, *Organometallics*, 2006, **25**, 1970–1977.
285 H.-Y. Tu, B.-L. Hu, C.-L. Deng and X.-G. Zhang, *Chem Commun*, 2015, **51**, 15558–15561.

Résumé

Cette thèse présente des travaux de méthodologie de synthèse et des études mécanistiques. Une approche complémentaire est utilisée, avec des résultats expérimentaux et des résultats théoriques issus de calculs DFT. Trois réactions ont été étudiées.

La première réaction est l'alpha-arylation de cétones énolisables en l'absence de métal de transition. Elle se déroule en présence de DMF et de *t*BuOK. L'étude mécanistique met en évidence la formation d'une espèce riche en électrons par déprotonation du solvant.

La deuxième réaction étudiée est la *N*-arylation de pyrazoles *via* la formation d'aryldiazoniums *in situ*. Cette réaction est catalysée au cuivre. Une évaluation de la méthode DFT la plus adaptée est présentée. Un double cycle catalytique est proposé, faisant intervenir le complexe de cuivre et l'acide acétique.

La dernière réaction étudiée est la formation stéréoselective d'alkényl thioethers fluorés trisubstitués par catalyse au cuivre. La méthodologie de synthèse est présentée, suivie d'une étude mécanistique. Celle-ci révèle un mécanisme radicalaire qui peut être généralisé à d'autres substrats.

Mots Clés

Catalyse homogène, mécanisme, DFT, méthodologie de synthèse, cuivre, radicalaire

Abstract

In this thesis, synthetic methodology development and mechanistic studies are presented. A complementary approach, using both experiments and theoretical outcomes from DFT, is used. Three reactions were studied.

The first reaction is the transition-metal free alpha-arylation of enolizable ketones. It proceeds using DMF and *t*BuOK. The mechanistic study reveals the formation of an electron-rich species by deprotonation of the solvent.

The second reaction studied is the copper-catalyzed *N*-arylation of pyrazoles with arenediazonium salts generated *in situ*. A benchmark is performed to evaluate the best DFT methodology. A double catalytic cycle is proposed, involving copper and acetic acid.

The last reaction studied is the copper-catalyzed stereoselective access to trisubstituted fluorinated alkenyl thioethers. The development of the methodology is presented. Then a mechanistic study reveals a radical mechanism that can be generalized to other substrates.

Keywords

Homogeneous catalysis, mechanism, DFT, synthetic methodology, copper, radical